Lecture Notes

Introduction to Plasma Physics

Summer Semester 2023

Ruhr-University Bochum

Prof. A. von Keudell

September 9, 2026

Preface

These notes have evolved from the lecture 'Introduction to Plasma Physics' in the summer semesters of 2004, 2006, 2014, and 2017. The main sources used were the books by Chen (*Plasma Physics and Controlled Fusion*), Liebermann and Lichtenberg (*Principles of Plasma Discharges and Materials Processing*), and Kaufmann (*Plasmaphysik und Fusionsforschung*). These notes are not intended to replace these books and are meant to supplement them.
Conceptually, the lecture begins with an *Introduction* followed by the *Description Forms* of plasma, the single-particle and multi-particle picture. After considering *Collision Processes*, a discussion of *Transport* in magnetized plasmas follows. The diagnostics and heating of plasmas are described in the chapter *Waves*. How this heating affects the distribution function of the particles in the plasma is treated in the chapter *Kinetics*. The boundary conditions of plasmas at walls are considered in the chapter *Plasma Boundary*. Finally, the application of plasmas in *Plasma Technology* and *Fusion Research* is discussed.
Excluded is an extended description of MHD equilibria and instabilities in toroidal plasmas. This is the subject of an advanced lecture "Fusion Plasma Physics". Also, in the description of kinetic phenomena, frequently used methods of low-temperature plasma physics have been emphasized.
My thanks go to my colleagues in Bochum for the numerous suggestions for the manuscript.
In the summer semester of 2023, animations of individual phenomena in plasma physics were added. These are linked to YouTube (https://www.youtube.com/@AchimvonKeudell) or the Python code is available on GitHub (https://github.com/AchimVonKeudell/PhysicsVisualisations).

Contents

1 Introduction **6**
1.1 Plasmas in Nature and Technology 7
1.1.1 Natural Plasmas 7
1.1.2 Plasmas in Technology 7
1.2 Definition Plasma 9
1.2.1 Concept of Temperature 9
1.2.2 Debye Shielding 10
1.2.3 Plasma Frequency 13
1.3 Classification of Plasmas 14

2 Description of Plasmas **17**
2.1 Single-Particle Picture 18
2.1.1 Particle Drifts 18
2.1.2 Adiabatic Invariants 38
2.2 Multi-Particle Picture 45
2.2.1 Hierarchy of Equations in Plasma Physics 45
2.2.2 Distribution Function 47
2.2.3 Temporal Evolution of the Distribution Function . . . 48
2.2.4 Moments of the Boltzmann Equation, Fluid Picture . . 51
2.2.5 Drifts in the Fluid Picture 57
2.2.6 Comparison Fluid Picture - Single-Particle Picture . . 62

3 Collisions **65**
3.1 Definitions 65
3.2 Differential Cross-Section 67
3.3 The Scattering Problem 69
3.4 Scattering Potentials 71
3.4.1 Coulomb Scattering, Coulomb Logarithm 71
3.4.2 Polarization Scattering 74
3.4.3 Ionization 76
3.5 Ionization Equilibria 79

4 Transport **83**
4.1 Transport in Partially Ionized Plasmas . . . 86
4.1.1 Ambipolar Diffusion . . . 86
4.1.2 Diffusion Perpendicular to the B Field . . . 89
4.2 Transport in Fully Ionized Plasmas . . . 92
4.2.1 Collisions Between Charge Carriers . . . 92
4.2.2 Specific Resistance or Conductivity of a Plasma . . . 92
4.2.3 Diffusion Perpendicular to the B Field, Magnetohydrodynamics . . . 95
4.3 Time-Dependent Effects of MHD . . . 102
4.3.1 Magnetic Field Diffusion . . . 104
4.3.2 Frozen-in Flux . . . 105
4.4 Equilibria and Instabilities . . . 106
4.4.1 Stability of a Cylindrical Plasma Column . . . 106
4.4.2 Instabilities . . . 109

5 Waves in Plasmas **119**
5.1 Electrostatic Waves . . . 120
5.1.1 Electron Oscillations . . . 120
5.1.2 Electron Waves . . . 122
5.1.3 Ion Waves . . . 124
5.1.4 Electron Waves Perpendicular to the B Field, Upper Hybrid Frequency . . . 126
5.1.5 Ion Waves Perpendicular to the B Field, Lower Hybrid Frequency . . . 127
5.2 Electromagnetic Waves . . . 130
5.2.1 EM Waves for $B_0 = 0$ . . . 131
5.2.2 EM Waves with $B_0 \neq 0$ . . . 133
5.3 Hydromagnetic Waves . . . 140
5.3.1 Alfven Waves . . . 141
5.3.2 Magnetosonic Waves . . . 142

6 Kinetics **144**
6.1 Distribution function in LTE, Maxwell distribution . . . 145
6.2 Distribution function under the influence of external fields . . . 146
6.2.1 2-term approximation . . . 146
6.2.2 Boltzmann equation in 2-term approximation . . . 149
6.3 Kinetic wave damping, Landau damping . . . 157

7 The Plasma Sheath **161**
7.1 sheath 161
7.1.1 Space Charge Zone 162
7.1.2 Presheath 164
7.2 Floating potential, Plasma potential 166
7.3 Sheaths with Applied Voltage 167
7.3.1 Matrix Sheath 168
7.3.2 Child-Langmuir Sheath 170
7.3.3 Collision-determined sheath 172
7.4 Probe Measurements 174

8 Application: Low-Temperature Plasmas **178**
8.1 DC Discharge 178
8.1.1 Townsend Discharge - Unself-Sustained Discharge . . . 178
8.1.2 Glow Discharge - Self-Sustained Discharge, Paschen Curve 180
8.1.3 Magnetically Assisted DC Discharge, Magnetron Plasmas 185
8.2 Capacitively Coupled RF Discharges 187
8.2.1 Voltage 187
8.2.2 Heating Methods 190
8.2.3 Asymmetric, Capacitive RF Discharge 194
8.3 Inductively Coupled RF Discharges 197
8.4 Plasmas with Wave Heating 201
8.4.1 Microwave Plasmas 201
8.4.2 ECR Plasmas 202
8.5 Atmospheric Pressure Plasmas 204
8.5.1 Arc Discharge 204
8.5.2 Dielectric Barrier Discharge 208
8.6 Global Plasma Models 211
8.6.1 Particle Balances 211
8.6.2 Energy Balance 212

9 Application: Nuclear Fusion **213**
9.1 Fusion Reactions 213
9.2 Ignition Criterion 215
9.3 Plasma Confinement 221
9.3.1 Tokamak 221
9.3.2 Limiter, Divertor 225
9.3.3 Transport in the Tokamak 228
9.4 Plasma Heating 232

9.5 Materials for Fusion 235

A Question Catalog 237

A.1 Chapter 1: Introduction 237
A.2 Chapter 2: Description of Plasmas 237
A.3 Chapter 3: Collisions 238
A.4 Chapter 4: Transport 238
A.5 Chapter 5: Waves 239
A.6 Chapter 6: Kinetics 240
A.7 Chapter 7: Plasma Sheath 240
A.8 Chapter 8: Low-Temperature Plasmas 241
A.9 Chapter 9: Fusion 241

Chapter 1

Introduction

Plasmas are partially or fully ionized gases that become visible to humans in luminous phenomena. Irving Langmuir coined the term "plasma" to describe the seemingly random ensemble of positive and negative charge carriers. Langmuir derived this designation from the well-known microscopic image of a biological "blood plasma". Unfortunately, the term plasma is almost always equated with this biological plasma by the public, even though many products of daily life come into contact with plasmas during their manufacturing process. Nevertheless, the designation plasma is not used to name an object. The most well-known example is the neon tube or fluorescent tube, which would be better described as a plasma lamp.

In this chapter, the peculiarities of a plasma are characterized, and the essential parameters are derived. In addition, a classification of plasmas is presented.

Plasmas are the most common form of visible matter. When energy is supplied to a solid, it undergoes several **states of aggregation**. As the temperature increases, it first begins to melt and becomes a liquid. With further increase, the liquid begins to evaporate. However, if the energy supply per particle is so high that atoms or molecules can be ionized, a plasma is created. Therefore, this is also referred to as the fourth state of matter. A preliminary **definition of the plasma state** is:

> "A plasma is a quasi-neutral gas of charged and uncharged particles that exhibits collective behavior."

In this sentence, the essential terms, quasi-neutral and collective, are included. This is intended to distinguish plasmas, for example, from an ion beam.

1.1 Plasmas in Nature and Technology

1.1.1 Natural Plasmas

Plasmas are natural components of the universe. In stars, fusion reactions occur at high pressure and temperature. The energy released keeps the plasma state in these systems alive. Here, the radiation pressure is in equilibrium with the gravitational force.
In the solar system, plasma continuously flows from our central star, the solar wind. These particles hit the Earth and mainly reach the polar regions along the magnetic field lines. There, ionization occurs in the atmosphere, which can be observed as auroras.
Lightning corresponds to discharges between potential differences between clouds or between clouds and the Earth, which are caused by friction phenomena in thunderclouds.

1.1.2 Plasmas in Technology

Nuclear Fusion

In the application of plasmas, controlled nuclear fusion plays a central role. It has been and continues to be essential for the advancement of plasma research. The goal is to replicate the nuclear fusion reactions that occur in the sun on Earth. Since the fuel for the fusion reaction is hydrogen isotopes, which are available in unlimited quantities, a fusion power plant represents an inexhaustible energy source for the future. To achieve this goal, the most promising fusion reaction with the largest cross-section is the DT reaction according to:

$$\mathrm{D} + \mathrm{T} \rightarrow \mathrm{He} + \mathrm{n} + 17.6\mathrm{MeV} \tag{1.1}$$

Here, the helium nucleus has an energy of ~ 4 MeV and the neutron has an energy of ~ 13 MeV. To realize nuclear fusion on Earth, there are two fundamentally different concepts of confinement:

- In the case of fusion in magnetically confined plasmas, a plasma is brought to temperatures of around 10^4 eV by coupling energy in the form of wave heating and neutral particle injection. At particle densities of 10^{20} m^{-3}, this confinement must be maintained for several seconds to obtain a plasma that continues to burn independently through the energy release in the nuclear fusion reactions.

- In contrast, in laser fusion, the fuel is compressed by irradiating laser power. The outer shell of a spherical pellet is ablated, and the inward-running shock front compresses the core of the pellet. The temperatures are again approximately 10^4 eV, but densities of 10^{30} m^{-3} are achieved. However, this form of confinement is only successful for nanoseconds.

Both situations are comparable because, for a successful fusion reactor, the so-called triple product (density $\times$ temperature $\times$ confinement time) must exceed a certain value.

Plasma Technology

In plasma technology, cold plasmas are usually considered, in which the temperature of the ions remains in the range of room temperature. The distinction between cold and hot plasmas is made with regard to the temperature of the ions.
Several application fields of plasma technology can be distinguished:

- **Lighting Technology**

  Light generation is a major application field of plasma technology. The fluorescent tube or energy-saving lamp are actually plasma lamps that are characterized by long life and high light efficiency.

- **Surface Techniques**

  Plasma processes are widely used in coating and modifying surfaces. For example, numerous manufacturing steps in the semiconductor industry are based on plasma etching processes or plasma coating processes. In these processes, a starting gas is dissociated in the plasma, and the dissociation products react with the surrounding walls, leading to coating or material removal.

- **Plasma Spraying**

  Thermal plasmas are used to produce thin films from metals or ceramics. In this process, a powder is injected into a plasma that burns at atmospheric pressure, a thermal arc. The particles melt in the arc and form a homogeneous film upon impact on the substrate.

- **Plasma Switches**

  Plasma switches are essential for switching high currents. Here, when opening an electrical connection that carries many kA, the formation of an electric arc must be suppressed. For this purpose, SF_6 is often used as a gas, as it is strongly electronegative and thus binds electrons that are formed by attachment reactions (formation of negative ions). The current transport through the light electrons is thus prevented.

1.2 Definition Plasma

1.2.1 Concept of Temperature

So far, various temperatures have been distinguished with regard to cold and hot plasmas. The energy content of a plasma can be characterized by means of the so-called distribution function. A typical example is the **Maxwell distribution**, which corresponds to a distribution function of maximum entropy. It forms when the particles experience sufficiently elastic collisions with each other.

$$f(v) = Ae^{\frac{-\frac{1}{2}mv^2}{k_BT}} \tag{1.2}$$

The distribution function must first be normalized. For this purpose, two conventions can be used. If the distribution function is normalized to one, i.e., indicates the probability of finding a particle in a velocity interval dv, one obtains:

$$f(v) = \left(\frac{m}{2\pi k_BT}\right)^{3/2} e^{\frac{-\frac{1}{2}mv^2}{k_BT}} \tag{1.3}$$

Alternatively, $f(v)$ can also directly indicate the density n of the particles in the velocity interval dv. One then obtains:

$$f(v) = n\left(\frac{m}{2\pi k_BT}\right)^{3/2} e^{\frac{-\frac{1}{2}mv^2}{k_BT}} \tag{1.4}$$

From this distribution function, the average energy of a particle can be derived.

$$\langle E\rangle = \frac{\int \frac{1}{2}mv^2 f(v)d^3v}{\int f(v)d^3v} = \frac{3}{2}k_BT \tag{1.5}$$

Here, $k_BT = 1$ eV $= 11594$ K. The concept of temperature is due to elastic collisions between the particles. If sufficient collisions occur, the temperatures

of the individual charge carriers can equalize each other. This is referred to as **thermal equilibrium** ($T_e = T_i$). However, the thermal coupling between electrons and ions is low due to the large mass difference, and a large number of collisions are required for temperature equalization. However, the concept of a temperature can still be used by assigning separate temperatures to ions and electrons.
With regard to the parameters charge carrier density n and temperature T, plasmas can be very roughly distinguished, as illustrated in Fig. 1.1.

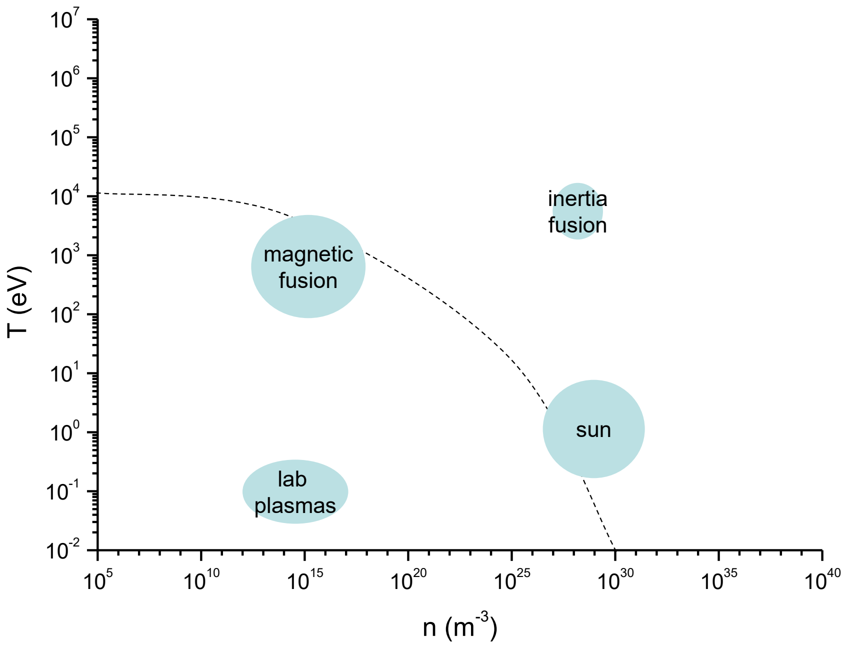

Figure 1.1: Classification of Plasmas

1.2.2 Debye Shielding

Initially, a plasma was described as a quasi-neutral gas. This means that the number of positive and negative charge carriers in a volume element must be exactly equal. But on what scale does this statement hold?
Consider a stationary ion background and examine the case where a local disturbance in the electric potential Φ_0 occurs. In Fig. 1.2, the case of an additional *negative* charge at a point $x = 0$ is illustrated. A new equilibrium is established, which balances the repulsion of the surrounding electrons by the presence of the additional electron with the backflow of these electrons

according to a density gradient (The case of an additional ion at the point $x = 0$ is entirely analogous).

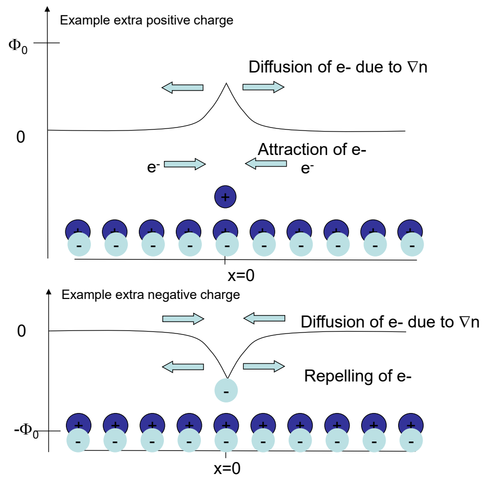

Figure 1.2: Debye Shielding

The electron density at the location of this disturbance is described by the **Boltzmann relation** (as will be proven later):

$$n_e = n_0 e^{\frac{e\Phi(x)}{k_B T}} \tag{1.6}$$

This is inserted into the Poisson equation:

$$\epsilon_0 \frac{d^2\Phi}{dx^2} = en_0 \left(e^{\frac{e\Phi(x)}{k_B T}} - 1 \right) \tag{1.7}$$

For $\frac{e\Phi}{k_B T} \ll 1$, we have:

$$\epsilon_0 \frac{d^2\Phi}{dx^2} = en_0 \left(1 + \frac{e\Phi(x)}{k_B T} + ... - 1 \right) \simeq en_0 \frac{e\Phi}{k_B T} \tag{1.8}$$

Animation

Youtube: Debye Shielding

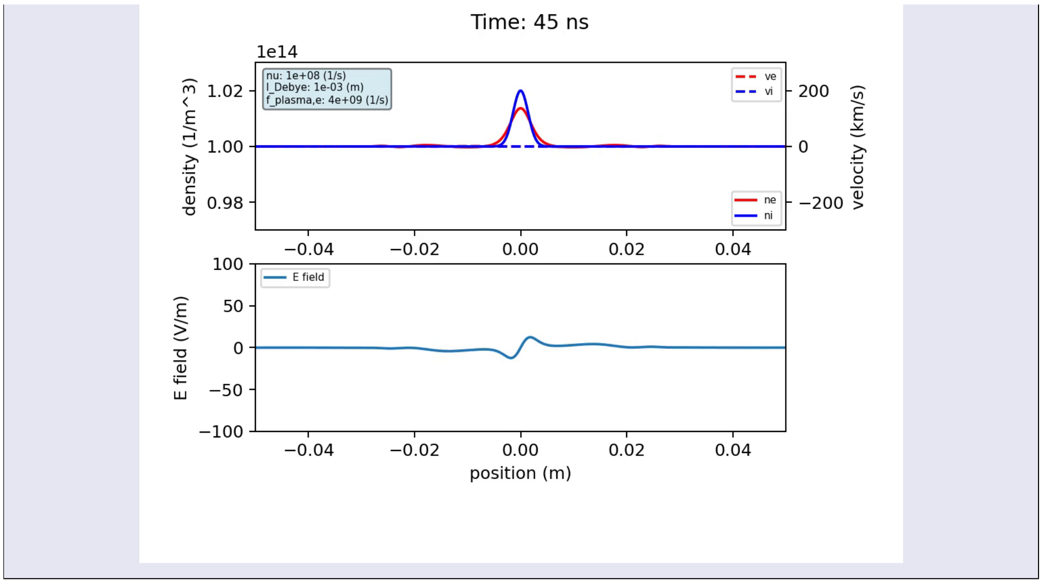

The solution of the differential equation

$$\frac{d^2\Phi}{dx^2} = \frac{n_0 e^2}{\epsilon_0 k_B T}\Phi \tag{1.9}$$

yields

$$\Phi = \Phi_0 e^{-\frac{|x|}{\lambda_D}} \tag{1.10}$$

with the so-called **Debye length**:

$$\boxed{\lambda_D = \left(\frac{\epsilon_0 k_B T}{n_0 e^2}\right)^{1/2}} \tag{1.11}$$

i.e., quasi-neutrality is satisfied if the considered region is larger than the Debye length. Thus, a scale is defined from which one can speak of a plasma. The volume with radius Debye length is referred to as the **Debye sphere**. Collective behavior is only ensured if the number of particles in this Debye sphere $\gg 1$ is.

$$N_D = \frac{4\pi}{3}\lambda_D^3 n \gg 1 \tag{1.12}$$

Microscopically, however, it becomes visible that a plasma is only quasi-neutral but consists of charged particles: an atom or molecule in the plasma "sees" the charge carriers electrons and ions in the vicinity. These generate a fluctuating electric field at the location of this atom or molecule, the **microfield**. This is important for the emission and absorption of radiation, as the electric microfield leads to a Stark splitting of the emission and absorption lines. The collisional interaction of an excited atom or molecule with the surrounding electrons and ions also leads to a reduction in the lifetime of the excited state and thus to a line broadening, the Stark broadening[1].

1.2.3 Plasma Frequency

Consider a plasma volume in which the electrons as a whole are deflected by a displacement δ from the background of the stationary ions, according to Fig. 1.3:

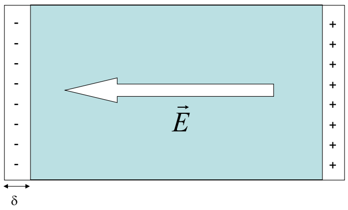

Figure 1.3: Plasma Frequency

The electric field of a surface charge is:

$$E = \frac{1}{\epsilon_0} en\delta \tag{1.13}$$

The equation of motion of the electrons in this field is:

$$m_e \frac{d\delta^2}{d^2t} = -eE \tag{1.14}$$

Thus, an oscillation equation is obtained according to

$$\frac{d^2\delta}{dt^2} + \frac{ne^2}{\epsilon_0 m}\delta = 0 \tag{1.15}$$

The natural frequency of this oscillation is the so-called **plasma frequency**:

$$\boxed{\omega_p = \left(\frac{ne^2}{\epsilon_0 m}\right)^{1/2}} \tag{1.16}$$

With these preliminary considerations, we can now more precisely define a plasma. Three conditions must be met:

[1] Similar disturbance effects are caused by collisions of the radiating atom with neutrals, which lead to the so-called pressure broadening and resonance broadening.

- $L > \lambda_D$

  The extent L of the plasma must be larger than the Debye length to ensure quasi-neutrality.

- $N_D \gg 1$

  The number of particles in the Debye sphere must be much larger than 1 to maintain collective behavior of the plasma.

- $\omega\tau \gg 1$

  The product of the plasma frequency with the collision time with neutrals τ should be much larger than 1 so that the electrostatic interaction dominates over normal gas kinetics.

1.3 Classification of Plasmas

Plasmas can be roughly divided into several categories:

- **ideal / non-ideal plasma**

  If the potential energy between two charge carriers:

$$\Phi_{AB} = \frac{q_A q_B}{4\pi\epsilon_0 r_{AB}} \tag{1.17}$$

  is compared with the thermal energy $E_{th} = \frac{3}{2}k_B T$, one speaks of

$$\text{ideal plasmas} \qquad \Phi_{AB} \ll E_{th} \tag{1.18}$$

$$\text{non}-\text{ideal plasmas} \qquad \Phi_{AB} \gg E_{th} \tag{1.19}$$

  Since the distance r_{ab} scales with the density n as $\propto n^{-1/3}$, the boundary between ideal plasma and non-ideal plasma is $T \propto n^{1/3}$

- **Degeneracy**

  Degeneracy occurs when the density of the charge carriers becomes so high that the Pauli exclusion principle has a significant share in the repulsive force. This is the case if the Fermi energy becomes larger than the thermal energy:

$$E_{Fermi} > E_{th} = \frac{3}{2}k_B T \tag{1.20}$$

With the Fermi energy

$$E_{Fermi} = \frac{\hbar^2}{2m_e}(3\pi^2 n_e)^{2/3} \tag{1.21}$$

the boundary between degenerate and non-degenerate plasmas is $T \propto n^{2/3}$

- **relativistic**

  Finally, at very high particle energies, it is necessary to calculate relativistically. This is the case for a thermal energy that is greater than the rest mass:

$$m_e c^2 \leq \frac{3}{2} k_B T \tag{1.22}$$

This classification is graphically illustrated in Fig. 1.4.

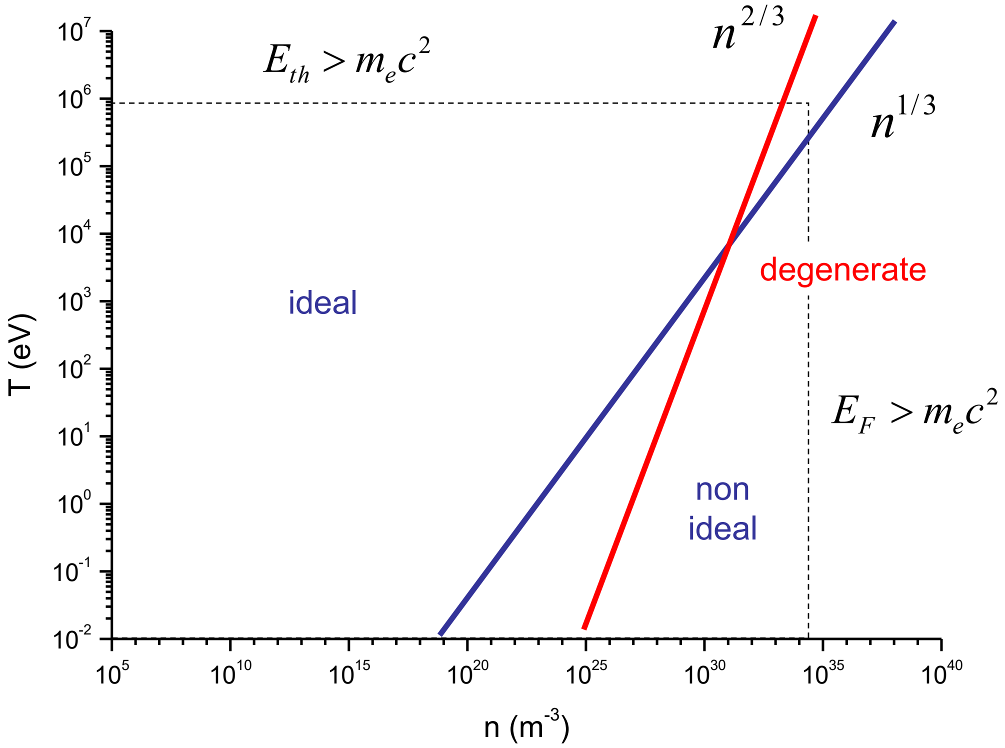

Figure 1.4: Classification of Plasmas

Chapter 2

Description of Plasmas

To describe the physics of a plasma, we need the appropriate tools. Important influencing factors are electric and magnetic fields, which determine the motion of the particles according to the Lorentz force. However, this entails a great complexity, since the induced motion of the particles in turn produces new internal electric and magnetic fields, which again determine the behavior. That is, the problem can only be solved self-consistently.

The most important component for controlling plasmas are magnetic fields, as they impart a preferred direction to the particles. That is, with a special magnetic field, plasmas can be well confined. However, this confinement can be strongly altered by the self-generated electromagnetic fields. The fundamental concepts for the successful magnetic confinement of a plasma are demonstrated in this chapter.

In the description of a plasma, one can start from the individual particle and calculate its motion in magnetic and electric fields. In this view, one moves with the particle. However, to describe an entire plasma, a multi-particle picture is more practical, where a stationary coordinate system is chosen and particles can enter and exit a volume element in the phase space (position and velocity).

In the description of plasmas, the following hierarchy can be established: (i) single-particle picture as the solution of the equation of motion of a particle given by the Lorentz force; (ii) multi-particle picture as the determination of the distribution function in the phase space of position and velocity (Vlasov or Boltzmann equation); (iii) multi-particle picture as the determination of the density and the center-of-mass velocity of a fluid (fluid picture, *moments of the Boltzmann equation).*

2.1 Single-Particle Picture

In the single-particle picture, the Newtonian equations of motion are solved for the motion of a charged particle in external force fields.

2.1.1 Particle Drifts

Constant E and B Fields

The starting point for the description of plasmas is initially the motion of a single charged particle in electric and magnetic fields. The determining factor here is always the **Lorentz force**:

$$\boxed{m\frac{d\vec{v}}{dt} = q(\vec{E} + \vec{v} \times \vec{B})} \tag{2.1}$$

- **Constant B Field**

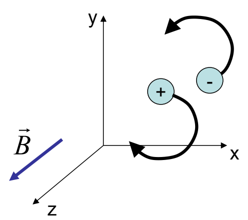

Figure 2.1: Coordinates for particle motion in a constant B field

Assume we have only a constant B field in the z direction. The equations of motion in the x,y plane are therefore:

$$m\frac{dv_x}{dt} = qB_z v_y \tag{2.2}$$

$$m\frac{dv_y}{dt} = -qB_z v_x \tag{2.3}$$

Differentiating once with respect to time and substituting into each other yields:

$$\frac{d^2 v_y}{dt^2} = -\left(\frac{qB}{m}\right)^2 v_y \tag{2.4}$$

This corresponds to an oscillation equation with the angular frequency ω_c of the **cyclotron frequency**:

$$\boxed{\omega_c = \frac{|q|B}{m}} \tag{2.5}$$

The solution of the oscillation equation is obtained with an ansatz according to:

$$v_{x,y} = v_\perp e^{\pm i\omega_c t} \tag{2.6}$$

Differentiating once gives the time dependence of the position coordinate:

$$x - x_0 = -i\frac{v_\perp}{\omega_c} e^{\pm i\omega_c t} \tag{2.7}$$

With the definition of the **Larmor radius** as

$$\boxed{r_L = \frac{v_\perp}{\omega_c} = \frac{m v_\perp}{|q|B}} \tag{2.8}$$

and

$$x - x_0 = r_L \sin \omega_c t \tag{2.9}$$

or

$$y - y_0 = \pm r_L \cos \omega_c t \tag{2.10}$$

The motion of the charge carriers in the magnetic field always has a **diamagnetic** character. That is, the magnetic field generated by the circular motion of the ions or electrons is always opposite to the externally applied magnetic field.

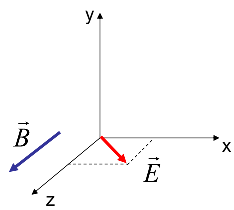

Figure 2.2: Coordinates for particle motion in constant E and B field

- **Constant B Field and E Field**

  In the case of constant E and B fields, the following equations are obtained according to the Lorentz force:

$$\dot{v}_z = \frac{q}{m} E_z \tag{2.11}$$

$$\dot{v}_x = \frac{q}{m} E_x \pm \omega_c v_y \tag{2.12}$$

$$\dot{v}_y = \mp \omega_c v_x \tag{2.13}$$

The signs take into account the case for ions and electrons, respectively. This is necessary here because the magnitude of the charge $|q|$ was chosen in the definition of ω_c.

Differentiating Eq. 2.12 once and substituting into Eq. 2.13 yields:

$$\ddot{v}_x = -\omega_c^2 v_x \tag{2.14}$$

Similarly,

$$\ddot{v}_y = \mp \omega_c \left[\frac{q}{m} E_x \pm \omega_c v_y \right] = -\omega_c^2 \left(\frac{E_x}{B_z} + v_y \right) \tag{2.15}$$

This is equivalent to a differential equation for the variable

$$\tilde{v}_y = \frac{E_x}{B_z} + v_y \tag{2.16}$$

The first term corresponds to a **drift motion**. This is illustrated in Fig. 2.3.

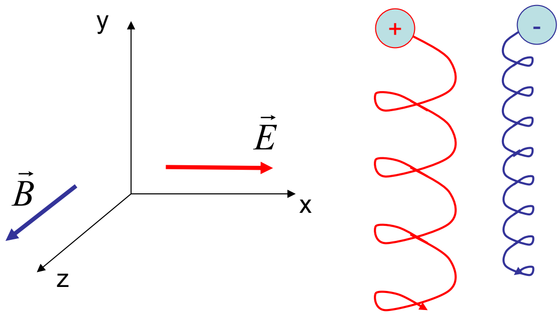

Figure 2.3: $\vec{E} \times \vec{B}$ Drift

Formally, this drift motion can be derived directly from the Lorentz force by not considering the trajectory directly, but the motion of the so-called **guiding center**, i.e., the center of mass of the gyration path. The time derivative describes this gyration motion explicitly. If one is only interested in the drift, the left side in Eq. 2.1 can be set to zero, and one obtains the expression:

$$0 = \vec{E} + \vec{v} \times \vec{B} \tag{2.17}$$

Now, both sides are multiplied by $\times\vec{B}$, and one obtains

$$0 = \vec{E} \times \vec{B} + (\vec{v} \times \vec{B}) \times \vec{B} \tag{2.18}$$

$$0 = \vec{E} \times \vec{B} - \vec{v}B^2 + \vec{B}(\vec{v}\vec{B}) \tag{2.19}$$

The last term is zero because the drift motion occurs perpendicular to the magnetic field. Finally, one obtains the so-called $\vec{E} \times \vec{B}$ **Drift**:

$$\boxed{\vec{v}_{E\times B} = \frac{\vec{E} \times \vec{B}}{B^2}} \tag{2.20}$$

This drift can be generalized by replacing the E field with a general external force field. With

$$\vec{F} = q\vec{E} \tag{2.21}$$

one obtains

$$\vec{v}_F = \frac{1}{q}\frac{\vec{F} \times \vec{B}}{B^2} \tag{2.22}$$

As an example, the **gravitational drift** is mentioned here.

$$\boxed{\vec{v}_g = \frac{m}{q}\frac{\vec{g} \times \vec{B}}{B^2}} \tag{2.23}$$

Intuitively, these drifts mean that in an external force field, the charge carriers are accelerated or decelerated depending on the direction. In doing so, the Larmor radius and accordingly the curvature of the path are always changed. Due to the change in the curvature of the path, the guiding center of the particle motion drifts.

The $\vec{E} \times \vec{B}$-drift is illustrated by three examples:

- **Magnetron**
  For the production of metal films using plasma processes, the sputtering of a metal surface in a noble gas plasma is used. A voltage is applied to the metal surface, and the ions that hit it are accelerated in the electric field and knock metal atoms out of this surface. The free metal atoms then settle again on a workpiece. The sputtering can be made more efficient by placing magnets behind the metal surface, as illustrated in Fig. 2.4. The electrons are forced onto paths according to the $E \times B$ motion. This corresponds to a better plasma confinement and very high electron densities can be generated. This also increases the ion density and accordingly the sputtering rate.
- **Hall Thruster**
  For the attitude control of satellites, so-called Hall thrusters are usually used. These ion thrusters generate a plasma in a concentric horseshoe magnet. As illustrated in Fig. 2.5, an electric field is superimposed. This forces the electrons onto $E \times B$ paths in the horseshoe magnet, while the ions are accelerated by the electric field and provide thrust through their momentum transfer. Since charged particles are emitted, the charge loss of the satellite must be compensated. For this reason, electrons are also added to the ion beam to neutralize it.

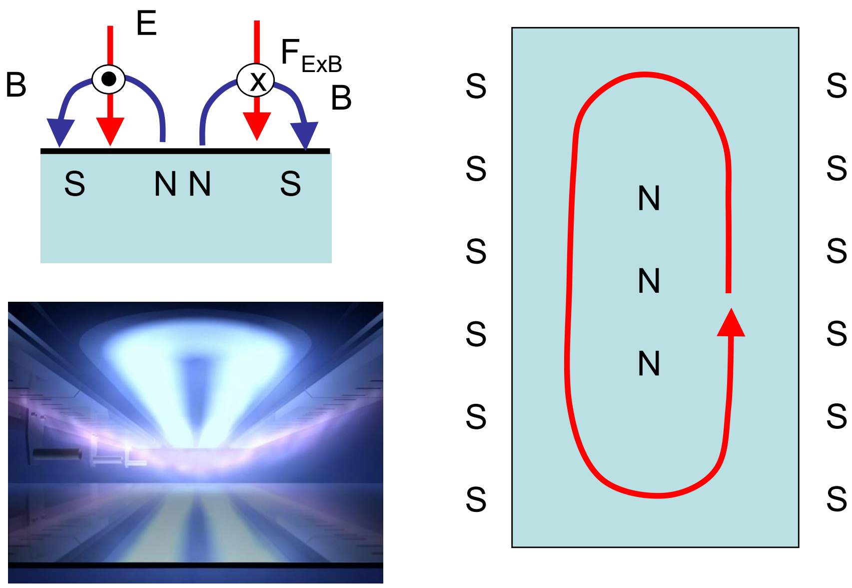

Figure 2.4: $E \times B$ motion of electrons in a magnetron discharge. Image: Uni Magdeburg

– **MHD Generator**

Another application of the forces on charged particles in electric and magnetic fields is the MHD generator (MHD, magnetohydrodynamics), as illustrated in Fig. 2.6. With this generator, chemical energy can be converted into electrical energy. Initially, a burner or flame is considered in which a reaction mixture, such as hydrocarbons plus oxygen or hydrogen and oxygen, is burned. The goal is to realize both a high degree of ionization and a high outflow velocity. When this thermal plasma flows through a magnetic field, charge carrier separation occurs according to the Lorentz force. These charges are collected at electrodes and can drive a consumer in an external circuit.

Non-Uniform Fields

In the following, we assume that the fields are no longer constant in space, but have a spatial variation.

- **Gradient of the B Field Perpendicular to the Direction of B**

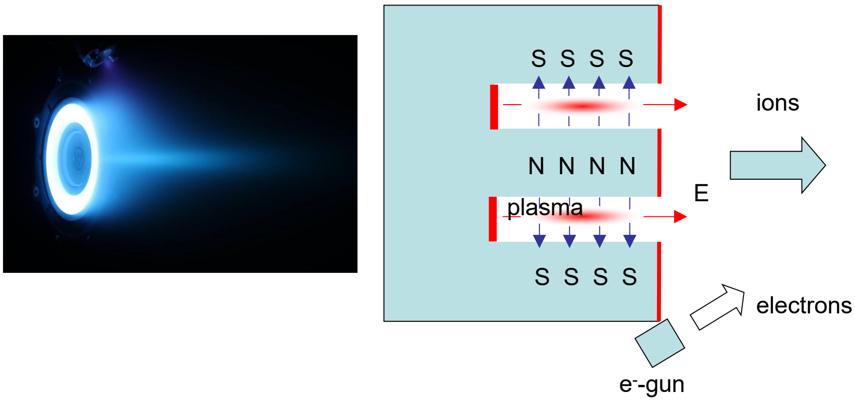

Figure 2.5: Hall Thruster. Image: Alta-Space

We assume that only a B field is present and that the gradient of the B field is perpendicular to the B field itself, as indicated in Fig. 2.7. The gradient in the B field is described by a Taylor expansion:

$$B_z(y) = B_0 + y\frac{\partial B}{\partial y} \tag{2.24}$$

An additional component of the force in the y direction is created because the B field changes in this direction:

$$F_y = -qv_x B_z(y) \tag{2.25}$$

We replace $v_x = v_\perp \cos\omega_c t$ and $y = \pm r_L \cos\omega_c t$. Thus, we obtain:

$$F_y = -qv_\perp \cos\omega_c t \left[B_0 \pm r_L \cos\omega_c t \frac{\partial B}{\partial y}\right] \tag{2.26}$$

Averaging over one revolution gives

$$\langle\cos^2\omega_c t\rangle = \frac{1}{2} \qquad \langle\cos\omega_c t\rangle = 0 \tag{2.27}$$

Thus, we obtain

$$F_y = \mp q v_\perp r_L \frac{1}{2}\frac{\partial B}{\partial y} \tag{2.28}$$

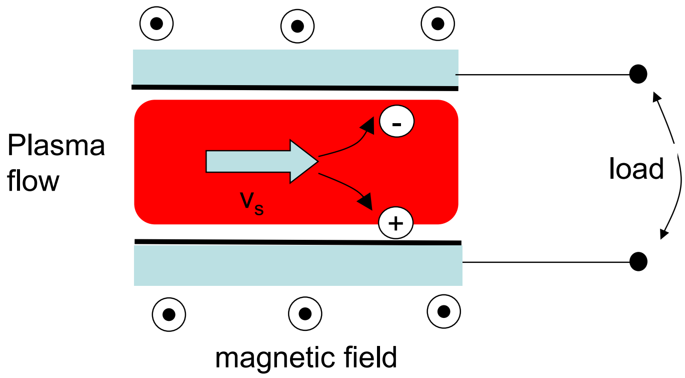

Figure 2.6: In an MHD generator, a plasma flows in a strong magnetic field. A charge separation occurs, which corresponds to a conversion of kinetic energy into electrical energy.

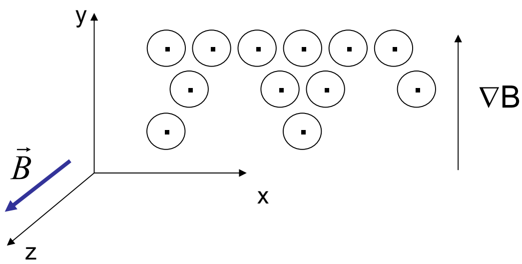

Figure 2.7: Coordinates for motion in the gradient of the B field

Substituting this back into the general relationship 2.22, we obtain:

$$v_{\nabla B} = \mp v_\perp r_L \frac{1}{2} \frac{\nabla B \times \vec{B}}{B^2} \tag{2.29}$$

or after swapping the cross product

$$\boxed{v_{\nabla B} = \pm v_\perp r_L \frac{1}{2} \frac{\vec{B} \times \nabla B}{B^2}} \tag{2.30}$$

This **∇ B Drift** is illustrated in Fig. 2.8. It is mainly caused by a change in the Larmor radius of the gyrating particle. However, this drift depends on the charge of the particle, unlike the $E \times B$ drift.

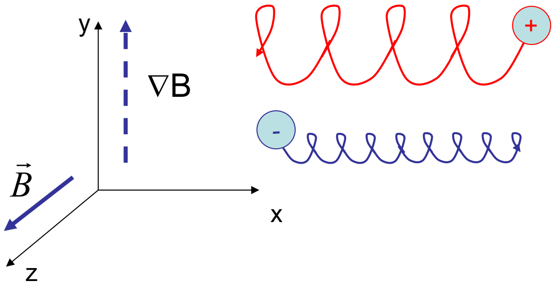

Figure 2.8: Gradient B Drift

- **Curved B Field Lines**

  If the B field lines are curved, the guiding center follows the trajectory of the particle path. This creates a centrifugal force, which in turn leads to a drift, **the curvature drift**. The centrifugal force can be described according to Fig. 2.9 by

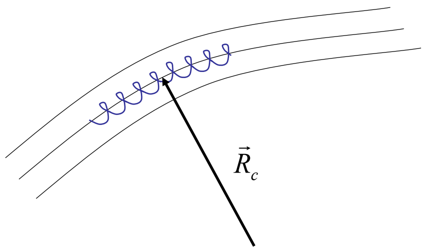

Figure 2.9: The centrifugal force creates a uniform force outward. In combination with the B field, the particle then experiences a curvature drift perpendicular to the plane.

$$\vec{F_{cf}} = m\frac{v_\parallel^2}{R_c}\hat{r} = m\frac{v_\parallel^2}{R_c^2}\vec{R_c} \tag{2.31}$$

Thus, the **curvature drift** with Eq. 2.22 gives:

$$\boxed{\vec{v_R} = \frac{1}{q}m\frac{v_\parallel^2}{R_c^2}\frac{\vec{R_c}\times\vec{B}}{B^2}} \tag{2.32}$$

These particle drifts have fundamental consequences for the field configuration in a toroidal plasma. Due to the curvature of the magnetic field lines and the gradient in the magnetic field in a torus, a charge carrier separation is created. This leads to an electric field, which in turn leads to an $E \times B$ drift that drives the plasma outward (Fig. 2.10. This can only be counteracted by shearing the magnetic field lines, i.e., a magnetic field line does not simply run around the torus in the toroidal direction but also in the poloidal direction. This is explained in more detail in Chapter 9.

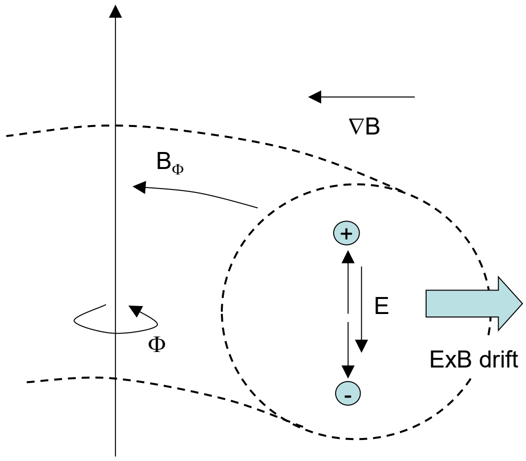

Figure 2.10: Drifts in a toroidal arrangement

- **Gradient of the B Field Parallel to the Direction of B**

Now, consider the case of a gradient of the B field parallel to the B field. The starting point is again the Lorentz force:

$$\vec{F} = q\vec{v} \times \vec{B} \tag{2.33}$$

The cylindrical symmetric configuration is represented by the three magnetic field components B_r, B_z, and B_Θ. The Lorentz force in this coordinate system is:

$$F_r = q\left(v_\Theta B_z - v_z B_\Theta\right) \tag{2.34}$$
$$F_\Theta = q\left(-v_r B_z + v_z B_r\right) \tag{2.35}$$
$$F_z = q\left(v_r B_\Theta - v_\Theta B_r\right) \tag{2.36}$$

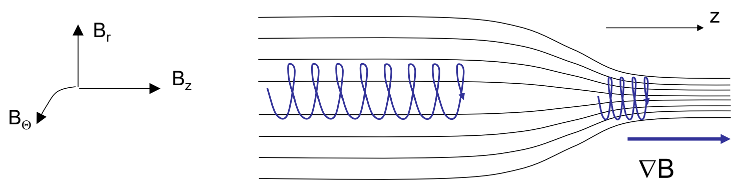

Figure 2.11: Motion parallel to B and ∇B. A magnetic mirror is created by a region of high magnetic field.

where $B_\Theta = 0$ applies. The gradient in the B field in the z direction can be linked to the radial B field via:

$$\vec{\nabla}\vec{B} = 0 \tag{2.37}$$

which in cylindrical coordinates for $B_\Theta = 0$

$$\frac{1}{r}\frac{\partial}{\partial r} r B_r + \frac{\partial B}{\partial z} = 0 \tag{2.38}$$

corresponds. This can be integrated under the approximation that $\frac{\partial B}{\partial z}$ depends only weakly on r.

$$r B_r = -\int_0^r r \frac{\partial B}{\partial z} dr = -\frac{1}{2} r^2 \left.\frac{\partial B}{\partial z}\right|_{r=0} \tag{2.39}$$

Thus, Eq. 2.36 can be written simply as

$$F_z = \frac{1}{2} q \vec{v}_\Theta \vec{r} \frac{\partial B}{\partial z} \tag{2.40}$$

With $v_\Theta = \mp v_\perp$ and the Larmor radius

$$r_L = \frac{m v_\perp}{|q| B} \tag{2.41}$$

one finally obtains

$$\bar{F}_z = -\frac{1}{2} \frac{m v_\perp^2}{B} \frac{\partial B}{\partial z} \tag{2.42}$$

This can be written as

$$\bar{F}_z = -\mu \frac{\partial B}{\partial z} \tag{2.43}$$

with the **magnetic moment** μ :

$$\boxed{\mu = \frac{1}{2}\frac{mv_\perp^2}{B}} \tag{2.44}$$

This magnetic moment is a conserved quantity of the motion of the charged particle in the magnetic field. This is shown below. First, we start from the equation of motion parallel to the z direction:

$$m\frac{dv_\parallel}{dt} = -\mu \frac{\partial B}{\partial z} \tag{2.45}$$

Both sides are multiplied by $v_\parallel$

$$mv_\parallel \frac{dv_\parallel}{dt} = -\mu v_\parallel \frac{\partial B}{\partial z} = -\mu \frac{dz}{dt}\frac{\partial B}{\partial z} = -\mu \frac{\partial B}{\partial t} \tag{2.46}$$

$v_\parallel$ is replaced by $\frac{dz}{dt}$. The left side can be rewritten and one obtains:

$$\frac{d}{dt}\left(\frac{1}{2}mv_\parallel^2\right) = -\mu \frac{\partial B}{\partial t} \tag{2.47}$$

Now we also need, for comparison, the consideration of the total energy, which remains constant because the Lorentz force always acts perpendicular to $\vec{v}$. This gives:

$$\frac{d}{dt}\left(\frac{1}{2}mv_\parallel^2 + \frac{1}{2}mv_\perp^2\right) = \frac{d}{dt}\left(\frac{1}{2}mv_\parallel^2 + \mu B\right) = 0 \tag{2.48}$$

This gives

$$-\mu \frac{dB}{dt} + \frac{d}{dt}(\mu B) = 0 \tag{2.49}$$

With the product rule for the second term, only the following relationship remains:

$$B\frac{d\mu}{dt} = 0 \tag{2.50}$$

Since the B field is given, the derivative of the magnetic moment with respect to time must be zero. Therefore, the magnetic moment of the particle motion remains constant during a movement along the B field gradient.

This constancy of the magnetic moment can be illustrated in a simple way by so-called mirror fields according to Fig. 2.12.

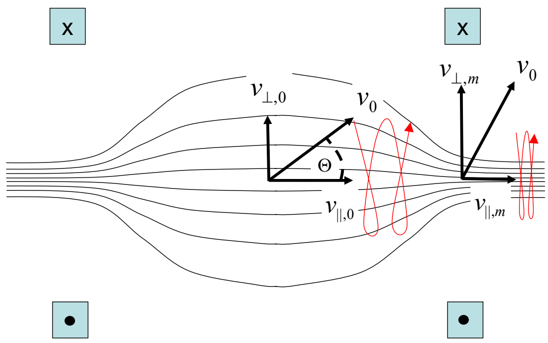

Figure 2.12: Magnetic bottle as a combination of two magnetic mirrors. In the center, the field is B_0 and on the axis in the middle of the coil B_m. The velocity of the particles is v_0. When moving through the magnetic bottle, the components v_{perp} and $v_{\parallel}$ are exchanged, while v_0 remains constant.

Consider a particle that at the location of minimal B field B_0 has a velocity $v_{\parallel,0}$ parallel and $v_{\perp,0}$ perpendicular to the magnetic field. At the location of maximum B field, the velocities are $v_{\parallel,m}$ parallel and $v_{\perp,m}$ perpendicular to the magnetic field. The constancy of the magnetic moment requires that:

$$\frac{1}{2}mv_{\perp,0}^2\frac{1}{B_0} = \frac{1}{2}mv_{\perp,m}^2\frac{1}{B_m} \tag{2.51}$$

From this it follows:

$$\frac{B_m}{B_0} = \frac{v_{\perp,m}^2}{v_{\perp,0}^2} \tag{2.52}$$

If we assume that the particle comes to a standstill in the axial direction at the location of maximum magnetic field, then energy conservation gives:

$$v_{\perp,0}^2 + v_{\|,0}^2 = v_{\perp,m}^2 \equiv v_0^2 \tag{2.53}$$

Thus, we have:

$$\frac{B_0}{B_m} = \frac{v_{\perp,0}^2}{v_0^2} = \sin^2 \Theta_m = \frac{1}{R_m} \tag{2.54}$$

with R_m the so-called **mirror ratio** . During the motion in this magnetic mirror, the total energy of the particle remains the same, since the magnetic field always acts perpendicular to the velocity. On its path, only parallel energy is exchanged with perpendicular energy. However, the angle between the vector $\vec{v}$ and the parallel component changes, the so-called **pitch angle** . In the center of the mirror arrangement at the lowest magnetic field, the particle has maximum parallel energy, and at the location of maximum B field, the particle has maximum perpendicular energy.

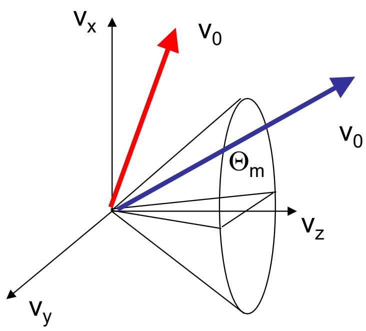

Figure 2.13: Particles whose velocity vector in the middle of the mirror machine lies within a loss cone with opening angle Θ_m can leave the mirror machine.

How does the Larmor radius change during the motion through the mirror field? Since the magnetic moment remains constant, $v_\perp^2 \propto B$, i.e., with increasing B field, $v_\perp$ only increases slowly. With $r_L = mv_\perp/(qB)$, this means that r_L is smaller in the region of the mirror point than in the center of the arrangement.

Whether a particle is trapped in this mirror field is determined by the initial conditions. If the vector of the particle velocity lies within the so-called **loss cone** , the particle can leave the mirror arrangement.

However, the confinement of particles is also not optimal independently of the consideration with the loss cone. In a mirror machine, there are regions of favorable and unfavorable curvature. In the middle of the mirror machine, the curvature drift leads to a charge separation in which the resulting electric field in combination with the magnetic field leads to an $E \times B$ drift that is directed outward. It drives the plasma apart as illustrated in Fig. 2.14. At the ends of the mirror machine, the curvature of the particle paths points in the opposite direction, and the resulting $E \times B$ drift points inward. This improves the confinement.

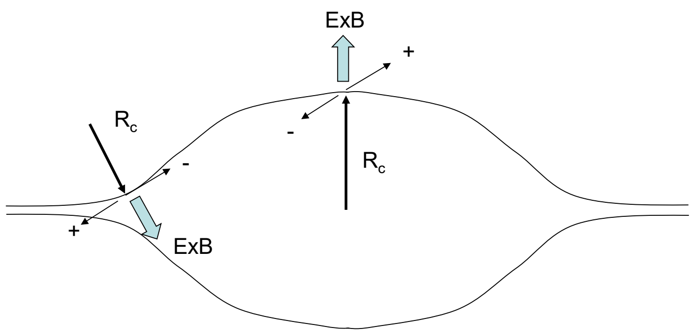

Figure 2.14: Regions of favorable and unfavorable curvature

Thus, depending on the curvature of the boundary between plasma and vacuum, one obtains a stable equilibrium or an unstable configuration (see Fig. 2.15).

The stability of the boundary between plasma and vacuum also has fundamental consequences for the shape of the toroidal confinement in magnetic fusion. In magnetic fusion, the magnetic field lines run around a torus. Here, these magnetic field lines are additionally *sheared*, as explained further below, so that a specific magnetic field line only returns to itself after several revolutions. The way in which the magnetic field lines are wrapped around the torus can be predetermined by the experimental setup or the shape of the external coils.

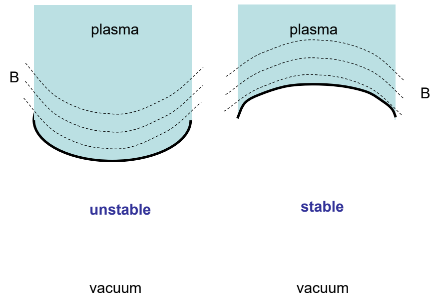

Figure 2.15: Stability of a boundary between plasma and vacuum depends on its curvature.

In a torus, the particle paths that run along the outside of the torus are unfavorable, while the particle paths on the inside are stable. For this reason, one tries to shape the magnetic field in such a way that a circulating magnetic field line leads around the inside of the torus as often as possible and only a few times around the outside. This results in a rather triangular cross-section of the torus surface as illustrated in Fig. 2.16.

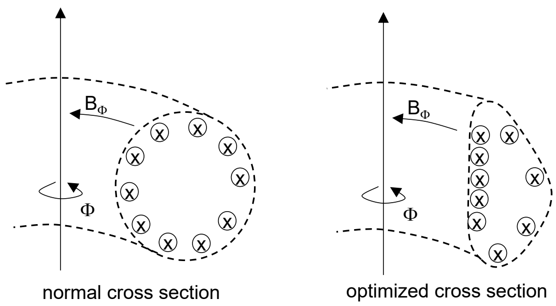

Figure 2.16: Optimization of the cross-section of a toroidal plasma.

To minimize the unfavorable curvature in the case of a linear mirror arrangement, the idea is to use a so-called cusp arrangement (Fig. 2.17). This increases the stability. However, this configuration has two disadvantages: on the one hand, in addition to the end losses, additional losses also occur around the circumference of the arrangement. Secondly, a so-called **X-point** has been created at the location with a magnetic field of 0. If a particle passes through this point, the magnetic moment loses its significance and is no longer a conserved quantity. That is, small disturbances can cause the particle to enter the loss cone.

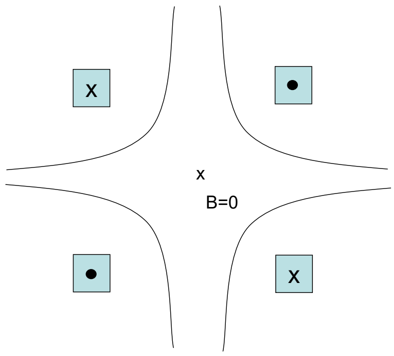

Figure 2.17: Cusp arrangement of a magnetic mirror

- **Non-Uniform E Field**

  In the case of a spatially non-uniform electric field, a drift only occurs if a curvature (i.e., second derivative not equal to zero) is present. Otherwise, the acceleration or deceleration cancels out again during one revolution. This is illustrated in Fig. 2.18.

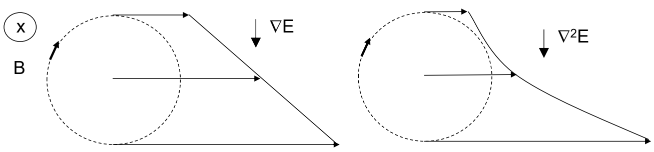

Figure 2.18: Drift due to non-uniform E fields

The drift velocity contains, in addition to the simple $E \times B$ drift, an additional term proportional to $\nabla^2 E$.

$$\boxed{v_{\nabla E} = \left(1 + \frac{1}{4} r_L^2 \nabla^2\right) \frac{\vec{E} \times \vec{B}}{B^2}} \tag{2.55}$$

Time-Dependent Fields

In the case of time-dependent fields, two cases can be distinguished: spatially constant but time-varying fields or spatially and temporally varying fields:

- *Polarization Drift*

  The **polarization drift** arises from time-varying electric fields that are spatially constant:

$$\boxed{\vec{v} = \pm\frac{1}{B\omega_c}\frac{\partial E}{\partial t}} \tag{2.56}$$

  If the electric field suddenly increases, the charge carriers are first accelerated in this direction before a gyration forms according to $\vec{v} \times \vec{B}$. Thus, a net drift in the direction of the electric field has taken place. This drift is greater the greater the inertia (given by the mass) is (see Fig. 2.19).

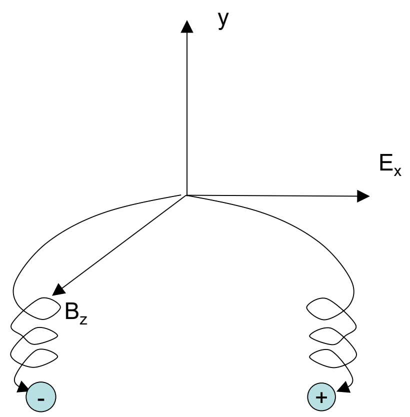

Figure 2.19: Polarization drift

- *Ponderomotive Force*

  Consider a charge carrier in a spatially and temporally varying field and assume that no static magnetic field B_0 exists. A classical example is the motion of a charge carrier in an electrostatic wave (see Chapter Waves), as illustrated in Fig. 2.20. The wave creates a disturbance of the quasi-neutrality according to $n(r) = n_0 + n_1(r)$, thereby creating a spatially and temporally varying electric field.

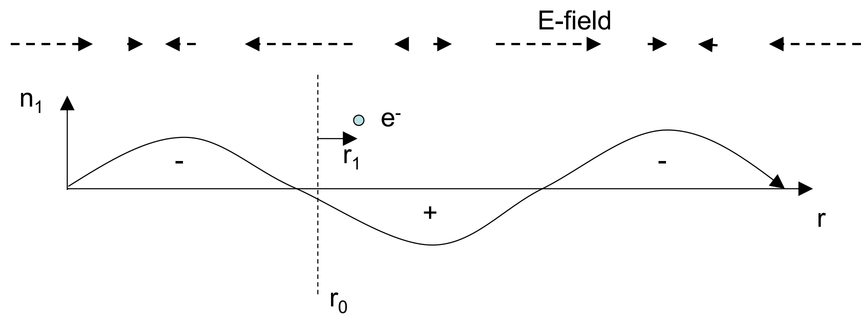

Figure 2.20: In an electrostatic wave, the electron density varies spatially as $n(r) = n_0 + n_1(r)$. The local variation of the charge creates a spatially varying electric field. We consider an electron at the location r_0, which is displaced by r_1 through the electric field.

For the electric field, we make the ansatz:

$$E(r,t) = E_0(r)\cos\omega t \tag{2.57}$$

The equation of motion that describes the motion of, for example, an electron in this variable field is the Lorentz force:

$$m\frac{dv}{dt} = -e\left[E_0(r)\cos\omega t + v \times B\right] \tag{2.58}$$

The magnetic field is generated by induction since the electric field changes over time. We now consider the change in velocity and position in different approximations. For the position, we write:

$$r = r_0 + r_1 \tag{2.59}$$

and the velocity v:

$$v = v_0 + v_1 + v_2 \tag{2.60}$$

In the first order, we consider the electron at the location r_0. Due to the temporal change of the electric field, we have a change in the velocity in the first order by v_1:

$$m\frac{dv_1}{dt} = -eE_0(r_0)\cos\omega t \tag{2.61}$$

Integrating this over time, we obtain the velocity v_1:

$$v_1 = -\frac{e}{m\omega}E_0(r_0)\sin\omega t \tag{2.62}$$

or after a further integration the displacement r_1:

$$r_1 = \frac{e}{m\omega^2}E_0(r_0)\cos\omega t \tag{2.63}$$

That is, the position of the electron oscillates like the electric field around the rest position r_0, and for the temporal averaging, $\langle v_1\rangle = \langle r_1\rangle = 0$ applies.

With this ansatz, we have not taken into account that the electric field changes spatially. That is, we must develop the electric field in order to be able to solve the equation of motion in the second order:

$$E(r,t) = E(r_0,t) + r_1\nabla\ E(r,t)|_{r=r_0} \tag{2.64}$$

In this case, we can no longer neglect the magnetic field. We obtain the equation of motion for the velocity v_2 in the first order.

$$m\frac{dv_2}{dt} = -e\left[r_1\nabla E(r) + v_1\times B_1\right] \tag{2.65}$$

At the same time, we consider the induction law:

$$\nabla\times E(r) = -\dot{B}_1 \tag{2.66}$$

which, when integrated over time, gives:

$$\frac{1}{\omega}\nabla\times E_0(r)\sin\omega t = -B_1 \tag{2.67}$$

That is, with Eq. 2.62, Eq. 2.63, and Eq. 2.67 in Eq. 2.65, we obtain:

$$\begin{aligned} m\frac{dv_2}{dt} &= -e\Big[\frac{e}{m\omega^2}E_0(r)\nabla E_0(r)\cos^2\omega t \\ &\quad + \frac{e}{m\omega^2}E_0(r)\times\nabla\times E_0(r)\sin^2\omega t\Big] \end{aligned} \tag{2.68}$$

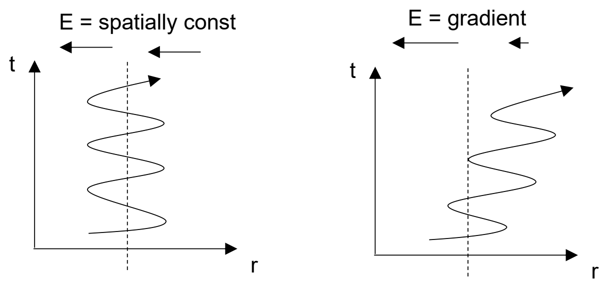

Figure 2.21: xt-diagram for the motion of a particle in a temporally oscillating but spatially homogeneous or inhomogeneous electric field.

The temporal averaging gives $\langle \sin^2 \omega t \rangle = \langle \cos^2 \omega t \rangle = 1/2$ in each case. Thus, we obtain:

$$m\langle \frac{dv_2}{dt} \rangle = -\frac{e^2}{m\omega^2}\frac{1}{2}\left[E_0(r)\nabla E_0(r) + E_0(r) \times \nabla \times E_0(r)\right] \tag{2.69}$$

After resolving the double cross product, the first term cancels out, and we obtain:

$$m\langle \frac{v_2}{dt} \rangle = -\frac{e^2}{m\omega^2}\frac{1}{4}\nabla (E_0(r))^2 \tag{2.70}$$

That is, a net force opposite to the gradient of the electric field is created. Electrons are thus always driven to regions of lower field strength. This so-called **ponderomotive force** has its origin in the fact that the oscillating electron moves from regions of high to regions of low field strength during its motion. Since the forces in the region of high field strength are greater, one does not obtain a symmetric motion but a drift. This is illustrated in an xt-diagram in Fig. 2.21.

2.1.2 Adiabatic Invariants

In mirror machines, there are several conserved quantities. If these conserved quantities remain constant even in the case of *slow* temporal changes in the fields, one speaks of **adiabatic invariants**. For this purpose, we consider the change in the momentum $\vec{p}$ on a closed path $\vec{q}$. If this integral is constant to first order, a conserved quantity is present.

$$\oint \vec{p} d\vec{q} \tag{2.71}$$

As an example, we take the magnetic moment. We integrate over one revolution of the gyration path according to Fig. 2.22.

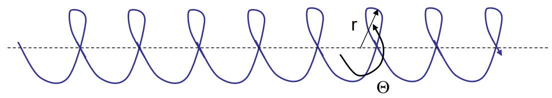

Figure 2.22: Conserved quantities in gyration

$$\oint \vec{p} d\vec{q} = \oint m v_\perp r_L d\Theta = 2\pi m v_\perp r_L \tag{2.72}$$

With the Larmor radius $r_L = v_\perp/\omega_c$ we obtain

$$\oint \vec{p} d\vec{q} = 2\pi \frac{m v_\perp^2}{\omega_c} = 4\pi \frac{m}{|q|}\mu \tag{2.73}$$

Thus, μ is a conserved quantity.

First Adiabatic Invariant

However, the claim was that the magnetic moment is also preserved if we *slowly change* the external field. When the magnetic field changes, an electric field is induced according to

$$\nabla \times \vec{E} = -\dot{\vec{B}} \tag{2.74}$$

In this electric field, the velocity of the particle and thus its kinetic energy increases. The change in the kinetic energy E_{kin} with time can be linked to the accelerating force $F = qE$, which acts over a distance ds via:

$$\frac{dE_{kin}}{dt} = F\frac{ds}{dt} \tag{2.75}$$

Thus, we obtain:

$$\frac{d}{dt}\left(\frac{1}{2} m v_\perp^2\right) = q\vec{E}\vec{v}_\perp = q\vec{E}\frac{dx}{dt} \tag{2.76}$$

Per revolution, the energy changes by an amount:

$$\delta\left(\frac{1}{2}mv_\perp^2\right) = \oint_0^{2\pi/\omega_c} q\vec{E}\frac{dx}{dt}dt = \oint_{Umfang} q\vec{E}dx \tag{2.77}$$

With the Stokes theorem, we obtain:

$$\oint_{Umfang} q\vec{E}dx = \int_{Flaeche} q(\nabla\times\vec{E})d\vec{S} = -q\int_{Flaeche}\dot{\vec{B}}d\vec{S} \tag{2.78}$$

with $\vec{S}$ the surface normal of the enclosed gyration path. Thus, we have:

$$\delta\left(\frac{1}{2}mv_\perp^2\right) = \pm q\dot{B}\pi r_L^2 \tag{2.79}$$

The sign changes because the direction of revolution around the surface S is different for ions and electrons. Thus, the direction of the surface normal of the gyration path also changes. In Eq. 2.79, the adiabatic approximation is included because for the surface integral, $r_L^2\pi$ was simply taken, which is only correct for small values of $\dot{B}$, as explained in Fig. 2.23.

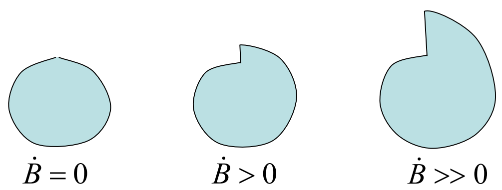

Figure 2.23: Adiabatic approximation when integrating the Larmor path.

$$\pm q\dot{B}\pi r_L^2 = \pm q\dot{B}\pi\frac{v_\perp^2}{\omega_c}\frac{m}{\pm qB} = \frac{1}{B}\frac{1}{2}mv_\perp^2\underbrace{\frac{2\pi\dot{B}}{\omega_c}}_{\delta B} = \mu\delta B \tag{2.80}$$

δB corresponds to the change in B per revolution. The change in the potential energy of a magnetic moment in the magnetic field μB corresponds to a change in the kinetic energy perpendicular to the magnetic field $\frac{1}{2}mv_\perp^2$:

$$\delta(\mu B) = \delta\left(\frac{1}{2}mv_\perp^2\right) \tag{2.81}$$

The left side can be expanded to

$$B\delta\mu + \mu\delta B = \delta\left(\frac{1}{2}mv_\perp^2\right) \tag{2.82}$$

Comparing equations 2.79 and 2.82 yields that

$$\boxed{\delta\mu = 0} \tag{2.83}$$

must hold. This also applies to a *slowly varying* B field. The invariance of the magnetic moment can be exploited to heat a plasma. If an alternating field is applied to a coil, a periodic variation of the magnetic field is obtained. Thus, $v_\perp$ also oscillates. The net energy gain would be zero, however, since the gyration motion always reverses. If, however, collisions occur, the increase in $v_\perp$ can also be transferred to $v_\parallel$. If the particle then moves parallel to the magnetic field, it no longer feels the Lorentz force and can therefore no longer be decelerated. Thus, on average, the energy of the particles increases, since energy can flow into the parallel component, but it is not removed again by the oscillating magnetic field alone. The increase in energy in a plasma by oscillating magnetic fields is referred to as **magnetic pumping** .

Second Adiabatic Invariant

The second adiabatic invariant refers to the pendulum motion between the turning points in a magnetic mirror arrangement, as illustrated in Fig. 2.24.

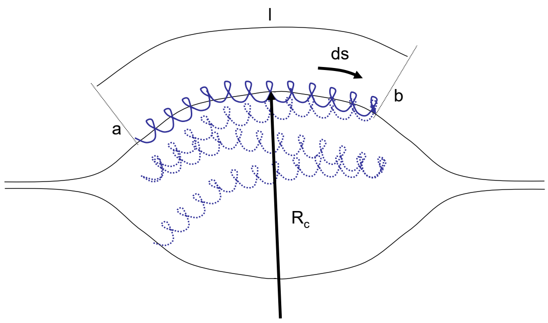

Figure 2.24: 2nd adiabatic invariant as pendulum motion between two turning points. The third adiabatic invariant corresponds to a slow drift of this pendulum motion around the circumference of the mirror machine.

The conserved quantity is given by the following path integral

$$J = \oint mv_\parallel ds \tag{2.84}$$

If we take the length of the path between the turning points to be l, the conserved quantity is given by

$$J = 2m\langle v_\parallel \rangle l \tag{2.85}$$

This raises the question of how the velocity $v_\parallel$ changes on the path. Initially, we start from the conservation of energy:

$$\frac{1}{2}mv_\parallel^2 + \frac{1}{2}mv_\perp^2 = \text{const.} \tag{2.86}$$

Taking the time derivative gives

$$mv_\parallel \frac{\partial v_\parallel}{\partial t} + \frac{d}{dt}(\mu B) = 0 \tag{2.87}$$

$$m\frac{\partial s}{\partial t}\frac{\partial v_\parallel}{\partial t} = -\frac{d}{dt}(\mu B) \tag{2.88}$$

Swapping the derivatives gives

$$m\frac{\partial v_\parallel}{\partial t} = -\frac{d}{ds}(\mu B) = -\frac{d}{ds}V \tag{2.89}$$

with V the potential energy. The energy balance gives:

$$\frac{1}{2}m\left(\frac{ds}{dt}\right)^2 + V(s) = \mu B_m \equiv W \tag{2.90}$$

with W the total energy and B_m the magnetic field at the turning point. The conserved quantity gives:

$$J = \oint m \underbrace{\frac{ds}{dt}}_{v\parallel} ds = \oint [2m(W-V)]^{1/2} ds = \oint [2m(\mu B_m - \mu B)]^{1/2} ds \tag{2.91}$$

Since μ is a conserved quantity of the motion according to the first adiabatic invariant, we must require that the expression:

$$\oint [B_m - B]^{1/2} ds \tag{2.92}$$

remains invariant. This applies if the B field changes *more slowly* over time than the pendulum motion of the charged particle between the turning points. With

$$v_{\parallel} = \left[\frac{2}{m}(\mu B_m - \mu B)\right]^{1/2} \tag{2.93}$$

The second adiabatic invariant must hold

$$\boxed{\oint v_{\parallel} ds = \text{invariant}} \tag{2.94}$$

However, if one considers the interaction of charged particles with time-varying magnetic fields, the velocity can change. A classic example is the so-called **Fermi acceleration** . Time-varying magnetic fields are always associated with an electrostatic field ($\nabla \times \vec{E} = -\dot{\vec{B}}$) in which charge carriers can be accelerated. This is an essential mechanism for describing high-energy cosmic radiation. Here, particles of the solar wind are accelerated when passing through the shock front ($\dot{B} \gg$) of the Earth's magnetic field in the heliosphere (see Fig. 2.25)

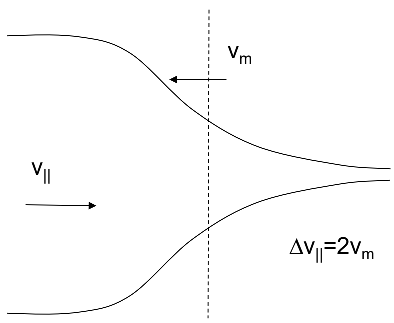

Figure 2.25: Fermi Acceleration

Another possibility for deriving Fermi acceleration is to initially write the second adiabatic invariant as

$$J = \oint v_{\parallel} ds = \langle v_{\parallel} \rangle 2l \tag{2.95}$$

with l the distance between the two turning points. If the magnetic field in a mirror machine is now increased, the turning points move closer together, i.e., the distance l decreases. Since the second adiabatic invariant holds, the parallel velocity $\langle v_{\parallel} \rangle$ must increase to the same extent. This is also Fermi acceleration.

Third Adiabatic Invariant

Finally, there is a third pendulum motion in a mirror arrangement. Here, the entire particle path rotates around the axis (see Fig. 2.24), since the curvature drift is superimposed on the pendulum motion. The conserved quantity here is the magnetic flux:

$$\boxed{\Phi = \int \vec{B} d\vec{S}} \tag{2.96}$$

In summary, it can be said that, depending on the collision frequency, the three adiabatic invariants are more or less conserved quantities. The fastest motion is the gyration, so the magnetic moment is usually a conserved quantity. The second adiabatic invariant, the pendulum motion between the turning points, is usually fulfilled at lower pressure, since the period is longer and the probability of suffering a collision with a neutral particle is greater. The third adiabatic invariant is rarely fulfilled, since the rotation of the pendulum motion around the axis of the mirror arrangement has the longest period. In summary, the validity of the individual adiabatic invariants can be seen in the following order

$$\mu > \int v_{\parallel} > \int \vec{B} d\vec{S} \tag{2.97}$$

An example of the realization of a magnetic bottle on a large scale is shown in Fig. 2.26. Particles that fall into the loss cone are guided to the end by special coils and reflected by electric fields.

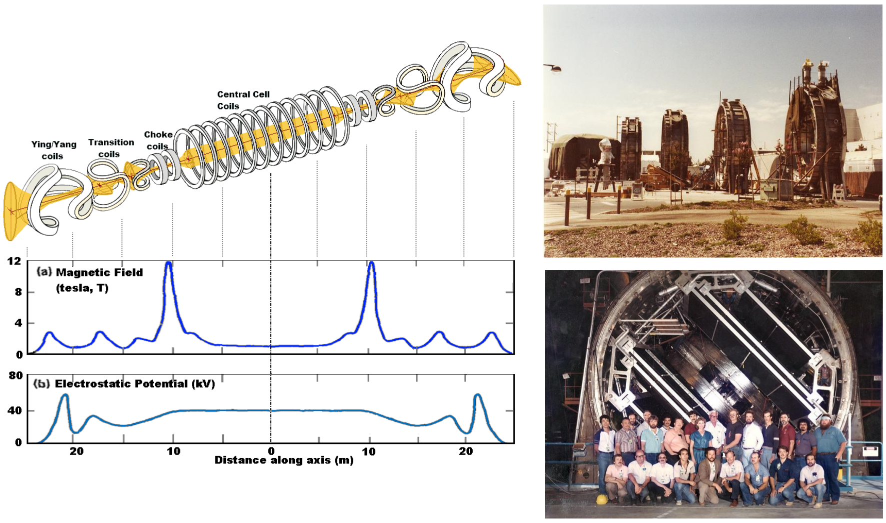

Figure 2.26: Mirror machine as used for nuclear fusion research. At the end of the mirror machine, special Ying-Yang coils and electric fields are mounted to reflect the particles that have fallen into the loss cone back into the magnetic bottle.

2.2 Multi-Particle Picture

In the single-particle picture, the drifts of charged particles in a given field configuration can be very successfully described. Any multi-particle effects remain unconsidered. Processes such as the formation of pressure in the plasma and the influence of collisions on transport can only be described in a multi-particle picture.
A subtle difference is the fact that the single-particle picture is based on the Lorentz force and always solves an equation for a trajectory. That is, the consideration always follows the particle and is *not stationary*. A much more practical description would be a stationary coordinate system with individual volume elements into which the particles can enter and exit. Exactly this is the "Eulerian description".

2.2.1 Hierarchy of Equations in Plasma Physics

In plasma physics, a hierarchy of equations can be established. This begins with a function f that completely describes N particles in the phase space of position and velocity.

$$f(\vec{x}_i, \vec{v}_i) \qquad i = 1..N \tag{2.98}$$

This problem has 6N dimensions and is simply the superposition of the solution of the equation of motion of N particles. This high dimensionality can be greatly reduced by defining a new function f that only represents the probability of finding a particle in an interval in the position and velocity space. This **distribution function** in the phase space has only 6 dimensions:

$$f(\vec{x}, \vec{v}) \tag{2.99}$$

Alternatively to the formulation as the probability of finding a particle, one can also take the number of particles in the phase space element $d\vec{x}d\vec{v}$. Both formulations, or normalization conditions for f, are equivalent. The problem can be further reduced by marginalizing the information about the velocity via

$$\int f(\vec{x}, \vec{v}) d^3v = n(\vec{x}) \tag{2.100}$$

and only being interested in the spatially resolved density $n(\vec{x})$ of the plasma. This description finally has only 3 dimensions. The latter corresponds to the fluid picture, where initially each particle species corresponds to a fluid. A further simplification exists only in fully ionized plasmas where the symmetry of the equations is exploited and 2-fluid equations (electrons and ions) are reduced to 1-fluid equations (MHD).
In addition to the fluid equations, the **Maxwell equations** naturally apply (*ho*...charge density):

$$\mathbf{div}\vec{E} = \frac{1}{\epsilon_0}\rho \tag{2.101}$$

$$\mathbf{div}\vec{B} = 0 \tag{2.102}$$

$$\mathbf{rot}\vec{E} = -\dot{\vec{B}} \tag{2.103}$$

$$\mathbf{rot}\vec{B} = \mu_0\vec{j} + \mu_0\epsilon_0\dot{\vec{E}} \tag{2.104}$$

and the **equation of state** of the plasma as an ideal gas:

$$p = nk_BT \tag{2.105}$$

For the state change, it is decisive in what form it takes place. In general, it is described by the **adiabatic equation** :

$$\boxed{\frac{\nabla p}{p} = \gamma \frac{\nabla n}{n}} \tag{2.106}$$

with

$$\gamma = \frac{C_p}{C_v} \tag{2.107}$$

For the ideal gas, we have

$$\gamma = \frac{2+N}{N} \tag{2.108}$$

In the case of adiabatic state changes, γ applies as described. In the case of isothermal state changes, $\gamma = 1$ applies. The latter is the case for the description of electrons, since the temperature equalization usually takes place quickly and thus isothermal conditions can be assumed.

2.2.2 Distribution Function

The distribution function in 6N dimensions (plus 1 dimension time) describes the plasma in the phase space of position and velocity (Fig. 2.27). A prominent example is the Maxwell velocity distribution , which is established when all particles can balance their velocity components through collisions and a distribution function of maximum entropy can be established. This is the Maxwell distribution. The distribution in the velocity space is:

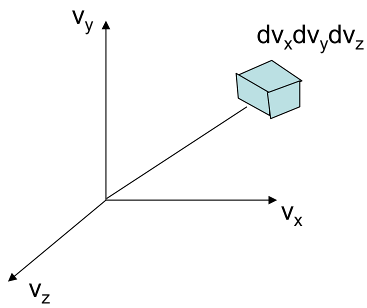

Figure 2.27: The distribution function f describes the number of particles in a phase space element $d\vec{x}d\vec{v}$. In the velocity space for a given position $\vec{x}$ we have a volume element $dv_xdv_ydv_z$.

$$f(\vec{v}) = \left(\frac{m}{2\pi k_B T}\right)^{3/2} e^{-\frac{1/2mv^2}{k_B T}} \tag{2.109}$$

In this notation, the distribution function $f(\vec{v})$ is normalized to one. From this distribution function, different quantities can be derived, such as the distribution function that corresponds to the probability of a certain speed magnitude.

$$f(|v|) = 4\pi v^2 \left(\frac{m}{2\pi k_B T}\right)^{3/2} e^{-\frac{1/2mv^2}{k_B T}} \tag{2.110}$$

Averaged quantities can be determined from the distribution function by integration. The average velocity of a Maxwell distribution is:

$$|\bar{v}| = \int |v| f(\vec{v}) d^3 v = \left(\frac{8 k_B T}{\pi m}\right)^{1/2} \tag{2.111}$$

The average velocity of a Maxwell distribution for a direction x is:

$$|\bar{v_x}| = \int |v_x| f(\vec{v}) d^3 v = \left(\frac{2 k_B T}{\pi m}\right)^{1/2} = \frac{1}{2}\bar{v} \tag{2.112}$$

If the normalization of the distribution function to the density of the particles $n(\vec{x})$ at a location $\vec{x}$ is used, one obtains:

$$f(\vec{v}) = n(\vec{x}) \left(\frac{m}{2\pi k_B T}\right)^{3/2} e^{-\frac{1/2mv^2}{k_B T}} \tag{2.113}$$

This formulation of the normalization condition is the one we want to use in the following.

2.2.3 Temporal Evolution of the Distribution Function

For the description of plasmas, of course, the temporal evolution of this distribution function under the influence of external fields is decisive. For this reason, we now consider the change of this distribution function in the phase space. For simplification, we consider the two-dimensional case as indicated in Fig. 2.28. A particle is at a location x, v at time t and moves to a new location x', v' at time $t + dt$. The equations that describe this are:

$$x' = x + v_x dt \tag{2.114}$$

$$v'_x = v_x + \dot{v}_x dt = v_x + \frac{F}{m} dt \tag{2.115}$$

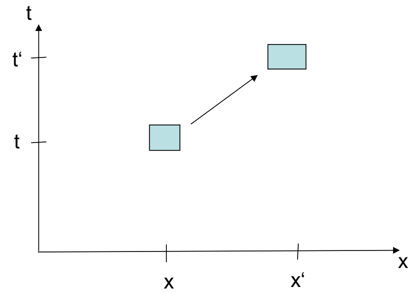

Figure 2.28: Temporal evolution of the distribution function

If no processes generate new particles, then:

$$f(x', v_x', t')dx'dv_x' = f(x, v_x, t)dxdv_x \tag{2.116}$$

How do we now transform the quantities x to x' and v_x to v_x'? The above equations can be interpreted as a transformation of the coordinate system. For this, in the two-dimensional case:

$$dx'dv_x' = |J|dxdv_x = \begin{vmatrix} \frac{\partial x'}{\partial x} & \frac{\partial x'}{\partial v_x} \\ \frac{\partial v_x'}{\partial x} & \frac{\partial v_x'}{\partial v_x} \end{vmatrix} dxdv_x \tag{2.117}$$

The Jacobian determinant J gives for this transformation

$$|J| = 1 + O(dt^2) \tag{2.118}$$

Thus, in the first order, $dxdv_x = dx'dv_x'$ must hold. Therefore, $f(x', v_x', t') = f(x, v_x, t)$. That is, the distribution function remains constant over time

$$\boxed{\frac{df}{dt} = 0} \tag{2.119}$$

This is called the **Liouville theorem** . However, this is the total derivative. When resolved into partial derivatives, one obtains:

$$\frac{df}{dt} = \frac{\partial f}{\partial t} + \frac{\partial f}{\partial \vec{x}}\frac{\partial \vec{x}}{\partial t} + \frac{\partial f}{\partial \vec{v}}\frac{\partial \vec{v}}{\partial t} = 0 \tag{2.120}$$

From this, one obtains the so-called **Vlasov equation** :

$$\boxed{\frac{df}{dt} = \frac{\partial f}{\partial t} + \vec{v}\frac{\partial f}{\partial \vec{x}} + \frac{\vec{F}}{m}\frac{\partial f}{\partial \vec{v}} = 0} \tag{2.121}$$

Considering collisions, a redistribution can take place, or new particles can be generated by ionization. This is described in the so-called **Boltzmann equation** .

$$\boxed{\frac{df}{dt} = \frac{\partial f}{\partial t} + \vec{v}\frac{\partial f}{\partial \vec{x}} + \frac{\vec{F}}{m}\frac{\partial f}{\partial \vec{v}} = \frac{\partial f}{\partial t}\Big|_{Stoesse}} \tag{2.122}$$

The term on the right side includes all processes that cause a change in the distribution function due to collision processes. In the image of the distribution function, we now have a stationary coordinate system.
Without the change in the velocity space, one can write the so-called **convective derivative** as:

$$\frac{df}{dt} = \frac{\partial f}{\partial t} + \vec{v}\nabla f \tag{2.123}$$

The left side corresponds to an observer who moves with the phase space element. The first term on the right side corresponds to an observer who considers a fixed volume element from the outside. The description in a coordinate system that moves with a fluid element is called **"Lagrangian description"** and the description with a stationary coordinate system is called **"Eulerian description"** .
Intuitively, this can be illustrated by the example of a wave in Fig. 2.26. Assuming that no new particles are generated, we have:

$$\frac{df}{dt} = 0 \tag{2.124}$$

That is, an observer who swims along with the wave does not even notice that he is sitting on a wave. If one now keeps the location fixed, an outside observer, however, sees that the number of particles at the location x_0 increases. This happens proportionally to the velocity of this wave and its density gradient.

$$\frac{\partial f}{\partial t} = -\vec{v}\nabla f \tag{2.125}$$

According to Fig. 2.29, the gradient in f is positive, while the velocity $\vec{v}$ points in the negative x direction. That is, according to Eq. 2.125, $\frac{\partial f}{\partial t}$ becomes positive at the location x_0, and the stationary observer sees an increase in the particle density at the location x_0.

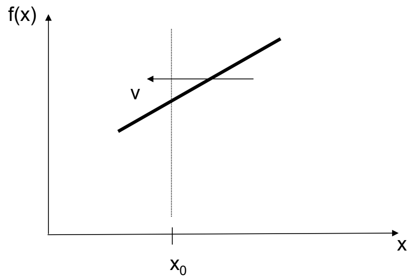

Figure 2.29: Idea of the convective derivative

2.2.4 Moments of the Boltzmann Equation, Fluid Picture

First, we consider a further simplification in the multi-particle picture by reducing the information of the distribution in the velocity space to a few moments. The nth moment of a distribution function or equation is defined as:

$$\int v^n f(v) d^3v \tag{2.126}$$

Principally, the complete information about the form of $f(v)$ in the velocity space is preserved by the specification of infinitely many moments. However, in many cases, this consideration can be broken off after the leading moments. We reduce the dimension of the problem to 3 by considering only the first three moments in the following. The temporal evolution of these moments is given by the moments of the Vlasov equation itself.

0th Moment, Particle Balance

First, we consider the 0th moment according to:

$$\int \frac{\partial f}{\partial t} d^3v + \int \vec{v} \frac{\partial f}{\partial \vec{x}} d^3v + \int \frac{\vec{F}}{m} \frac{\partial f}{\partial \vec{v}} d^3v = 0 \tag{2.127}$$

This is a *balance equation* about the number of particles, since

$$\int f(v) d^3v = n(\vec{x}) \tag{2.128}$$

applies and $\frac{df}{dt}$ corresponds to a change in the number of particles. In Eq. 2.127, the integration and the derivative with respect to the location can be interchanged. The third term yields zero as will be proven immediately. Thus, we initially obtain:

$$\frac{\partial}{\partial t}\int f d^3v + \frac{\partial}{\partial \vec{x}}\int \vec{v} f d^3v = 0 \tag{2.129}$$

This yields the continuity equation , or the **particle balance**:

$$\boxed{\frac{\partial n}{\partial t} + \nabla \cdot (n\vec{v}_s) = 0} \tag{2.130}$$

after the first moment over the velocity, the center-of-mass velocity $\vec{v}_s$ is given:

$$\int \vec{v} f d^3v = \vec{v}_s \cdot n(\vec{x}) \tag{2.131}$$

We claimed that the third term in equation 2.127 becomes zero. This is shown below. The force on charged particles is again the Lorentz force, i.e., a term proportional to $\vec{E}$ and to $\vec{v} \times \vec{B}$.

$$\int \vec{E}\frac{\partial f}{\partial \vec{v}} d^3v = \int \frac{\partial}{\partial \vec{v}}\vec{E} f d^3v = \int_S \vec{E} f d\vec{S} = 0 \tag{2.132}$$

Here, Gauss's theorem was used, which links the divergence of a field with the surface integral. This must become zero because at a surface at infinity the distribution function f must become zero to describe a finite energy content. This has the consequence that the entire integral becomes zero. Similarly, the argumentation for the second term:

$$\int \vec{v} \times \vec{B}\frac{\partial f}{\partial \vec{v}} d^3v = \int \frac{\partial}{\partial \vec{v}}(f\vec{v} \times \vec{B}) d^3v - \int f\frac{\partial}{\partial \vec{v}}(\vec{v} \times \vec{B}) d^3v \tag{2.133}$$

The first term is again zero because it can be linked to a surface integral via Gauss's theorem. The second term is also zero because the change in velocity and the velocity itself are perpendicular to each other ($\vec{v} \times \vec{B}$ always acts perpendicular to the velocity). Thus, this term also becomes zero.

1st Moment, Momentum Balance

The first moment of the distribution function is given as

$$\int v f(v) d^3v = n(\vec{x}) v_s \tag{2.134}$$

with v_s the center-of-mass velocity. If this is multiplied by the mass m of the considered particle, the first moment of the Vlasov equation becomes a balance equation for the total momentum in the fluid:

$$\int m\vec{v}\frac{\partial f}{\partial t}d^3v + \int m\vec{v}\left(\vec{v}\frac{\partial f}{\partial \vec{x}}\right)d^3v + \int m\vec{v}\left(\frac{\vec{F}}{m}\frac{\partial f}{\partial \vec{v}}\right)d^3v \tag{2.135}$$

The first term in Eq. 2.135 gives:

$$m\frac{\partial}{\partial t}\left(n\vec{v}_s\right) \tag{2.136}$$

To resolve the third term, we first use the product rule for derivatives[1]:

$$\frac{\partial}{\partial \vec{v}}f\vec{v}\vec{F} = f\vec{v}\frac{\partial}{\partial \vec{v}}\vec{F} + \vec{F}\vec{v}\frac{\partial}{\partial \vec{v}}\vec{f} + \vec{F}f\frac{\partial}{\partial \vec{v}}\vec{v} \tag{2.137}$$

The third term in Eq. 2.135 gives:

$$\int \frac{\partial}{\partial \vec{v}}f\vec{v}\vec{F}d^3v - \int f\vec{v}\frac{\partial \vec{F}}{\partial \vec{v}}d^3v - \int f\vec{F}\underbrace{\frac{\partial \vec{v}}{\partial \vec{v}}}_{=1}d^3v = -n\vec{F} \tag{2.138}$$

The first term in Eq. 2.138 gives zero according to the argumentation via Gauss's theorem. The second term in Eq. 2.138 gives zero because $\vec{v}$ always stands perpendicular to $\frac{\partial}{\partial v}$, due to $\vec{F} = \vec{v}\times\vec{B}$. The second term in Eq. 2.135 gives:

$$m\int v^2\frac{\partial}{\partial \vec{x}}fd^3v = m\frac{\partial}{\partial \vec{x}}\int v^2 fd^3v \tag{2.139}$$

For further consideration, the velocity component is divided into a center-of-mass component and a thermal component, as illustrated in Fig. 2.30:

$$v = v_s + v_t \tag{2.140}$$

These differ in the results of their averaging:

$$\int vfdv = nv_s \tag{2.141}$$

Thus,

[1]This is only presented very briefly here. For the explicit derivation, the components of the vectors must be distinguished exactly according to the individual directions x, y, and z.

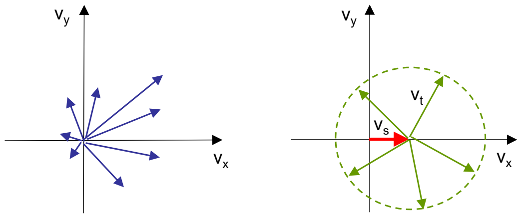

Figure 2.30: The distribution in the velocity space is divided into a component for the center of mass and a thermal component for the isotropic velocity.

$$\int v_t f dv = 0 \tag{2.142}$$

With this definition, we have

$$\int v^2 f d\vec{v} = n\langle v^2\rangle = n\langle v_s^2 + 2v_s v_t + v_t^2\rangle = n\langle v_s^2\rangle + n\langle v_t^2\rangle \tag{2.143}$$

Thus, from

$$m\frac{\partial}{\partial\vec{x}}\int nfv^2 d\vec{v} = m\frac{\partial}{\partial\vec{x}}nv_s^2 + m\frac{\partial}{\partial\vec{x}}nv_t^2 \tag{2.144}$$

At this point, the pressure is introduced as a macroscopic quantity to describe the multi-particle character of the plasma. In its microscopic definition , the pressure is given as:

$$p = \frac{1}{3}mn\langle v_t^2\rangle = mn\langle v_{tx}^2\rangle \tag{2.145}$$

with $\langle v_t^2\rangle = \langle v_{tx}^2\rangle + \langle v_{ty}^2\rangle + \langle v_{tz}^2\rangle$, or in the case of isotropic conditions $\langle v_t^2\rangle = 3\langle v_{tx}^2\rangle$. In general, the pressure p is a tensor since, according to the definition of averaging, it can contain not only terms of the form $\langle v_{tx}v_{tx}\rangle$ but also mixed terms such as $\langle v_{tx}v_{ty}\rangle$. This corresponds to the simple isotropic pressure or shear stresses. In the following, we want to consider only the simple isotropic case. The connection between pressure and thermal velocity can be understood intuitively: the pressure in thermodynamics is given for the ideal gas by $p = nk_BT$, i.e., it is hidden in the isotropic movement of the gas particles, and is thus linked to v_t. If such a particle hits a wall, it transfers its momentum there. The transfer of momentum from n particles to a wall per time interval corresponds to a force F on this surface. In this interpretation, the pressure is

$$p = \underbrace{mv_{tx}}_{Impuls} \underbrace{nv_{tx}}_{Teilchen/Zeit} \tag{2.146}$$

the product of particle momentum mv_t and the impact rate of n particles nv_t. Thus, one finally obtains:

$$m\frac{\partial}{\partial \vec{x}} \int nfv^2 d^3v = m\frac{\partial}{\partial \vec{x}} \left(nv_s^2\right) + \frac{\partial}{\partial \vec{x}} p \tag{2.147}$$

The first term is resolved to:

$$\frac{\partial}{\partial \vec{x}} nv_s^2 = v_s \frac{\partial}{\partial \vec{x}} nv_s + nv_s \frac{\partial}{\partial \vec{x}} v_s \tag{2.148}$$

After substitution, we finally obtain:

$$\underbrace{m\frac{\partial}{\partial t} nv_s}_{mn\frac{\partial v_s}{\partial t} + mv_s\frac{\partial n}{\partial t}} + mv_s \underbrace{\frac{\partial}{\partial \vec{x}} nv_s}_{-\frac{\partial n}{\partial t}} + mnv_s \frac{\partial}{\partial \vec{x}} v_s + \frac{\partial}{\partial \vec{x}} p - n\vec{F} = 0 \tag{2.149}$$

The first term is differentiated according to the product rule, and the term $\frac{\partial}{\partial \vec{x}} nv_s$ corresponds to $-\frac{\partial n}{\partial t}$ from the particle balance. Thus, two terms cancel out, and one obtains as the final result the **momentum balance**:

$$\boxed{mn\left[\frac{\partial \vec{v}_s}{\partial t} + \vec{v}_s \nabla \vec{v}_s\right] = n\vec{F} - \nabla p = nq(\vec{E} + \vec{v}_s \times \vec{B}) - \nabla p} \tag{2.150}$$

In a more general formulation, the pressure is a tensor that can also contain shear forces, which can arise from the off-diagonal elements in $\langle v_t v_t \rangle$ (terms $\nabla v_x v_y$ etc).
From this momentum balance, the Navier-Stokes equation for fluids with friction can also be derived. In a fluid with a certain viscosity γ, shear forces arise when adjacent fluid elements move past each other at different speeds. This shear force is $\propto n\gamma\nabla^2 v_s$. Here, not the first derivative but the second derivative of the velocity from the location is decisive, since in the case of a linear dependence, the retarding and accelerating shear force would cancel each other out at the two sides of the fluid element. With this consideration, one obtains the Navier-Stokes equation:

$$mn\left[\frac{\partial \vec{v}_s}{\partial t} + \vec{v}_s \nabla \vec{v}_s\right] = n\vec{F} - \nabla p + n\gamma\nabla^2 \vec{v}_s \tag{2.151}$$

2nd Moment, Energy Balance

The second moment of the Vlasov equation corresponds to the energy balance in the collision-free case. For this purpose, the second moment of the Vlasov equation is multiplied by $\frac{1}{2}m$ and integrated over the velocity space. One obtains

$$\int \frac{1}{2}mv^2\frac{\partial f}{\partial t}d^3v + \int \frac{1}{2}mv^2\vec{v}\frac{\partial f}{\partial \vec{x}}d\vec{v} + \int \frac{1}{2}mv^2\frac{\vec{F}}{m}\frac{\partial f}{\partial \vec{v}}d^3v = 0 \tag{2.152}$$

Here, too, the derivative and integration can be interchanged for the components of location and time. From the first term, one obtains the change in the total energy with time:

$$\int \frac{1}{2}mv^2\frac{\partial f}{\partial t}d^3v = \frac{\partial}{\partial t}\int \frac{1}{2}mv^2 f d^3v = \frac{\partial}{\partial t}n\langle\epsilon\rangle \tag{2.153}$$

From the last term, the change in energy due to an external force according to:

$$\begin{aligned}\int \frac{1}{2}mv^2\frac{\vec{F}}{m}\frac{\partial f}{\partial \vec{v}}d\vec{v} &= \int \frac{\partial}{\partial \vec{v}}\frac{1}{2}mv^2\frac{\vec{F}}{m}fd^3v - \int \frac{1}{2}m2v\frac{F}{m}fd^3v \\ &= -n\vec{F}\vec{v}_s \end{aligned}\tag{2.154}$$

This term arises analogously to above, since now $\frac{1}{2}\nabla_v v^2 = v$. From the second term in Eq. 2.152, terms according to:

$$\langle v^3\rangle = \langle v^2\rangle v_s + \langle v^2 v_t\rangle = \langle v^2\rangle v_s + \langle v_s^2 v_t\rangle + \langle 2v_s v_t^2\rangle + \langle v_t^3\rangle \tag{2.155}$$

The first term gives an expression according to the transport of the average energy $\epsilon = \frac{1}{2}mv^2$ by convection

$$\nabla n\langle\epsilon\rangle v_s \tag{2.156}$$

The second term in Eq. 2.155 is 0, and from the third term, an expression according to energy gain or dissipation by compression or expansion, respectively, is obtained:

$$p\nabla v_s \tag{2.157}$$

The last term in Eq. 2.155 finally corresponds to the transport of energy by heat conduction :

$$\nabla q \qquad \text{with} \qquad q = -\kappa\nabla T \tag{2.158}$$

with κ the thermal conductivity. If all this is inserted, one finally obtains the **energy balance**:

$$\boxed{\frac{\partial}{\partial t}n\langle\epsilon\rangle + \underbrace{\nabla n\langle\epsilon\rangle v_s}_{Convection} + \underbrace{p\nabla v_s}_{Compression/Expansion} + \underbrace{\nabla q}_{Heatconduction} - \underbrace{n v_s \vec{F}}_{e.g.\ ohmic\ heating} = 0} \tag{2.159}$$

From this equation, simple cases can be constructed. Thus, the change in energy due to expansion or compression corresponds to a term:

$$\frac{\partial}{\partial t}n\langle\epsilon\rangle = -p\nabla v_s \tag{2.160}$$

or an energy gain due to ohmic heating in an external electric field:

$$\frac{\partial}{\partial t}n\langle\epsilon\rangle = n v_s \vec{F} = \vec{j}\vec{E} \tag{2.161}$$

In the comparison of average energy, pressure, and center-of-mass velocity, there are different simplifications in the literature. In low-pressure plasmas, the thermal energy is often much higher than the energy in the center-of-mass velocity. Thus, one can set

$$\langle\epsilon\rangle = \frac{3}{2}k_B T = \frac{3}{2}\frac{p}{n} \tag{2.162}$$

2.2.5 Drifts in the Fluid Picture

Drift Parallel to the B Field

After the introduction of the fluid picture, we are now able to derive the Debye length. The momentum balance of the electrons is given by:

$$mn\left[\frac{\partial v_s}{\partial t} + v_s\nabla v_s\right] = n\vec{F} - \nabla p = nq\vec{E} - \nabla p \tag{2.163}$$

In equilibrium, under the assumption of a stationary fluid, we have

$$nq\vec{E} = \nabla p \tag{2.164}$$

With $q = -e$ and $\vec{E} = -\nabla\Phi$, one obtains here under the assumption of an isothermal state change for the electrons:

$$en\nabla\Phi = \nabla p = \nabla n k_B T \tag{2.165}$$

or

$$e\nabla\Phi = \frac{1}{n}\nabla n k_B T = \nabla \ln n k_B T \tag{2.166}$$

Integrating this equation gives

$$e\Phi = k_B T_e \ln n + c \tag{2.167}$$

with the integration constant c, which corresponds to the normalization of the plasma density n_0. One thus obtains the solution for n as:

$$\boxed{n = n_0 e^{\frac{e\Phi}{k_B T_e}}} \tag{2.168}$$

This is referred to as the **Boltzmann relation** . It corresponds to the equilibrium between the thermal energy of the electrons and the electric potential that arises when the electrons are shifted relative to the ions. In high-density plasmas, the Pauli exclusion principle is added, which limits the density of the electrons at a location.
The shielding of a disturbance of the quasi-neutrality is again derived from the Poisson equation:

$$\epsilon_0 \nabla^2 \Phi = -e(n_i - n_e) \tag{2.169}$$

$$\epsilon_0 \nabla^2 \Phi = -e\left(n_0 - n_0 e^{\frac{e\Phi}{k_B T_e}}\right) \tag{2.170}$$

For the case where the thermal energy is much greater than the potential disturbance, the exponential function can be developed according to:

$$\epsilon_0 \nabla^2 \Phi = e n_0 \left[e^{\frac{e\Phi}{k_B T_e}} - 1\right] = e n_0 \left[1 + \frac{e\Phi}{k_B T_e} + ... - 1\right] = e n_0 \frac{e\Phi}{k_B T_e} \tag{2.171}$$

This equation has the solution

$$\Phi = \Phi_0 e^{-\frac{|x|}{\lambda_D}} \tag{2.172}$$

with the **Debye length** :

$$\boxed{\lambda_D = \left(\frac{\epsilon_0 k_B T_e}{n e^2}\right)^{1/2}} \tag{2.173}$$

Drift Perpendicular to the B Field, Diamagnetic Drift, Plasma β

By introducing the fluid picture, we now have an additional term ∇p in the momentum balance, the pressure gradient. For particle drifts perpendicular to the magnetic field, the following picture emerges. Initially, we again have:

$$mn\left[\frac{\partial v_s}{\partial t} + v_s \nabla v_s\right] = n\vec{F} - \nabla p = nq(\vec{E} + \vec{v} \times \vec{B}) - \nabla p \tag{2.174}$$

We initially neglect the explicit time derivative, since we are only interested in the drift motion. The second term on the left side is also neglected because the drift motion is perpendicular to the velocity gradient, as will be shown. As the starting equation, we thus have

$$0 = nq\left(\vec{E} + \vec{v} \times \vec{B}\right) - \nabla p \tag{2.175}$$

We multiply from the right by $\times\vec{B}$ and obtain

$$0 = nq\left(\vec{E} \times \vec{B} + \vec{v} \times \vec{B} \times \vec{B}\right) - \nabla p \times \vec{B} \tag{2.176}$$

$$0 = nq\left(\vec{E} \times \vec{B} + \vec{B}(\vec{v}_\perp \vec{B}) - \vec{v}_\perp B^2\right) - \nabla p \times \vec{B} \tag{2.177}$$

The second term cancels out because $v_\perp$ always stands perpendicular to $\vec{B}$. Finally, one obtains the drift velocity as

$$v_\perp = \frac{\vec{E} \times \vec{B}}{B^2} - \frac{\nabla p \times \vec{B}}{qnB^2} \tag{2.178}$$

The first term is the known E $\times$ B drift and the second term is the **diamagnetic drift** . It leads to the fact that, given a pressure gradient, the electrons and the ions are driven in different directions perpendicular to the magnetic field. Thus, a diamagnetic current is created that shields the external magnetic field. A cylindrical plasma column in an external magnetic field begins to rotate as a whole.

This drift velocity changes with the distance from the center of the plasma column, i.e., $\nabla\vec{v}$ is perpendicular to $\vec{v}$ itself. This justifies the assumption made at the beginning that the term $\vec{v}\nabla\vec{v}$ is zero.

We now consider the configuration of a plasma column again. The following must apply:

$$\nabla p = qn(\vec{v} \times \vec{B}) = \vec{j} \times \vec{B} \tag{2.179}$$

In addition, Ampere's law applies

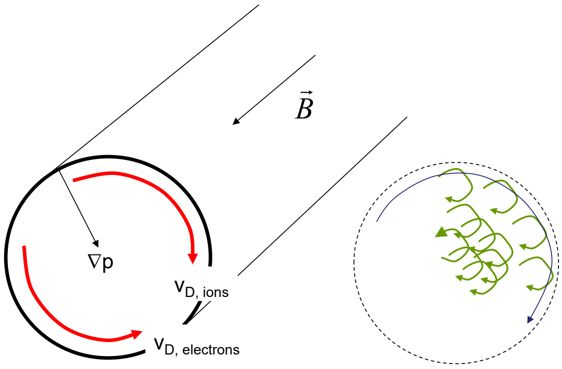

Figure 2.31: Through a gradient in the plasma pressure, a diamagnetic drift is created, which corresponds to a shielding current in a plasma column.

$$\nabla \times \vec{B} = \mu_0 \vec{j} \tag{2.180}$$

Multiplying Eq. 2.179 by $\times \vec{B}$ now directly gives the diamagnetic current:

$$\vec{j}_\perp = \frac{\vec{B} \times \nabla p}{B^2} \tag{2.181}$$

Substituting Eq. 2.180 into 2.179 gives:

$$\nabla p = \frac{1}{\mu_0}(\nabla \times \vec{B}) \times \vec{B} = \frac{1}{\mu_0}\left[\vec{B}\nabla\vec{B} - \frac{1}{2}\nabla B^2\right] \tag{2.182}$$

From this it follows that

$$\nabla\left(p + \frac{B^2}{2\mu_0}\right) = \frac{1}{\mu_0}\vec{B}\nabla\vec{B} \simeq 0 \tag{2.183}$$

Since the gradient along the magnetic field is usually very small, the right side can be set to nearly zero. Thus, the following must apply:

$$p + \frac{B^2}{2\mu_0} = \text{const.} \tag{2.184}$$

The first term is the plasma pressure and the second term corresponds to the magnetic field pressure. The sum of both remains constant over the cross-section of a plasma column. This is also expressed by the so-called **plasma** β :

$$\boxed{\beta = \frac{p(0)}{\frac{B(R)^2}{2\mu_0}}} \tag{2.185}$$

By definition, the pressure in the center of the plasma column is taken and the magnetic field at the edge of the plasma. A high beta thus means that the magnetic field in the interior becomes very small, while in the case of a small β value, the magnetic field can well penetrate the plasma column.
The currents in a cylindrical plasma can be measured by different arrangements. In the simplest case, the magnetic field is first determined by Hall detectors. From the magnetic field, the generating currents can then be calculated. Alternatively, however, the induced voltages in a coil can also be measured if the current in the plasma varies (e.g., $\nabla \times \vec{E} = -\dot{\vec{B}}$). This creates a time-varying magnetic field. Depending on the arrangement of the coil, different contributions to the plasma current can be measured 2.32:

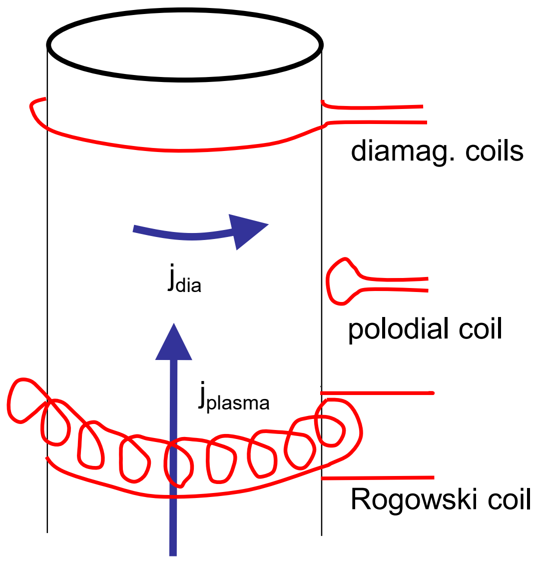

Figure 2.32: Measurement of plasma currents using coils.

- **diamagnetic coil**

  In a diamagnetic coil, a simple loop is placed around the plasma. When the plasma is turned on, a pressure gradient from the inside to the outside is created, which drives a diamagnetic current. This generates a time-varying magnetic flux through the cross-sectional area of the coil and thus a voltage at the ends. The change in the plasma current along the cylinder axis does not generate a change in the magnetic flux in this coil. Thus, here *only* the diamagnetic component of the plasma current is measured.

- **poloidal field coil**

  In a poloidal field coil, mainly the component of the plasma current is measured that flows along the cylinder axis. Only this generates a time-varying magnetic field around the circumference of the plasma column (cf. current-carrying conductor). However, the signal still contains components of the diamagnetic current, since the current density distribution in the entire column partially contributes to the time-varying flux in the poloidal field coil.

- **Rogowski coil**

  With a Rogowski coil , it is finally possible to measure exclusively the component of the plasma current that flows along the cylinder axis. In this arrangement, poloidal field coils are placed in series around the circumference and thus measure the plasma current. The lead is, however, once again returned around the circumference so that no closed conductor loop around the circumference is created.

2.2.6 Comparison Fluid Picture - Single-Particle Picture

When comparing the single-particle and fluid pictures, one notices that some drifts occur in only one description. To combine both pictures, one considers an infinitesimal fluid element and examines the particle trajectories that pass through this fluid element. Averaging over the particle velocities of these individual particles then corresponds to a center-of-mass velocity of the fluid:

- **diamagnetic drift**

  The diamagnetic drift cannot exist in the single-particle picture, since the interaction of many particles is not considered. In the fluid picture, there is a drift motion because particles pass a certain point more frequently in one direction than in the other. A prerequisite is a density gradient in the plasma, as illustrated in Fig. 2.33.

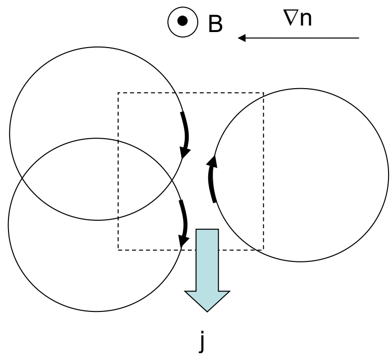

Figure 2.33: Comparison single-particle-fluid picture: diamagnetic drift

- **∇B drift**

  The ∇B drift exists in the single-particle picture, but not in the fluid picture. Particles enter a certain volume element in arbitrary directions. Since the direction of the particle motion is changed but not its velocity by a varying magnetic field, the center-of-mass velocity of the plasma remains zero, as illustrated in Fig. 2.34.

- **$\vec{E} \times \vec{B}$-drift**

  In the case of the $\vec{E} \times \vec{B}$-drift, however, the electric field changes the velocity of the particles. This changes the Larmor radius and the drift of the single-particle picture arises. In the fluid picture, this is retained because when summing the particle velocities in a small volume element, the individual contributions do not cancel each other out.

The comparison of the further drifts, such as polarization drift, drift in non-uniform electric fields, etc., is more complex because the particle density used in the fluid picture is not identical to the density of the guiding centers, which forms the basis of the single-particle picture.
The single-particle picture is a good description of plasmas when the transport *along* the magnetic field lines is considered. Here, the mean free paths are large and many gyration radii are traversed without collisions. For the transport of plasma perpendicular to the field lines, however, the fluid picture is better suited because here the collisions of the particles with each other are important, which lead to an exchange of particles between adjacent field lines.

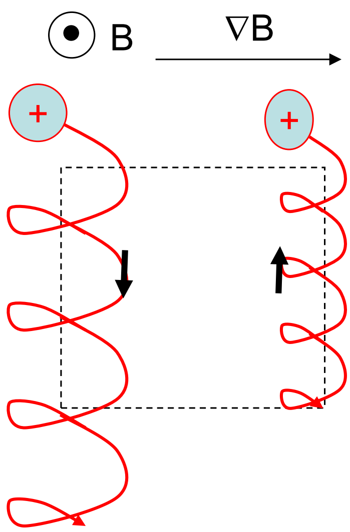

Figure 2.34: Comparison single-particle-fluid picture: ∇B drift

Chapter 3

Collisions

For the description of transport phenomena in plasmas, it is necessary to treat collision processes. Every diffusion process is driven by gradients in density and temperature, where collision processes between the particles or with the background gas limit this particle motion. This is expressed by mean free paths or collision frequencies. To derive these quantities, a microscopic picture of a collision process is needed, which is described by a cross-section according to the type of interaction.

Important processes in plasmas are scattering processes of the charged particles among each other as well as ionization processes. By quantitatively describing the generation rate of ions and their annihilation, the degree of ionization of a plasma can be determined.

3.1 Definitions

The transport of particles in a plasma is limited by collisions with other components of this plasma. If one considers a directed particle flux Γ, it is reduced over a distance dx according to:

$$d\Gamma = -\sigma_{sc} n_g \Gamma dx \tag{3.1}$$

Here, σ_{sc} denotes the so-called **cross-section** for scattering on a collision partner with density n_g. This results in the differential equation:

$$\frac{d\Gamma}{dx} = -\sigma_{sc} n_g \Gamma \tag{3.2}$$

with the following solution:

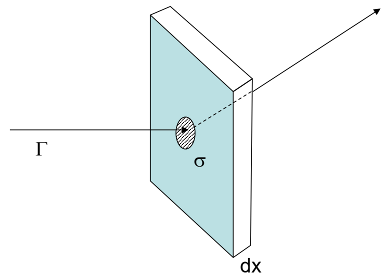

Figure 3.1: Collision Interaction

$$\Gamma = \Gamma_0 e^{-\frac{x}{\lambda}} \tag{3.3}$$

The length λ is referred to as the **mean free path** :

$$\boxed{\lambda = \frac{1}{\sigma_{sc} n_g}} \tag{3.4}$$

Accordingly, one can also define other quantities. The average **collision time** τ is:

$$\boxed{\tau = \frac{\lambda}{v}} \tag{3.5}$$

Or the **collision frequency** ν is:

$$\boxed{\nu = \tau^{-1} = n_g \langle \sigma_{sc} v \rangle} \tag{3.6}$$

The collisions of the particles with another collision partner are taken into account in the momentum balance as follows:

$$mn \left[\frac{\partial \vec{v}}{\partial t} + \vec{v} \nabla \vec{v} \right] = n\vec{F} - \nabla p - \underbrace{m\vec{v}}_{Impulseloss} \underbrace{n\nu_m}_{Frequency of collisions} \tag{3.7}$$

The index m in the collision frequency ν_m takes into account the collision frequency for the loss of momentum, not the entire particle (see below). The continuity equation is modified by particle generation and particle recombination. For both processes, collision frequencies can also be specified.

$$\frac{\partial n}{\partial t} + \nabla \vec{v} n = n\nu_{Ionization} - n\nu_{Recombination} \tag{3.8}$$

In general, $\nu_m \gg \nu_{ionization}$

3.2 Differential Cross-Section

The scattering of two particles from each other leads to an energy and momentum transfer, where the incident projectile is scattered at an angle Θ. The scattering angle itself changes in a characteristic manner with the **impact parameter** b, as illustrated in Fig. 3.2. As the impact parameter b becomes smaller, the scattering angle generally increases.
Such a scattering process is described by a **cross-section**. For the description of a scattering process with a given impact parameter, the differential cross-section is used as the portion of the total cross-section that leads to scattering into a certain solid angle element $d\Omega$. Particle conservation requires that the flux through an area $d\sigma$, which is given by a ring of width db and radius b:

$$d\sigma = 2\pi b db \tag{3.9}$$

is identical to the flux through an area dA, which is given by a ring with an opening angle $d\Theta$ on a spherical surface with radius R:

$$dA = R\sin\Theta 2\pi R d\Theta \tag{3.10}$$

This area dA is converted into a solid angle $d\Omega$ via:

$$d\Omega = dA\frac{1}{R^2} \tag{3.11}$$

Thus, the differential cross-section is:

$$\boxed{\frac{d\sigma}{d\Omega} = \frac{b}{\sin\Theta}\frac{db}{d\Theta}} \tag{3.12}$$

That is, for the determination of the differential cross-section, we need a relationship between the so-called **impact parameter** b and the angle at which the particle is scattered.
The total cross-section is finally obtained by integrating over the entire solid angle:

$$\sigma_{sc} = 2\pi\int_0^\pi \frac{d\sigma}{d\Omega}\sin\Theta d\Theta \tag{3.13}$$

For transport, however, it is not the loss of the particle that is interesting, or the probability of whether a scattering process has occurred, but to what extent this scattering process has reduced the momentum. The corresponding cross-section for momentum transfer must be corrected by the factor:

$$dp = p - p\cos\Theta \tag{3.14}$$

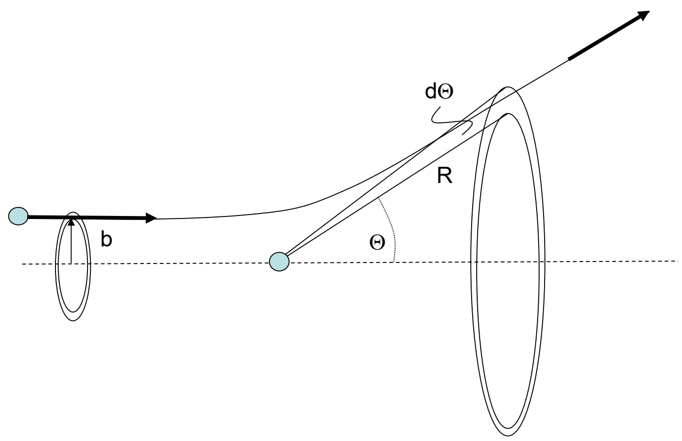

Figure 3.2: The differential cross-section links the scattering for a given impact parameter b with the solid angle element $d\Omega$ into which it is scattered.

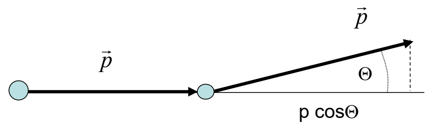

Figure 3.3: In the cross-section for momentum loss, the change in the direction of the particle is decisive.

$$\frac{dp}{p} = 1 - \cos\Theta \tag{3.15}$$

Thus, we obtain:

$$\sigma_m = 2\pi \int_0^\pi (1 - \cos\Theta) \frac{d\sigma}{d\Omega} \sin\Theta d\Theta \tag{3.16}$$

That is, if the particle is hardly deflected, i.e., $\Theta \sim 0$, $\cos\Theta$ becomes one and the cross-section σ_m vanishes.

3.3 The Scattering Problem

So far, the type of scattering process has not been specified. The goal in solving the scattering problem is to determine the dependence between the impact parameter b and the scattering angle Θ. For this purpose, one practically starts from the **center-of-mass system** . The center-of-mass velocity is:

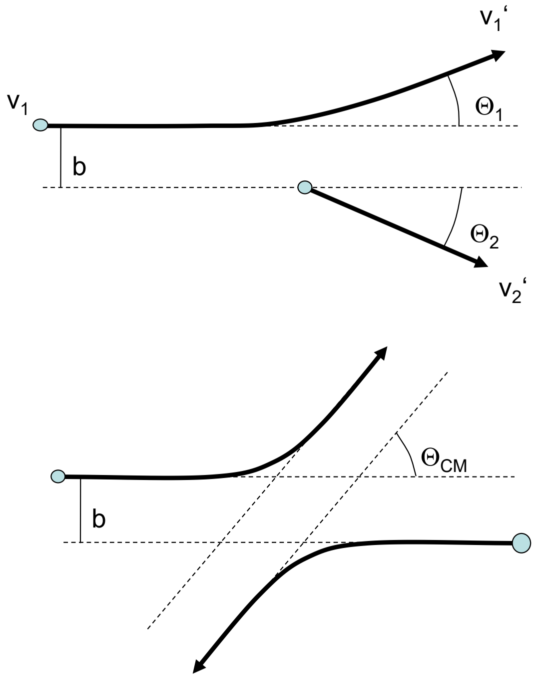

Figure 3.4: Laboratory System - Center-of-Mass System

$$v_{cm} = \frac{m_1 v_1 + m_2 v_2}{m_1 + m_2} \tag{3.17}$$

The reduced mass m_{cm} is:

$$m_{cm} = \frac{m_1 m_2}{m_1 + m_2} \tag{3.18}$$

The relative velocity before the collision:

$$v_R = v_1 - v_2 \tag{3.19}$$

The scattering angles Θ_1 and Θ_2 in the laboratory system are linked to the scattering angle in the center-of-mass system Θ_{cm} according to Fig. 3.4:

$$\tan\Theta_1 = \frac{m_2 \sin\Theta_{cm}}{m_1 + m_2\cos\Theta_{cm}} \tag{3.20}$$

$$\Theta_2 = \frac{1}{2}(\pi - \Theta_{cm}) \tag{3.21}$$

The energy loss results from the solution of energy and momentum conservation for a given scattering angle. This is referred to as the **kinematic factor** γ .

$$\boxed{\frac{\Delta E}{E} = \gamma = \frac{2m_1m_2}{(m_1+m_2)^2}(1-\cos\Theta_{cm})} \tag{3.22}$$

The kinematic factor reaches its maximum in a central collision. One obtains:

$$\gamma = 4\frac{m_1m_2}{(m_1+m_2)^2} \tag{3.23}$$

After introducing these new quantities for the center-of-mass system, the energy conservation must be solved on the trajectory:

$$\frac{1}{2}m_{cm}\left(\dot{r}^2 + r^2\dot{\Theta}_{cm}^2\right) + V(r) = \frac{1}{2}m_{cm}v_R^2 \tag{3.24}$$

as well as the angular momentum conservation:

$$m_{cm}v_R b = m_{cm}r^2\dot{\Theta}_{cm} \tag{3.25}$$

Equations 3.24 and 3.25 can be substituted into each other using the relationship:

$$\frac{d\Theta}{dr} = \frac{d\Theta}{dt}\frac{1}{\frac{dr}{dt}} \tag{3.26}$$

One finally obtains the so-called **scattering integral** :

$$\boxed{\Theta_{cm} = \pi - 2b\int_{r_{min}}^{\infty} \frac{1}{r^2\left[1 - \frac{V}{\frac{1}{2}m_{cm}v_R^2} - \left(\frac{b}{r}\right)^2\right]^{1/2}}dr} \tag{3.27}$$

Here, the scattering potentials $V(r)$ are inserted according to the type of interaction, and the integral is solved. This results in the dependence $\Theta(b)$, with which the differential cross-section is subsequently determined.

3.4 Scattering Potentials

3.4.1 Coulomb Scattering, Coulomb Logarithm

First, let's consider Coulomb scattering . The potential is given by:

$$V = \frac{q_1 q_2}{4\pi\epsilon_0 r} \tag{3.28}$$

If this is inserted into the scattering integral, the following solution for the relationship between b and Θ is obtained:

$$b = \frac{q_1 q_2}{4\pi\epsilon_0} \frac{1}{m_{cm} v_R^2} \frac{1}{\tan\Theta/2} \tag{3.29}$$

This equation can be written more compactly by denoting b_0 as the distance of closest approach between the collision partners. It is obtained by equating the kinetic and potential energy.

$$\frac{q_1 q_2}{4\pi\epsilon_0 b_0} = \frac{1}{2} m_{cm} v_R^2 \tag{3.30}$$

Thus, we obtain:

$$b = \frac{1}{2} b_0 \frac{1}{\tan\Theta/2} \tag{3.31}$$

and the differential cross-section for the so-called **Rutherford scattering** :

$$\boxed{\frac{d\sigma}{d\Omega} = \frac{1}{4}\left(\frac{b_0}{\sin^2\Theta/2}\right)^2 \propto \frac{1}{E^2}} \tag{3.32}$$

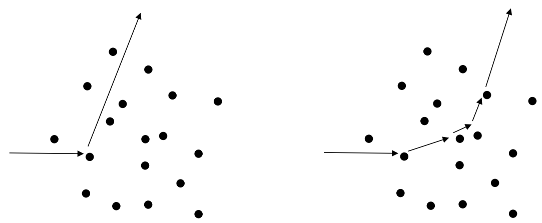

Figure 3.5: Single Collision vs. Small-Angle Collisions

In plasmas, these Coulomb collisions dominate the scattering of the charged particles. To calculate the total cross-section, the differential cross-section must be integrated over all directions. Since the range of the Coulomb potential is infinite, the integral diverges. This problem can be solved by defining a maximum impact parameter or minimum deflection angle, which is determined by the Debye length: in a plasma, a projectile ”sees” the target only if the impact parameter is smaller than the Debye length, otherwise the target charge is shielded. However, for evaluating the transport properties of charge carriers in plasmas, another estimation is even more important. The deflection by, for example, 90 degrees can occur within a single collision or as a sequence of small-angle collisions. As can be shown, the latter case is dominant:

- Approximation of a Single Collision

  A collision with a scattering angle of at least 90Â° can be calculated from the differential cross-section for scattering angles between $\pi/2$ and π:

$$\sigma_{90^\circ,sc} = \int_{\pi/2}^{\pi} \frac{1}{4}\left(\frac{b_0}{\sin^2\Theta/2}\right)^2 2\pi\sin\Theta d\Theta = \frac{1}{4}\pi b_0^2 \tag{3.33}$$

  By restricting the integration limits, one avoids the diverging integral when $\Theta \rightarrow 0$.

- Approximation of Small-Angle Collisions

  In comparison, many small-angle collisions can add up to a deflection of 90Â°. The dependence $\Theta(b)$ is:

$$\tan\Theta/2 = \frac{q_1 q_2}{4\pi\epsilon_0 m_{cm} v_R^2}\frac{1}{b} \tag{3.34}$$

  For small deflection angles, the tangent can be expanded, and one obtains:

$$\Theta/2 \simeq \frac{1}{2}\underbrace{\frac{q_1 q_2}{4\pi\epsilon_0 \frac{1}{2} m_{cm} v_R^2}}_{b_0}\frac{1}{b} \tag{3.35}$$

  This finally becomes:

$$\Theta \simeq \frac{b_0}{b} \tag{3.36}$$

Subsequently, we ask how many of these small deflections must be summed to obtain a total deflection by an angle of 90Â°. For this purpose, we consider the quadratic deviation of:

$$\langle\Theta^2\rangle = \frac{1}{\pi b_{max}^2}\int_{b_{min}}^{b_{max}} \frac{b_0^2}{b^2} 2\pi b db \tag{3.37}$$

This becomes:

$$\langle\Theta^2\rangle = 2\frac{b_0^2}{b_{max}^2}\ln\frac{b_{max}}{b_{min}} \tag{3.38}$$

Here, one again encounters the problem with the infinite range of the Coulomb potential. If one sets $b_{max} \rightarrow \infty$, one does not obtain a finite expression for $\langle\Theta^2\rangle$. For this reason, the following estimation is made: in plasmas, the maximum allowed impact parameter is the Debye length, since at distances greater than the Debye length, the potential of the collision partner is completely shielded. As an approximation for the minimum impact parameter, the minimum distance b_0 is used. Thus, the so-called **Coulomb logarithm** is defined:

$$\boxed{\ln\Lambda = \ln\frac{\lambda_D}{b_0}} \tag{3.39}$$

The quadratic deviation should be exactly 90Â° after a time τ_m. That is, within a collision time τ_m, we need a certain number $N_{Collisions}$ of collision processes with an average deflection $\langle\Theta\rangle$, which add up to $\pi/2$. That is, we require:

$$\langle\Theta^2\rangle N_{Collisions} = \left(\frac{\pi}{2}\right)^2 \tag{3.40}$$

This number of collisions can be calculated as:

$$N_{Collisions} = \underbrace{(\pi b_{max}^2)}_{Maximumarea}\underbrace{n_g v_R}_{Fluxdensity}\tau_m \tag{3.41}$$

This collision time τ_m is inversely proportional to our sought cross-section $\sigma_{90°,m}$ according to:

$$\sigma_{90°,m} = \frac{1}{n_g\lambda} = \frac{1}{n_g\tau_m v_R} \tag{3.42}$$

If we substitute everything, we finally obtain:

$$\sigma_{90^\circ,m} = \frac{8}{\pi} b_0^2 \ln \Lambda \tag{3.43}$$

The comparison between single collision σ_{sc} and multiple scattering σ_m shows that multiple scattering dominates the transport:

$$\frac{\sigma_{90^\circ,m}}{\sigma_{90^\circ,sc}} = \frac{32}{\pi^2} \ln \Lambda \simeq 30 \tag{3.44}$$

The Coulomb logarithm is approximately $\ln \Lambda = 10$ for many plasmas.
The scattering of charged particles among each other is essential for the description of fully ionized plasmas. In particular, when heating a fusion plasma to high temperatures, the resistance of the plasmas decreases increasingly due to the Coulomb cross-section.

3.4.2 Polarization Scattering

In partially ionized plasmas of plasma technology, the most frequent collision processes of ions and electrons are those with the neutral background gas.
In the so-called polarization scattering , the scattering of a charged particle on a neutral gas atom is considered. Here, the electron shell of the neutral particle is polarized by the electric field of the passing charged particle. The field of the charged particle is initially:

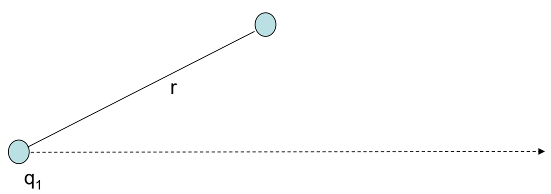

Figure 3.6: Polarization Scattering

$$\vec{E} = \frac{1}{4\pi\epsilon_0} \frac{q_1}{r^2} \tag{3.45}$$

This field induces a dipole moment in the neutral atom. The magnitude of the dipole moment depends on the polarizability α of the atom:

$$\vec{p} = \alpha \vec{E} \tag{3.46}$$

The potential energy V of this dipole in the field of the charged particle becomes:

$$V = \vec{p}\vec{E} = \alpha E^2 = \frac{1}{(4\pi\epsilon_0)^2}\frac{q_1^2}{r^4}\alpha \propto \frac{\alpha}{r^4} \tag{3.47}$$

A potential proportional to $1/r^4$ is obtained. This expression is inserted into the scattering integral, and the cross-section is calculated again. In the analysis of the trajectories, it is observed that for small impact parameters, the charged particle is captured by the neutral particle (see Fig. 3.7). The impact parameter at which the transition between deflection and capture occurs defines the **Langevin capture cross-section** :

$$\boxed{\sigma_L = \pi b_L^2 = \left(\frac{\pi\alpha q^2}{\epsilon_0 m_{cm}}\right)^{1/2}\frac{1}{v_R}} \tag{3.48}$$

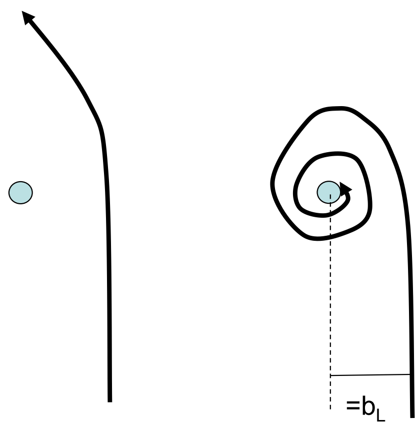

Figure 3.7: In polarization scattering, capture of the charged particle occurs below a certain impact parameter. The cross-sectional area with this impact parameter is referred to as the Langevin capture cross-section.

The essential scaling of the Langevin cross-section is proportional to v^{-1}. That is, with higher velocities of the charge carriers, the cross-section decreases. This decrease to high particle velocities occurs more slowly than in Coulomb scattering (v^{-4}). The scattering cross-section depends, in particular, on the polarizability of the neutral gas. Table 3.1 lists the polarizabilities of some elements.

Element	Relative Polarizability
H	4.5
Ar	11.08
Cl_2	31
SF_6	30
CCl_4	69

Table 3.1: Relative polarizability $\alpha_R = \frac{\alpha}{a_0^3}$ (a_0 Bohr radius)

In particular, halides are characterized by a high polarizability. In applications, this fact is utilized in fluorescent tubes or plasma lamps (see Fig. 3.8). There is always a small amount of mercury in the discharge. Due to the large cross-section, the electrical resistance in the plasma can be increased, and thus the charge can be operated with high voltages but small currents. Also for heating with electrical alternating fields, collisions of the electrons with the background gas are essential for the efficiency of the heating. However, in newer plasma lamps, the mercury or other halides must first vaporize. This happens after switching on the lamp by the slow heating of the lamp bulb. This takes some time. With increasing halide concentration in the plasma, the efficiency of the energy coupling increases, and the light intensity of new plasma lamps (energy-saving lamp) slowly increases until it reaches the equilibrium value.
Another peculiarity of polarization scattering is the **Ramsauer minimum** in the scattering of electrons on noble gas atoms. Here, quantum mechanical interference occurs between the incident electron wave and the wave function of the electrons in the atom. Due to this interference, a minimum in the cross-section is obtained at small electron energies. In molecules, this effect usually does not occur because there are a variety of excitation possibilities (rotation and vibrations) that continue to lead to a large scattering cross-section (see Fig. 3.9).

3.4.3 Ionization

Ionization by electron impact can only be correctly described by the laws of quantum mechanics. As a simple classical approximation, one can also consider the momentum transfer to a bound electron in the atomic shell. The energy transfer in such a collision process is:

$$\Delta E = E\, 2\frac{m_1 m_2}{(m_1+m_2)^2}(1-\cos\Theta_{cm}) \tag{3.49}$$

Since small angles dominate, we make the approximation:

Figure 3.8: Adding mercury to an energy-saving lamp increases the electrical resistance of the plasma and thus the dissipated power in the plasma itself. With this dissipated power, the light output simultaneously increases.

$$\cos\Theta_{cm} \simeq 1 - \frac{\Theta_{cm}^2}{2} \tag{3.50}$$

Eq. 3.49 applies to the scattering angle in the center-of-mass system (CM). In the laboratory system (LB), $\Theta_{LB} \to \Theta_{CM}/2$ for collision partners with equal mass $m_1 = m_2$. In the following, we denote by Θ the scattering angle in the laboratory system. The energy transfer in the laboratory system becomes:

$$\Delta E = \Theta^2 E \tag{3.51}$$

Similarly, the differential cross-section in the center-of-mass system (CM) for small scattering angles Θ can be written ($\sin^4\Theta_{CM}/2 = \Theta^4$):

$$\left.\frac{d\sigma}{d\Omega}\right|_{CM} = \left(\frac{e^2}{4\pi\epsilon_0}\right)^2 \frac{1}{E^2}\frac{1}{\Theta^4} \tag{3.52}$$

Convert to the laboratory system via $E_{CM} = \frac{1}{2}E_{LB}$ and $m_{cm} = \frac{1}{2}m_{LB}$:

$$d\sigma|_{LB} = \left(\frac{e^2}{4\pi\epsilon_0}\right)^2 \frac{1}{E^2}\frac{1}{\Theta^4} 2\pi \underbrace{\sin\Theta}_{\propto\Theta} d\Theta \tag{3.53}$$

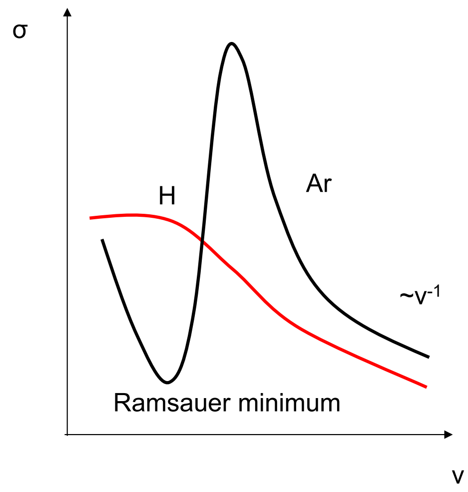

Figure 3.9: Typical course of the Langevin cross-section (red).

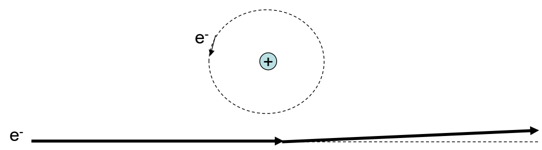

Figure 3.10: Ionization in classical consideration

We transition from a solid angle element to an energy transfer ΔE with:

$$d(\Delta E) = E2\Theta d\Theta \tag{3.54}$$

Thus, we obtain:

$$d\sigma = \pi \left(\frac{e^2}{4\pi\epsilon_0}\right)^2 \frac{1}{E}\frac{1}{(\Delta E)^2} d(\Delta E) \tag{3.55}$$

We integrate this equation from the minimum energy transfer given by the ionization energy to the total energy E of the electron.

$$\sigma(E) = \int_{E_{Ionization}}^{E} \pi \left(\frac{e^2}{4\pi\epsilon_0}\right)^2 \frac{1}{E}\frac{1}{(\Delta E)^2} d(\Delta E) \tag{3.56}$$

Thus, we finally obtain the **Thomson cross-section** for ionization:

$$\boxed{\sigma_{Ionization} = \pi \left(\frac{e^2}{4\pi\epsilon_0}\right)^2 \frac{1}{E}\left(\frac{1}{E_{Ionization}} - \frac{1}{E}\right)} \tag{3.57}$$

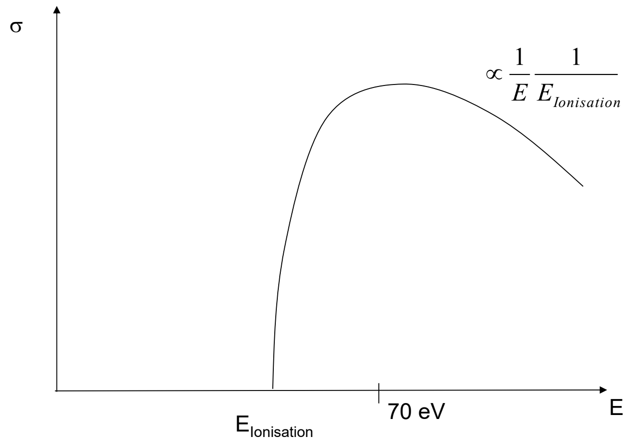

Figure 3.11: Typical course of the cross-section for ionization.

3.5 Ionization Equilibria

In the description of plasmas, the degree of ionization, i.e., the concentration of charge carriers relative to the total particle number density, is crucial for the behavior of the plasma. In plasma technology, the degree of ionization is usually small, in the range of a few percent, while in fusion physics, the plasmas are usually fully ionized. In addition, in these hot plasmas, the atoms are ionized multiple times.

For the density of a singly ionized atom with atomic number Z, the following rate equation can be set up:

$$\frac{dn_{Z+1}}{dt} = S_Z n_Z n_e - \beta_{Z+1} n_{Z+1} n_e n_e - \frac{n_{Z+1}}{\tau} \tag{3.58}$$

The first term describes the electron impact-induced ionization of the atoms in the ground state. The second term describes the recombination of the ion with the electrons. This is usually a three-body recombination, as only then can momentum and energy conservation be ensured. In principle, one could still add additional terms, e.g., double ionization. However, these reactions have a small cross-section so that for the concentration of the ions, essentially only the neighboring ionization states are important. The third term describes the finite confinement time τ of the ionized atoms in the plasma. This confinement time can be given by the diffusion or drift of the particles to the boundaries of the system, as discussed in more detail in the following chapter.

The dominance of the terms in Eq. 3.58 depends on the system considered. In very dense plasmas with a sufficient number of collisions, recombination of the ions is crucial for their loss. An example would be thermal high-pressure plasmas, such as flames, etc. At the same time, in a magnetically confined plasma, such as in fusion experiments, the confinement time can become very long. In such systems, the first two terms in Eq. **??** dominate. In contrast, there are cold thin plasmas of low-pressure plasma technology. There, the confinement time is often short, and at low pressures, the terms 1 and 3 in Eq. 3.58 dominate.

However, we want to consider the case where sufficient collisions occur and the confinement time τ becomes very long. An example of such an equilibrium between the concentration of atoms and ions in a hydrogen plasma would be:

$$\mathrm{H} + \mathrm{e}^- \rightleftarrows \mathrm{H}^+ + 2\mathrm{e}^- \tag{3.59}$$

In steady-state equilibrium, Eq. 3.58 thus gives:

$$S_z n_z n_e = \beta_{Z+1} n_e^2 n_{Z+1} \tag{3.60}$$

This has the form of a mass action law. The equilibrium constant $f(T_e)$ is only a function of temperature.

$$\frac{n_e n_{Z+1}}{n_Z} = \frac{S_Z}{\beta_{Z+1}} = f(T_e) \tag{3.61}$$

Based on our assumption that collisions between the particles lead to thermalization (the type of microscopic processes is irrelevant), we can describe the occupation of the individual atomic or ionization levels using Boltzmann statistics:

$$\frac{n_{Z+1}}{n_Z} = \frac{g_{Z+1}}{g_Z} e^{-\frac{E_{Z+1}-E_Z}{k_B T_e}} = \frac{g_{Z+1}}{g_Z} e^{-\frac{\chi_Z}{k_B T_e}} \tag{3.62}$$

with E_{Z+1} and E_Z the binding energies of the levels and $\chi_Z = E_{Z+1} - E_Z$ the ionization energy. g_{Z+1} and g_Z denote the corresponding degeneracies. The density of the electrons at a given temperature T_e results from the density of states.

$$\frac{dN_e}{dE} = g(E)\frac{1}{e^{\frac{E-E_F}{k_BT}}+1} \tag{3.63}$$

The Fermi distribution can be approximated with the Boltzmann distribution for thin plasmas where $E_F \ll k_BT_e$, as illustrated in Fig. 3.10.

$$\frac{dN_e}{dE} = g(E)e^{-\frac{E}{k_BT}} \tag{3.64}$$

The degeneracy $g(E)$ of a free electron gas results from counting the states in phase space:

$$\frac{dN_e}{dE} = V\frac{8\pi\left(2m_e^3\right)^{1/2}}{h^3}\sqrt{E}e^{-\frac{E}{k_BT_e}} \tag{3.65}$$

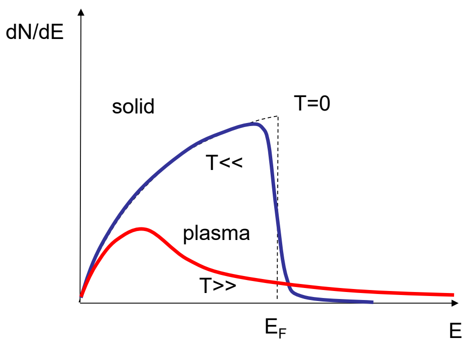

Figure 3.12: State density of electrons in a solid and in a plasma.

Thus, the electron density as a function of their temperature is:

$$n_e = \frac{2\left(2\pi m_e k_B T_e\right)^{3/2}}{h^3} \tag{3.66}$$

If we substitute this into Eq. 3.61, we finally obtain the so-called **Saha equation** for the ratio of the occupation densities to each other.

$$\boxed{\frac{n_e n_{Z+1}}{n_Z} = \frac{g_{Z+1}}{g_Z}\frac{2\left(2\pi m_e k_B T_e\right)^{3/2}}{h^3}e^{-\frac{\chi}{k_BT_e}}} \tag{3.67}$$

Given a temperature, we still have three unknowns on the left side of the equation. In addition to the Boltzmann occupation 3.62, we need two more equations to determine the unknowns. These are the quasi-neutrality

$$n_e = \sum_{Z=1}^{Z_{max}} Z n_Z \tag{3.68}$$

and the specification of a pressure or total particle density

$$n_0 = \sum_{Z=0}^{Z_{max}} n_Z \tag{3.69}$$

Let us consider the simple case of a weakly ionized hydrogen plasma. The ground state density of the atoms n_Z is much larger here than the ion density n_{Z+1}. Thus, we obtain:

$$\frac{n_e^2}{n_0} = \frac{g_{H^+}}{g_H} \frac{2\left(2\pi m_e k_B T_e\right)^{3/2}}{h^3} e^{-\frac{13.6eV}{k_B T_e}} \tag{3.70}$$

However, the collision rate is often lower, so that the assumption of thermalization of the states is not justified. For excited ionization stages, however, a condition of equilibrium can still be assumed. In the case of a highly excited ion, the electronic states become strongly hydrogen-like, and the levels lie close together on the energy scale (principal quantum number $n \to \infty$). Since the states of these excited ions thus overlap well, the cross-section for the collision interaction is very large. That is, the excited states thermalize among themselves. For this subset of excited states, a **partial local thermal equilibrium** (PLTE partial local thermal equilibrium) can be specified. The describing equation is the **Saha-Boltzmann equation**, where the index k indicates the excitation state of the ion ($k = 1$ corresponds to the ground state). One obtains:

$$\frac{n_e n_{Z+1,1}}{n_{Z,k}} = \frac{g_{Z+1,1}}{g_{Z,k}} \frac{2\left(2\pi m_e k_B T_e\right)^{3/2}}{h^3} e^{-\frac{E_{Z+1,1}-E_{Z,k}}{k_B T_e}} \tag{3.71}$$

Chapter 4

Transport

Transport processes determine the quality of the confinement of a plasma. Particles and energy are driven by a density gradient or electric fields. This transport changes fundamentally in magnetized plasmas, as the magnetic field lines define a preferred direction of particle motion. Transport perpendicular to this direction is suppressed in the first approximation. Nevertheless, the plasma confinement is not arbitrarily good, as numerous processes such as macroscopic and microscopic instabilities, turbulence, reconnection, and drift processes increase the transport perpendicular to the field lines.

To describe transport processes, one starts with the fluid picture, which is extended by a collision term. In fully ionized plasmas, the fluid picture can be further simplified with MHD (magnetohydrodynamics).

To describe transport processes, one starts in the fluid picture, which is extended by a simple approach for the collision term, the relaxation approximation. The change in momentum in a fluid element is given by the momentum lost in a collision ($\sim m\vec{v}$) multiplied by the frequency of this process ($\sim n\nu_m$). Thus, one obtains:

$$mn\left[\frac{\partial}{\partial t}\vec{v} + (\vec{v}\nabla)\vec{v}\right] = qn\vec{E} - \nabla p - m\vec{v}n\nu_m \tag{4.1}$$

In the steady-state case, the time derivative is set to zero. Assuming that $\nu_m \gg v$ (we consider the case of high collision frequencies), the second term on the left side, proportional to v^2, can be neglected. Thus, one obtains:

$$\vec{v} = \frac{1}{mn\nu_m}\left(\pm en\vec{E} - \nabla p\right) \tag{4.2}$$

Using the ideal gas law, two cases arise. For an isothermal state change, we have:

$$\nabla p = kT\nabla n \tag{4.3}$$

For an adiabatic state change (i.e., the temperature does not remain constant with a pressure change), the adiabatic equation applies:

$$\frac{\nabla p}{p} = \gamma\frac{\nabla n}{n} \tag{4.4}$$

Here, γ is given by

$$\gamma = \frac{2+N}{N} \tag{4.5}$$

with N the number of degrees of freedom. For an isothermal state change, the following expression for the velocity of the electrons or ions in the fluid picture is obtained:

$$\vec{v} = \pm\frac{e}{m\nu_m}\vec{E} - \frac{kT}{m\nu_m}\frac{\nabla n}{n} \tag{4.6}$$

$$\vec{j} = n\vec{v} = n\frac{\pm e}{m\nu_m}\vec{E} - \frac{k_BT}{m\nu_m}\nabla n \tag{4.7}$$

The first term describes the particle flux driven by an electric field, the drift. The second term corresponds to a particle flux driven by a density gradient, diffusion. Accordingly, the so-called **mobility** is obtained to describe the drift as:

$$\boxed{\mu = \frac{|q|}{m\nu_m}} \tag{4.8}$$

and the **diffusion constant** as:

$$\boxed{D = \frac{k_BT}{m\nu_m}} \tag{4.9}$$

The connection between drift and diffusion is given by the **Einstein relation** :

$$\boxed{\mu = \frac{|q|}{k_bT}D} \tag{4.10}$$

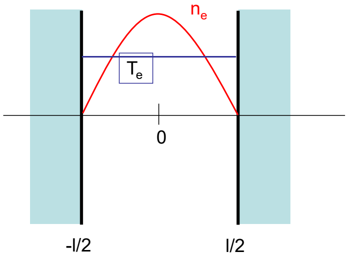

Figure 4.1: Geometry for solving the diffusion equation in one dimension.

As an example, consider the solution of the continuity equation for planar geometry for a neutral gas, i.e., the drift term is negligible. The geometry is sketched in Fig. 4.1.
The ansatz yields:

$$\frac{\partial n}{\partial t} + \nabla(-D\nabla n) = 0 \tag{4.11}$$

Assuming that D is spatially constant (due to the high thermal conductivity, a rapid temperature equalization often occurs in a plasma, i.e., the temperature does not change spatially), one obtains:

$$\frac{\partial n}{\partial t} = D\nabla^2 n \tag{4.12}$$

We make a separation ansatz for the density n according to

$$n = u(t)w(x) \tag{4.13}$$

and separate the variables.

$$\frac{1}{u}\frac{\partial u}{\partial t} = D\frac{1}{w}\nabla^2 w = \text{const.} = -\frac{1}{\tau} \tag{4.14}$$

Since the left side depends only on time and the right side only on location, both sides must each yield a constant. We define this meaningfully as -$1/\tau$. The time dependence is obtained from the solution of the differential equation:

$$\frac{\partial u}{\partial t} = -\frac{1}{\tau}u \tag{4.15}$$

Thus, we obtain

$$u(t) = u_0 e^{-\frac{t}{\tau}} \tag{4.16}$$

The solution of the spatial dependence is obtained from the differential equation:

$$-\frac{1}{D\tau} = \frac{1}{w}\nabla^2 w \tag{4.17}$$

With the definition of a geometric constant $\Lambda = \sqrt{D\tau}$, we obtain

$$-\frac{1}{\Lambda^2} w = \nabla^2 w \tag{4.18}$$

with the solution

$$w(x) = w_0 \cos\frac{x}{\Lambda} + ...+ \tag{4.19}$$

In planar geometry with the boundary condition $n = 0$ for $x = \pm l/2$, the geometric constant Λ is:

$$\Lambda = \frac{l}{\pi} \tag{4.20}$$

For other geometries such as cylindrical geometry or spherical problems, correspondingly different geometric constants are obtained (in cylindrical geometry, the spatial dependence is given by Bessel functions). The solution in one dimension is:

$$n(x,t) = n_0 e^{-\frac{t}{\tau}} \cos\left(\frac{\pi}{l}x\right) \tag{4.21}$$

That is, the density profile created by the diffusion of neutrals corresponds to a cosine. This is referred to as the fundamental mode of diffusion. This density profile decays exponentially over time. Even if an initial density distribution deviates from the cosine profile, the cosine distribution quickly forms through the decay of higher modes, which then decreases exponentially. Depending on the geometry, typical solutions of the diffusion equation are obtained. In cylindrical geometry, these are Bessel functions.

4.1 Transport in Partially Ionized Plasmas

4.1.1 Ambipolar Diffusion

So far, we have considered the diffusion of neutral particles, i.e., the drift term did not play a role. In the case of electrons and ions, one might assume that they have different density profiles since their transport coefficients, diffusion and mobility, are strongly different due to the mass. This would mean, however, that the electron profile decays much faster than the ion profile. An electric field builds up that counteracts this decay to maintain quasi-neutrality in the plasma. Assuming that the ion and electron fluxes must be equal:

$$\vec{j} = \mu_i n_i \vec{E} - D_i \nabla n_i = -\mu_e n_e \vec{E} - D_e \nabla n_e \tag{4.22}$$

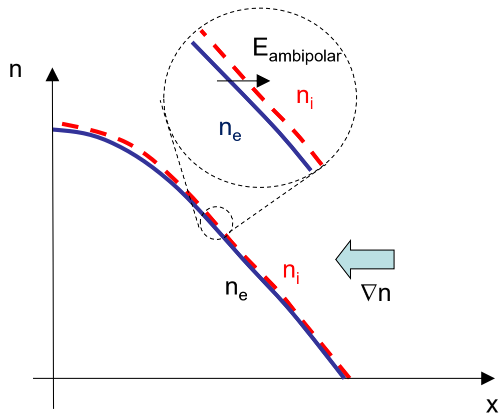

Figure 4.2: The ambipolar electric field arises in a plasma with a density gradient to accelerate the ions and decelerate the electrons. This compensates for the different mobilities and diffusion constants of electrons and ions and thus ensures quasi-neutrality.

The electric field that arises in this process ensures that the electrons, which are ahead, are followed by the ions. This is referred to as **ambipolar field**:

$$\vec{E}_{amb} = \frac{D_i - D_e}{\mu_i + \mu_e} \frac{\nabla n}{n} \tag{4.23}$$

Here, it was assumed that $j_i = j_e$, $n_e = n_i$, and $\nabla n_e = \nabla n_i$ holds. The particle flux is thus

$$\vec{j} = \mu_i n \frac{D_i - D_e}{\mu_i + \mu_e} \frac{\nabla n}{n} - D_i \nabla n = -\frac{\mu_i D_e + \mu_e D_i}{\mu_i + \mu_e} \nabla n \tag{4.24}$$

This again corresponds formally to a diffusion equation with a new **ambipolar diffusion coefficient**:

$$\boxed{D_{amb} = \frac{\mu_i D_e + \mu_e D_i}{\mu_i + \mu_e}} \tag{4.25}$$

In general, $\mu_e \gg \mu_i$. Therefore, we have

$$D_{amb} = \frac{\frac{\mu_i}{\mu_e} D_e + D_i}{\frac{\mu_i}{\mu_e} + 1} \simeq D_i + \frac{\mu_i}{\mu_e} D_e = D_i \left(1 + \frac{T_e}{T_i}\right) \tag{4.26}$$

Here, the Einstein relation was used for the last transformation. If the electron temperature is greater than the ion temperature (as in low-pressure plasmas), we obtain:

$$D_{amb} = D_i \frac{T_e}{T_i} = \frac{k_B T_e}{M \nu_{m,Ionen}} \tag{4.27}$$

That is, the transport is driven by the temperature of the electrons, but with the inertia of the ions.
For the case of a plasma, we want to use ambipolar diffusion to derive the equilibrium condition of a confined plasma volume. This corresponds to the idea of the **global model** . We again start from the continuity equation, with the assumption that the particle flux is driven by ambipolar diffusion. In addition, we seek steady-state solutions (i.e., the time derivative is set to zero). We also assume that ionization occurs in our volume (i.e., new particles are generated). Thus, we obtain

$$\frac{\partial n}{\partial t} + \nabla(-D\nabla n) = n\nu_{ionization} \tag{4.28}$$

with a steady-state solution assuming that $T_e \gg T_i$

$$0 = n\nu_{ionsation} + D_{amb}\nabla^2 n \tag{4.29}$$

This differential equation also has a solution of the form

$$n(x) = n_0 \cos \frac{\pi}{l} x \tag{4.30}$$

Comparing with the solution of the diffusion equation for neutrals according to Eq. 4.20 automatically gives:

$$\left(\frac{\pi}{l}\right)^2 = \frac{\nu_{ionization}}{D_{amb}} \tag{4.31}$$

or

$$\nu_{ionization} = \left(\frac{\pi}{l}\right)^2 \frac{k_B T_e}{M\nu_m} \tag{4.32}$$

If one now simply assumes an exponential law for the ionization frequency (according to an excitation energy for ionization), one obtains:

$$\nu_{ionization} = \nu_0 e^{-\frac{E_{ionization}}{k_B T_e}} = \left(\frac{\pi}{l}\right)^2 \frac{k_B T_e}{M \nu_m} \tag{4.33}$$

On the left side, there is an expression with an exponential function in T_e, and on the right side, a function linear in T_e. The dependencies of the global model on the size of the discharge (l), the electron temperature (T_e), and the ionization energy ($E_{ionization}$) are illustrated in Fig. 4.3.

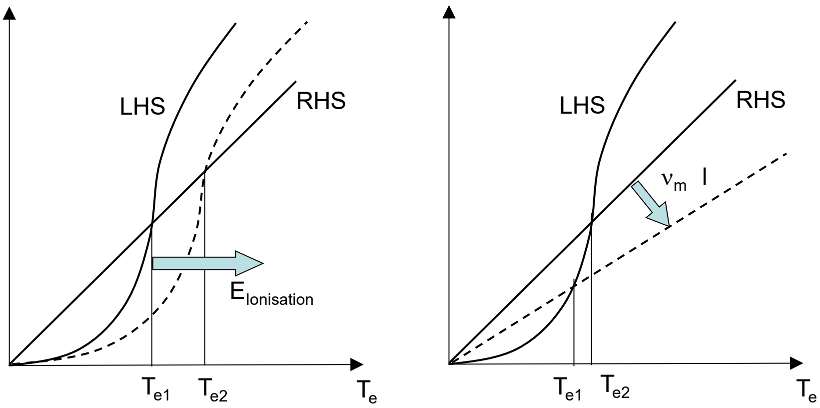

Figure 4.3: Global model according to Eq. 4.33 . The transport of the ions is diffusion-limited.

One can see that the temperature increases or decreases depending on the geometry and gas type: A gas with high ionization energy leads to a high electron temperature. Increasing the plasma volume improves the surface-to-volume ratio. The electron temperature decreases because the ion loss rate decreases, and a lower ionization rate is sufficient to maintain a given charge carrier density.
In analogy, a global model for ions can be constructed, in which the loss of ions is given by the Bohm velocity (see Chapter 7) at the sheath edge.

4.1.2 Diffusion Perpendicular to the B Field

So far, we have considered transport without a B field or transport along the B field lines. Transport perpendicular to the B field lines can only occur if collisions take place, as illustrated in Fig. 4.4:

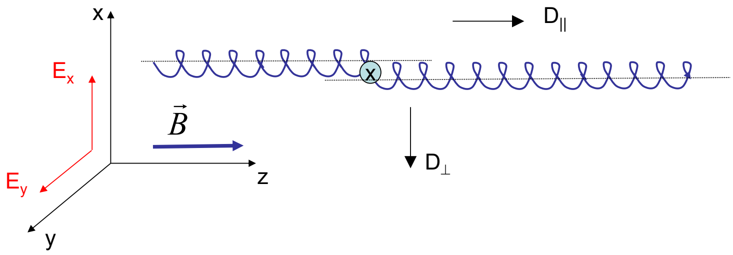

Figure 4.4: Transport perpendicular to the magnetic field only occurs through collisions.

This is an important difference: transport along the field lines is hindered by collisions with neutrals, while for transport perpendicular to the magnetic field, collisions are essential! One can imagine the transport perpendicular to the magnetic field as a **random walk** of the guiding center (Fig. 4.5).

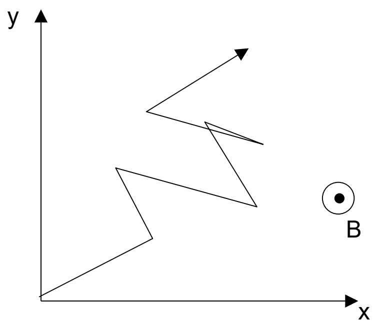

Figure 4.5: Diffusion perpendicular to the magnetic field corresponds to a random walk of the guiding center.

The equation of motion of a charged particle is obtained from:

$$mn\frac{dv_\perp}{dt} = qn(\vec{E} + \vec{v}_\perp \times \vec{B}) - k_B T \nabla n - mn\nu_m \vec{v} \tag{4.34}$$

The left side of Eq. 4.34 describes only the explicit gyration motion. However, we want to determine only the drift motion and can therefore set the left side to zero again. Thus, in the x-direction, we obtain:

$$mn\nu_m v_x = \pm enE_x - k_B T_e \frac{\partial n}{\partial x} \pm env_y B \tag{4.35}$$

The upper sign applies to ions, and the lower sign applies to electrons. In the y-direction, we obtain:

$$mn\nu_m v_y = \pm enE_y - k_B T_e \frac{\partial n}{\partial y} \mp env_x B \tag{4.36}$$

Thus, the expression for v_x is:

$$v_x = \pm \frac{e}{m\nu_m} E_x - \frac{1}{n} \frac{k_B T}{m\nu_m} \frac{\partial n}{\partial x} \pm \frac{eB}{m\nu_m} v_y \tag{4.37}$$

or

$$v_x = \pm \mu E_x - \frac{D}{n} \frac{\partial n}{\partial x} \pm \frac{\omega_c}{\nu_m} v_y \tag{4.38}$$

Now, v_y is substituted, and $\tau = \nu_m^{-1}$ is replaced. Thus, we obtain the following expression:

$$v_x(1 + \omega_c^2\tau^2) = \pm \mu E_x - \frac{D}{n} \frac{\partial n}{\partial x} + \omega_c^2\tau^2 \frac{E_y}{B} \mp \omega_c^2\tau^2 \frac{k_B T}{eB} \frac{1}{n} \frac{\partial n}{\partial y} \tag{4.39}$$

For v_y, one obtains an analogous expression:

$$v_y(1 + \omega_c^2\tau^2) = \pm \mu E_y - \frac{D}{n} \frac{\partial n}{\partial y} - \omega_c^2\tau^2 \frac{E_x}{B} \pm \omega_c^2\tau^2 \frac{k_B T}{eB} \frac{1}{n} \frac{\partial n}{\partial x} \tag{4.40}$$

The first and second terms denote the known drift and diffusion. The third term describes the E × B drift, and the last term corresponds to the diamagnetic drift . Formally, we can now bring the term $(1 + \omega_c^2\tau^2)$ to the right side and obtain modified expressions for the **diffusion and drift perpendicular to the magnetic field** :

$$\boxed{\mu_\perp = \frac{\mu_\parallel}{1 + \omega_c^2\tau^2}} \tag{4.41}$$

and

$$\boxed{D_\perp = \frac{D_\parallel}{1 + \omega_c^2\tau^2}} \tag{4.42}$$

The term $\frac{1}{1+\omega_c^2\tau^2}$ shows that the diffusion constant perpendicular to the magnetic field is strongly reduced compared to the diffusion parallel to the magnetic field. If we now approximately consider the case of a strong magnetic field with $\omega^2\tau^2 \gg 1$, we obtain

$$D_\perp = \frac{k_B T}{m\nu_m}\frac{\nu_m^2}{\omega_c^2} \propto \frac{\nu_m}{B^2} \propto \frac{r_L^2}{\tau_m} \tag{4.43}$$

That is, the transport increases with increasing collision frequency. The step size here corresponds to a random walk with a step size of the Larmor radius. For comparison, classical diffusion:

$$D_\parallel = \frac{k_B T}{m\nu_m} \propto \frac{1}{\nu_m} \propto v_{therm}^2 \tau_m = \frac{\lambda_m^2}{\tau_m^2}\tau_m = \frac{\lambda_m^2}{\tau_m} \tag{4.44}$$

Here, the diffusion decreases with increasing collision frequency, and the transport corresponds to a random walk with a step size of the mean free path λ_m.

4.2 Transport in Fully Ionized Plasmas

4.2.1 Collisions Between Charge Carriers

So far, we have always considered the diffusion of charged particles in front of a neutral gas background. What changes if we only consider collisions between charged particles, as is the case in fully ionized plasmas. Fig. 4.6 illustrates that only the transport of *unlike* charge carriers leads to net transport: (i) if two like charge carriers collide on their gyration path, they change their direction in an elastic collision and begin their gyration anew. If, however, the center of mass of the two guiding centers is formed, this does not change in a collision process; (ii) in the case of unlike charge carriers, the center of mass of the two guiding centers changes by the order of a Larmor radius.

4.2.2 Specific Resistance or Conductivity of a Plasma

Before we consider the transport in fully ionized plasmas, we first want to determine the resistance of a plasma for the case where only charged particles are collision partners. The current is driven by an electric field according to Ohm's law:

$$\vec{j} = \sigma_{cond}\vec{E} = en\mu\vec{E} \tag{4.45}$$

The **conductivity** σ_{cond} is thus

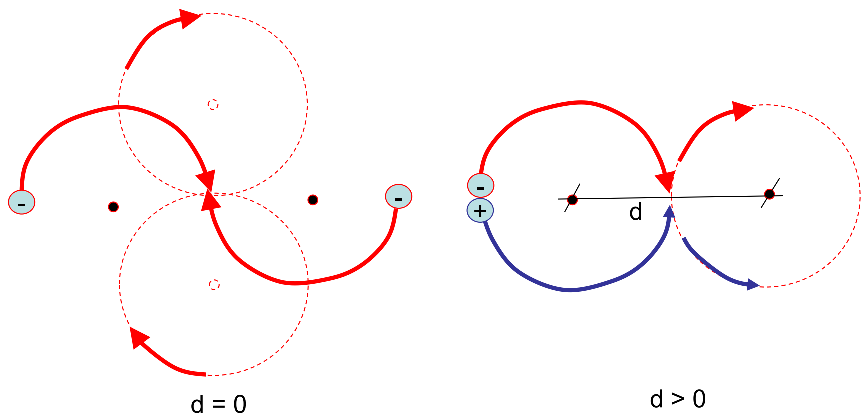

Figure 4.6: Only collisions between unlike charge carriers lead to transport

$$\sigma = \frac{ne^2}{m\nu_m} = \frac{1}{\eta} \tag{4.46}$$

η is by definition the **specific resistance** . The collision frequency is given by:

$$\nu_m = n\langle\sigma_{coll} v\rangle \tag{4.47}$$

Here, σ_{coll} is the cross-section, and n is the density of the collision partners, which in this case are the charge carriers themselves. Equations 4.46 and 4.47 together give:

$$\eta = \frac{m}{ne^2}\nu_m = \frac{m}{ne^2}n\langle\sigma_{coll} v\rangle = \frac{m}{e^2}\langle\sigma_{coll} v\rangle \tag{4.48}$$

Here, the density can be canceled, since the carriers of the current are also the collision partners. This is in contrast to diffusion via collisions with neutrals. Finally, the cross-section for momentum transfer through small-angle collisions is used:

$$\sigma_{90^\circ}|_m = \frac{8}{\pi}b_0^2 \ln\Lambda \tag{4.49}$$

b_0 is the distance of closest approach ($b_0^2 \sim v^{-4}$). The velocity is expressed by a temperature, and the **specific resistance according to Spitzer** is obtained:

$$\boxed{\eta \simeq \frac{\pi e^2 m^{1/2}}{(4\pi\epsilon_0)^2 (k_B T_e)^{3/2}} \ln \Lambda} \tag{4.50}$$

The specific resistance scales as follows:

- The resistance does not depend on the charge carrier density, since charge carriers simultaneously carry current but are also collision partners. That is, the current does not increase with increasing charge carrier density. This is in contrast to current transport in partially ionized plasmas, where the current is limited by collisions with the neutral gas. Here, the current increases with increasing electron density, as sketched in Fig. 4.7.

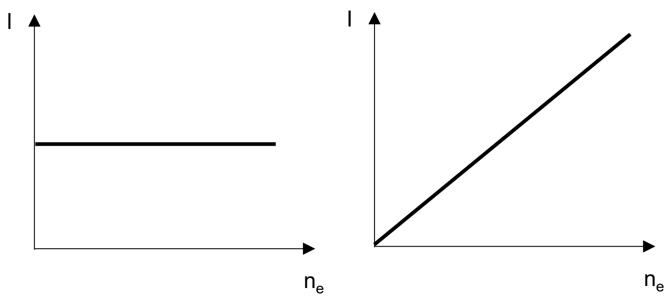

Figure 4.7: Dependence of the current on the electron density in fully and partially ionized plasmas.

- The specific resistance scales with v^{-3}. That is, fast electrons carry the current. If a disturbance in the electric field occurs that leads to an acceleration of the particles, it can happen that these are no longer decelerated by friction and can leave the plasma. This is a kinetic effect: a deviation from the Maxwell distribution of the electrons in the high-energy region of the distribution function cannot be compensated by thermalization. These fast electron beams are referred to as *runaway electrons*, which can reach relativistic energies. At these high energies, however, bremsstrahlung losses become significant. This bremsstrahlung is partly re-absorbed in a fusion plasma and the radiation of the electrons is thus not completely lost to the energy content of the fusion plasma.

- The specific resistance scales with $T_e^{-3/2}$, i.e., at high plasma temperatures, ohmic heating becomes increasingly ineffective. For this reason, in today's fusion experiments, the injection of waves or, in particular, the injection of high-energy neutral particles are the most important heating methods.

The last two points are a direct consequence of the property of the Coulomb cross-section to become very small at high energies ($\sigma \sim v^{-4}$).

4.2.3 Diffusion Perpendicular to the B Field, Magnetohydrodynamics

After these preliminary remarks, we are now able to set up the momentum balance equations for the electron and ion fluid in fully ionized plasmas. For ions, we have

$$Mn\frac{\partial v_i}{\partial t} = en(E + v_i \times B) - \nabla p_i + P_{ie} \tag{4.51}$$

The last term describes the momentum transfer in collisions of the ions with electrons. A term for collisions of ions with ions does not occur, since no transport takes place here! Analogously, an expression for the momentum balance of the electrons is obtained:

$$mn\frac{\partial v_e}{\partial t} = -en(E + v_e \times B) - \nabla p_e + P_{ei} \tag{4.52}$$

Since we consider elastic collisions between electrons and ions, by symmetry, we must have:

$$P_{ei} = -P_{ie} \tag{4.53}$$

Through this symmetry, we can now create new simplified equations by adding and subtracting the momentum balance of the electrons and ions, respectively. By adding Eqs. 4.51 and 4.52, the following expression is obtained:

$$n\frac{\partial}{\partial t}(Mv_i + mv_e) = en(v_i - v_e) \times B - \nabla(p_e + p_i) \tag{4.54}$$

The *electrical* current density is given by:

$$j = en(v_i - v_e) \tag{4.55}$$

That is, electrical current only occurs if the velocities of the ions and electrons are different. If this is not the case, the plasma as a whole fluid can flow, but no net transport of charges occurs.
The total pressure is

$$p = p_i + p_e \tag{4.56}$$

and the center-of-mass velocity is

$$v = \frac{1}{\rho}(n_i M v_i + n_e m v_e) \tag{4.57}$$

with the mass density $\rho = n_i M + n_e m$. With this notation, the following momentum balance for the center-of-mass velocity of the fluid is obtained:

$$\boxed{\rho \frac{\partial v}{\partial t} = \vec{j} \times \vec{B} - \nabla p} \tag{4.58}$$

This is referred to as the **single-fluid equation** . Fig. 4.8 illustrates how external electric or magnetic fields can influence the center-of-mass velocity or charge transport:

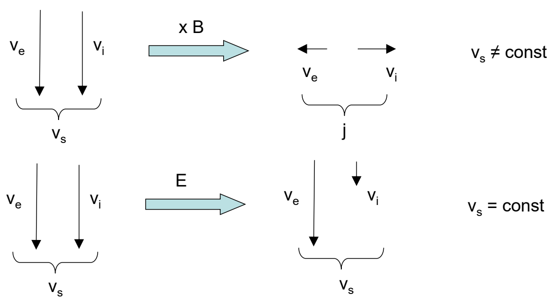

Figure 4.8: Illustration of the single-fluid equation. Only a magnetic field changes the center-of-mass velocity of the fluid and a current is created.

- *Magnetic field* If one considers a plasma in which the electrons and ions move uniformly, the Lorentz force deflects positive and negative charge carriers in different directions. This changes the center-of-mass velocity.

- *Electric field* If one considers a plasma in which the electrons and ions move uniformly, an electric field increases the velocity of the electrons, for example, but decreases that of the ions. Net, this does not result in a change in the center-of-mass velocity.

A second relationship of magnetohydrodynamics (MHD) can be derived by forming the difference between Eqs. 4.51 and 4.52. Here, Eq. 4.51 is multiplied by the electron mass m and Eq. 4.52 by the ion mass M. Thus, one obtains:

$$\begin{aligned} Mmn\frac{\partial}{\partial t}(v_i - v_e) &= en(M+m)\vec{E} + en(m\vec{v}_i + M\vec{v}_e)\times\vec{B} \\ &\quad -m\nabla p_i + M\nabla p_e - (M+m)P_{ei} \end{aligned} \tag{4.59}$$

The individual terms in this equation can be further simplified. The mass density is:

$$\rho = n(M+m) \tag{4.60}$$

The collision term is

$$P_{ei} = mn(v_i - v_e)\nu_m = mn(v_i - v_e)\frac{ne^2}{m}\eta = e^2n^2(v_i - v_e)\eta = en\eta\vec{j} \tag{4.61}$$

At this point, it is important to note that η itself is a constant and independent of n. The term $mv_i + Mv_e$ in Eq. 4.59 gives:

$$mv_i + Mv_e = Mv_i + mv_e + M(v_e - v_i) + m(v_i - v_e) = \frac{1}{n}\rho v - (M-m)\frac{j}{ne} \tag{4.62}$$

These transformations are substituted back into Eq. 4.59, divided by $(e\rho)$, and one obtains

$$\begin{aligned} \frac{Mmn}{e\rho}\frac{\partial}{\partial t}\frac{\vec{j}}{en} &= \vec{E} + \vec{v}\times\vec{B} - \frac{M-m}{e\rho}\vec{j}\times\vec{B} \\ &\quad -\frac{m}{e\rho}\nabla p_i + \frac{M}{e\rho}\nabla p_e - (M+m)en\eta\vec{j}\frac{1}{e\rho} \end{aligned} \tag{4.63}$$

Neglecting the time derivative, which here corresponds to the inertia term, and under the assumption that $M \gg m$, one obtains the so-called **generalized Ohm's law** :

$$\boxed{\vec{E} + \vec{v}\times\vec{B} = \eta\vec{j} + \frac{1}{en}\left(\vec{j}\times\vec{B} - \nabla p_e\right)} \tag{4.64}$$

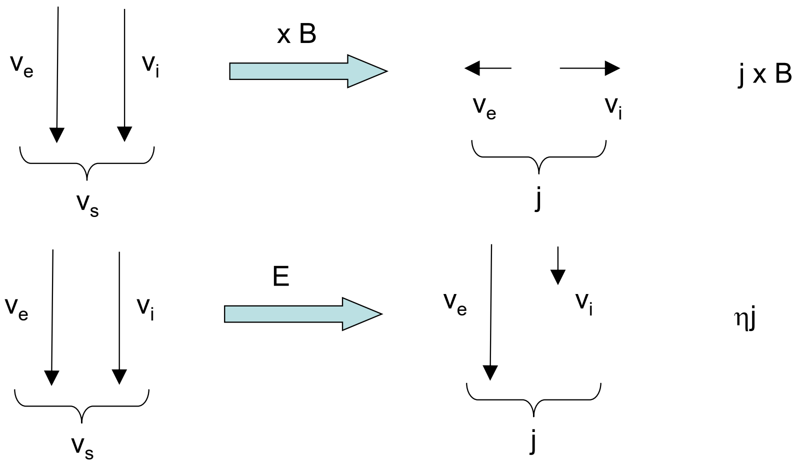

Figure 4.9: Illustration of the generalized Ohm's law. An electric or magnetic field generates a current flow in the plasma.

In most cases, the first term on the right side is dominant. The second term is referred to as the Hall term. Fig. 4.9 describes intuitively how external fields can drive a current in the plasma.

- *Electric field* Again, consider a plasma in which the electrons and ions initially move uniformly. An electric field increases the velocity of the electrons, for example, but decreases that of the ions. This corresponds to a current, since the term $v_i - v_e$ is now different from zero.

- *Magnetic field* The Lorentz force deflects positive and negative charge carriers in different directions. This creates a current that is stronger the greater the magnetic field and the center-of-mass velocity is.

The system of MHD equations is closed by the conservation equations for mass and charge. Thus, one obtains:

$$\rho\frac{\partial\vec{v}}{\partial t} = \vec{j}\times\vec{B} - \nabla p \tag{4.65}$$

$$\vec{E} + \vec{v}\times B = \eta\vec{j} + \frac{1}{en}\left(\vec{j}\times\vec{B} - \nabla p_e\right) \tag{4.66}$$

$$\frac{\partial\rho}{\partial t} + \nabla(\rho\vec{v}) = 0 \tag{4.67}$$

$$\frac{\partial \sigma}{\partial t} + \nabla j = 0 \tag{4.68}$$

In the last equation, σ denotes the charge of the fluid $\sigma = e(n_e - n_i)$
Based on the MHD equations, we can now describe the diffusion perpendicular to the magnetic field. Since we now consider the entire plasma as a single-fluid problem, the diffusion automatically corresponds to the transport of both charge carriers together, i.e., an ambipolar diffusion. The equations for describing the transport are the momentum balance 4.58 and Ohm's law 4.64. We consider the steady-state case, so the time derivatives are zero. We obtain:

$$\vec{j} \times \vec{B} = \nabla p \tag{4.69}$$

$$\vec{E} + \vec{v} \times \vec{B} = \eta \vec{j} \tag{4.70}$$

The Hall term and the pressure gradient were neglected in Eq. 4.70 compared to ηj. In the direction parallel to the magnetic field, we simply obtain

$$E_{\|} = \eta_{\|} j_{\|} \tag{4.71}$$

In the direction perpendicular to $\vec{B}$, we obtain the velocity of the fluid by multiplying Ohm's law 4.64 by $\times \vec{B}$:

$$\vec{E} \times \vec{B} + (\vec{v}_\perp \times \vec{B}) \times \vec{B} = \eta_\perp (\vec{j} \times \vec{B}) = \eta_\perp \nabla p \tag{4.72}$$

The double cross product is resolved again, where the term $\vec{v}_\perp \vec{B}$ becomes zero, since the components are perpendicular to each other. That is, from the double cross product, only a term $-\vec{v}_\perp B^2$ remains. Thus, the fluid velocity perpendicular to the magnetic field is:

$$\vec{v}_\perp = \frac{\vec{E} \times \vec{B}}{B^2} - \frac{\eta_\perp}{B^2} \nabla p \tag{4.73}$$

Here, two terms arise. The first term corresponds to the $\vec{E} \times \vec{B}$ drift, and the second term corresponds to diffusion driven by a density gradient.

Diffusion Term

First, consider the second term in Eq. 4.73, which corresponds to diffusion. A gradient in pressure or density drives a particle flux Γ:

$$\Gamma = n \vec{v}_\perp = -\eta_\perp \frac{n(k_B T_i + k_B T_e)}{B^2} \nabla n \tag{4.74}$$

Here, isothermal state changes were assumed. In the case of an adiabatic state change of the ions, one obtains with the adiabatic coefficient γ:

$$\Gamma = n\vec{v}_\perp = -\eta_\perp \frac{n(\gamma k_B T_i + k_B T_e)}{B^2} \nabla n \tag{4.75}$$

The diffusion coefficient perpendicular to the magnetic field in fully ionized plasmas is thus given for isothermal changes as:

$$D_\perp = \frac{\eta n}{B^2} \sum_i k_B T_i \tag{4.76}$$

where the index i describes the type of charge carrier involved. Compared to the diffusion coefficients for transport in partially ionized plasmas with

$$D_\perp = \frac{kT}{m\nu_m} \frac{1}{1+\omega_c^2 \tau_m^2} \tag{4.77}$$

An explicit dependence on the ion density is now obtained, since the ions are collision partners here! Moreover, the diffusion coefficient decreases with increasing temperature in fully ionized plasmas, since the temperature dependence of η is stronger than the temperature dependence in the numerator. This is again due to the strong velocity dependence of the Coulomb cross-section.

Due to the explicit density dependence of the diffusion coefficient, the diffusion equation can no longer be solved as easily as in the case of partially ionized plasmas. One initially obtains:

$$\frac{\partial n}{\partial t} + \nabla(-D\nabla n) = 0 \tag{4.78}$$

with a diffusion coefficient that depends on the density n:

$$D = \frac{\eta}{B^2} n \sum_n K_B T_n = 2nA \tag{4.79}$$

Thus, the continuity equation becomes

$$\frac{\partial n}{\partial t} = \nabla(2An\nabla n) = A\nabla^2 n^2 \tag{4.80}$$

With a separation ansatz according to

$$n = T(t)S(x) \tag{4.81}$$

one obtains

$$\frac{1}{T^2}\frac{\partial T}{\partial t} = \frac{A}{S}\nabla^2 S^2 = -\frac{1}{\tau} \tag{4.82}$$

Here, both sides must again yield a constant, which we define as -1/τ. The time dependence can still be easily solved. One obtains:

$$\frac{1}{T} = \frac{1}{T_0} + \frac{t}{\tau} \tag{4.83}$$

That is, for very large times t, the density profile decays with $T \propto 1/t$ and not exponentially, as in the case of transport in partially ionized plasmas. The spatial dependence can no longer be easily solved.

Drift Term, Bohm Diffusion

The diffusion coefficient for describing the perpendicular transport in fully ionized plasmas decreases with increasing temperature and increasing B field squared. This is in itself favorable, as at high plasma temperatures and high magnetic fields, as in fusion, good confinement should be ensured. According to this estimate, one would expect fusion conditions in small fusion experiments with diameters of about 1 meter. Many experiments in the 1950s were initially designed on this basis. However, in the experiment, it turned out that, on the one hand, the perpendicular transport increases with temperature instead of decreasing, and on the other hand, the dependence scales more with 1/B than with 1/B^2.

The assumption is that the transport perpendicular to the magnetic field is given by the first drift term in Eq. 4.73. The dependence on temperature and magnetic field was initially described empirically by the **Bohm diffusion** with

$$D_\perp = \frac{1}{16}\frac{k_B T}{eB} = D_{\text{Bohm}} \tag{4.84}$$

The drift term in Eq. 4.73 is:

$$\vec{v}_\perp = \frac{\vec{E}\times\vec{B}}{B^2} \tag{4.85}$$

But where does the electric field come from? This can arise from disturbances in the plasma equilibrium, plasma waves, and instabilities. A disturbance in quasi-neutrality automatically creates an electric field.

Such a disturbance creates a change in the local particle density by δn and thus a particle flux according to:

$$\delta\Gamma_\perp = \delta n \frac{\vec{E}\times\vec{B}}{B^2} \propto \delta n \frac{E}{B} \tag{4.86}$$

The electric field can be created by a displacement of the electrons over a characteristic length R, analogous to the Debye shielding. The potential energy corresponding to this displacement and the thermal energy must be equal $e\Phi = k_B T_e$. Therefore, we have:

$$E = \frac{\Phi}{R} \simeq \frac{k_B T_e}{eR} \tag{4.87}$$

Thus, the following expression for the particle flux driven by this disturbance is obtained:

$$\Gamma_\perp = \frac{\delta n}{R}\frac{k_B T_e}{eB} \simeq \frac{k_B T}{eB}\nabla n \tag{4.88}$$

Apart from the empirical factor 1/16, this corresponds exactly to the scaling of Bohm diffusion. That is, all processes that lead to electric fields in the plasma can dominantly contribute to the perpendicular transport.

The transport perpendicular to the magnetic field can exhibit some peculiarities, especially in toroidal arrangements. Due to the shearing of the field lines, a particle on its trajectory sees alternately high and low B fields. If its parallel velocity is too small, it can be trapped like in a mirror machine and oscillate between two turning points. This pendulum motion must still be superimposed by the curvature drift perpendicular to the magnetic field direction. This leads to a particle trajectory that, when projected onto the cross-section of the torus, has a banana-shaped contour.

On this contour trajectory, a particle runs from the center to the edge of the discharge and back. That is, the step size for the perpendicular transport is now rather the width of this banana-shaped path. This is referred to as **neoclassical transport** . If the collision frequency becomes very large, the mean free path is very small, and the particles cannot complete a full orbit in a mirror arrangement. The perpendicular transport now again has the step size of the Larmor radius.

4.3 Time-Dependent Effects of MHD

Based on the MHD equations, one can also discuss the case of how a magnetized plasma reacts to temporal changes in the field or the plasma position. We start again with Ohm's law:

$$\vec{E} + \vec{v}\times\vec{B} = \eta\vec{j} \tag{4.89}$$

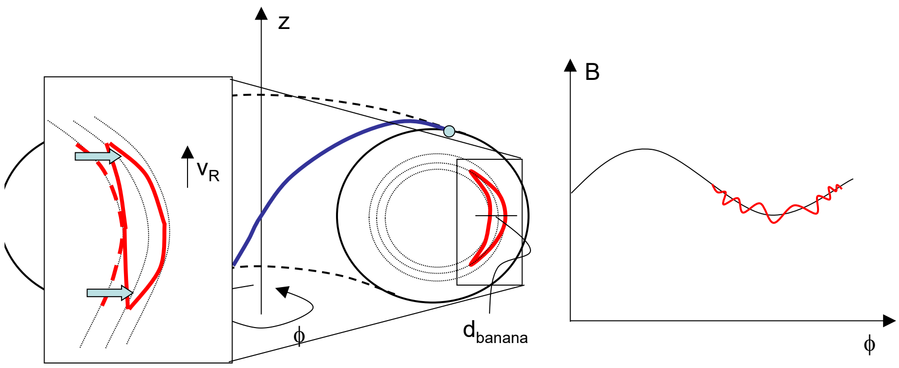

Figure 4.10: In toroidal plasmas where the magnetic field is sheared, particles can be trapped in mirror fields. Due to the curvature drift, they do not remain on a magnetic surface but also oscillate between adjacent magnetic surfaces. This short circuit perpendicular to the magnetic field is referred to as neoclassical transport.

in conjunction with Ampere's law (neglecting the displacement current):

$$\nabla \times \vec{B} = \mu_0 \vec{j} \tag{4.90}$$

one obtains

$$\vec{E} + \vec{v} \times \vec{B} = \frac{\eta}{\mu_0} \nabla \times \vec{B} \tag{4.91}$$

Now, both sides are multiplied by $\nabla\times$ from the left, and one obtains:

$$\nabla \times \vec{E} + \nabla \times \vec{v} \times \vec{B} = \frac{\eta}{\mu_0} \nabla \times (\nabla \times \vec{B}) \tag{4.92}$$

From this, with $\nabla \times E = -\dot{B}$ and $\nabla B = 0$, one obtains:

$$\boxed{-\frac{\partial B}{\partial t} + \nabla \times \vec{v} \times \vec{B} = \frac{\eta}{\mu_0}(-\nabla^2 B)} \tag{4.93}$$

Two cases can be considered. On the one hand, the case of a stationary fluid ($v = 0$) and on the other hand, the case of infinite conductivity ($\eta = 0$).

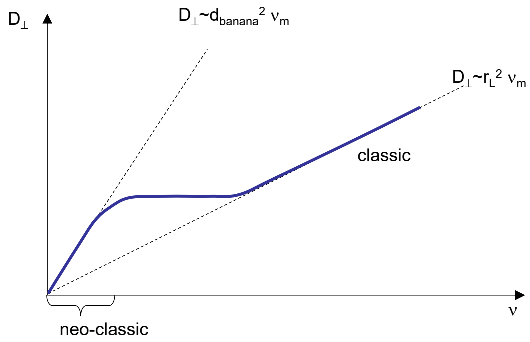

Figure 4.11: Neoclassical transport is particularly visible at low collision frequencies.

4.3.1 Magnetic Field Diffusion

We first assume that the plasma is at rest and thus $v = 0$ applies. Thus, we obtain:

$$\frac{\partial B}{\partial t} = \frac{\eta}{\mu_0} \nabla^2 B \tag{4.94}$$

This is a diffusion equation for the magnetic field and describes the penetration of the magnetic field into a plasma, as illustrated in Fig. 4.12. This equation is linearized and describes the decay of the magnetic field over a characteristic length l in the plasma. One obtains:

$$\frac{\partial B}{\partial t} = \frac{\eta}{\mu_0} B \frac{1}{l^2} \tag{4.95}$$

This equation has the solution

$$B = B_0 e^{-t/\tau} \tag{4.96}$$

with

$$\tau = \frac{\mu_0 l^2}{\eta} \tag{4.97}$$

That is, the magnetic field penetrates the plasma, and through the driving of dissipative currents ($\eta \neq 0$), magnetic field energy is converted into thermal energy. This transition from magnetic field energy to heat can be derived from the dissipated Ohmic power P:

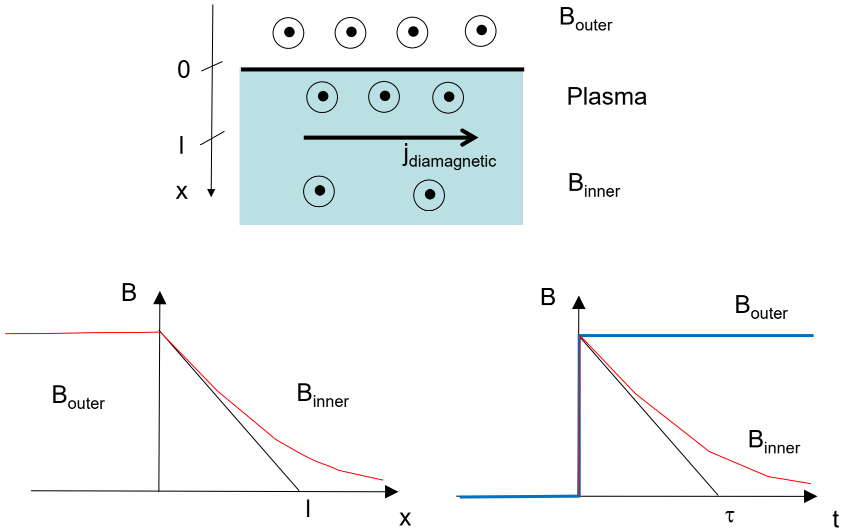

Figure 4.12: Diffusion of the magnetic field into a plasma.

$$P = \eta j^2 \tag{4.98}$$

With $\mu_0 \vec{j} = \nabla \times \vec{B} = \frac{B}{l}$ and $\tau = \frac{\mu_0 l^2}{\eta}$, the dissipated energy $\Delta E = P\tau$ is:

$$\Delta E = \eta j^2 \tau = \eta \left(\frac{B}{\mu_0 l}\right)^2 \left(\frac{\mu_0 l^2}{\eta}\right) = \frac{B^2}{\mu_0} \tag{4.99}$$

One can see that the dissipated energy exactly corresponds to the magnetic field energy $\frac{B^2}{\mu_0}$.

4.3.2 Frozen-in Flux

In the so-called **ideal MHD** , one assumes an infinite conductivity of the plasma. Now, $\eta = 0$, but $\vec{v}$ can be arbitrary.

$$\frac{\partial B}{\partial t} = \nabla \times (\vec{v} \times \vec{B}) \tag{4.100}$$

Thus, one obtains

$$\frac{\partial B}{\partial t} = (\vec{B} \cdot \nabla)\vec{v} + \vec{v}(\nabla \cdot \vec{B}) - (\vec{v} \cdot \nabla)\vec{B} - \vec{B}(\nabla \cdot \vec{v}) \tag{4.101}$$

$$= (\vec{B}\nabla)\vec{v} - \vec{B}(\nabla\vec{v}) \tag{4.102}$$

Here, the term $\vec{v}(\nabla\vec{B})$ vanishes because $divB = 0$. The term $(\vec{v}\nabla)\vec{B}$ vanishes because the change in B is perpendicular to $\vec{v}$. With the continuity equation for the mass density of the flowing plasma.

$$\frac{\partial\rho}{\partial t} + \nabla\vec{v}\rho = 0 \tag{4.103}$$

The term $\vec{v}\nabla\rho$ can also be approximated to be zero. Substituting this for the term $\nabla\vec{v}$ gives

$$\frac{\partial B}{\partial t} = (\vec{B}\nabla)\vec{v} + \vec{B}\frac{1}{\rho}\frac{\partial\rho}{\partial t} \tag{4.104}$$

With the relation

$$\frac{d}{dt}\frac{B}{\rho} = \frac{1}{\rho}\frac{\partial B}{\partial t} - \frac{1}{\rho^2}B\frac{\partial\rho}{\partial t} \tag{4.105}$$

one obtains

$$\frac{d}{dt}\left(\frac{B}{\rho}\right) = \left(\frac{\vec{B}}{\rho}\nabla\right)\vec{v} \tag{4.106}$$

Since the plasma flow is usually bound to the magnetic field lines, the right side is very small or becomes zero. Thus, the ratio of the magnetic field to the mass density of the plasma remains constant. This is referred to as **frozen-in flux** . That is, if the plasma moves, the magnetic field is carried along with it, and vice versa.

$$\boxed{\frac{\vec{B}}{\rho} = \text{const.}} \tag{4.107}$$

The phenomenon of frozen-in flux can explain the presence of magnetic fields in interstellar space: during supernova explosions, the ejected plasma carries the star's magnetic field out into interstellar space.

4.4 Equilibria and Instabilities

4.4.1 Stability of a Cylindrical Plasma Column

If one considers a cylindrical plasma column in a magnetic field, the following equations from MHD apply in equilibrium:

$$\vec{j} \times \vec{B} = \nabla p \tag{4.108}$$

$$\nabla \times \vec{B} = \mu_0 \vec{j} \tag{4.109}$$

From this, it follows that

$$\vec{j}_\perp = -\frac{\nabla p \times \vec{B}}{B^2} \tag{4.110}$$

In addition, the generalized Ohm's law applies.

$$\vec{E} + \vec{v} \times \vec{B} = \eta_\perp \vec{j}_\perp + \eta_\| \vec{j}_\| \tag{4.111}$$

Thus, the velocity (see Fig. 4.13) perpendicular to the axis is obtained as:

$$v_\perp = \underbrace{\frac{\vec{E} \times \vec{B}}{B^2}}_{shortens\ theplasma\ together} - \underbrace{\frac{\eta_\perp}{B^2}\nabla p}_{drives\ plasma\ apart} \tag{4.112}$$

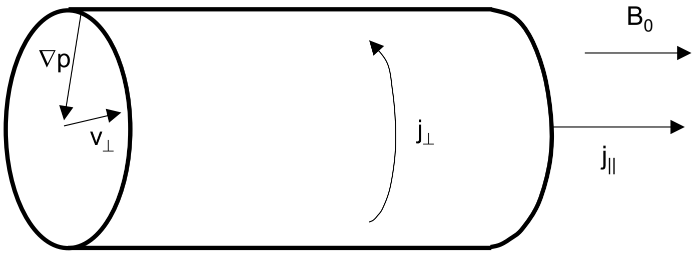

Figure 4.13: Cylindrical plasma column

In equilibrium, one can set $v_\perp = 0$. These equilibria are used to compress a plasma in the so-called **pinch discharges** (Fig. 4.14). By time-varying magnetic fields, a diamagnetic current is induced that leads to a pinching of the plasma. In the Θ-pinch, this is a ring current perpendicular to the magnetic field. In the z-pinch, the current is an axial current. The compression of the plasma is usually triggered by a high current pulse. If the resulting variation in the magnetic field is faster than the penetration time of this increased magnetic field into the plasma, the diamagnetic currents pinch the plasma.

The equilibrium of the plasma column is unstable against its deflection during pinching. If the magnetic field increases locally, this increases the $\vec{j} \times \vec{B}$ term.

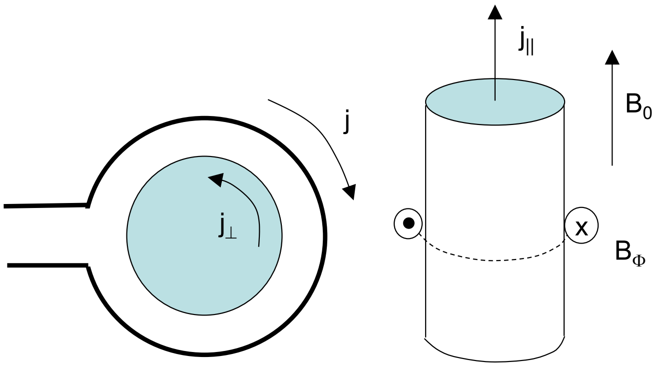

Figure 4.14: Θ-pinch, z-pinch

A pressure increase cannot compensate for this, since the pressure quickly equalizes along the plasma column (the plasma as an incompressible fluid). A so-called **sausage instability** arises (Fig. 4.15). If a kink occurs, the magnetic field increases on one side while it decreases on the other side. Thus, the $\vec{j} \times \vec{B}$ term wins on one side, while the ∇p term dominates on the opposite side (Fig. 4.15).

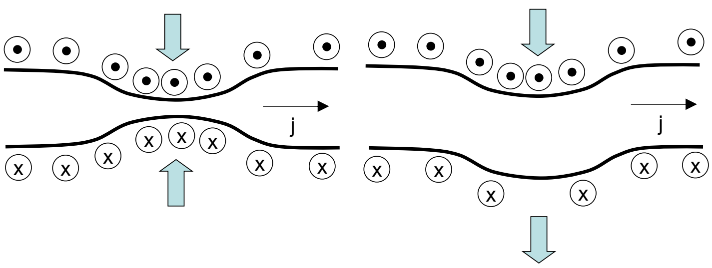

Figure 4.15: Sausage and kink instability

The kink instability is counteracted by the tension of the field lines. A deflection of a plasma column increases the magnetic field energy, since the magnetized volume becomes larger.

4.4.2 Instabilities

In the following, we want to consider instabilities. As already discussed, in magnetized plasmas, one observes a different dependence for perpendicular diffusion than one would classically expect. One possible explanation is an $\vec{E} \times \vec{B}$ driven diffusion, the Bohm diffusion. The necessary electric fields can arise from instabilities, which are discussed below.
The principal approach to describing instabilities is initially again the momentum balance, which is developed into small disturbances in density and velocity. With a Fourier ansatz, one obtains a dispersion relation. If ω can become imaginary, it depends on the sign whether this disturbance is damped or whether it grows into an instability.

Rayleigh-Taylor Instability

In the Rayleigh-Taylor instability, we consider a plasma boundary in a gravitational field according to Fig. 4.16

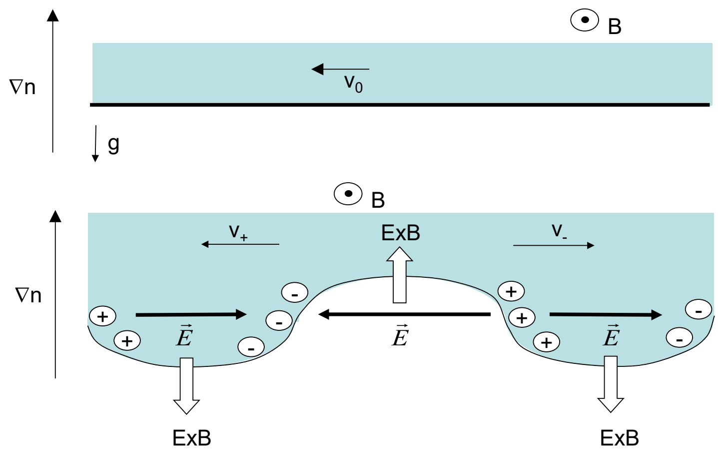

Figure 4.16: Rayleigh-Taylor instability

A flow occurs in the plasma according to the gravitational drift with:

$$v_0 = \frac{m\vec{g} \times \vec{B}}{|q|B^2} \tag{4.113}$$

The momentum balance of the ions for $T_e = T_i = 0$ is

$$Mn\left[\frac{\partial \vec{v}}{\partial t} + \vec{v}\nabla\vec{v}\right] = en(\vec{E} + \vec{v} \times \vec{B}) + Mn\vec{g} \tag{4.114}$$

The velocity and density are developed with $v = v_0 + v_1$ and $n = n_0 + n_1$. In equilibrium without disturbance, one obtains:

$$Mn_0\left[\vec{v_0}\nabla\vec{v_0}\right] = en_0(\vec{v_0}\times\vec{B}) + Mn_0\vec{g} \tag{4.115}$$

In equilibrium, there is no electric field present. If a disturbance of the plasma boundary now occurs, an electric field arises according to Fig. 4.16. Due to the inertia of the ions, the charge distribution is not compensated quickly enough by the electrons. The disturbance can be written as:

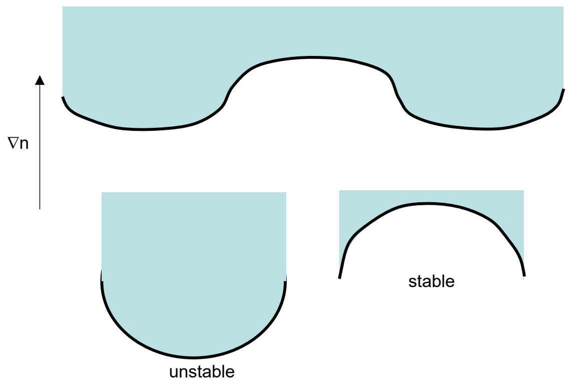

Figure 4.17: Rayleigh-Taylor instability occurs when the density gradient and an additional force are oppositely directed.

$$\begin{aligned} M(n_0+n_1)\left[\frac{\partial(\vec{v}_0+\vec{v}_1)}{\partial t} + (\vec{v}_0+\vec{v}_1)\nabla(\vec{v}_0+\vec{v}_1)\right] &= \\ e(n_0+n_1)(E_1 + (\vec{v}_0+\vec{v}_1)\times\vec{B}_0) + M(n_0+n_1)\vec{g} & \end{aligned} \tag{4.116}$$

One multiplies Eq. 4.115 by $1{+}n_1/n_0$ and subtracts it from 4.116 and obtains for the left side:

$$M(n_0+n_1)\left[\frac{\partial(\vec{v}_0+\vec{v}_1)}{\partial t} + \vec{v}_0\nabla(\vec{v}_0+\vec{v}_1) + \vec{v}_1\nabla(\vec{v}_0+\vec{v}_1)\right] = \tag{4.117}$$

Here, one can set $n_0 + n_1 \simeq n_0$, $\vec{v}_1\nabla\vec{v}_1 \simeq n_0$, and $\nabla v_0 = 0$ in each case and obtains overall:

$$Mn_0\left[\frac{\partial\vec{v}_1}{\partial t} + \vec{v}_0\nabla v_1\right] = en_0(\vec{E}_1 + \vec{v}_1\times\vec{B}_0) \tag{4.118}$$

In this formulation, the term $\vec{g}$ has now disappeared. However, it should be noted that the velocity $\vec{v}_0$ is always a function of $\vec{g}$. In the Fourier space, one obtains:

$$M(\omega - \vec{k}\vec{v}_0)\vec{v}_1 = ie(\vec{E}_1 + \vec{v}_1 \times \vec{B}_0) \tag{4.119}$$

In the y-direction, one obtains:

$$M(\omega - \vec{k}\vec{v}_0)v_{1,y} = ie(E_{1,y} - v_{1x}B_z) \tag{4.120}$$

In the x-direction,

$$M(\omega - kv_0)v_{1,x} = iev_{1,y}B_z \tag{4.121}$$

Thus, one obtains:

$$M(\omega - kv_0)v_{1,x} = ieB_z\frac{ie\left(E_y - v_{1,x}B_z\right)}{M(\omega - kv_0)} \tag{4.122}$$

This can be solved to:

$$M^2\frac{(\omega - kv_0)^2}{e^2B^2}v_{1,x} = -\frac{E_y}{B_z} + v_{1,x} \tag{4.123}$$

With $\Omega_c = \frac{eB}{M}$ and $\Omega_c^2 \gg (\omega - kv_0)^2$, one obtains the approximation:

$$v_{1,x} = \frac{E_y}{B_z} \tag{4.124}$$

$$v_{1,y} = -i\frac{\omega - kv_0}{\Omega_c}\frac{E_y}{B_z} \tag{4.125}$$

v_x corresponds to the $E \times B$ drift, and v_y corresponds to the polarization drift in the oscillating field. For the electrons, one obtains:

$$v_{1x,e} = \frac{E_y}{B_z} \tag{4.126}$$

$$v_{1y,e} = 0 \tag{4.127}$$

The continuity equation can also be developed into the disturbance, and one obtains:

$$\frac{\partial n}{\partial t} + \nabla(n_0 + n_1)(v_0 + v_1) = 0 \tag{4.128}$$

This yields:

$$\frac{\partial n}{\partial t}+\nabla(v_0 n_0)+(v_0\nabla n_1)+n_1\nabla v_0+(v_1\nabla)n_0+n_0\nabla v_1+\nabla(n_1 v_1)=0 \quad (4.129)$$

Under the approximation that for terms of higher order $n_1 v_1 \ll n_1 v_0 \ll n_0 v_0$, $\nabla v_0 = 0$, and $\nabla n_0 \perp v_0$ holds, one obtains:

$$\frac{\partial n}{\partial t}+(v_0\nabla n_1)+(v_1\nabla)n_0+n_0\nabla v_1=0 \quad (4.130)$$

or in the Fourier space, for the ions, one obtains:

$$-i\omega n_{1,i}+ikv_0 n_{1,i}+v_{x,i}\frac{\partial n_0}{\partial x}+ikn_0 v_{y,i}=0 \quad (4.131)$$

For the electrons, the gravitational drift is very small, and thus $v_{0,e}=0$

$$-i\omega n_{1,e}+v_{x,e}\frac{\partial n_0}{\partial x}=0 \quad (4.132)$$

If one now substitutes the velocities into the continuity equations, one obtains for the ions:

$$(\omega-kv_0)n_{1,i}+i\frac{E_y}{B}\frac{\partial n_0}{\partial x}+ikn_0\frac{\omega-kv_0}{\Omega_c}\frac{E_y}{B}=0 \quad (4.133)$$

and for the electrons:

$$\omega n_{1,e}+i\frac{E_y}{B}\frac{\partial n_0}{\partial x}=0 \quad (4.134)$$

With $n_{1,e}=n_{1,i}$, one finally obtains

$$(\omega-kv_0)n_1-\omega n_1-kn_0\frac{\omega-kv_0}{\Omega_c}\omega\frac{n_1}{\frac{\partial n}{\partial x}}=0 \quad (4.135)$$

With the expression for v_0

$$v_0=\frac{M}{e}\frac{\vec{g}\times\vec{B}}{B^2}=-\frac{g}{\Omega_c}\hat{y} \quad (4.136)$$

Thus, one obtains the following dispersion:

$$\omega^2-kv_0\omega-g\frac{1}{n_0}\frac{\partial n_0}{\partial x}=0 \quad (4.137)$$

This is a quadratic equation in ω. The solution can become imaginary if:

$$-\vec{g}\frac{1}{n_0}\frac{\partial n_0}{\partial x}>\frac{1}{4}k^2 v_0^2 \quad (4.138)$$

That is, this equation can only be satisfied if the directions of $\vec{g}$ and $\frac{\partial n}{\partial x}$ are different. $kv_0 = \omega$ corresponds to the fundamental frequency of the wave at a small density gradient. That is, the above inequality is well satisfied when this frequency is very small. Thus, the Rayleigh-Taylor instability is dominant at low-frequency excitations. This is consistent with the polarization drift, which also only becomes dominant at slowly varying fields.
This instability has great importance for the optimization of a toroidal plasma. By shearing the field lines, the plasma is repeatedly brought to the inside of the torus to compensate for the $E \times B$ drift (see Chap. 2). On the outside of the torus, the centrifugal force and the density gradient point in opposite directions. Thus, this area is susceptible to a Rayleigh-Taylor instability. With a small shearing of the field lines (small rotational transform q, see Chap. 9), particles move on their magnetic field line for a longer time on the outside. That is, a corresponding disturbance of these trajectories has a long wavelength and is low-frequency. These are prerequisites for the occurrence of a Rayleigh-Taylor instability. This can be suppressed by choosing a larger shearing of the field lines and thus keeping the wavelength of a possible instability short. This makes the formation of the instability more difficult. Thus, a natural lower limit for the shearing (or rotational transform q) is obtained below which a fusion plasma becomes unstable.

Drift Waves

Another important instability that limits the energy confinement and particle confinement in a fusion plasma is the drift wave instability. Consider a cylindrical plasma column in the z-direction. In equilibrium, the contour of constant density (isobar) is symmetric to the cylinder axis. Now, let this contour be disturbed, resulting in a density fluctuation around the circumference of the column that is twisted relative to the longitudinal axis as sketched in Fig. 4.18 ("twisted Greek column").
This has fundamental consequences for the development of the instability. The electrons can quickly compensate for the density fluctuation *along the magnetic field*: the motion of the electrons along the axial magnetic field occurs quickly, as it is driven by a gradient in the density. This diffusion to regions of lower density occurs ambipolar, as the ions follow the electron motion. If one considers the isobars of the electrons and ions, a density disturbance *only* in the ion density around the circumference is obtained, while the electrons compensate for this density disturbance by diffusion. The isobar of the electrons remains cylindrical. If one now considers a cross-section of the torus, one recognizes regions with a positive and a negative excess of charge carriers, as illustrated in Fig. 4.18.

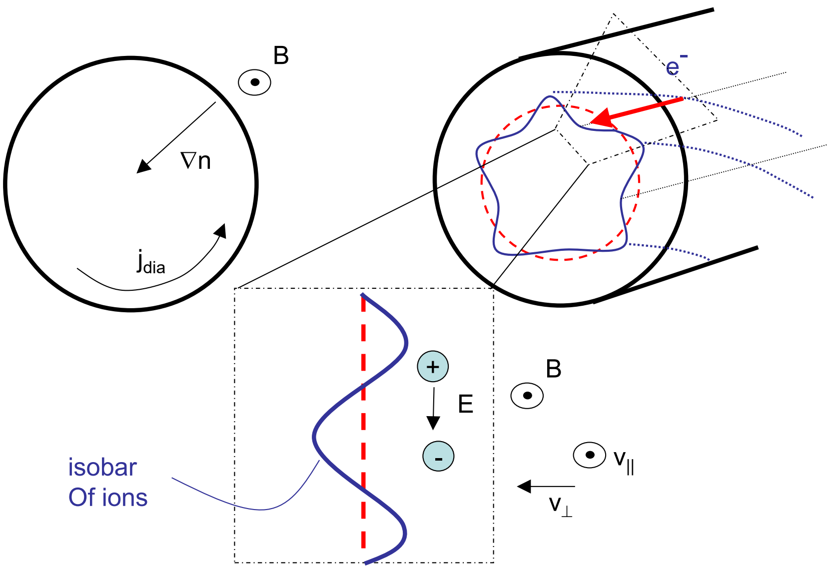

Figure 4.18: Drift wave instability

The equation of motion of the ions along the axis of the plasma column corresponds to ambipolar diffusion. This can be written as:

$$Mn_0\frac{\partial v_\parallel}{\partial t} = -\nabla p \tag{4.139}$$

In the Fourier space, one obtains:

$$-Mn_0 i\omega v_\parallel = -\nabla p = -ik_\parallel n_1 k_B T_e \tag{4.140}$$

The pressure was expressed here by the electron pressure, since the electrons follow the gradient and, through the resulting electric field, pull the ions along, corresponding to ambipolar diffusion. Thus, one obtains

$$v_\parallel = \underbrace{\frac{k_B T_e}{M}}_{c_s^2} k_\parallel \frac{n_1}{n_0}\frac{1}{\omega} \tag{4.141}$$

With c_s the ion sound velocity. Perpendicular to the external magnetic field, the $E \times B$ force acts according to:

$$Mn\frac{\partial v_\perp}{\partial t} = en(\vec{E} + \vec{v}_\perp \times \vec{B}) \tag{4.142}$$

The time derivative is a small term here, since only the velocity parallel to the magnetic field changes significantly.

$$v_\perp = \frac{E_y}{B} = -ik_\perp \frac{\Phi_1}{B} \tag{4.143}$$

The disturbance in the potential is now described by the Boltzmann relation, since the density gradient and potential along the magnetic field are compensated. One obtains:

$$n = n_0 + n_1 = n_0 exp\left[\frac{e\Phi_1}{k_B T_e}\right] \tag{4.144}$$

Developed for small disturbances, one obtains:

$$\frac{n_1}{n_0} = \frac{e\Phi_1}{k_B T_e} \tag{4.145}$$

Thus, one obtains

$$v_\perp = -ik_\perp \frac{n_1}{n_0}\frac{k_B T_e}{eB} \tag{4.146}$$

With the continuity equation, one obtains

$$\frac{\partial n}{\partial t} + \nabla(v_\perp + v_\parallel)n = 0 \tag{4.147}$$

In the Fourier space, this gives:

$$-i\omega n_1 + v_\perp \nabla n + v_\parallel i k_\parallel n_0 = 0 \tag{4.148}$$

Now, the velocities can be substituted to:

$$-\omega n_1 - k_\perp \frac{n_1}{n_0}\frac{k_B T_e}{eB}\nabla n + k_\parallel^2 c_s^2 n_0 \frac{n_1}{n_0}\frac{1}{\omega} = 0 \tag{4.149}$$

With $v_{dia} = -\frac{1}{n_0}\frac{k_B T_e}{eB}\nabla n$ the diamagnetic drift velocity, one obtains:

$$\omega^2 - k_\perp v_{dia}\omega - k_\parallel^2 c_s^2 = 0 \tag{4.150}$$

This quadratic equation has two real solutions. That is, damping or instability can only occur if one of the factors becomes imaginary.
This happens if a finite conductivity is assumed, so that a change in the potential is not instantaneously compensated by the electrons. This can be expressed by assigning a phase shift to the Boltzmann relation according to:

$$\frac{n_1}{n_0} = \frac{e\Phi}{k_B T_e}(1 - i\Delta) \tag{4.151}$$

Thus, the diamagnetic drift velocity formally becomes an imaginary number, and thus the solution for ω also becomes imaginary. This is referred to as **resistive drift wave instability** .
In the Rayleigh-Taylor instability, there were directly imaginary solutions for ω, so this is referred to as a *reactive* instability. In the drift wave instability, a coefficient must become imaginary. This is referred to as a *dissipative* instability.
The drift wave instability grows strongly according to the factor

$$\frac{k_B T_e}{n_0 e B} \nabla n \tag{4.152}$$

That is, if, for example, the density gradient becomes too large, the plasma becomes unstable. This process thus sets a maximum gradient at which a stable plasma can still be maintained. Because of these finite gradients, fusion reactors must be sufficiently large to guarantee fusion conditions given a central density and temperature.
The condition of a maximum gradient in the density means, however, that an improvement of the fusion plasma at the edge (e.g., higher plasma density) automatically also results in an increase in the density in the center of the fusion plasma. This improvement of the edge plasma can be achieved through special wall materials or through special heating methods.
In recent years, it has also been possible to create transport barriers in the plasma through special heating methods. These discontinuities in the density gradient significantly improve the plasma confinement. These are referred to as **internal transport barriers (ITB)**.

Plasma-Beam Instability

In the plasma-beam instability, an electron beam penetrating a plasma is considered. The ions are considered to be at rest, while the electrons are to have a velocity v_0, as sketched in Fig. 4.19:
For the stationary ions, we again write the momentum balance for the disturbed quantities:

$$M n_0 \frac{\partial v_{1,i}}{\partial t} = e n_0 E_1 \tag{4.153}$$

For the electrons, we have:

$$m n_0 \left[\frac{\partial v_{1,e}}{\partial t} + v_0 \nabla v_{1,e} \right] = -e n_0 E_1 \tag{4.154}$$

These momentum balances in the Fourier space thus give:

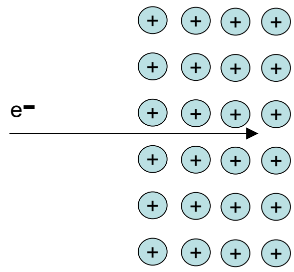

Figure 4.19: Plasma-beam instability

$$-i\omega M n_0 v_{1,i} = e n_0 E_1 \tag{4.155}$$

$$m n_0(-i\omega + ikv_0) v_{1,e} = -e n_0 E_1 \tag{4.156}$$

From the continuity equation of the ions, one obtains

$$\frac{\partial n_{1,i}}{\partial t} + n_0 \nabla v_{1,i} = 0 \tag{4.157}$$

In the Fourier space, this gives:

$$-i\omega n_{i,1} = -ikn_0 v_{1,i} \tag{4.158}$$

Thus, one obtains:

$$n_{1,i} = \frac{ien_0 k}{M\omega^2} E_1 \tag{4.159}$$

From the continuity equation of the electrons

$$\frac{\partial n_{1,e}}{\partial t} + v_0 \nabla n_{1,e} + n_0 \nabla v_{1,e} = 0 \tag{4.160}$$

One obtains in the Fourier space:

$$n_{1,e} = -\frac{ien_0 k}{m(\omega - kv_0)^2} E_1 \tag{4.161}$$

This corresponds to the disturbance of the ions only with a Doppler-shifted frequency ($\omega' = \omega - kv_0$). The densities are inserted into the Poisson equation, and one obtains from

$$\epsilon_0 \nabla E_1 = e(n_{1,i} - n_{1,e}) \tag{4.162}$$

the dispersion relation:

$$1 = \omega_p^2 \left[\frac{m/M}{\omega^2} + \frac{1}{(\omega - kv_0)^2} \right] \tag{4.163}$$

This equation can be solved graphically. One finds that an instability arises if

$$\Omega_p^2 = (\omega_p - kv_0)^2 \tag{4.164}$$

That is, if the plasma frequency of the ions is the same as the Doppler-shifted plasma frequency of the moving electrons, the instability occurs because the density fluctuations in both fluids (electrons and ions) are such that positive and negative charges exactly cancel each other out, and the potential energy is minimized (Fig. 4.20).

$$\langle \frac{1}{2} m \left(n_0 + n_1\right) \left(v_0 + v_1\right)^2 \rangle < \frac{1}{2} m n_0 v_0^2 \rangle \tag{4.165}$$

That is, the average energy in the system with disturbance (potential energy given by the potential and the kinetic energy given by v_1) becomes so much smaller than the energy in the system without disturbance. This has the consequence that the amplitude of an initial oscillation always becomes larger, and an instability arises.

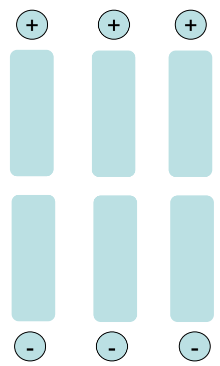

Figure 4.20: Fulfilment of the Poisson equation by electron oscillations in the moving reference system.

Chapter 5

Waves in Plasmas

The stability of a magnetized plasma is described by the fundamental equations of magnetohydrodynamics, assuming quasi-neutrality in general. This quasi-neutrality can be locally disturbed, and the associated electric and magnetic fields influence the surrounding plasma, leading to the generation of waves.

The propagation or absorption of waves is a central tool to observe the state of a plasma from the outside. Each plasma can be assigned a refractive index. By measuring the phase shift when an electromagnetic wave passes through a plasma, the plasma density can thus be determined. Moreover, injected waves can be absorbed by the plasma and thus serve as a heating method.

To describe waves in plasmas, we start with an equilibrium density n_0 that changes by a small amount n_1 when a wave passes through. This disturbance is described by a Fourier ansatz:

$$n_1 e^{i(kx-\omega t)} \tag{5.1}$$

The same disturbance ansatz is also chosen for the components of velocity, electric, and magnetic field.
We distinguish in principle:

- **parallel and perpendicular** for the direction of propagation with respect to the static magnetic field
- **longitudinal and transverse** for the direction of propagation with respect to the electric field
- **electrostatic and electromagnetic** In the case of electrostatic waves, only a disturbance in $\vec{E}_1$ occurs, while in the case of electromagnetic

waves, a disturbance in $\vec{E}$ and $\vec{B}$ occurs. In the case of electrostatic waves, this implies that the right side of the equation:

$$\nabla \times \vec{B} = \mu_0 \vec{j} + \mu_0 \epsilon_0 \dot{\vec{E}} \tag{5.2}$$

must become zero so that a change in $\vec{E}$ does not automatically cause a change in $\vec{B}$. This can only be ensured by a special choice of $\vec{j}$, which immediately illustrates that electrostatic waves can only occur in media. The typical example is an electrostatic plasma oscillation, in which $\vec{j}$ and $\vec{E}$ alternate as illustrated in Fig. 5.1.

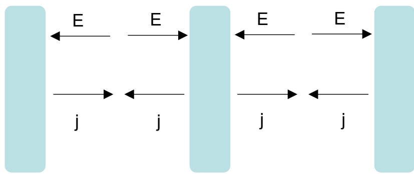

Figure 5.1: In electrostatic waves, $\dot{\vec{E}}$ and particle current $\vec{j}$ cancel each other out.

5.1 Electrostatic Waves

5.1.1 Electron Oscillations

The momentum balance for describing electron oscillations (assuming $T_e = 0$) is:

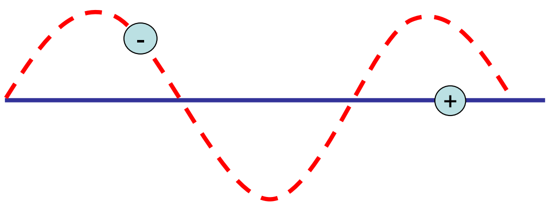

Figure 5.2: Electrostatic electron waves. The ions are considered to be stationary.

$$mn\left[\frac{\partial v_e}{\partial t} + v_e \nabla v_e\right] = -en\vec{E} \tag{5.3}$$

the continuity equation

$$\frac{\partial n_e}{\partial t} + \nabla n_e v_e = 0 \tag{5.4}$$

We develop into a small disturbance in density and velocity, with $v_0 = 0$ and $\nabla n_0 = 0$. The momentum balance thus gives:

$$m\left[\frac{\partial v_1}{\partial t} + \underbrace{v_1 \nabla v_1}_{\to 0 \text{ ,because } v_1^2 \ll v_1}\right] = -e\vec{E}_1 \tag{5.5}$$

and the particle balance

$$\frac{\partial n_e}{\partial t} + \nabla(n_0 v_1 + n_1 v_1) = 0 \tag{5.6}$$

The term $n_1 v_1$ can be neglected compared to $n_0 v_1$.

$$\frac{\partial n_e}{\partial t} + n_0 \nabla v_1 = 0 \tag{5.7}$$

With the Poisson equation for stationary ions ($n_{i,1} = 0$), we obtain

$$\nabla E_1 = -\frac{e}{\epsilon_0} n_1 \tag{5.8}$$

By transforming into the Fourier space, we obtain

$$-im\omega v_1 = -eE_1 \tag{5.9}$$

$$-i\omega n_1 = -n_0 ikv_1 \tag{5.10}$$

$$ikE_1\epsilon_0 = -en_1 \tag{5.11}$$

If we eliminate v_1, E_1, and n_1 from these equations, we obtain the solution for ω:

$$\boxed{\omega_p = \left(\frac{ne^2}{\epsilon_0 m}\right)^{1/2}} \tag{5.12}$$

This corresponds to the **plasma frequency** for an oscillation of the electrons in front of a stationary ion background.

This oscillation is not yet a wave that propagates. If we consider a plasma with an oscillating region adjacent to a non-oscillating region, the non-oscillating region does not see an oscillating E-field, as the local deviation from quasi-neutrality cancels out in the Gaussian integration. That is, only through edge effects in finite volumes does the electric field extend to adjacent regions.

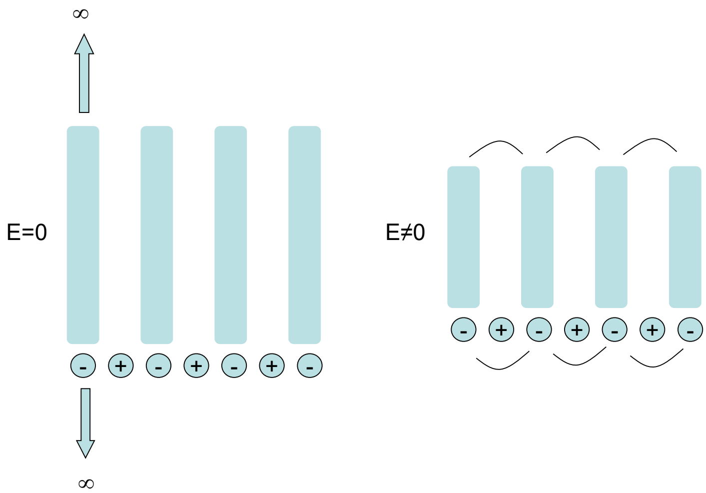

Figure 5.3: Electrostatic plasma oscillations cannot propagate in infinitely extended plasmas at $T_e = 0$. In bounded plasmas, edge effects cause the oscillations to propagate into adjacent regions.

5.1.2 Electron Waves

From plasma oscillations to electrostatic electron waves, we arrive by considering the finite temperature of the electrons.
Now, the following must hold:

$$mn\left[\frac{\partial v_e}{\partial t} + v_e\nabla v_e\right] = -en\vec{E} - \nabla p = -en\vec{E} - 3k_BT_e\nabla n_e \tag{5.13}$$

Here, we have converted the pressure into a gradient in the density using the adiabatic equation. Here, we assume (in contrast to isothermal) adiabatic conditions, i.e., the wave is so fast that the temperature does not have time to equalize in adjacent regions. Therefore, the factor 3, which comes from the relationship:

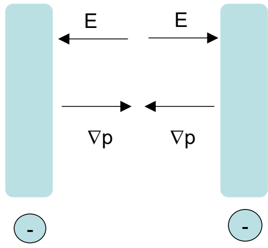

Figure 5.4: The gradient in the pressure creates an additional term in the momentum balance of the electrons. This results in the electrostatic electron waves.

$$\gamma = \frac{2+N}{N} \tag{5.14}$$

with N the number of degrees of freedom. Since we are considering the propagation in one direction, N here is 1, and thus $\gamma = 3$.
We again obtain similar equations as for the plasma oscillations, only expanded by the term ∇p:

$$-in_0 m\omega v_1 = -en_0 E_1 - 3k_B T_e ikn_1 \tag{5.15}$$

$$-i\omega n_1 = -n_0 ikv_1 \tag{5.16}$$

$$ikE_1\epsilon_0 = -en_1 \tag{5.17}$$

If we eliminate v_1, E_1, and n_1 from these equations, we obtain the solution for ω:

$$\boxed{\omega^2 = \frac{ne^2}{\epsilon_0 m} + \frac{3k_B T_e}{m}k^2 = \omega_p^2 + \frac{3}{2}v_{th}^2 k^2} \tag{5.18}$$

The dispersion relation is illustrated in Fig. 5.5:
We see that the maximum propagation speed of the electron waves is the thermal velocity. For small values of k, i.e., long wavelengths, the propagation speed is at 0, since the gradient also becomes zero, and thus diffusion cannot carry the information from oscillating regions to non-oscillating regions.

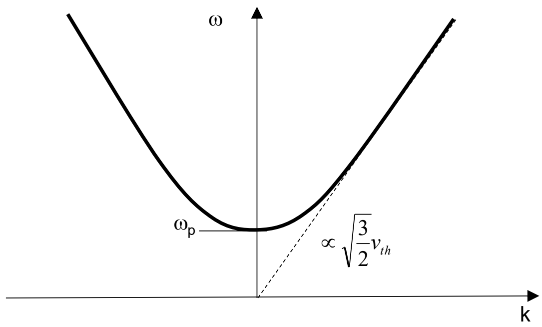

Figure 5.5: Dispersion of electrostatic electron waves.

5.1.3 Ion Waves

In describing the oscillation of the ions, we can no longer ad hoc assume that the much lighter electrons remain at rest. Rather, the electrons compensate for the disturbance of the potential by a density fluctuation of the ions instantaneously according to the Boltzmann relation.

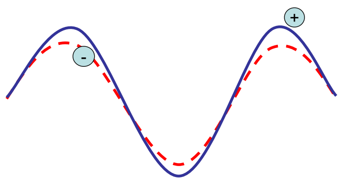

Figure 5.6: In electrostatic ion waves, the electrons follow the density fluctuations of the ions. This does not happen completely, but a difference between electron and ion density according to the Boltzmann relation remains.

For the momentum balance of the ions, we again set:

$$Mn\left[\frac{\partial v_i}{\partial t} + \underbrace{v_i \nabla v_i}_{\ll}\right] = enE - \nabla p = -en\nabla\Phi - \gamma_i k_B T_i \nabla n_i \tag{5.19}$$

In the Fourier space, we obtain:

$$-i\omega M n_0 v_{i,1} = -en_0 ik\Phi_1 - \gamma_i k_B T_i ik n_1 \tag{5.20}$$

The deviation from the equilibrium density that can build up is given by the Boltzmann relation.

$$n_e = n = n_0 + n_1 = n_0 e^{\frac{e\Phi_1}{k_B T_e}} = n_0(1 + \frac{e\Phi_1}{k_B T_e} + ...) \tag{5.21}$$

From this, it follows that

$$n_1 = n_0 \frac{e\Phi_1}{k_B T_e} \tag{5.22}$$

The particle balance again gives, as usual

$$i\omega n_1 = n_0 ikv_{i,1} \tag{5.23}$$

We again eliminate n_1, v_1, and Φ_1 and obtain:

$$i\omega M n_0 v_{i,1} = \left(en_0 ik \frac{k_B T_e}{en_0} + \gamma_i k_B T_i ik \right) \frac{n_0 ikv_{i,1}}{i\omega} \tag{5.24}$$

Thus, we obtain

$$\boxed{\omega^2 = k^2 \left(\frac{k_B T_e}{M} + \gamma_i \frac{k_B T_i}{M} \right)} \tag{5.25}$$

We see that ion waves can only occur at finite temperature. Only at finite temperature can the electrons move far enough away from the ions so that an electric field can build up at all. This separation of the electrons from the ions can be given by the temperature of the electrons, which occurs isothermally ($\propto k_B T_e$, here the frequency of the ion waves is much smaller than that of the electron waves so that the isothermal assumption is valid). The separation of the ions from the electrons occurs adiabatically ($\propto \gamma_i k_B T_i$).

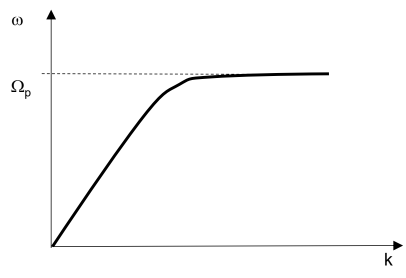

Figure 5.7: Dispersion of electrostatic ion waves.

At large wavenumbers, the oscillation transitions into an ion plasma frequency oscillation. This limit is obtained only if the deviation of the electron density from the equilibrium value is explicitly considered and inserted into the Poisson equation to determine Φ_1.

5.1.4 Electron Waves Perpendicular to the B Field, Upper Hybrid Frequency

Now we consider electrostatic waves perpendicular to a stationary B field. Again, we consider the ions to be stationary. The momentum balance is now

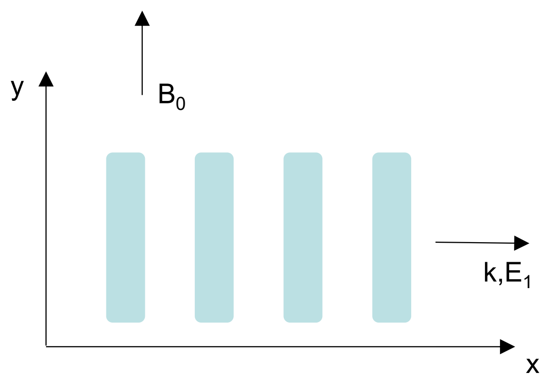

Figure 5.8: Coordinate system for electron waves perpendicular to the B field.

$$mn\frac{\partial v_1}{\partial t} = -e(E_1 + v_1 \times B_0) \tag{5.26}$$

The particle balance again gives

$$\frac{\partial n_1}{\partial t} + n_0 \nabla v_1 = 0 \tag{5.27}$$

The Poisson equation finally

$$\epsilon_0 \nabla E_1 = -en_1 \tag{5.28}$$

The momentum balance in the Fourier space resolved by directions:

$$-i\omega m v_x = -eE_1 - ev_y B_0 \tag{5.29}$$
$$-i\omega m v_y = +ev_x B_0 \tag{5.30}$$
$$-i\omega m v_z = 0 \tag{5.31}$$

Solving gives:

$$i\omega m v_x = eE_1 + eB_0 \frac{ieB_0}{m\omega} v_x \tag{5.32}$$

From the particle balance

$$n_1 = \frac{k}{\omega} n_0 v_x \tag{5.33}$$

Thus, into the Poisson equation

$$\epsilon_0 ikE_1 = -e\frac{k}{\omega} n_0 \frac{eE_1}{im\omega}\left(1 - \frac{\omega_c^2}{\omega^2}\right)^{-1} \tag{5.34}$$

From this, we obtain

$$\left(1 - \frac{\omega_c^2}{\omega^2}\right) = \frac{\omega_p^2}{\omega^2} \tag{5.35}$$

and thus

$$\boxed{\omega^2 = \omega_p^2 + \omega_c^2 = \omega_{oh}^2} \tag{5.36}$$

This is referred to as the **upper hybrid frequency**. This frequency is slightly higher than the plasma frequency, as the gyration motion in the magnetic field is superimposed on the plasma oscillation, as illustrated in Fig. 5.9.

5.1.5 Ion Waves Perpendicular to the B Field, Lower Hybrid Frequency

Finally, we now consider the propagation of electrostatic ion waves perpendicular to B_0. First, we consider the case of a finite angle close to 90Â° of the propagation direction to the magnetic field. Due to this small deviation from 90Â°, there is a possibility for the electrons to compensate for the density fluctuations and to determine the disturbance according to the Boltzmann relation, as illustrated in Fig. 5.10. This is analogous to the discussion of drift wave instabilities.

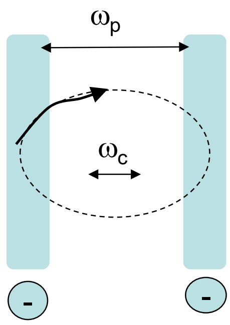

Figure 5.9: The electron oscillation according to the plasma frequency is superimposed by the gyration frequency. This leads to a resonance frequency that is higher than that of the gyration alone.

We start again with the momentum balance according to:

$$M\frac{\partial v_1}{\partial t} = -e\nabla\Phi_1 + ev_1 \times B_0 \tag{5.37}$$

The particle balance again gives

$$\frac{\partial n_1}{\partial t} + n_0\nabla v_1 = 0 \tag{5.38}$$

- $\Theta \approx 90°$

  First, we consider the case that the direction of propagation is only approximately 90Â° to the direction of the magnetic field. For the electric field or the potential disturbance, we can thus again use the Boltzmann relation.

  $$n_1 = n_0\frac{e\Phi_1}{k_B T_e} \tag{5.39}$$

  From the momentum balance, we again obtain:

  $$-i\omega M v_{i,x} = eik\Phi_1 + ev_{i,y}B_0 \tag{5.40}$$

  $$-i\omega M v_{i,y} = -ev_{i,x}B_0 \tag{5.41}$$

  From this, it follows again

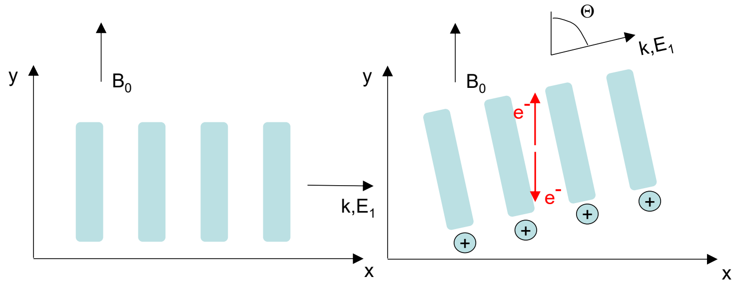

Figure 5.10: In electrostatic ion waves perpendicular to the magnetic field, the electrons can only compensate for the density fluctuations of the ions if the angle between the direction of wave propagation and the B field is not exactly 90Â°.

$$v_{i,x} = \frac{ek}{M\omega}\Phi_1 \left(1 - \frac{\Omega_c^2}{\omega^2}\right)^{-1} \tag{5.42}$$

With the particle balance for propagation in the x-direction

$$n_1 = n_0 \frac{k}{\omega} v_x \tag{5.43}$$

We again eliminate the velocity v_x and n_1 and obtain

$$\boxed{\omega^2 = \Omega_c^2 + k^2 \frac{k_B T_e}{M}} \tag{5.44}$$

Now, the resonance frequency increases by an amount $k^2 \frac{k_B T}{M}$, since the ions, in addition to their gyration, are driven by ambipolar diffusion (in the case of electron waves, this was directly a contribution of the electron plasma frequency, see Eq. 5.36). This is referred to as **ion cyclotron waves**.

- $\Theta = 90°$

  Now, we consider the case where the direction of propagation is exactly 90Â° to the magnetic field. Now, we must, analogous to the momentum balance for the ions, set up the momentum balance for the electrons:

$$v_{e,x} = -\frac{ek}{m\omega}\Phi_1 \left(1 - \frac{\omega_c^2}{\omega^2}\right)^{-1} \tag{5.45}$$

The continuity equation for the electrons gives:

$$n_{e,1} = n_0 \frac{k}{\omega} v_{e,x} \tag{5.46}$$

With $n_e = n_i$ and $v_{e,1} = v_{i,1}$ we obtain

$$\frac{1}{M}\left(1 - \frac{\Omega_c^2}{\omega^2}\right)^{-1} = -\frac{1}{m}\left(1 - \frac{\omega_c^2}{\omega^2}\right)^{-1} \tag{5.47}$$

With $M \gg m$ we obtain

$$\boxed{\omega = (\Omega_c \omega_c)^{1/2} = \omega_{lh}} \tag{5.48}$$

The **lower hybrid frequency**. These waves can only oscillate at a wave propagation angle of less than 90Â° to the magnetic field.

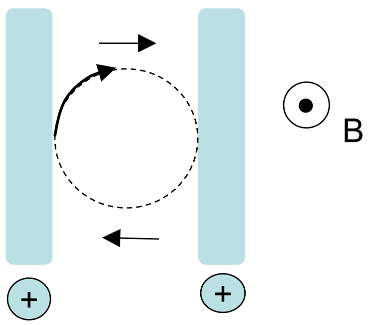

Figure 5.11: In the lower hybrid, the resonance condition of the electrons is superimposed with that of the ions.

5.2 Electromagnetic Waves

In the case of electromagnetic waves, a change in B_1 also occurs. These waves are the only ones that can propagate in a vacuum. All waves that are irradiated onto plasmas are therefore necessarily electromagnetic waves. These can couple to the electrostatic waves in the plasma if frequencies are identical and the electric field components point in the same direction.

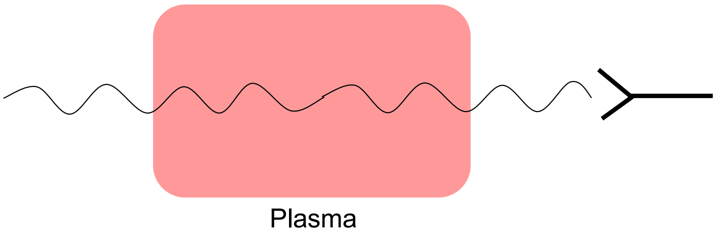

Figure 5.12: Transmission of electromagnetic waves through a plasma.

In general, we have

$$\nabla \times \vec{E} = -\dot{B} \tag{5.49}$$

and

$$\nabla \times \vec{B} = \mu_0 \vec{j} + \epsilon_0 \mu_0 \dot{\vec{E}} \tag{5.50}$$

Differentiating this with respect to time and substituting into Eq. 5.49 gives

$$-\nabla \times \nabla \times \vec{E} = \mu_0 \dot{\vec{j}} + \epsilon_0 \mu_0 \ddot{\vec{E}} \tag{5.51}$$

$$-\left(\nabla(\nabla \vec{E}) - \nabla^2 \vec{E}_1\right) = \mu_0 \dot{\vec{j}} + \frac{1}{c^2} \ddot{\vec{E}} \tag{5.52}$$

In the Fourier space, this gives the general **wave equation**:

$$+\vec{k}(\vec{k}\vec{E}) - k^2 \vec{E} = -i\omega\mu_0 \vec{j} - \frac{1}{c^2}\omega^2 \vec{E} \tag{5.53}$$

5.2.1 EM Waves for $\mathbf{B}_0 = \mathbf{0}$

For the case of transverse electromagnetic waves, $\vec{E}$ and the wave vector k are perpendicular to each other. Thus, the first term in Eq. 5.53 vanishes, and we obtain:

$$k^2 E = i\omega\mu_0 j + \frac{\omega^2}{c^2} E \tag{5.54}$$

We consider the case of the momentum balance in a medium for $T_e = 0$ and $v_{e,0} = 0$. The collision frequency is ν_m.

$$j = -n_0 e v_{e,1} \tag{5.55}$$

$$nm\left[\frac{\partial}{\partial t}v_1 + \underbrace{v_1 \nabla v_1}_{\ll}\right] = -enE_1 - mn\nu_m v_1 \tag{5.56}$$

From this, in the Fourier space, we obtain

$$-mi\omega v_1 = -eE_1 - m\nu_m v_1 \tag{5.57}$$

or

$$v_1 = \frac{eE_1}{-im\omega + m\nu_m} \tag{5.58}$$

This can now be inserted into the wave equation 5.53, and we obtain

$$k^2 = -i\omega\mu_0 n_0 e \frac{e}{-im\omega + m\nu_m} + \frac{\omega^2}{c^2} \tag{5.59}$$

or

$$k^2 = \omega \frac{1}{c^2}\omega_p^2 \frac{1}{\omega + i\nu_m} + \frac{\omega^2}{c^2} \tag{5.60}$$

By rearranging, we finally obtain

$$\boxed{c^2 k^2 = \omega^2 \underbrace{\left[1 - \frac{\omega_p^2}{\omega^2}\frac{1}{1 + i\frac{\nu_m}{\omega}}\right]}_{n^2\text{...refractiveindex}^2}} \tag{5.61}$$

That is, for high frequencies, the dispersion approaches the dispersion in a vacuum, i.e., the wave can propagate and "does not see" the plasma. Only when the frequency of the wave approaches the plasma frequency do the electrons begin to be able to follow the oscillating E-field, and dispersion occurs. For frequencies below the plasma frequency, the inertia of the electrons is small enough so that they can follow the electric field oscillations of the EM wave in phase, and the wave can no longer propagate. Damping occurs.
The refractive index of a plasma is widely used for diagnostic purposes. A typical example is interferometry , where the phase shift is used to determine the refractive index and, via the plasma frequency, the density in the plasma.

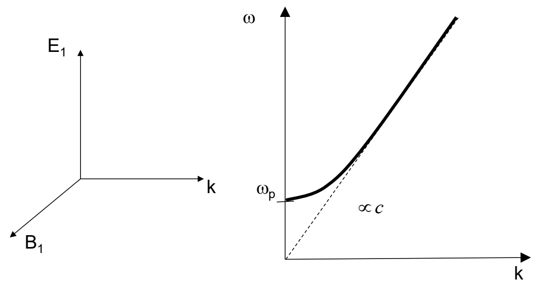

Figure 5.13: Dispersion of electromagnetic waves for zero magnetic field.

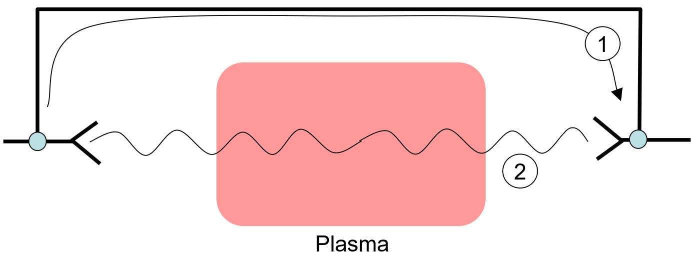

Figure 5.14: The refractive index of a plasma can be measured using interferometry.

5.2.2 EM Waves with $\mathbf{B}_0 \neq 0$

Direction of Propagation $\perp B_0$

Here, we can again distinguish two cases. First, we consider the case where the disturbance in the electric field E_1 is parallel to B_0.
Thus, the motion of the electrons is parallel to the magnetic field, and thus no additional component due to the Lorentz force occurs. This is referred to as **ordinary wave** with the dispersion:

$$\omega^2 = \omega_p^2 + c^2 k^2 \tag{5.62}$$

If the disturbance in the electric field E_1 is perpendicular to B_0, as sketched in Fig. 5.16, this is referred to as **extraordinary wave**.
We start again with the wave equation for our case.

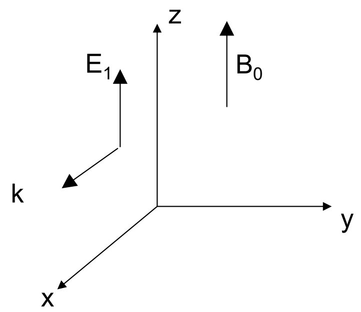

Figure 5.15: Ordinary EM wave.

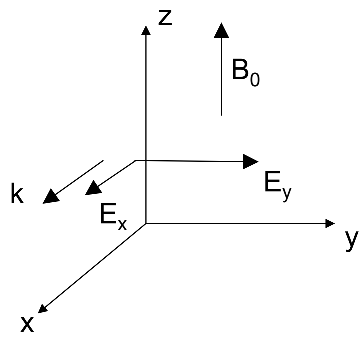

Figure 5.16: Extraordinary EM wave.

$$-\vec{k}(\vec{k}\vec{E}_1) + k^2\vec{E} = i\omega\mu_0\vec{j} + \frac{\omega^2}{c^2}\vec{E}_1 \tag{5.63}$$

The momentum balance for the case without damping and $T_e = 0$ and $v_0 = 0$ gives:

$$m\frac{\partial v_1}{\partial t} = -eE_1 - e(\vec{v}_1 \times \vec{B}_0) \tag{5.64}$$

We solve this for the x- and y-direction and obtain:

$$v_x = -i\frac{e}{m\omega}(E_x + v_y B_0) \tag{5.65}$$

$$v_y = -i\frac{e}{m\omega}(E_y - v_x B_0) \tag{5.66}$$

This is inserted into the wave equation 5.53

$$(\omega^2 - c^2k^2)\vec{E}_1 + c^2\vec{k}(\vec{k}\vec{E}_1) = -i\omega\frac{1}{\epsilon_0}\vec{j}_1 = in\omega\frac{1}{\epsilon_0}e\vec{v}_1 \tag{5.67}$$

This wave equation is solved under the condition that E_x points in the direction of the wave propagation $\vec{k}$. Thus, we obtain:

$$(\omega^2 - c^2k^2)\vec{E}_1 + c^2k\vec{k}E_x = in\omega\frac{1}{\epsilon_0}e\vec{v}_1 \tag{5.68}$$

Now, the velocities $\vec{v}_1$ can be solved and resolved into the x- and y-direction to:

$$\omega^2 E_x = -\frac{i\omega n_0 e}{\epsilon_0}\frac{e}{m\omega}\left(iE_x + \frac{\omega_c}{\omega}E_y\right)\left(1 - \frac{\omega_c^2}{\omega^2}\right)^{-1} \tag{5.69}$$

$$\left(\omega^2 - c^2k^2\right)E_y = -\frac{i\omega n_0 e}{\epsilon_0}\frac{e}{m\omega}\left(iE_y - \frac{\omega_c}{\omega}E_x\right)\left(1 - \frac{\omega_c^2}{\omega^2}\right)^{-1} \tag{5.70}$$

Now, we have two equations for the field components E_x and E_y, which can be written as a matrix:

$$\begin{pmatrix} A & B \\ C & D \end{pmatrix}\begin{pmatrix} E_x \\ E_y \end{pmatrix} = 0 \tag{5.71}$$

This system of equations has a solution if the determinant is zero. Thus, we obtain the condition:

$$\frac{c^2k^2}{\omega^2} = \frac{\omega^2 - \omega_{oh}^2 - \left[\left(\frac{\omega_p^2\omega_c}{\omega}\right)^2\frac{1}{\omega^2-\omega_{oh}^2}\right]}{\omega^2 - \omega_c^2} \tag{5.72}$$

Finally, we obtain the dispersion relation for electromagnetic waves perpendicular to the magnetic field with:

$$\boxed{c^2k^2 = \omega^2\underbrace{\left[1 - \frac{\omega_p^2}{\omega^2}\frac{\omega^2 - \omega_p^2}{\omega^2 - \omega_{oh}^2}\right]}_{n^2 \text{...refractiveindex}^2}} \tag{5.73}$$

- **Resonances**

  Resonances occur for $k \to \infty$, i.e., the wavelength approaches zero. Or, because

$$ck = n\omega \tag{5.74}$$

  a refractive index $n \to 0$. This corresponds to an absorption of the wave by exciting plasma oscillations with the resonance frequency of the upper hybrid:

$$\omega^2 = \omega_{oh}^2 = \omega_p^2 + \omega_c^2 \tag{5.75}$$

  Here, the component E_x of the electromagnetic wave, which runs in the x-direction, is in phase with the electric field E_1 of the plasma oscillation in this direction. This energy transfer corresponds to upper hybrid heating.

- **Cutoff**

  Cutoffs occur for $k \to 0$. That is, the wavelength approaches infinity. Here, the refractive index is 0, and the EM wave can no longer propagate. For this condition, we obtain.

$$1 = \frac{\omega_p^2}{\omega^2} \frac{1}{1 - \omega_c^2 \frac{1}{\omega^2 - \omega_p^2}} \tag{5.76}$$

  This can be reduced to.

$$1 - \frac{\omega_p^2}{\omega^2} = \pm \frac{\omega_c}{\omega} \tag{5.77}$$

  The different signs correspond to the left- and right-handed cutoff. This is illustrated in Fig. 5.17.

  The extraordinary wave has a resonance at ω_{oh} because here the wave can couple to the plasma oscillation. The ordinary wave has no resonance because there is no component E_1 along the direction of propagation.

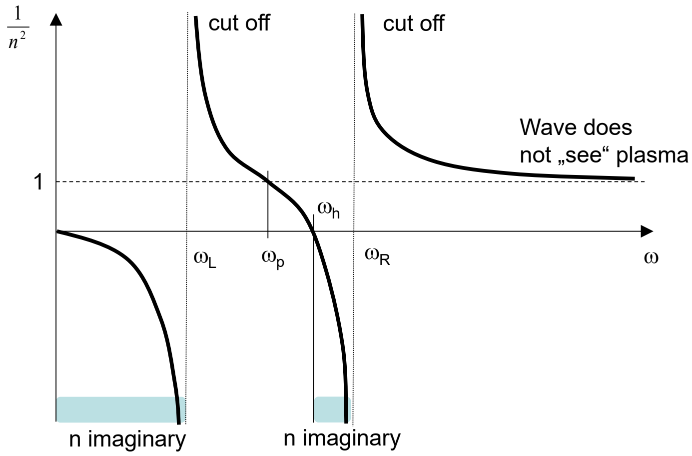

Figure 5.17: 1/refractiveindex^2 of electromagnetic waves with propagation direction perpendicular to the magnetic field.

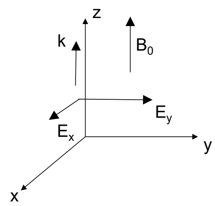

Figure 5.18: Coordinate system for the propagation of waves parallel to the magnetic field.

Direction of Propagation $\| B_0$

For the derivation of the dispersion, we start again with a coordinate system according to Fig. 5.18.
We start with the wave equation.

$$-\vec{k}(\vec{k}\vec{E}_1) + k^2\vec{E} = i\omega\mu_0\vec{j} + \frac{\omega^2}{c^2}\vec{E}_1 \tag{5.78}$$

The momentum conservation

$$-i\omega m\vec{v}_1 = -e\vec{E}_1 - e\vec{v}_1 \times \vec{B}_0 \tag{5.79}$$

and

$$\vec{j} = -en_0\vec{v}_1 \tag{5.80}$$

Again, this can be resolved into the components in the x- and y-direction to:

$$\left(\omega^2 - c^2k^2\right) E_x = \frac{\omega_p^2}{1-\frac{\omega_c^2}{\omega^2}}\left(E_x - i\frac{\omega_c}{\omega}E_y\right) \tag{5.81}$$

$$\left(\omega^2 - c^2k^2\right) E_y = \frac{\omega_p^2}{1-\frac{\omega_c^2}{\omega^2}}\left(E_y + i\frac{\omega_c}{\omega}E_x\right) \tag{5.82}$$

$$\tag{5.83}$$

In analogy to the solution for wave propagation perpendicular to the magnetic field, we obtain from the condition that the determinant of the system of equations vanishes the following solution for the **refractive index**:

$$\boxed{n^2 = 1 - \frac{\omega_p^2}{\omega^2}\frac{1}{1\mp\frac{\omega_c}{\omega}}} \tag{5.84}$$

The signs correspond again to an R and an L wave corresponding to the phase shift between the field strength components. R corresponds to right-circular and L corresponds to left-circular.

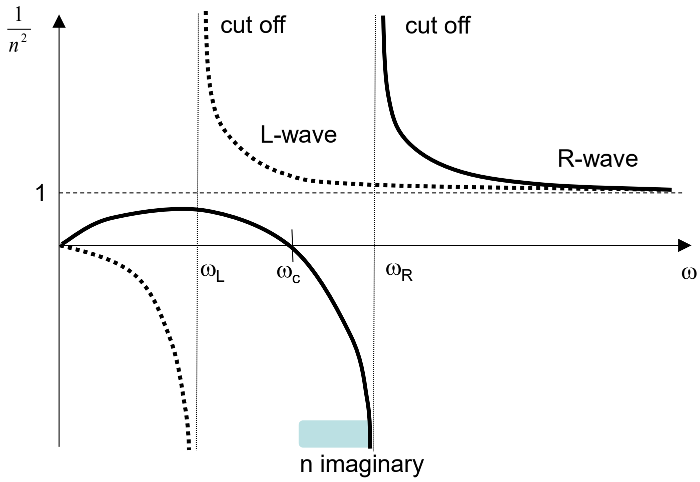

Figure 5.19: 1/refractiveindex^2 of electromagnetic waves parallel to the magnetic field.

The course of 1/refractiveindex^2 is shown in Fig. 5.19. We obtain a resonance at the cyclotron frequency. However, this only applies to one polarization direction, as here the electric field rotates in phase with the gyration. The other polarization direction is not absorbed, as illustrated in Fig. 5.20.

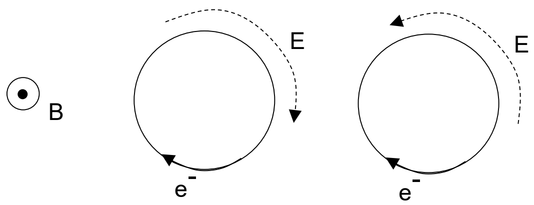

Figure 5.20: Absorption of electromagnetic waves only occurs for one polarization.

- **Whistler Modes**

  These are electromagnetic waves parallel to the magnetic field that travel back and forth between the poles in the ionosphere. In the acoustic range $< \omega_c$, the dispersion has positive curvature. Accordingly, low frequencies arrive later than higher ones, and one hears a falling tone.

- **Helicon Plasmas**

  If we consider the whistler modes in bounded plasmas, we refer to these waves as helicon waves (”helicon”, since they correspond to circularly polarized plasma waves). A typical arrangement is a corresponding antenna that is driven at 13.56 MHz and can excite these modes by its shape. The magnetic field is typically 100 mT. The cyclotron resonance frequency ω_c at these magnetic fields is in the several GHz range, i.e., the excitation frequency is significantly below ω_c. The electromagnetic wave has only a finite penetration depth, which, however, is so large that it can almost fill the typical technical plasmas. An optimum in the power coupling occurs when a standing wave is excited in the plasma vessel. In plasma technology, this is an attractive type of discharge for the efficient generation of a highly dense plasma. However, this state is too sensitive to discharge geometry, etc., and could therefore not prevail on a broad front.

- **Faraday Rotation**

  The phase velocity is different for right- and left-circularly polarized light, i.e., the polarization state of the light that penetrates a plasma can thus be changed.

- **High-Field Coupling**

  For heating a plasma at the electron cyclotron resonance frequency, a corresponding frequency (ω_{mw} several GHz) is irradiated from a microwave generator. It is important that this wave also reaches the location of the resonance ($\omega = \omega_c$). There is only one successful variant for this, the so-called **high-field coupling**. That is, the window of the microwave source to the plasma chamber must be in an area of the plasma vessel where the magnetic field is *higher* than the resonance field (position 2 in Fig. 5.21). Thus, the electromagnetic wave passes through an area where $\omega_{mw} < \omega_c$ always applies. If the radiation is coupled from the low-field side (position 1 in Fig. 5.21), it inevitably runs into the cutoff and is simply reflected.

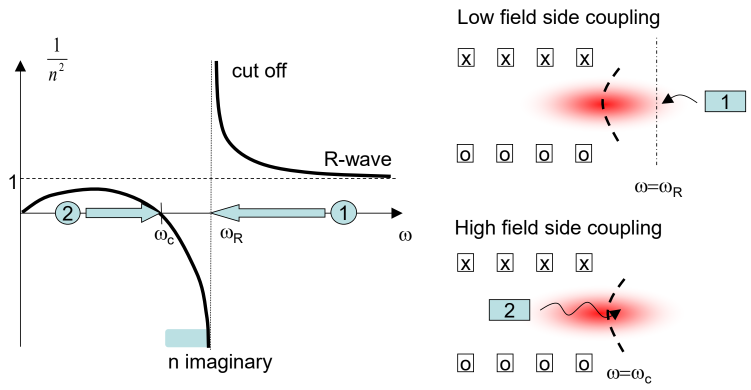

Figure 5.21: For an electromagnetic wave parallel to B_0 to reach the resonance zone, it must be coupled from the high-field side (position 1). From the low-field side, it automatically runs into the cutoff.

5.3 Hydromagnetic Waves

Finally, we consider the case of hydromagnetic waves. These are the slowest wave phenomena, where the inertia of the ions and the different velocities of the ions and electrons are taken into account. That is, we can no longer assume stationary ions or a change in the electron density according to the Boltzmann relation. Now, we have

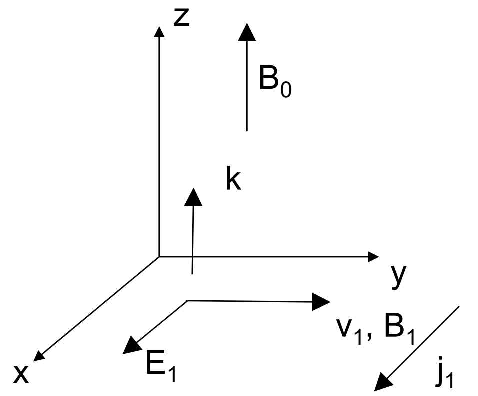

Figure 5.22: Coordinate system for the propagation of hydromagnetic waves parallel to the magnetic field.

$$\vec{j} = en_0(v_{i,1} - v_{e,1}) \tag{5.85}$$

The starting point is again the wave equation here

$$-\vec{k}(\vec{k}\vec{E}_1) + k^2\vec{E} = i\omega\mu_0\vec{j} + \frac{\omega^2}{c^2}\vec{E}_1 \tag{5.86}$$

5.3.1 Alfven Waves

Alfven waves are hydromagnetic waves that propagate parallel to the magnetic field, according to Fig. 5.22. From the momentum balance of the ions, we obtain the x and y components.

$$v_{i,x} = i\frac{e}{M\omega}\left(1 - \frac{\Omega_c^2}{\omega^2}\right)^{-1} E_1 \tag{5.87}$$

$$v_{i,y} = \frac{e}{M\omega}\frac{\Omega_c}{\omega}\left(1 - \frac{\Omega_c^2}{\omega^2}\right)^{-1} E_1 \tag{5.88}$$

These are the same equations that we had already derived for the derivation of electrostatic ion waves $\perp$ to B_0. Unlike this analysis, we now explicitly also consider the velocity components of the electrons under the approximation $m \ll M$ and $\omega_c \gg \omega$:

$$v_{e,x} = 0 \tag{5.89}$$

$$v_{e,y} = -\frac{E_1}{B} \tag{5.90}$$

This corresponds to the E $\times$ B drift in the y-direction. Now, the velocities are again inserted into the relationship for the current, and this is inserted into 5.53. We obtain:

$$\omega^2 - c^2k^2 = \Omega_p^2 \left(1 - \frac{\Omega_c^2}{\omega^2}\right)^{-1} \tag{5.91}$$

For very low-frequency waves, we obtain for $\omega \ll \Omega_c$:

$$\omega^2 - c^2k^2 = -\omega^2 \frac{\Omega_p^2}{\Omega_c^2} = -\omega^2 \frac{ne^2}{\epsilon_0 M} \frac{M^2}{e^2 B_0^2} = -\omega^2 \frac{nM}{\epsilon_0 B_0^2} \tag{5.92}$$

Thus, we have

$$\frac{c^2k^2}{\omega^2} = 1 + \frac{nM}{\epsilon_0 B_0^2} \simeq \underbrace{\frac{nM}{\epsilon_0 B_0^2}}_{n^2} \tag{5.93}$$

From this, we obtain the phase velocity as the so-called **Alfven velocity** v_A:

$$\boxed{\frac{\omega}{k} = \frac{B_0}{(\mu_0 nM)^{1/2}} = v_A} \tag{5.94}$$

Alfven waves correspond to an oscillation in the plasma in which the frozen-in flux oscillates around its equilibrium position. The electric field arises from a charge separation due to the inertia of the ions compared to that of the electrons.

5.3.2 Magnetosonic Waves

In the case of wave propagation perpendicular to the magnetic field, the terms E $\times$ B and ∇ p are decisive.

$$Mn_0 \frac{\partial}{\partial t} v_{i,1} = en_0(E_1 + v_1 \times B_0) - \nabla p \tag{5.95}$$

In analogy to the derivation of Alfven waves, we again obtain a dispersion relation.

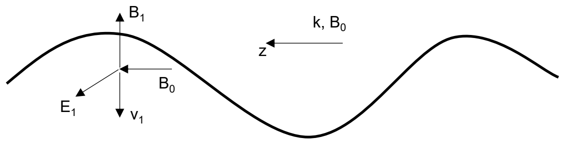

Figure 5.23: Alfven waves correspond to low-frequency oscillations of the frozen-in flux.

$$\boxed{\frac{\omega^2}{k^2} = c^2 \frac{v_s^2 + v_A^2}{c^2 + v_A^2}} \tag{5.96}$$

with

$$v_s = \left(\frac{\gamma k_B T_i + k_B T_e}{M} \right)^{1/2} \tag{5.97}$$

The magnetosonic wave is an MHD wave in which the density fluctuations are driven by an E $\times$ B and ∇ p term.

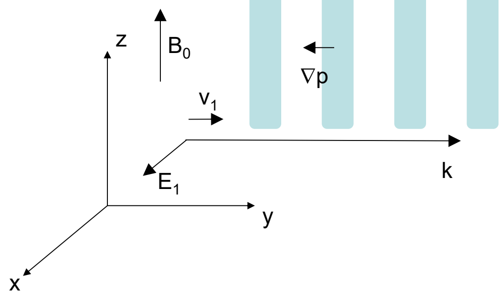

Figure 5.24: Magnetosonic waves.

For the case of vanishing magnetic field, i.e., $B_0 \rightarrow 0$, Eq. 5.96 reduces to the dispersion of ion-acoustic waves. In the case of cold plasmas given by $T \rightarrow 0$ or $v_s \rightarrow 0$, we obtain the so-called fast hydromagnetic waves:

$$\frac{\omega^2}{k^2} = c^2 \frac{v_A^2}{c^2 + v_A^2} > v_A \tag{5.98}$$

Chapter 6

Kinetics

The kinetic picture is more general than the fluid picture, as it does not assume a temperature of the plasma, but allows for arbitrary velocity distributions. Non-equilibrium phenomena, such as the injection of fast particles into plasmas or selective wave heating, initially only change small regions of this distribution function. Through collisions of the particles with each other, the energy can then be transferred to other regions in the distribution function. The shape of the distribution function thus carries information about the generation and heating mechanisms in a plasma.

So far, we have treated the confinement of plasmas and the heating of plasmas by means of waves. Within the plasma itself, the energy content was characterized by a temperature within the framework of the fluid picture. The more complete description, however, is the knowledge of the entire distribution function in velocity space. This is determined within the framework of the kinetic description. The aim of this approach is to gain information about how the distribution function $f(v)$ forms under the influence of electric fields, which, for example, are present when waves are coupled into the plasma. Collisions of the particles among each other then lead to a redistribution in velocity space. The starting point is the **Vlasov equation**:

$$\boxed{\frac{df}{dt} = \frac{\partial f}{\partial t} + \vec{v}\frac{\partial f}{\partial \vec{x}} + \frac{\vec{F}}{m}\frac{\partial f}{\partial \vec{v}} = 0} \tag{6.1}$$

Taking into account collisions, the **Boltzmann equation** applies:

$$\boxed{\frac{df}{dt} = \frac{\partial f}{\partial t} + \vec{v}\frac{\partial f}{\partial \vec{x}} + \frac{\vec{F}}{m}\frac{\partial f}{\partial \vec{v}} = \left.\frac{\partial f}{\partial t}\right|_{collisions}} \tag{6.2}$$

6.1 Distribution function in LTE, Maxwell distribution

We now consider the collision term on the right-hand side of the Boltzmann equation and require that this must become zero in equilibrium. The distribution function can be changed by collision processes, in that particles can be scattered into or out of a phase space element. This is illustrated in Fig. 6.1.

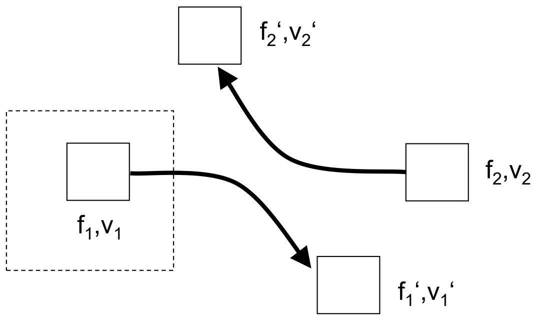

Figure 6.1: Collisions between phase space elements d^3v_1 and d^3v_2

Particles f_1 and f_2 with velocities v_1 and v_2 scatter off each other, and after the collision we obtain particles f_1' and f_2' with the velocities v_1' and v_2'. The loss of f_1 particles in the phase space element $\mathrm{d}^3\mathrm{v}_1$ due to collisions with particles f_2 from the phase space $\mathrm{d}^3\mathrm{v}_2$ is described by:

$$f_1 f_2 d^3v_1 d^3v_2 |v_1 - v_2| \frac{d\sigma}{d\Omega} d\Omega \tag{6.3}$$

$\frac{d\sigma}{d\Omega}$ is the differential cross section. The gain of particles through scattering processes that create new particles in the volume element $\mathrm{d}^3\mathrm{v}_1$ can be obtained by time reversal.

$$f_1' f_2' d^3v_1' d^3v_2' |v_1' - v_2'| \frac{d\sigma'}{d\Omega'} d\Omega' \tag{6.4}$$

For elastic collisions, the following must hold:

$$|v_1 - v_2| = |v_1' - v_2'| \tag{6.5}$$

and

$$\frac{d\sigma'}{d\Omega'}d\Omega' = \frac{d\sigma}{d\Omega}d\Omega \tag{6.6}$$

If we take the loss and gain terms together, we obtain:

$$\frac{\partial f_1}{\partial t} = \frac{\Delta N}{d^3v_1} = \int\int(-f_1f_2 + f_1'f_2')|v_1 - v_2|\frac{d\sigma}{d\Omega}d\Omega d^3v_2 \tag{6.7}$$

For the collision term, integration is performed here over the differential cross section. In the case of Coulomb scattering, no finite integral is obtained. Therefore, for the kinetics in the case of Coulomb scattering, an expansion is made under the assumption that a collision only slightly changes the distribution function, i.e. small-angle scattering. This leads to the Fokker-Planck equation.
In equilibrium, we require that the distribution function should not change. This implies that:

$$f_1'f_2' - f_1f_2 = 0 \tag{6.8}$$

or

$$\ln f_1' + \ln f_2' = \ln f_1 + \ln f_2 \tag{6.9}$$

This equation can be solved by the ansatz of a Maxwell distribution. If we set

$$f \sim e^{-\alpha m v^2} \tag{6.10}$$

then the above equation yields

$$v_1'^2 + v_2'^2 = v_1^2 + v_2^2 \tag{6.11}$$

This corresponds to the conservation of energy.

6.2 Distribution function under the influence of external fields

6.2.1 2-term approximation

When deviating from equilibrium, the general approach is to assume that the perturbation is small. In many cases, the system also has a preferred direction, e.g. due to the alignment of the electric field, which accelerates the charge carriers. This is taken into account in the so-called **2-term approximation**. The distribution function is divided into an isotropic part f_0 and an anisotropic part f_1 according to Fig. 6.2.

$$f(\vec{v}) = f_0(|v|) + \frac{v_z}{v} f_1(|v|) \tag{6.12}$$

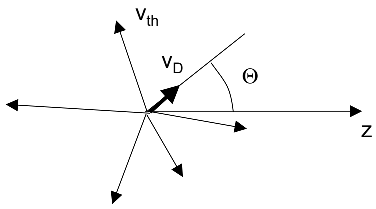

Figure 6.2: Anisotropic part in the distribution function due to e.g. superimposed drift velocity v_D

i.e. the directional information is now in the prefactor of the anisotropic part, while the parts of the distribution function f_0 and f_1 become functions of a scalar. The form of f_0 and f_1 is illustrated in Fig. 6.3. With $\cos\Theta = \frac{v_z}{v}$ we can write:

$$f(\vec{v}) = f_0(|v|) + \cos\Theta f_1(|v|) \tag{6.13}$$

Depending on the angle Θ at which the distribution function is considered, a different shape results. If the distribution function is considered for $\Theta = 0$, i.e. in the direction of the external electric field, one sees the completely shifted distribution function $f_0 + f_1$. If the distribution function is considered for directions perpendicular to the electric field $\Theta = \pi/2$, one notices no change and only gets f_0. This is illustrated in Fig. 6.4.
Now let us consider collisions of the electrons with neutral gas particles, which are characterized by a distribution function f_g. f_g does not change due to collisions in the first approximation, since, due to the mass difference, the momentum transfer is small, i.e., $f_g = f_g'$. In this approximation, the collision term is, for example:

$$\left.\frac{\partial f}{\partial t}\right|_{collisions} = \int\int (f_1 f_g - f_1' f_g)|v| \frac{d\sigma}{d\Omega} d\Omega d^3 v_g \tag{6.14}$$

Here it is taken into account that the distribution function of the heavy particles does not change and that their velocity is much smaller than that of the electrons. In the 2-term approximation, this becomes:

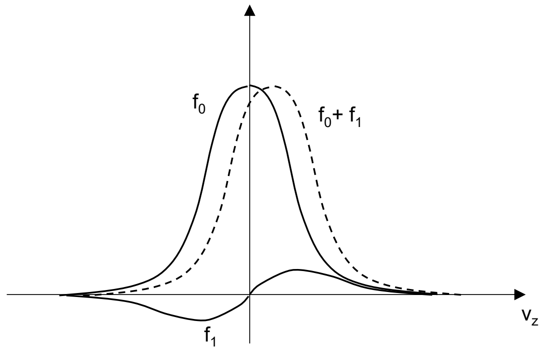

Figure 6.3: Isotropic part f_0 and anisotropic part f_1 of the distribution function

$$(f_1' f_g - f_1 f_g)|v| = (f_0 f_g - f_0 f_g)|v| + f_1 f_g v_z' - f_1 f_g v_z = f_1 f_g (v_z' - v_z) \quad (6.15)$$

Here, the fact that the magnitude of the velocity remains the same during the collision was used. i.e. $v' = v$ and $f_0' = f_0$ and $f_1' = f_1$. However, the direction changes through the collision process, and it holds:

$$v_z' = v_z \cos\Theta \quad (6.16)$$

Thus, the collision term becomes:

$$\left.\frac{\partial f}{\partial t}\right|_{collisions} = \underbrace{\int f_g d^3 v_g}_{n_g} \underbrace{\int f_1 (\cos\Theta - 1)|v|}_{-v(1-\cos\Theta)} \underbrace{\frac{d\sigma}{d\Omega} d\Omega}_{\sigma} \quad (6.17)$$

The term on the right-hand side is already known. It corresponds to the collision frequency for momentum transfer ν_m, characterized by the factor $(1 - \cos\Theta)$. Thus, we have:

$$\boxed{\left.\frac{\partial f}{\partial t}\right|_{collisions} = -\nu_m f_1} \quad (6.18)$$

i.e. the anisotropic part of the distribution function decays through collisions. i.e., by turning on the collisions, equilibrium is sought, and the distribution function f_0 is reached.

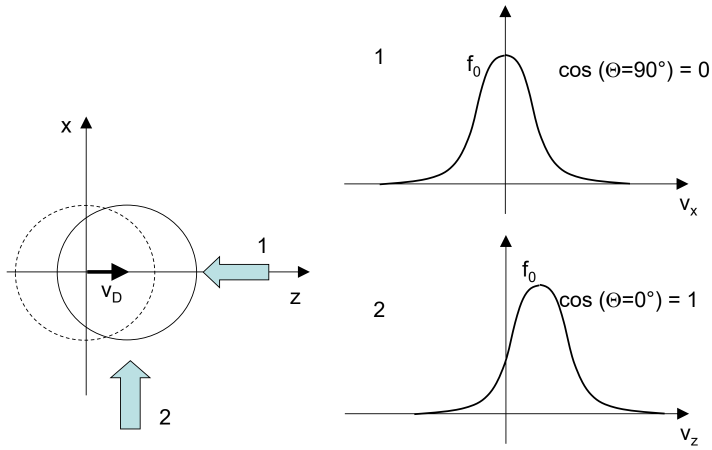

Figure 6.4: Isotropic part f_0 and anisotropic part f_1 of the distribution function. Depending on the direction considered, the anisotropic part contributes to f.

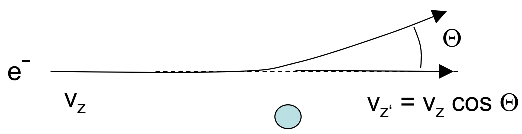

Figure 6.5: Change of the z-component through a collision process.

6.2.2 Boltzmann equation in 2-term approximation

Now let us consider the Boltzmann equation for electrons for a selected direction z in one dimension:

$$\frac{\partial f}{\partial t} + v_z \frac{\partial f}{\partial t} - \frac{eE_z}{m}\frac{\partial f}{\partial v_z} = \left.\frac{\partial f}{\partial t}\right|_{collisions} \tag{6.19}$$

In this equation, the 2-term approximation can now be inserted; f becomes:

$$\frac{\partial f_0}{\partial t} + \cos\Theta \frac{\partial f_1}{\partial t} + ... \tag{6.20}$$

or.

$$v_z = v \cos\Theta \tag{6.21}$$

Subsequently, the equation is either multiplied by $\sin\Theta$ or $\sin 2\Theta$ and integrated from 0 to π. By this type of averaging over space, the symmetric or antisymmetric part of the equation is separated, and a balance equation for the part f_0 or f_1 of the distribution function is created:

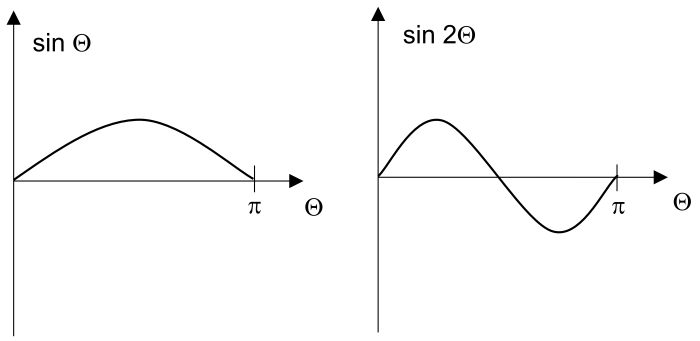

Figure 6.6: Integration with the factors $\sin\Theta$ and $\sin 2\Theta$ yield rate equations for the isotropic and anisotropic part.

- **Symmetric part** f_0

  After substituting the variable substitution from Eq. 6.20 and 6.21 into Eq. 6.19 and the corresponding integration over $\sin\Theta d\Theta$, the following terms remain:

$$\int_0^\pi \frac{\partial f_0}{\partial t} \sin\Theta + \int_0^\pi \cos\Theta \sin\Theta \frac{\partial f_1}{\partial t} + ... = 2\frac{\partial f_0}{\partial t} + 0 + ... \tag{6.22}$$

  Thus, a balance equation for f_0 is created

$$\frac{\partial f_0}{\partial t} + \frac{1}{3} v \frac{\partial f_1}{\partial z} - \frac{e\vec{E}_z}{m} \frac{1}{3v^2} \frac{\partial v^2 f_1}{\partial v} = 0 \tag{6.23}$$

  The right-hand side of this equation becomes zero only if the isotropic distribution function cannot change through, for example, collisions with heavy particles. This is only true for a mass $M \to \infty$ of the heavy particles. For finite mass, the right-hand side of Eq. 6.23 from the collision term becomes instead:

$$\frac{m}{m+M}\frac{1}{v^2}\frac{\partial}{\partial v}\left[v^3\nu_m\left(f_0+\frac{k_BT}{mv}\frac{\partial f_0}{\partial v}\right)\right] \tag{6.24}$$

This term must also become zero if the isotropic distribution function f_0 is a Maxwell distribution, since any collision processes always lead to a Maxwell distribution in equilibrium. This is satisfied if the right-hand side becomes zero or if:

$$f_0 = -\frac{k_BT}{mv}\frac{\partial f_0}{\partial v} \tag{6.25}$$

This is a differential equation for f_0. The simple solution immediately shows that the dependence $f_0 \propto e^{mv^2/kT}$ satisfies this condition.

- **Antisymmetric part** f_1

  As a second variant, the equation 6.19 is multiplied by $\sin 2\Theta$ and integrated from 0 to π to obtain a rate equation for f_1. The first terms remaining now are

$$\int_0^\pi \frac{\partial f_0}{\partial t}\sin 2\Theta + \int_0^\pi \cos\Theta\sin 2\Theta\frac{\partial f_1}{\partial t} + ... = 2\frac{\partial f_1}{\partial t} + 0 + ... \tag{6.26}$$

  This results in an equation for the temporal evolution of the anisotropic part.

$$\frac{\partial f_1}{\partial t} + v\frac{\partial f_0}{\partial z} - \frac{e\vec{E}_z}{m}\frac{\partial f_0}{\partial v} = -\nu_m f_1 \tag{6.27}$$

  One can see that the anisotropic part f_1 is changed by three terms: (i) by a flow in the spatial domain according to $\frac{\partial f_0}{\partial z}$ where particles flow from neighboring phase space elements into the phase space element of f_1; (ii) by an acceleration or deceleration according to an electric field E_z; (iii) or the loss of anisotropy through collision processes according to a collision frequency ν_m.

Transport quantities

For the description of plasmas, it is often expedient to describe the complex variation in the spatial domain by a simpler fluid model, while the heating processes in plasmas and thus the energy content are better captured with a

kinetic model. The spatial dependence of the shape of the distribution function is thereby neglected (see local approximation below). For the coupling of the kinetic model to the fluid model, the derivation of the transport quantities, mobility and diffusion constant, of the fluid model from the microscopic description in the kinetic model is important.
Mobility and diffusion constant can be derived from the formulation of the Boltzmann equation in a 2-term approximation. The particle flux in one direction is given by the anisotropic part in the distribution function. This can be shown from:

$$j = \int v f d^3v = \int v \left(f_0 + \frac{v_z}{v} f_1 \right) d^3v \tag{6.28}$$

The terms proportional to f_0 average out and we obtain

$$j_z = \frac{4\pi}{3} \int_0^\infty v_z f_1 v^2 dv \tag{6.29}$$

Here, $4\ \pi v^2$ comes from the spherical shell and the term $1/3$ from considering only one direction. i.e., the directed particle flux is determined only by the anisotropic part of the distribution function. The rate equation for the anisotropic part is given by Eq. 6.27. In the steady state, we obtain

$$f_1 = -\frac{1}{\nu_m} \left(v \frac{\partial f_0}{\partial z} - \frac{e}{m} E_z \frac{\partial f_0}{\partial v} \right) \tag{6.30}$$

Thus, for the particle flux we obtain

$$j = -\frac{4\pi}{3} \frac{1}{n} \int_0^\infty v^4 \frac{f_0}{\nu_m} dv \frac{\partial n}{\partial z} + \frac{4\pi e}{3mn} \int \frac{v^3}{\nu_m} \frac{\partial f_0}{\partial v} n E_z dv \tag{6.31}$$

From the comparison for the electron flux in the fluid picture with:

$$j = -D \nabla n - \mu n E_z \tag{6.32}$$

we obtain:

$$\boxed{D = \frac{4\pi}{3} \frac{1}{n} \int \frac{v^4}{\nu_m} f_0 dv} \tag{6.33}$$

and

$$\boxed{\mu = -\frac{4\pi e}{3mn} \int \frac{v^3}{\nu_m} \frac{\partial f_0}{\partial v} dv} \tag{6.34}$$

These equations are important to determine the transport quantities diffusion D and mobility μ from the velocity-dependent collision frequency.
A typical hybrid plasma modeling arises from the following sequence: (i) first, the distribution function for the entire plasma is determined from the Boltzmann equation in 2-term approximation; (ii) then, the transport quantities μ and D are determined from the solution, taking into account the velocity dependence of the collision frequency; (iii) finally, the spatial distribution of the electron density is determined from the fluid model with these transport parameters. However, since the transport coefficients also depend on the particle densities, a self-consistent solution can be enforced by iterating steps (i) to (iii) until convergence.

Heavy particle collisions, Druyvesteyn distribution

We now consider the case of the shape of the distribution function under the assumption of heavy particle collisions. From the rate equation of the anisotropic part 6.27 we obtain:

$$f_1 = \frac{eE_z}{m\nu_m}\frac{\partial f_0}{\partial v} \tag{6.35}$$

Here, the spatial derivative $\frac{\partial f_0}{\partial z}$ was set to zero. This corresponds to the so-called **local approximation**, i.e., the shape of the distribution function does not change with the location in the discharge, and the consideration in a phase space element is valid for the entire discharge. This approximation is based on the idea that energy transport in a discharge is much more efficient than particle transport. i.e., there are gradients in the particle density corresponding to a diffusion profile, while the temperature distribution, or more precisely the distribution in velocity space, is spatially constant. However, this local approximation is often only insufficiently valid.
Alternatively, however, a **non-local approximation** can be defined. This assumes that in a plasma in which the electrons have long mean free paths, the total energy as the sum of potential energy $e\Phi(x)$ and kinetic energy $\frac{1}{2}mv^2(x)$ remains constant. i.e. the potential $\Phi(x)$ and the velocity $v(x)$ may change *spatially* but the expression

$$E = e\Phi(x) + \frac{1}{2}mv(x)^2 \tag{6.36}$$

remains constant. With this assumption, balance equations for the distribution function $f(v)$ can be transformed into balance equations for $f(E)$ in which the spatial derivative disappears again. After solving the problem for

$f(E)$, the spatial dependence $f(v(x))$ can be directly derived by inserting the potential $\Phi(x)$.
For the derivation of the distribution function in the case of collisions with heavy particles, we use equation 6.23 and obtain:

$$-\frac{eE_z}{m}\frac{1}{3v^2}\frac{\partial}{\partial v}v^2 f_1 = 0 \tag{6.37}$$

This was valid for the approximation of infinitely massive heavy particles. For particles of finite mass in local approximation and with $m \ll M$ and $T = 0$ one obtains instead:

$$-\frac{eE_z}{m}\frac{1}{3v^2}\frac{\partial}{\partial v}v^2 f_1 = -\frac{m}{M}\frac{1}{v^2}\frac{\partial}{\partial v}\left(v^3\nu_m f_0\right) \tag{6.38}$$

Thus, we obtain:

$$f_1 = -\frac{3m^2}{eE_zM}v\nu_m f_0 \tag{6.39}$$

From equations 6.35 and 6.39 we obtain:

$$\frac{\partial f_0}{\partial v} = -\frac{m\nu_m}{eE_z}\frac{3m^2}{eE_zM}v\nu_m f_0 = -\frac{3m^3}{eE_z^2M}v\nu_m^2 f_0 \tag{6.40}$$

This yields a solution of the form:

$$f_0 \propto exp\left[-\frac{3m^3}{eE_z^2M}\int_0^v v'\nu_m^2 dv'\right] \tag{6.41}$$

Assuming that the collision frequency

$$\nu_m = n_g\sigma v \tag{6.42}$$

is a distribution function of the form

$$\boxed{f_0 \propto exp[-\alpha v^4]} \tag{6.43}$$

This is referred to as the **Druyvesteyn distribution**. The course of different distribution functions is illustrated in Fig. 6.7.
It should be noted that the shape of the distribution function does not necessarily imply the dominance of a process. For example, ionization above a certain threshold leads to a kink in the distribution function at higher electron energies; the shape of f_0 thus resembles that of a Druyvesteyn distribution, although the mechanism is not heavy particle collisions. In the opposite case, it may be that the distribution function is more populated at high energies

compared to the Maxwell distribution. This can be caused by special heating mechanisms (wave heating, γ effect, super-elastic collisions...).
To characterize the variety of distribution functions, a parameterized version of the distribution function is often used.

$$f_0 \propto exp\left[-\left(\frac{E}{k_B T}\right)^n\right] \tag{6.44}$$

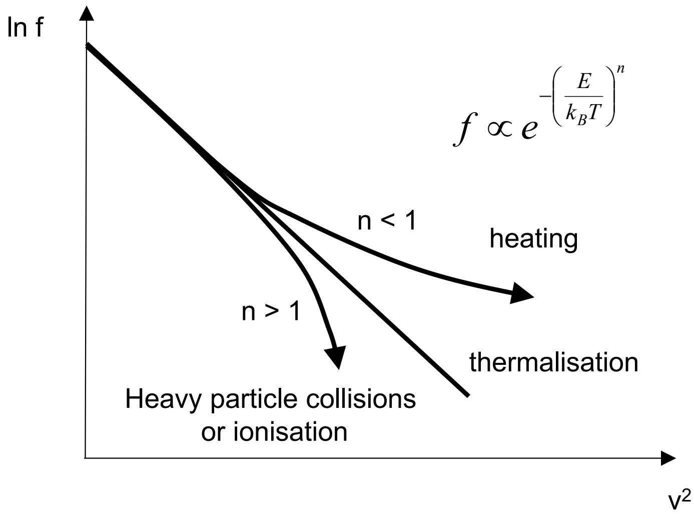

Figure 6.7: Variety of the distribution function

Time-dependent E fields

Based on this consideration, one can finally discuss the change of the distribution function by time-dependent electric fields. Since an electric field now oscillates according to $E_z \sin \omega t$, the anisotropic part of the distribution function also oscillates (Fig. 6.8). In local approximation, one again obtains:

$$\frac{\partial f_1}{\partial t} - \frac{eE_z}{m}\frac{\partial f_0}{\partial v} = -\nu_m f_1 \tag{6.45}$$

In the Fourier space, this results in $f_1 \rightarrow f_1 e^{i\omega t}$ and $E_z \rightarrow E_z e^{i\omega t}$:

$$f_1 = \frac{eE_z}{m(i\omega + \nu_m)}\frac{\partial f_0}{\partial v} \tag{6.46}$$

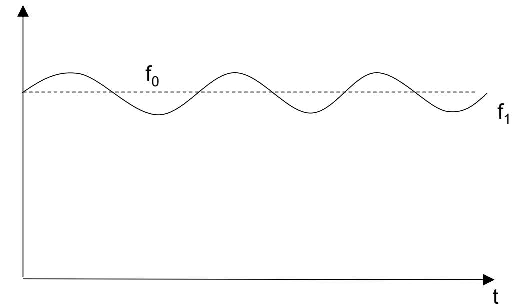

Figure 6.8: Isotropic part f_0 and anisotropic part f_1 of the distribution function for temporally modulated fields.

The real part gives:

$$f_1 = -\frac{eE_z}{m}\frac{\partial f_0}{\partial v}\frac{\nu_m}{(\omega 2^{+}\nu_m^2)} \tag{6.47}$$

For the case of collisions with neutral particles of finite mass, equation 6.23 yields:

$$\frac{eE_z}{m}\frac{1}{3v^2}\frac{\partial}{\partial v}(v^2 f_1) = -\frac{m}{M}\frac{1}{v^2}\frac{\partial}{\partial v}(v^3\nu_m f_0) \tag{6.48}$$

This simplifies again to:

$$f_1 = -\frac{3m^2}{eE_z M} v\nu_m f_0 \tag{6.49}$$

The distribution function is thus again:

$$f_0 \propto exp\left[-\frac{3m^3}{e^2E_z^2M}\int_0^v v'[\omega^2+\nu_m^2]dv'\right] \tag{6.50}$$

For $\omega \gg \nu_m$ the Maxwell distribution is obtained, since the collisions with the heavy particles are not significant. And for $\omega \ll \nu_m$, the Druyvesteyn distribution is obtained because heavy particle collisions dominate. From this approach, one can also gain insight into the dependence of the temperature that forms in the plasma. For a temperature to make sense, the velocity distribution must correspond to a Maxwell distribution.
For the exponent, the following must therefore hold, assuming that ν_m does not depend on the velocity.:

$$-\frac{1}{2}mv^2\frac{1}{k_BT_e} = -\frac{3m^3}{e^2E_z^2M}\frac{1}{2}v^2[\omega^2+\nu_m^2] \tag{6.51}$$

or

$$k_BT_e = \frac{e^2E_z^2M}{3m2}\frac{1}{[\omega^2+\nu_m^2]} = \frac{e^2M}{3m^2}\left[E_z\frac{1}{\sqrt{\omega^2+\nu_m^2}}\right]2 \tag{6.52}$$

The latter describes the effective field:

$$E_{eff} = E_z\frac{1}{\sqrt{\omega^2+\nu_m^2}} \propto \frac{1}{\omega} \tag{6.53}$$

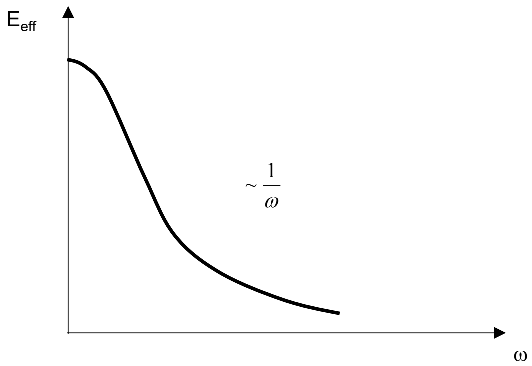

Figure 6.9: The effective electric field decreases with increasing frequency.

i.e., at higher frequencies, the acceleration of the electrons becomes less effective. This is explainable, since at HF fields, the electrons are accelerated and decelerated again in one cycle. If the frequency is very high, the electrons can no longer follow this frequency and the heating becomes ineffective.

6.3 Kinetic wave damping, Landau damping

So far, we have considered the influence of electric fields on the distribution function in order to describe phenomena such as wave heating and the anisotropy of the distribution function due to drifting, etc. As a last example, we want to describe collisionless damping of a plasma wave, the so-called **Landau damping**. Now we again develop the distribution function into an isotropic part and a perturbation.

$$f = f_0 + f_1 \tag{6.54}$$

This is inserted into the Vlasov equation, neglecting non-linear terms (e.g. $E_1 f_1$) and in local approximation ($\nabla f_0 = 0$), yields:

$$\frac{\partial f_1}{\partial t} + v\nabla f_1 - \frac{eE_1}{m}\frac{\partial f_0}{\partial v} = 0 \tag{6.55}$$

In the Fourier space, this results in:

$$\imath\omega f_1 + \imath vkf_1 = \frac{e}{m}E_1\frac{\partial f_0}{\partial v} \tag{6.56}$$

From the Poisson equation, we obtain:

$$\epsilon_0 \nabla E_1 = -en_1 = -e\int f_1 d^3v \tag{6.57}$$

or

$$\epsilon_0 \imath k E_1 = -e\int f_1 d^3v \tag{6.58}$$

Together, this gives the following integro-differential equation:

$$1 = -\frac{e^2}{km\epsilon_0}\int \frac{\frac{\partial f_0}{\partial v}}{\omega - kv} d^3v \tag{6.59}$$

Finally, a solution for ω of the form[1] is obtained:

$$\boxed{\omega = \omega_p\left[1 + i\frac{\pi}{2}\frac{\omega_p^2}{k^2}\left[\frac{\partial \hat{f}_0}{\partial v}\right]_{v_\Phi}\right]} \tag{6.60}$$

i.e. the wave is damped if the gradient of the distribution function at v_Φ is negative (see chapter Instabilities). For this, the section of the distribution function at the phase velocity v_Φ of the wave is important. The damping is the greater the greater the slope at the location of the phase velocity. The physical cause is illustrated in Figs. 6.10 and 6.11:

If the velocity of the electrons is close to the phase velocity, the electrons can follow the potential change and be pushed into the potential minimum of the wave, i.e., slower electrons are slightly accelerated, and faster ones are decelerated. In the case of a falling distribution function, this means that more electrons are accelerated than decelerated, i.e., net energy is transferred from the wave to the electron velocity, and thus the wave is damped. However,

[1] $\hat{f}_0$ expresses that the distribution function should be normalized to 1 here.

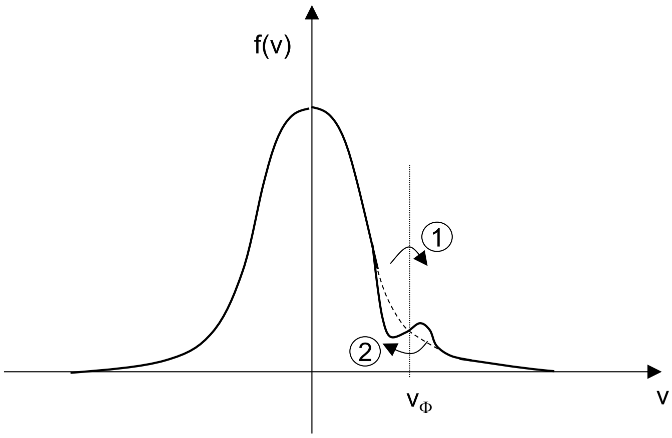

Figure 6.10: Change of the distribution function at the location of the phase velocity v_Φ of a wave.

if the distribution function of the electrons has a positive slope at the phase velocity, energy is transferred from the motion of the electrons into the wave, and it is exponentially amplified.
This damping of the wave is referred to as collisionless damping or **Landau damping**.
The acceleration of electrons in velocity space by the damping of a plasma wave is equivalent to the acceleration of electrons by externally irradiated E-fields in the form of electromagnetic radiation. A prominent example is the acceleration of charge carriers by intense laser pulses. According to the group velocity of an intense laser pulse that is passed through a plasma, the electrons are brought to high energy. This is referred to as **wake-field (=wake) acceleration**.

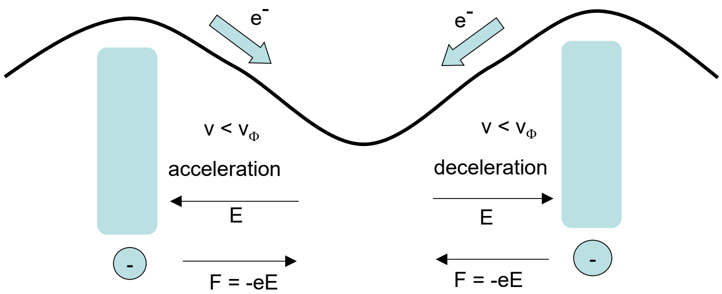

Figure 6.11: Schematic representation of the acceleration (part 1) and deceleration (part 2) of electrons that move at almost exactly the phase velocity of a wave.

Chapter 7

The Plasma Sheath

When generating plasmas on Earth, a confinement of the plasma to a surface of the vacuum vessel is automatically created. This transition between plasma and surface has a complex structure, since the quasi-neutrality of the plasma must be ensured despite the different mobilities of ions and electrons; a space charge zone, the sheath, is formed. This sheath can take on different forms and extensions, depending on the operating conditions of the plasma. The description of this sheath is of central importance for applications of plasma technology in which the particle flux to a surface to be processed is decisive.

7.1 sheath

Given a quasi-neutral plasma in front of a surface. This surface is not grounded. Since the electrons are much more mobile, they leave the plasma at the edge. This locally violates the quasi-neutrality, and an sheath potential is formed that counteracts the loss of electrons. A new equilibrium is established. In this sheath, the electron density is much smaller than the ion density, as illustrated in Fig. 7.1:
At this point, it is well illustrated that there are three types of electric fields in a plasma:

- **Microfield**: The microfield is a fluctuating small electric field that prevails due to the statistical motion of the charge carriers in the vicinity of a given atom or molecule. It is important for the absorption and emission properties of excited atoms and molecules.

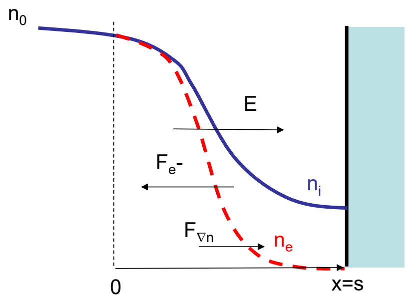

Figure 7.1: Profile of the charge carrier density in the sheath

- **Ambipolar field**: If a gradient in the plasma density is present, electrons and ions can only diffuse simultaneously, otherwise the quasi-neutrality would be violated. The ambipolar field builds up in such a way that the different mobilities of ions and electrons are compensated by accelerating the ions and decelerating the electrons.
- **Field of the sheath**: When transitioning to a surface, the electric field of the sheath is formed to counteract the loss of electrons at the surface.

7.1.1 Space Charge Zone

First, energy conservation applies to the ions according to:

$$\frac{1}{2}Mv_i^2(x) + e\Phi(x) = \frac{1}{2}Mv_0^2 \tag{7.1}$$

v_0 is the velocity with which ions enter this space charge zone. In addition, current conservation applies:

$$n_i(x)v_i(x) = n_0 v_0 \tag{7.2}$$

Solving for $n_i(x)$ with $E_0 = \frac{1}{2}Mv_0^2$ gives:

$$n_i(x) = n_0 \left(1 - \frac{2e\Phi(x)}{Mv_0^2}\right) -1/2 = n_0 \left(1 - \frac{e\Phi(x)}{E_0}\right)^{-1/2} \tag{7.3}$$

For the description of the electron density, the Boltzmann relation is used again:

$$n_e(x) = n_0 e^{\frac{e\Phi(x)}{k_B T_e}} \tag{7.4}$$

Substituting both into the Poisson equation gives:

$$\frac{d^2\Phi(x)}{dx^2} = e\frac{n_0}{\epsilon_0}\left[\exp\left(\frac{e\Phi(x)}{k_BT_e}\right) - \left(1-\frac{e\Phi(x)}{E_0}\right)^{-1/2}\right] \tag{7.5}$$

This equation corresponds to a differential equation for the potential profile $\Phi(x)$ in the sheath. However, this transcendental equation can only be solved numerically.

However, an estimate for the range of the sheath at $x \sim 0$ can be derived as follows. First, the equation is multiplied by $\frac{d\Phi(x)}{dx}$ and integrated over x. On the left side, we obtain

$$\begin{aligned} \int_0^x \frac{d\Phi(x)}{dx}\frac{d^2\Phi(x)}{dx}dx &= \\ \int_0^x \frac{d\Phi(x)}{dx}\frac{d}{dx}\frac{d\Phi(x)}{dx}dx &= \\ \int_0^x \frac{d\Phi(x)}{dx}d\left(\frac{d\Phi(x)}{dx}\right) &= \\ \frac{1}{2}\left(\frac{d\Phi(x)}{dx}\right)^2 & \end{aligned} \tag{7.6}$$

On the right side, we obtain

$$\begin{aligned} \int_0^x \frac{d\Phi(x)}{dx}e\frac{n_0}{\epsilon_0}\left[exp\left(\frac{e\Phi(x)}{k_BT_e}\right) - \left(1-\frac{e\Phi(x)}{E_0}\right)^{-1/2}\right]dx &= \\ \int_{\Phi(0)}^{\Phi(x)} e\frac{n_0}{\epsilon_0}\left[exp\left(\frac{e\Phi(x)}{k_BT_e}\right) - \left(1-\frac{e\Phi(x)}{E_0}\right)^{-1/2}\right]d\Phi & \end{aligned} \tag{7.7}$$

Thus, with the integration over Φ under the assumption that $\Phi(0) = \frac{d\Phi}{dx}\Big|_{x\sim 0}$=0, we obtain:

$$\frac{1}{2}\left(\frac{d\Phi(x)}{dx}\right)^2 = \frac{en_0}{\epsilon_0}\left[k_BT_e e^{\frac{e\Phi(x)}{k_BT_e}} - k_BT_e + 2E_0\left(1-\frac{e\Phi(x)}{E_0}\right)1/2 - 2E_0\right] \tag{7.8}$$

This equation requires that the right-hand side becomes greater than zero for meaningful solutions.

In the region $x \simeq 0$, both $e\Phi \ll k_BT_e$ and $e\Phi \ll E_0$ hold. Thus, an interesting relation can be derived if the right-hand side is expanded to the second order:

$$k_B T_e \left(1 + \frac{e\Phi}{k_B T_e} + \frac{1}{2}\left(\frac{e\Phi}{k_B T_e}\right)^2\right) k_B T_e + \tag{7.9}$$

$$2E_0 \left(1 - \frac{1}{2}\frac{e\Phi}{E_0} - \frac{1}{8}\left(\frac{e\Phi}{E_0}\right)^2\right) 2E_0 \leq 0 \tag{7.10}$$

This term must be greater than or equal to zero. Therefore, it can be concluded that:

$$\frac{1}{2}\frac{(e\Phi)^2}{k_B T_e} - \frac{1}{4}\frac{(e\Phi)^2}{E_0} > 0 \tag{7.11}$$

With $E_0 = \frac{1}{2}Mv_0^2$, the condition for the initial velocity v_0 is obtained:

$$\boxed{v_0 > \sqrt{\frac{k_B T_e}{M}} = v_B} \tag{7.12}$$

This is referred to as the **Bohm velocity**. This is an important result, as it provides a boundary condition for the ion current leaving the plasma. Thus, the energetic particle flux onto a given surface can also be easily estimated. Due to the acceleration of the ions in the sheath, they automatically have a preferred direction. While the direction of the ions in the volume is isotropically distributed, the unidirectional acceleration in the sheath leads to a very narrow angular distribution. i.e. the ions only hit the surface perpendicularly. This is of fundamental importance for the anisotropy of plasma etching in plasma technology: when structuring a trench on a silicon wafer, chemical etching reactions are driven by the ion bombardment. i.e., only at the bottom of the trench do the directed ions hit, and only there is the etch rate high. On the sidewalls of the trench, on the other hand, the incident ion flux is low, and the etch rate is low.

7.1.2 Presheath

In the description of the space charge zone, we have assumed the energy conservation of the ions and found a boundary condition, the Bohm velocity, which must be satisfied for the ions to enter this sheath. This naturally raises the question of how the ions are brought to this velocity.
The acceleration of the ions to the Bohm velocity occurs in the so-called **presheath** (Fig. 7.2). In this presheath, quasi-neutrality must prevail:

$$n_i(x) = n_e(x) \tag{7.13}$$

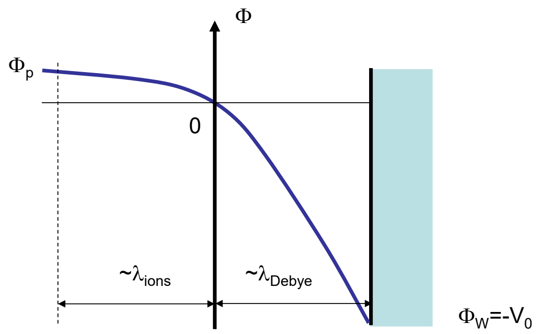

Figure 7.2: Potential profile in presheath and sheath

From this, the following can be derived:

$$\frac{1}{n_i(x)}\frac{dn_i(x)}{dx} = \frac{1}{n_e(x)}\frac{dn_e(x)}{dx} \tag{7.14}$$

With $j_i = n_i e v_i(x)$ we obtain:

$$\frac{1}{n_e(x)}\frac{dn_e(x)}{dx} = \frac{ev_i(x)}{j_i(x)}\frac{d}{dx}\frac{j_i}{ev_i(x)} = \frac{1}{j_i(x)}\frac{dj_i(x)}{dx} - \frac{1}{v_i(x)}\frac{dv_i(x)}{dx} \tag{7.15}$$

With the Boltzmann relation for the electrons, we finally obtain:

$$\frac{1}{v_i(x)}\frac{dv_i(x)}{dx} + \frac{e}{k_B T_e}\frac{d\Phi(x)}{dx} = \frac{1}{j_i(x)}\frac{dj_i(x)}{dx} \tag{7.16}$$

In the presheath, the local ion velocity $v_i(x)$ must always be less than the Bohm velocity v_B. Therefore, the inequality according to Eq. 7.16 is obtained:

$$\frac{1}{v_B}\frac{dv_i(x)}{dx} + \frac{e}{k_B T_e}\frac{d\Phi}{dx} < \frac{1}{j_i}\frac{dj_i}{dx} \tag{7.17}$$

This equation can be satisfied by several conditions:

- **Ion friction**: In the case of current conservation ($\frac{dj_i(x)}{dx} = 0$), the left side must explicitly become less than 0. This can be achieved if the increase in ion velocity is reduced by ion friction. i.e. the change in $v_i(x)$ is not equivalent to a change in $\Phi(x)$.

- **Geometry, Contraction:** Geometric effects can cause the current density to increase as the sheath is penetrated. e.g. $\frac{dj_i}{dx} > 0$ in a cylindrical arrangement.

- **Ionization:** The current through the presheath can increase due to the assumption of additional ionization. Here, $\frac{dj_i}{dx} > 0$ also applies.

It can be seen that collision processes, whether friction or ionization, are essential for the formation of the presheath in the plasma. Thus, it can be immediately concluded that the extent of the presheath must be of the order of the mean free path of the ions. For the description of the plasma edge, two dominant but strongly different scales are thus obtained: the mean free path of the ions for the presheath in the range of typically several cm, and the Debye length for the space charge zone typically in the range of mm to μm.

7.2 Floating potential, Plasma potential

Due to the violation of quasi-neutrality in the sheath, a potential difference builds up. If we denote the charge carrier density at the edge of the sheath with n_0, the currents that hit the surface can be determined. The ion current is given by the Bohm flux:

$$\Gamma_i = n_0 v_B \tag{7.18}$$

and the electron flux that hits the surface corresponds to the directed flux from the volume element directly in front of the surface. If the location of the surface is denoted by $x = s$ and a potential Φ_W prevails there, we obtain using the Boltzmann relation ($n(x = s) = n(x = 0) exp\left(\frac{e\Phi_W}{k_B T}\right)$):

$$\Gamma_e = \frac{1}{4} n(x = s) v_{e,th} = \frac{1}{4} n_0 v_{e,th} e^{\frac{e\Phi_W}{k_B T_e}} \tag{7.19}$$

For the case of a so-called **floating** surface, (i.e. the surface is not grounded) $\Gamma_e = \Gamma_i$ must hold, which implies:

$$n_0 v_B = \frac{1}{4} n_0 v_{e,th} e^{\frac{e\Phi_W}{k_B T_e}} \tag{7.20}$$

$$\left(\frac{k_B T_e}{M}\right)^{1/2} = \frac{1}{4}\left(\frac{8 k_B T_e}{\pi m}\right)^{1/2} e^{\frac{e\Phi_W}{k_B T_e}} \tag{7.21}$$

Thus, the so-called **floating potential** is obtained:

$$\boxed{\Phi_W = -\frac{k_B T_e}{e} \ln\left(\frac{M}{2\pi m}\right)^{1/2}} \tag{7.22}$$

Also, between the sheath and the plasma volume, a potential must drop in which the ions are brought to the Bohm velocity. This can be easily derived from:

$$\frac{1}{2} M v_B^2 = e\Phi_P \tag{7.23}$$

From this, the so-called **plasma potential** is obtained:

$$\Phi_P = \frac{k_B T_e}{2e} \tag{7.24}$$

All potentials are defined here with respect to the sheath edge ($v_i = v_B$). The total potential difference between the plasma potential and an external experimental mass of a plasma reactor includes the entire sheath voltage.

7.3 Sheaths with Applied Voltage

In technical plasmas, the energy of the incident ions is an essential parameter. Processes such as sputtering (the physical dislodging of atoms from a solid by momentum transfer) depend in detail on the energy of the projectiles. Due to the formation of the electric field in the sheath, the ions also hit the surface perpendicularly. This is an essential component of anisotropic etching, where the etching chemistry depends both on the isotropic flux of neutral etching species (fluorine atoms, oxygen atoms, etc.) and on the anisotropic flux of energetic ions. The direction of the ions determines the etching direction of the microstructure. This is of fundamental importance in semiconductor technology for the production of electronic components such as memory cells. To vary the energy of the ions, an arbitrary potential difference is created by applying a negative voltage. With the external voltage source, the electric field in the sheath can be changed, and thus the acceleration of the ions can be adjusted. In plasma technology, however, there is often the problem that cavities or trenches need to be coated or etched: when coating gears, the coating of the flanks is desired, while in anisotropic plasma etching the etching of the sidewalls of a trench is undesirable. The anisotropy or isotropy of the plasma process depends on whether the plasma can penetrate into a cavity or not, as illustrated in Fig. 7.3. Given a certain sheath voltage V and plasma density n, a thickness of the sheath s will be established as a

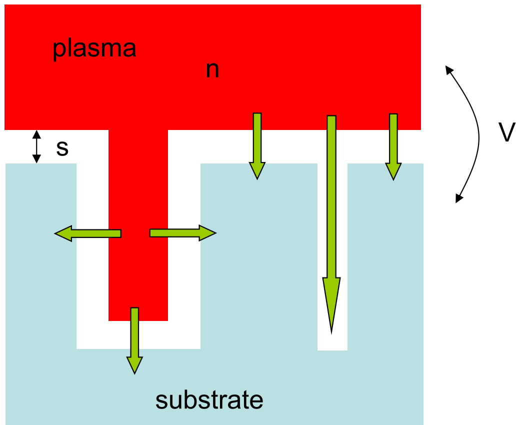

Figure 7.3: The relationship between sheath voltage V, plasma density n and sheath thickness s determines the penetration of plasmas into cavities.

characteristic minimum length scale. Fig. 7.3 illustrates that only the left cavity is filled with plasma and only there the ions also reach the sidewalls. For the evaluation of the penetration of plasmas into small cavities, we need a relationship between the thickness of the sheath s, the sheath voltage V, and the plasma density n. This relationship depends strongly on the assumptions made for the formation of the sheath. A distinction is made between the matrix sheath, the Child-Langmuir sheath and collision-determined sheaths.

7.3.1 Matrix Sheath

In plasma processes, a voltage is often explicitly applied to an electrode. This creates a high voltage drop across the sheath. This high voltage pushes the electrons back further and strongly accelerates the ions. In the simplest approximation, the violation of quasi-neutrality in the sheath can be described as a step function. If the ion density is described as constant in the sheath, one speaks of the so-called **matrix sheath** (Fig. 7.4).

$$\frac{dE}{dx} = \frac{1}{\epsilon_0} e n_0 \tag{7.25}$$

$$E(x) = \frac{1}{\epsilon_0} e n_0 x \tag{7.26}$$

This gives the potential profile:

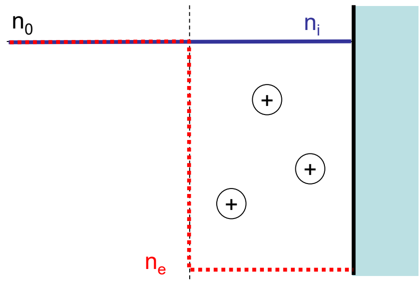

Figure 7.4: Profile of the charge carrier density in the matrix sheath

$$\Phi(x) = -\frac{e}{\epsilon_0} n_0 \frac{1}{2} x^2 \tag{7.27}$$

With $\Phi(s) = -V$ we obtain

$$s = \left(\frac{2\epsilon_0 V}{e n_0}\right)^{1/2} = \lambda_D \left(\frac{2eV}{k_B T_e}\right)^{1/2} \tag{7.28}$$

In practical units, a sheath thickness of:

$$s[\mathrm{cm}] = 1052 \left(\frac{V[\mathrm{V}]}{n[\mathrm{cm}^{-3}]}\right)^{1/2} \tag{7.29}$$

This result shows that the sheath can be many Debye lengths thick. In the description of the matrix sheath, the acceleration of the ions in the electric field was neglected. This acceleration would, under the assumption of current conservation ($j_0 = n(x)v(x)$), lead to the ion density having to decrease towards the surface. The matrix sheath is a good model for describing **Plasma Immersion Ion Implantation PIII**, where a negative high-voltage pulse is applied to a workpiece. This causes the electrons to be quickly repelled back into the plasma, while the ions cannot initially follow the pulse; the matrix sheath is formed. In this matrix sheath, the ions then pass through the electric field and are implanted into the workpiece with high energies.
The advantage of this pulsed approach is the fact that the thickness of the sheath can be much thinner compared to a permanently applied voltage (Child-Langmuir sheath, see below). i.e. with a given plasma density n and voltage V, a cavity *can still* be filled, while the sheath thickness s would be larger in a uniformly operated plasma.

7.3.2 Child-Langmuir Sheath

The assumption of a constant ion density in the sheath is only valid if collisions in the sheath counteract the acceleration of the ions. In the case of a collision-free sheath, the ion density decreases with increasing acceleration, as illustrated in Fig. 7.5. As an approach, we obtain:

$$\frac{1}{2}Mv^2(x) = -e\Phi(x) \tag{7.30}$$

Here we have neglected v_0, since the ions in the sheath are strongly accelerated and their initial energy according to v_0 is of minor importance. Current conservation gives:

$$en(x)v(x) = j_0 \tag{7.31}$$

From Eq. 7.30 and 7.31 we obtain:

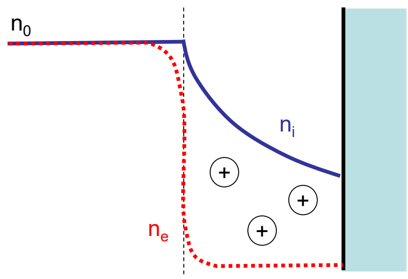

Figure 7.5: Profile of the charge carrier density in the Child-Langmuir sheath

$$n(x) = \frac{1}{e}j_0\left(-\frac{2e\Phi(x)}{M}\right)^{-1/2} \tag{7.32}$$

Thus, the Poisson equation gives:

$$\frac{d^2\Phi(x)}{dx^2} = -\frac{j_0}{\epsilon_0}\left(-\frac{2e\Phi(x)}{M}\right)^{-1/2} \tag{7.33}$$

At this point, the electron density in the sheath is neglected. This is a good approximation at high sheath voltage, since the electrons are effectively repelled back into the plasma volume.
Multiplication by $\frac{d\Phi(x)}{dx}$ and integration over x gives:

$$\frac{1}{2}\left(\frac{d\Phi}{dx}\right)^2 = 2\frac{j_0}{\epsilon_0}\left(\frac{2e}{M}\right)-1/2(-\Phi)^{1/2} \tag{7.34}$$

In the integration, the boundary conditions were used that $\Phi(0) = 0$ and $\left.\frac{d\Phi(x)}{dx}\right|_{x=0} = 0$. From this, for $\Phi(s) = -V$ we obtain:

$$\boxed{j_0 = \frac{4}{9}\epsilon_0\left(\frac{2e}{M}\right)^{1/2}\frac{V^{3/2}}{s^2}} \tag{7.35}$$

This corresponds to the space charge-limited current according to the **Child-Langmuir law** ($V^{3/2}$-law). With the condition

$$j_0 = en_0 v_B \tag{7.36}$$

an expression for the sheath thickness s can also be derived:

$$s = \frac{\sqrt{2}}{3}\lambda_D\left(\frac{2eV}{k_B T_e}\right)^{3/4} \tag{7.37}$$

These relationships provide a link between the particle density n_0, the thickness of the sheath s, the temperature of the electrons T_e, and the applied voltage V. The comparison with the matrix sheath shows that the extent of the Child-Langmuir sheath is greater. Due to the decrease in ion density according to the acceleration, the extent of the space charge zone must be greater in order to achieve the same charge quantity for the same voltage drop. In practical units, the sheath thickness can be calculated as:

$$s[\mathrm{cm}] = 590\frac{(V[\mathrm{V}])^{3/4}}{(T_e[\mathrm{eV}])^{1/4}(n[\mathrm{cm}^{-3}])^{1/2}} \tag{7.38}$$

For a given plasma process, the extent of the sheath can be estimated to decide to what extent a plasma can penetrate into the opening of a workpiece or not. These dependencies can be illustrated as follows:

- The sheath thickness increases with increasing voltage.
- With increasing electron density at a given sheath voltage, the sheath thickness decreases.
- With increasing electron temperature, the sheath thickness decreases.

For practical application, however, the exact quantitative relationship is essential. This, however, depends on the assumption of whether collisions of the ions in the sheath can be neglected or not.

7.3.3 Collision-determined sheath

So far, we have assumed a sheath in which the velocity of the ions increases according to energy conservation. Collisions of the ions in the sheath were neglected. The other limiting case arises from the assumption that collisions in the sheath limit the velocity, as expressed by the mobility. First, flux conservation applies in the sheath.

$$n_i(x)v_i(x) = n_0 v_B \tag{7.39}$$

but the velocity is given by

$$v_i(x) = \mu E \tag{7.40}$$

The mobility is given as:

$$\mu = \frac{e}{m\nu_m} \tag{7.41}$$

with $\nu_m = n_g \sigma v$. For the description of the collision frequency, the velocity is important. Here, two different approaches can be chosen: (i) at high pressure, the collision frequency is given by the thermal velocity (ii) at low pressure and large mean free paths, the velocity is rather the drift velocity. These two cases give:

- **Constant mean free path $\lambda =$ const.**

  At low pressure, the mean free path $\lambda = 1/n_g\sigma$ is constant, and for the collision frequency we directly set $\nu_m = n_g \sigma v$. The mobility becomes:

  $$v_i(x) = \mu E = \frac{e}{M\nu_m} E = \frac{e\lambda}{M v_i(x)} E \tag{7.42}$$

  This gives for a velocity-independent mean free path:

  $$v_i(x) = \left(\frac{e\lambda}{M} E(x)\right)^{1/2} \tag{7.43}$$

  The ion density is obtained:

  $$n_i(x) = \frac{v_B}{v_i(x)} n_0 = v_B n_0 \left(\frac{e\lambda}{M} E(x)\right)^{-1/2} \tag{7.44}$$

  This is substituted into the Poisson equation, neglecting the electron density in the sheath:

$$\frac{dE}{dx} = \frac{e}{\epsilon_0} n_0 v_B \left(\frac{e\lambda}{M} E(x) \right)^{-1/2} = \frac{1}{\epsilon_0} j_0 \left(\frac{e\lambda}{M} E \right)^{-1/2} \tag{7.45}$$

As current density, we obtain:

$$j_0 = \frac{2}{3} \left(\frac{5}{3} \right)^{3/2} \epsilon_0 \left(\frac{2e\lambda}{\pi M} \right)^{1/2} \frac{V^{3/2}}{s^{5/2}} \tag{7.46}$$

It can be seen that the scaling is very similar to the Child-Langmuir law. Only the dependence on the sheath thickness is somewhat different, since the ion density cannot decrease as quickly compared to free fall. A further comparison also shows that the collision-determined sheath is equal to the Child-Langmuir sheath multiplied by $(\lambda/s)^{1/2}$. i.e., the space charge-limited current is only reduced if the mean free path becomes smaller than the space charge zone.

In practical units, a sheath thickness is obtained under the assumption of a cross section $\sigma = 10^{-19} m^2$ for ion-neutral particle collisions:

$$s[\text{cm}] = 277 \frac{1}{\left(p[\text{Pa}] T_e[\text{eV}]\right)^{1/5}} \frac{\left(V[\text{V}]\right)^{3/5}}{\left(n[\text{cm}^{-3}]\right)^{2/5}} \tag{7.47}$$

- **Constant mobility ν_m = const.**

  At high pressure, the collision frequency is independent of the velocity and the mobility becomes a constant. Thus, we obtain:

$$\frac{dE}{dx} = \frac{j_0}{\epsilon_0} \mu{-1} E{-1} \tag{7.48}$$

  This solves to:

$$j_0 = \frac{9}{8} \epsilon_0 \mu \frac{V^2}{s^3} \tag{7.49}$$

The average velocity used to determine μ or ν_m can be the thermal velocity. This is particularly true at high pressure and many collisions.
It can be seen that depending on the boundary condition and prior assumption, the relationship between potential, voltage, and sheath thickness is different. Accordingly, the models for describing low-temperature plasmas, which are treated in the next chapter, are also diverse.

7.4 Probe Measurements

The currents through a sheath to a surface depend on the potential of this surface and on the electron temperature according to the Bohm velocity. i.e., by recording a current-voltage characteristic, it should be possible to obtain information about the distribution function of the charge carriers and their density. This circumstance is utilized by a probe measurement:

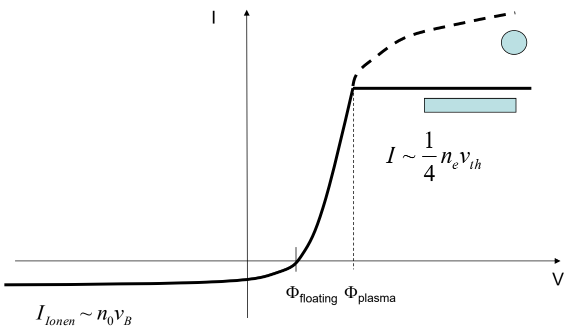

Figure 7.6: Probe characteristic

Three regions in the current-voltage characteristic can be distinguished (probe is planar) (see Fig. 7.6).

- **Ion saturation current**

  At strongly negative bias of the surface, the electrons are repelled, and the current is essentially carried by the ions. From this region, the charge carrier density is generally determined. The current density is given by.

$$j_{\text{Ions}} = -en_0 v_B \tag{7.50}$$

- **Floating region**

  At medium voltages, the electrons are no longer completely repelled, and the electron current can compensate for the ion current (this corresponds to the floating potential), or the electrons are no longer repelled (this corresponds to the plasma potential). The current is proportional to

$$j_{\text{e}} = \frac{1}{4} en_0 v_{e,th} \exp\left(\frac{eV - e\Phi_P}{k_B T_e}\right) \tag{7.51}$$

The total current that the probe sees is of course the ion current plus the electron current; i.e., to correctly determine the electron current, the ion current must still be subtracted in the floating region.

- **Electron saturation current**

  At voltages above the plasma potential, all electrons are collected, and the current obtained is

$$j_{\rm e} = \frac{1}{4} e n_0 v_{e,th} \tag{7.52}$$

In general, from the floating region not only the electron temperature can be determined but of course also the distribution function of the electrons. With increasing voltage V, fewer and fewer electrons are repelled. Therefore, from the velocity space of the electrons, an increasingly larger volume in phase space contributes to the current:

$$j_e = e \int_{v_{min}}^{\infty} v^2 f(v) dv \int_0^{2\pi} d\phi \int_0^{\Theta_{min}} \underbrace{v \cos\Theta}_{z-projection} \sin\Theta d\theta \tag{7.53}$$

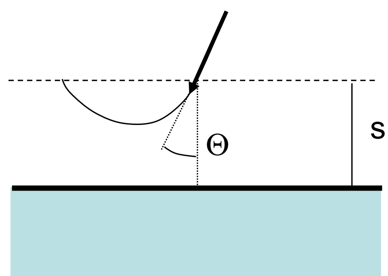

Figure 7.7: The sheath as a velocity filter of the incident ions or electrons

The connection between azimuthal angle and minimum velocity is:

$$\cos\Theta_{min} = \frac{v_{min}}{v} \tag{7.54}$$

Thus, we obtain:

$$j = e\pi \int_{v_{min}}^{\infty} v^3 \left(1 - \frac{v_{min}^2}{v^2}\right) f(v) dv \tag{7.55}$$

We now consider the distribution function not as a function of velocity but as dependent on the energy ϵ with

$$\epsilon = \frac{1}{2}mv^2 \tag{7.56}$$

Furthermore, we consider the minimum velocity v_{min} expressed by the potential difference V, which drops between probe and plasma ($V = \Phi_p - V_{Probe}$) and which holds back the electrons with velocities smaller than v_{min}. Through this coordinate transformation, we obtain:

$$I = \frac{2\pi e^3}{m^2}A\int_V^\infty \epsilon\left(1-\frac{eV}{\epsilon}\right)f(\epsilon)d\epsilon \tag{7.57}$$

The derivative with respect to the potential difference V gives:

$$\frac{dI}{dV} = -\frac{2\pi e^3}{m^2}A\int_V^\infty f(\epsilon)d\epsilon \tag{7.58}$$

or:

$$\frac{d2I}{dV2} = \frac{2\pi e^3}{m^2}Af(\epsilon) \tag{7.59}$$

i.e., the second derivative of the characteristic is directly proportional to the distribution function of the electrons. In practice, this determination of the distribution function is made difficult by the necessity (i) to subtract the ion current from the measured total current, (ii) to determine the plasma potential, and (iii) to form the second derivative with noisy data.

In addition to these aspects of evaluation, it should be noted that often a small cylindrical probe is chosen in order not to disturb the plasma. However, with a cylindrical probe, the conservation of angular momentum and the expansion of the sheath with increasing negative or positive voltage of the probe must be taken into account when considering the electron and ion currents. Here, two cases can be distinguished: (i) in the collision-free case, the currents result from the OML (orbital motion limited) theory, while in the case with collisions in the sheath, the current is determined by the radial transport. These two cases are illustrated in Fig. 7.8.

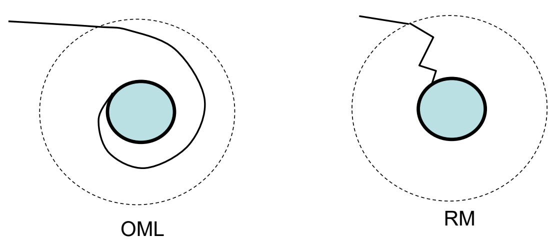

Figure 7.8: Orbital-Motion-Limited (OML) current, Radial-Motion-Limited (RML) current

Chapter 8

Application: Low-Temperature Plasmas

A prominent application of plasma physics is technical plasmas for light generation, plasma etching, or plasma synthesis of thin films or nanoparticles. In these low-temperature plasmas, the electron temperatures are usually very high, while the ion temperatures are low. Moreover, the degree of ionization is $\ll 1$. For the description of these plasmas, the ignition criterion is initially decisive, which determines when a plasma can be maintained. For the operation of the plasma, there are then several preferred configurations in which different forms of electric DC and AC fields are irradiated. All these discharge forms have different fields of application, which differ in terms of the charge carrier density and the scalability of the plasmas.

8.1 DC Discharge

8.1.1 Townsend Discharge - Unself-Sustained Discharge

If a voltage is applied across a gas-filled gap, charge carriers can be accelerated therein and ionize the gas. At sufficiently high voltage, the ionization can be amplified by an electron avalanche. If the first charge carrier of this avalanche must be generated by an external source, such as cosmic rays, photoeffect, etc., one speaks of an **unself-sustained discharge**.
The increase in current over a path length dx with an amplification factor α and an external source term S is:

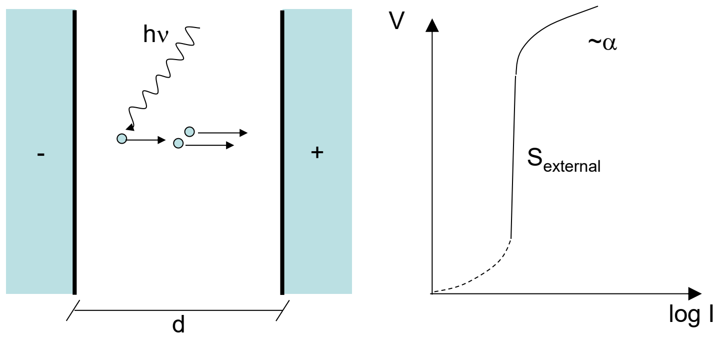

Figure 8.1: Townsend Discharge

$$d\Gamma = \alpha\Gamma dx + S_{extern}dx \tag{8.1}$$

This gives:

$$\Gamma = S_{\text{extern}}\frac{1}{\alpha}(e^{\alpha x} - 1) \tag{8.2}$$

The coefficient α is referred to as the **first Townsend coefficient**. It corresponds to the number of ionization processes per path length and electron:

$$\alpha = \underbrace{\frac{1}{\lambda}}_{Collisions\ \ per\ length} \underbrace{\exp\left[\frac{E_{Ionization}}{E_{e^-}}\right]}_{Probability\ for\ ionization} \tag{8.3}$$

with the energy E_{e^-} that an electron can absorb between two collisions. This is obtained from the field strength $\vec{E}$ and the mean free path λ as:

$$E_{e^-} = \lambda\vec{E} \tag{8.4}$$

If, in addition, it is taken into account that the mean free path $\lambda \propto 1/p$, one obtains

$$\alpha = Ap\exp\left(-B\frac{p}{E}\right) \tag{8.5}$$

with the parameters A and B. For a given plate spacing d and voltage V with $E = V/d$, one obtains:

$$\alpha = Ap\exp\left[-B\frac{pd}{V}\right] \tag{8.6}$$

The electron multiplication is thus a function of the ratio of field strength to pressure or particle density. The value E/n is often given in the unit *Townsend* Td[$= 10^{-17}$ Vcm^2].
Applications of this discharge are corona discharges for charge application in copiers or for flue gas cleaning in power plants.

8.1.2 Glow Discharge - Self-Sustained Discharge, Paschen Curve

For the ignition of a *self-sustained* discharge in a gas-filled gap, several conditions must be met. Over a distance corresponding to the mean free path, the electrons must have absorbed so much energy that ionization can take place.

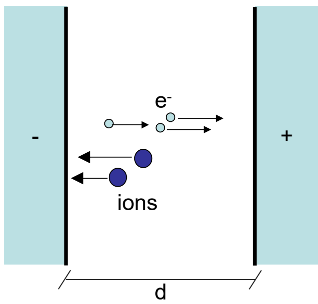

Figure 8.2: Ignition criterion

The electron multiplication is characterized by a coefficient α. The local electron flux is thus:

$$\frac{d\Gamma_e}{dx} = \alpha\Gamma_e \tag{8.7}$$

or

$$\Gamma_e(d) = \Gamma_e(0)e^{\alpha d} \tag{8.8}$$

The number of electrons generated in this avalanche is:

$$\Gamma_e(d) - \Gamma_e(0) = \Gamma_e(0)e^{\alpha d} - \Gamma_e(0) \tag{8.9}$$

For each ionization, an ion is naturally also generated. This requires that:

$$\Gamma_i(0) - \Gamma_i(d) = \Gamma_e(d) - \Gamma_e(0) \tag{8.10}$$

This discharge becomes self-sustained when the generation of the first electrons according to $\Gamma(0)$ does not depend on an external source. A possible process is the generation of secondary electrons by the impinging ions at the cathode. The connection between ion current and generation of secondary electrons can be written as:

$$\Gamma_e(0) = \gamma_i \Gamma_i(0) \tag{8.11}$$

The secondary electrons triggered by the electrons cannot contribute to plasma generation, as they are generated at the *wrong electrode* and thus are not accelerated in the field. Assuming that $\Gamma_i(d) = 0$, one can thus write:

$$\frac{1}{\gamma_i}\Gamma_e(0) = \Gamma_e(0)e^{\alpha d} - \Gamma_e(0) \tag{8.12}$$

γ is referred to as the **second Townsend coefficient**. The equation can be reduced to the following condition for the ignition of a self-sustained discharge:

$$\alpha d = \ln\left(1 + \frac{1}{\gamma}\right) \tag{8.13}$$

So far, α has not been specified in more detail. The first Townsend coefficient contains the electron multiplication, which should depend on the mean free path, the ionization energy, and the field strength. As an approach for α, one uses:

$$\alpha \propto n_g \exp\left(-\frac{E_{Ionization}}{\frac{V}{d}\lambda}\right) \tag{8.14}$$

The term $\frac{V}{d}\lambda$ describes the energy that an electron can absorb between two collisions. For the pressure p, $n_g \propto p$ and $\lambda \propto p^{-1}$. Thus, one obtains:

$$\alpha = Ap \exp\left(-B\frac{pd}{V}\right) \tag{8.15}$$

Substituting this gives

$$Apd \exp\left(-B\frac{pd}{V}\right) = \ln\left(1 + \frac{1}{\gamma}\right) \tag{8.16}$$

Solving for V gives:

$$\boxed{V = \frac{Bpd}{\ln(Apd) - \ln[\ln(1+\gamma^{-1})]}} \tag{8.17}$$

This equation gives the so-called **Paschen curve**. For large values of pd, the voltage at which ignition is possible increases linearly with Bpd. The factor B contains the ionization energy and thus corresponds to a term that depends on the type of gas.

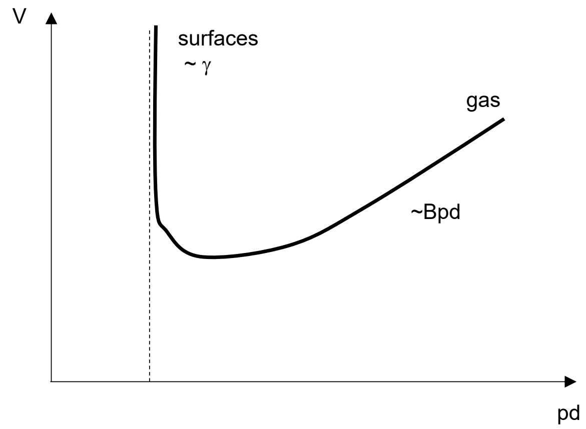

Figure 8.3: Paschen Curve

For small values of pd, a minimum value is obtained below which ignition is no longer possible. This limit is set by the condition $Apd - \ln(1+\gamma^{-1}) = 0$. This includes the coefficient γ, i.e. this limit depends on the electrode material. A glow discharge can be divided into several zones:

- **Cathode Sheath**

  The cathode sheath is generated by secondary electrons, which are accelerated in the electric field. Initially, they still have low energies and can effectively excite gas atoms to luminescence. With further acceleration, the cross section decreases, and a dark space follows.

- **Cathodic Dark Space**

  In the cathodic dark space, the electrons are strongly accelerated, and their density is thus still small. This dark space corresponds to the space charge zone.

- **Negative Glow**

  The electrons accelerated in the sheath can be multiplied by gas collisions. At some point, the electron current is so large that it is effectively

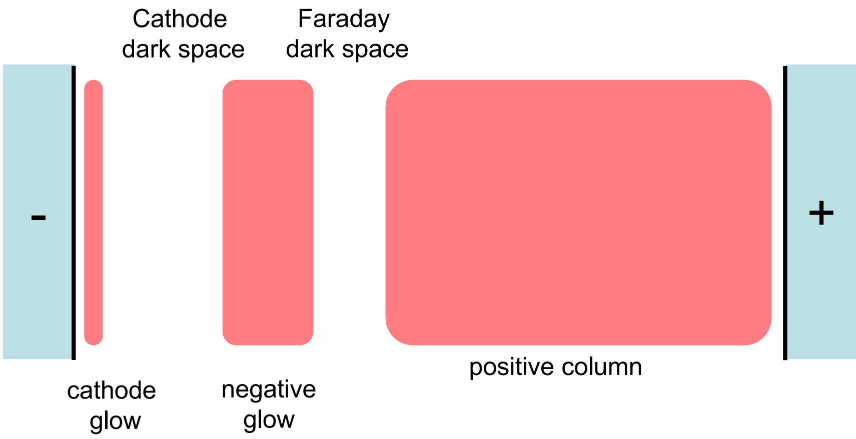

Figure 8.4: Regions of the DC Glow Discharge

sufficient to excite the neutral particles, and the negative glow is created. Through this avalanche, a high density of electrons is created at the end of the cathodic dark space, which creates a negative space charge zone. The corresponding electric field limits this negative glow to the Faraday dark space.

- **Faraday Dark Space**

  The Faraday dark space separates the negative glow from the positive column in which the electric field is very small.

- **Positive Column**

  The positive column represents the connection between the individual cathode layers and the counter electrode. The positive column can be arbitrarily long. Its existence is not essential for the operation of the discharge.

- **Anodic Dark Space**

  In the anodic dark space, the same conditions apply as in the cathodic dark space. It is less extended, since only a small voltage drop occurs here.

The current-voltage characteristics of a DC glow discharge can be described as follows. If a current source is assumed and the resulting voltage is observed, the characteristic in Fig. 8.7 is obtained:

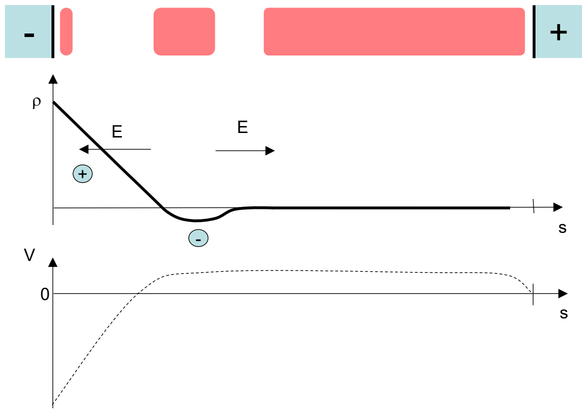

Figure 8.5: Space charge zones of a DC discharge

- **Townsend Discharge:**

  At low currents, the discharge burns unself-sustained. To allow a higher current to flow, the voltage must be increased to increase the charge carrier density according to the first Townsend coefficient α.

- **Normal Glow Discharge:**

  The ignition condition according to the Paschen curve is reached, and the discharge burns self-sustained. An increase in current is now ensured by an increase in the plasma (see Fig. 8.6).

- **Abnormal Glow Discharge:**

  Once the entire electrode is filled, a further increase in current can only be achieved by a higher voltage. According to the Child-Langmuir law, the current increases proportionally to $V^{3/2}$.

- **Arc Discharge:**

  If the current becomes very large, the surface heats up considerably and new charge carriers are formed by thermionic emission. The transition to an arc plasma takes place. This arc plasma is characterized by a high current at low voltage.

In the transition from an unself-sustained to a steady discharge, two types can be distinguished in terms of appearance, the α and the γ-mode. This distinction refers to the essential ionization mechanism, which is characterized by the two Townsend coefficients.

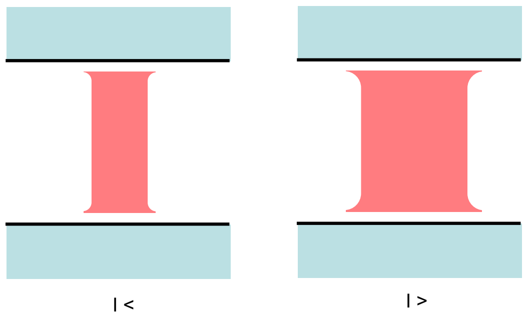

Figure 8.6: Normal glow discharge

- In the α-mode, the ionization is carried by the accelerated electrons in the volume. The luminescence emission in a parallel plate arrangement takes place essentially homogeneously distributed between the plates.
- In the γ-mode, the ionization is carried by secondary electrons at the electrodes. These are injected into the discharge by the high electric field in the sheath and lead to strong luminescence directly in front of the respective electrodes. The luminescence emission in a parallel plate arrangement is strongly inhomogeneous.

8.1.3 Magnetically Assisted DC Discharge, Magnetron Plasmas

In a so-called magnetron discharge , the efficiency of the discharge is increased by attaching magnets behind a DC electrode. In this magnetic field, the electrons are magnetized and can follow the field lines. With a suitable geometry and magnetic field, the secondary electrons are initially accelerated in the sheath and can then oscillate back and forth on an electrode along their gyration path, as shown in Fig. 8.8.
The discharge burns particularly optimally in a region given by the field line whose radius of curvature is in a certain ratio to the Larmor radius. Initially, the secondary electrons are accelerated in the sheath. Depending on the radius of curvature of the field lines emerging at this location, a different Larmor radius results. If the radius of curvature is very large, the Larmor radius remains very small. However, the field lines no longer hit the surface, and a pendulum motion does not take place. If the radius of curvature is very small, the Larmor radius is very large, and the electrons no longer hit the surface after one revolution. An optimum is achieved for an extension of the

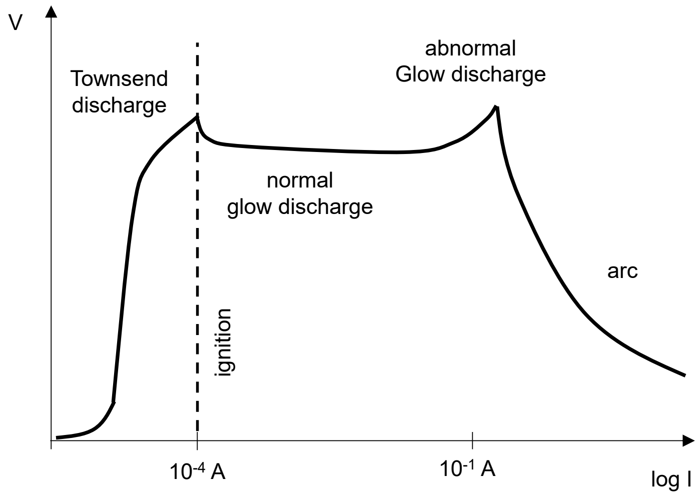

Figure 8.7: Characteristic of a DC discharge

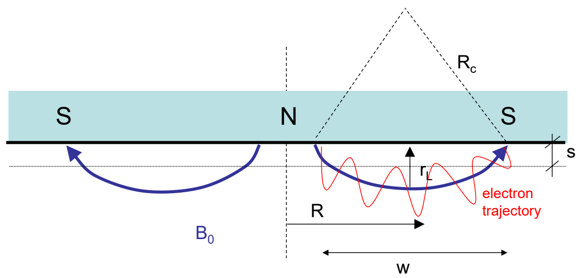

Figure 8.8: Geometry of the magnetron discharge

plasma w (corresponding to the width of a ring on a cylindrical electrode) according to Fig. 8.8:

$$w \simeq 2(2r_L R_c)^{1/2} \tag{8.18}$$

with r_L the Larmor radius:

$$r_L = \frac{v_\perp}{\omega_c} \simeq \frac{1}{B_0}\left(\frac{2mV_{dc}}{e}\right)^{1/2} \tag{8.19}$$

The number of secondary electrons N generated within one pendulum motion is given by:

$$N = \frac{V}{\epsilon_{ionization}} \tag{8.20}$$

with the average energy that an electron must have absorbed to ionize effectively once ($\epsilon_{ionization} \sim 30eV$). Due to charge conservation, the number of ions that trigger secondary electrons and the number of electrons that are generated per period by the pendulum motion must be equal. Thus, we have:

$$1 = \gamma N \tag{8.21}$$

The current across the sheath is again described by the Child-Langmuir law.

8.2 Capacitively Coupled RF Discharges

In a DC discharge, the power coupling is bound to the ohmic DC current flowing between the parallel plates. If this system is operated with alternating current, much higher charge carrier densities can be achieved (Fig. 8.9). Now the plasma is essentially heated by the displacement current, and the ohmic current represents only a very small fraction.

8.2.1 Voltage

To describe the voltage characteristic of a high-frequency discharge (typical frequency 13.56 MHz), we start with the simplest sheath model, the matrix sheath. The field in the space charge zone is calculated as:

$$\nabla E = \frac{e}{\epsilon_0} n \tag{8.22}$$

$$E(x,t) = \frac{en}{\epsilon_0}\left[x - s_a(t)\right] \tag{8.23}$$

The displacement current, which is created by the oscillation of the sheath between the electrode **a** and the plasma **p** (see Fig. 8.9), is given by:

$$I_{ap} = \epsilon_0 A \frac{\partial E}{\partial t} = -enA\frac{\partial s_a}{\partial t} \tag{8.24}$$

with A the area of electrode a. This displacement current must be equal to the rf current in the external circuit:

$$I_{ap} = I_{rf}\cos\omega t \tag{8.25}$$

This implies that the thickness of the sheath is obtained by integrating Eq. 8.24 as:

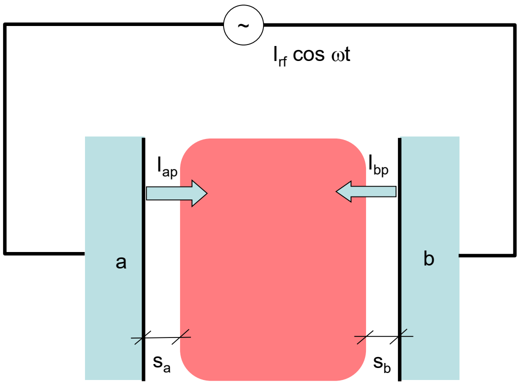

Figure 8.9: Capacitive rf discharge

$$s_a(t) = -\underbrace{\frac{I_{rf}}{en\omega A}}_{s_0}\sin\omega t + \bar{s} \tag{8.26}$$

Here, $\bar{s}$ is the integration constant. The voltage across the sheath **ap** from Eq. 8.23 is:

$$V_{ap} = -\frac{e}{\epsilon_0}n\frac{1}{2}s_a^2(t) \tag{8.27}$$

Substituting $s_a(t)$ gives:

$$V_{ap} = -\frac{1}{2}\frac{en}{\epsilon_0}(\bar{s}^2 + \frac{1}{2}s_0^2 - 2\bar{s}s_0\sin\omega t\frac{1}{2}s_0^2\cos 2\omega t) \tag{8.28}$$

Analogously, we have

$$I_{bp} = -enA\frac{\partial s_a}{\partial t} \tag{8.29}$$

Since $I_{ap} = I_{pb} = -I_{bp}$ must hold, we have

$$\frac{d}{dt}(s_a + s_b) = 0 \tag{8.30}$$

i.e. the extension of the plasma volume (plate spacing-$(s_a + s_b)$) does not change, but oscillates in its position back and forth between the electrodes during the rf cycle. It immediately follows for the sheath at electrode b:

$$s_b(t) = \underbrace{\frac{I_{rf}}{en\omega A}}_{s_0} \sin \omega t + \bar{s} \tag{8.31}$$

The voltage across the sheath **bp** is:

$$V_{bp} = -\frac{1}{2}\frac{en}{\epsilon_0}(\bar{s}^2 + \frac{1}{2}s_0^2 + 2\bar{s}s_0 \sin \omega t \frac{1}{2}s_0^2 \cos 2\omega t) \tag{8.32}$$

With

$$V_{rf} = V_{ab} = V_{ap} + V_{pb} = V_{ap} - V_{bp} \tag{8.33}$$

we obtain the total voltage that drops across the plasma:

$$V_{rf} = \frac{2e}{\epsilon_0} n\bar{s}\frac{I_{rf}}{en\omega A} \sin \omega t \tag{8.34}$$

So far, the average sheath thickness $\bar{s}$ has not been specified. This is obtained from the condition that the electron flux to a surface must compensate for the Bohm flux of the ions. This can only be achieved for the case of the matrix sheath if it is assumed that the sheath briefly collapses during an rf cycle ($s_a(t) = 0$). i.e. according to Eq. 8.26, we must have:

$$0 = -s_0 + \bar{s} \tag{8.35}$$

With this boundary condition, the voltage drop across an sheath is:

$$V_{ap} = \frac{e}{2\epsilon_0} n s_0^2 (1 - \sin \omega t)^2 = \frac{1}{2\epsilon_0}\frac{I_{rf}^2}{enA^2}\frac{1}{\omega^2}(1 - \sin \omega t)^2 \tag{8.36}$$

This gives the relationship between rf current and rf voltage:

$$\boxed{V_{rf} = \frac{2e}{\epsilon_0} n \left(\frac{I_{rf}}{en\omega A}\right)^2 \sin \omega t} \tag{8.37}$$

The course of the individual components of the voltage is shown in Fig. 8.10. One can see that the sheath voltages in front of the electrodes are small for long periods of time within the rf cycle. The sheath voltage is alternately large at electrode a and then at b. In the external circuit, however, the voltage follows a simple law $V_{rf} \sin \omega t$ again.
Fig. 8.10 also shows the spatial distribution of the potential under the assumption that electrode b is grounded and an alternating voltage is applied to electrode a. This behavior can be easily understood if one realizes that the *potential of the plasma must always be the most positive in the system*

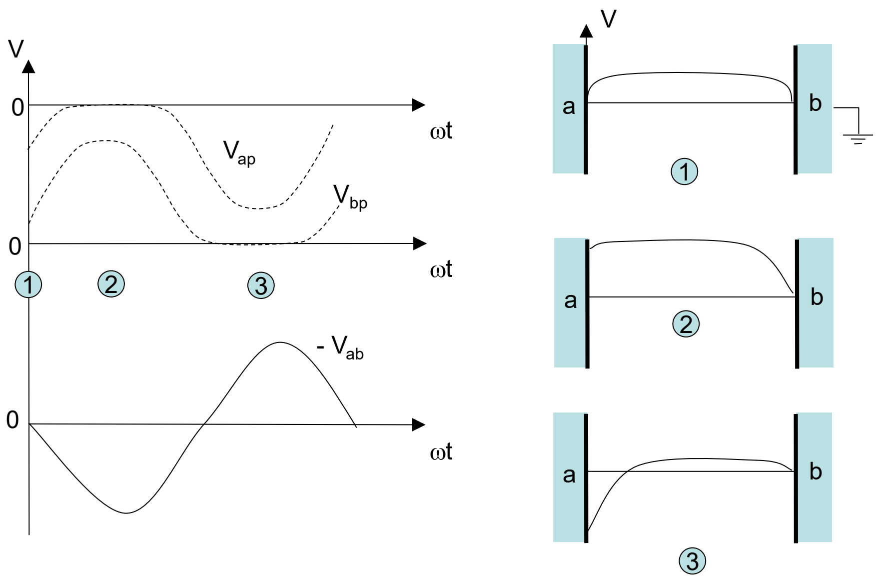

Figure 8.10: Voltage profile between electrodes a and b and plasma p, and between the electrodes.

electrode-plasma-electrode. If this were not the case, the electrons could simply leave the plasma[1].
In the positive half-cycle of the voltage source, the plasma potential follows the potential of electrode a in order to always remain more positive than the external potentials. The potential difference drops in front of electrode b. In the negative half-cycle, the sheath forms in front of electrode a, while the sheath voltage at electrode b remains low.

8.2.2 Heating Methods

Ohmic Heating

In rf discharges, the oscillation of the potential at the electrode leads to time-varying electric fields in which the charge carriers are accelerated:

[1]Only in a few cases does this rule not apply. Thus, in hydrogen plasmas, a so-called **field reversal** occurs for a short period of time in the rf cycle, in which the electric field no longer points in the direction of the plasma volume. This enhances the electron current out of the plasma. This is necessary, otherwise the quasi-neutrality cannot be maintained, since the ion current cannot be compensated by the loss of thermal electrons in front of the surface due to the very light and thus fast hydrogen ions.

$$m\ddot{x} + m\nu_m\dot{x} = eE_0 \sin \omega t \tag{8.38}$$

With the ansatz:

$$x = c_1 \sin \omega t + c_2 \cos \omega t \tag{8.39}$$

we obtain as a solution

$$\dot{x} = -\frac{eE_0\omega}{m}\frac{1}{\omega^2 + \nu_m^2}\left(\cos \omega t - \frac{\nu_m}{\omega}\sin \omega t\right) \tag{8.40}$$

The absorbed power per electron is:

$$p = \frac{d\epsilon}{dt} = \frac{1}{dt}(-)\vec{F}dx = \frac{1}{dt}eE_0 \sin \omega t dx = eE_0 \sin \omega t \dot{x} \tag{8.41}$$

Average power per e$^-$

$$\bar{p} = \int_0^{2\pi} eE_0 \sin \omega t \dot{x} dt \tag{8.42}$$

If the expression for $\dot{x}$ is inserted, the following expression for the absorbed power of an electron is obtained:

$$\bar{p} = \frac{e^2E_0^2}{2m}\frac{\nu_m}{\omega^2 + \nu_m^2} \tag{8.43}$$

The total absorbed power for a particle density n of electrons per volume gives:

$$P = \underbrace{\underbrace{\frac{ne^2}{m\nu_m}}_{\sigma_{dc}}\frac{\nu_m^2}{\omega^2 + \nu_m^2}}_{\sigma_{rf}}\frac{1}{2}E_0^2 = \frac{1}{2}\sigma_{rf}E_0^2 \tag{8.44}$$

or

$$P = \frac{1}{2}\sigma_{rf}E_0^2 = \frac{1}{2}\frac{1}{\sigma_{rf}}j_{rf}^2 \tag{8.45}$$

The total absorbed power per area, which is dissipated by a current I_{rf} flowing through a plasma of thickness d, is given by:

$$P_{total} = \frac{1}{2}I_{rf}^2\frac{1}{\sigma_{rf}}d \tag{8.46}$$

With the relationship between I_{rf} and V_{rf} from Eq. 8.37 for $\nu_m \gg \omega$, we obtain:

$$I_{rf}^2 \propto V_{rf}\omega^2 \tag{8.47}$$

and thus

$$P_{ohmic} \propto \omega^2 V_{rf}\frac{1}{\sigma} \propto \omega^2 V_{rf}\nu_m \tag{8.48}$$

One can see that the absorbed power scales with the voltage V_{rf} and the frequency ω^2. Moreover, collisions according to a collision frequency ν_m are necessary.

Stochastic Heating

In the experiment, it is observed that the power absorption does not completely disappear at low pressures (ν_m becomes small because $\nu_m = n_g\langle\sigma v\rangle$). i.e. despite the lack of collisions with the neutral gas, the electrons apparently can absorb energy from the oscillating field. An explanation is offered by the reflection of the electrons at the oscillating sheaths. For the electrons to experience a net energy gain, the phase of the electron relative to the oscillating field must change after a collision with the moving sheath. The electrons must therefore only hit the sheath in random phase. For this reason, one speaks of **stochastic heating**. The acceleration of the electrons takes place analogously to Fermi acceleration:

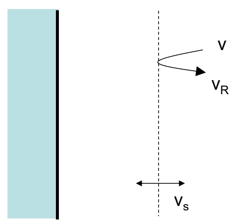

Figure 8.11: Stochastic heating by Fermi acceleration

$$v_R = -v + 2v_s \tag{8.49}$$

The number of incident particles Δn with velocity v, which collide with the sheath per unit time Δt is $\frac{\Delta n}{\Delta t} = (v - v_s)f(v)dv$. The absorbed power is thus per electron of velocity v:

$$dP = d\epsilon\frac{\Delta n}{\Delta t} = \frac{1}{2}m(v_R^2 - v^2)(v - v_s)f(v)dv \tag{8.50}$$

The absorbed power by n electrons is obtained by integrating over the entire velocity space:

$$P = -2m \int_{v_s}^{\infty} v_s (v - v_s)^2 f(v) dv \tag{8.51}$$

If we now substitute Eq. 8.49, we obtain:

$$P = -2m \int_{v=v_s}^{\infty} v_s f(v) v^2 - 2 v_s^2 v f(v) + v_s^3 f(v) dv \tag{8.52}$$

The velocity of the sheath is given as $v_s = v_0 \cos \omega t$. The absorbed power corresponds to the temporal average over an rf cycle. As a result, the odd powers of v_s cancel out by averaging, and we obtain:

$$\bar{P} = -2m v_0^2 \int_{v=\bar{v_s}=0}^{\infty} v f(v) dv = -2m v_0^2 \frac{1}{4} v_{th} n = \frac{1}{2} m v_0^2 v_{th} n \tag{8.53}$$

Here, it should be noted that the integration over the velocity space considers the directed flux in one direction. The dynamics of the sheath is given by

$$j_{rf} \cos \omega t = e n v_s(t) = e n v_0 \cos \omega t \tag{8.54}$$

Thus, we have

$$v_0 = \frac{j_{rf}}{en} \tag{8.55}$$

Thus, the absorbed power by stochastic heating becomes

$$\bar{P} = \frac{1}{2} m \frac{j_{rf}^2}{e^2 n^2} v_{th} n \tag{8.56}$$

The power scales as

$$P_{stochastic} \propto \omega^2 V_{rf} v_{th} = \omega^2 V_{rf} T_e^{1/2} \tag{8.57}$$

One can see that the power coupling in rf plasmas always scales with $\omega^2 V_{rf}$. In plasma processes, it is often desirable to decouple the generation of charge carriers (n_e) from the energy of the impinging ions (V_{rf}). In a simple rf discharge driven at a frequency, the charge carrier generation scales according to $\omega^2 V_{rf}$ and the sheath voltage according to V_{rf}. In multifrequency discharges , however, a high frequency and a small rf amplitude V_{rf} are used to ensure high power coupling while keeping the voltage swing small. For the acceleration of the ions in the sheath, the sheath potential is set by a second, lower frequency with correspondingly higher voltage. Thus, the setting of the charge carrier density and the sheath voltage can be decoupled from each other.

8.2.3 Asymmetric, Capacitive RF Discharge

In a symmetric RF discharge, the voltage swing at both sheaths is identical due to symmetry. If a parallel plate discharge with different electrode sizes is used, a different voltage drop can be forced.

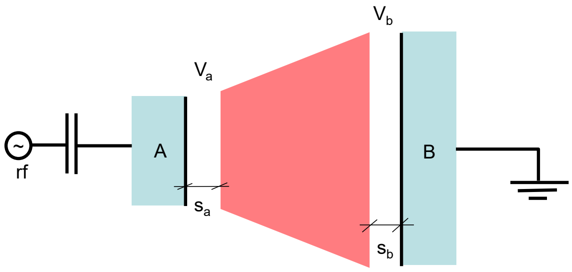

Figure 8.12: Asymmetric RF Discharge

The DC component of the voltage between the two electrodes is, according to Fig. 8.12:

$$V_{bias} = -(\bar{V}_a - \bar{V}_b) \tag{8.58}$$

The plasma can be seen as a series connection of two capacitors C_a and C_b. Each sheath (or capacitor) maintains a charge amount Q that is maintained by the time-averaged voltage $\bar{V}_a$ or $\bar{V}_b$. According to the expression for the capacitance of a plate capacitor, we obtain for the two sheaths:

$$Q = \bar{V}_a C_a = \bar{V}_a \frac{A}{s_a} \epsilon_0 \tag{8.59}$$

$$Q = \bar{V}_b C_b = \bar{V}_b \frac{B}{s_b} \epsilon_0 \tag{8.60}$$

With A and B the areas of electrodes a and b and s_a and s_b the thicknesses of the sheaths. From this consideration of the capacitances, it immediately follows:

$$\frac{\bar{V}_a}{s_a} A = \frac{\bar{V}_b}{s_b} B \tag{8.61}$$

Since the plasma is characterized by a unique density, a second relationship between sheath thicknesses and sheath voltages can be derived. According to the Child-Langmuir law, sheath voltage and sheath thickness are linked as:

$$j_0 \propto n v_B \propto \frac{V^{3/2}}{s^2} \tag{8.62}$$

Since the current density on both electrodes a and b must be equal, we obtain as a second equation:

$$\frac{V_a^{3/2}}{s_a^2} = \frac{V_b^{3/2}}{s_b^2} \tag{8.63}$$

Dividing Eq. 8.61 by Eq. 8.63, we obtain:

$$\frac{\bar{V}_a}{\bar{V}_b} = \left(\frac{B}{A}\right)^4 \tag{8.64}$$

i.e., by a very asymmetric choice of electrode sizes, the average voltage that drops between surface and plasma becomes very large for small electrodes. The exponent 4 essentially arises from the assumption of the Child-Langmuir law. In the experiment, a dependence with an exponent of 2.5 is rather observed. The course of the sheath voltage at an rf electrode is shown in Fig. 8.13.

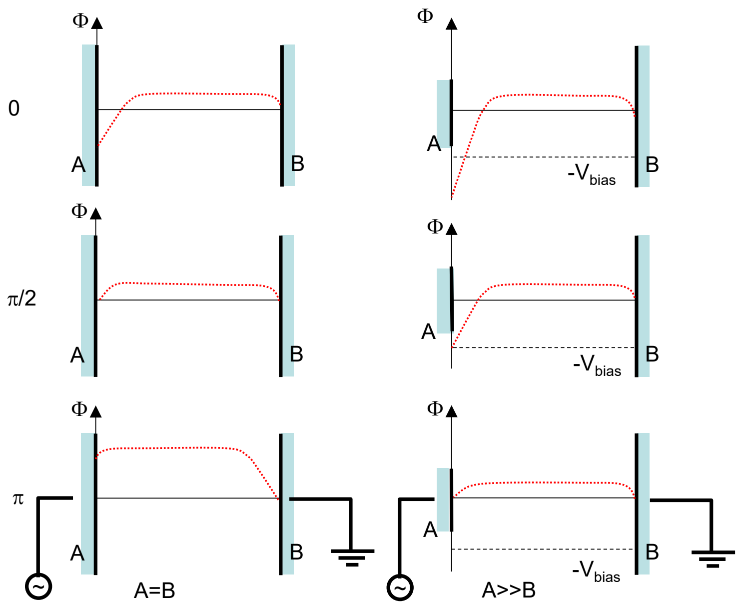

Figure 8.13: Profile of the potential between two electrodes with symmetric electrode size $A = B$ and asymmetric electrode size $A \ll B$.

To ensure the asymmetry of the voltage drop on the two electrodes a and b according to Eq. 8.64, a DC self-bias V_{bias} is established at electrode a: the generator initially generates an alternating voltage V_{rf} with an average of 0, which is connected to the electrode via a capacitor. This capacitor galvanically isolates the generator from the electrode. Thus, it is possible for an additional DC voltage to be established at the electrode, which is superimposed on the alternating voltage. At the electrode, an amplitude of V_{rf} is obtained, but the average of this amplitude is shifted to negative voltages by V_{bias}.

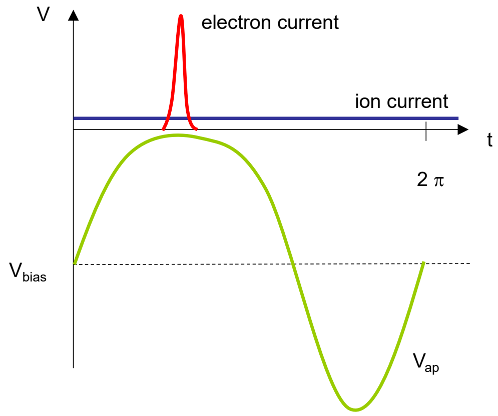

Figure 8.14: Profile of the currents in front of electrode A.

This DC self-bias, however, cannot take on arbitrary values, since the net currents to electrode a must always result in zero. i.e., during an rf cycle, the sheath must collapse at a certain point to allow the electrons to reach the electrode. This is illustrated in Fig. 8.14. The voltage across the sheath at electrode a shows an almost sinusoidal profile. A *maximum* DC self-bias $V_{bias,max}$ is established such that $V_{bias,max}$ is *exactly equal* to the amplitude of the externally applied alternating voltage V_{rf}. This ensures that the sheath collapses at one point and the electron current to electrode a is exactly equal to the ion current to electrode a.
For arbitrary ratios of the electrode sizes, a DC self-bias voltage V_{bias} is established so that Eq. 8.64 can be satisfied. The temporal course of the voltages at the electrode Φ_a and in the plasma Φ_p is illustrated in Fig. 8.15. The ions falling through the sheath can now follow the oscillating field depending on their mass. For very light ions (H^+), the ion energy distribution is correspondingly broad. A characteristic double peak structure is formed, as shown in Fig. 8.16.

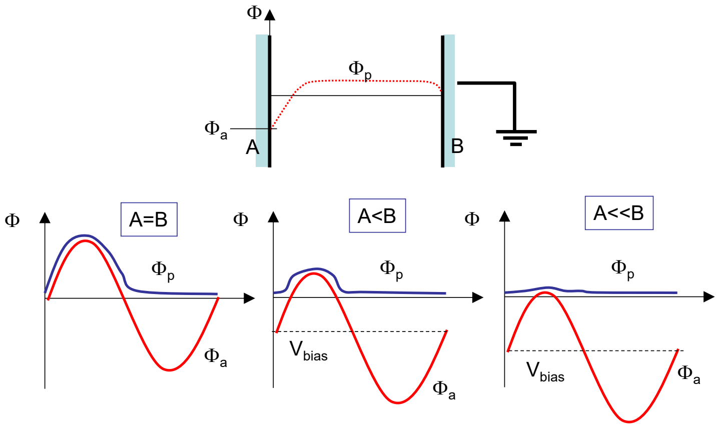

Figure 8.15: Temporal course of the plasma potential Φ_p and the potential Φ_a at electrode a for different ratios of the electrode areas A and B.

8.3 Inductively Coupled RF Discharges

In inductive discharges, an electric field is induced in the plasma via a coil and a dielectric (quartz window). The plasma represents a single secondary winding of a transformer. For this inductive coupling, there are cylindrical or planar configurations. The displacement current flows essentially parallel to the dielectric in the inductive case, while it runs normal to the dielectric in the capacitive case (see Fig. 8.17).

The absorbed power in the plasma depends on the efficiency of the transformer and the volume in which the plasma current flows.

$$P = \frac{1}{2} j_\Theta^2 \frac{1}{\sigma} V \tag{8.65}$$

With this method, high-density plasmas can be generated. Here, the density can reach a value that leads to a penetration depth of the electromagnetic wave that is smaller than the vessel dimension.

The refractive index of a plasma is given by:

$$n^2 = \left[1 - \frac{\omega_p^2}{\omega^2} \frac{1}{1 - i\frac{\nu_m}{\omega}}\right] \tag{8.66}$$

The frequency at which these plasmas are operated (13.56 MHz) is usually smaller than the plasma frequency, so the wave is damped. The penetration depth, or **skin depth** δ is defined as the decay of the wave amplitude to 1/e according to:

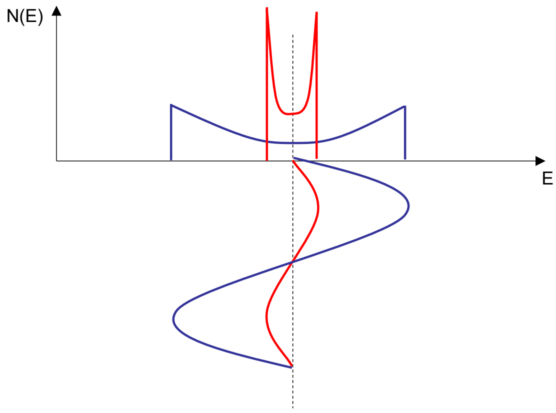

Figure 8.16: Depending on the mass of the ions, they can follow the oscillating field in the sheath more or less. Their energy upon impact on the surface depends on their phase relative to the electric field in the rf cycle. Since the E-field remains maximal or minimal for a longer time, a characteristic double peak structure of the ion energy distribution is formed.

$$\exp(-\alpha x) \qquad \text{with} \qquad \alpha = \frac{1}{\delta} \tag{8.67}$$

In typical inductively coupled plasmas, $\omega < \omega_p$ often applies. Thus, we obtain the following estimates for the **normal skin effect** depending on the ratio between collision frequency ν_m and rf frequency ω:

$$\nu_m \ll \omega \qquad \delta = \frac{c}{\omega_p} = \left(\frac{\epsilon_0 m c2}{ne2}\right)^{1/2} \tag{8.68}$$

and the **anomalous skin effect** in which the penetration depth is frequency-dependent (cf. rf conductivity in metals):

$$\nu_m \gg \omega \qquad \delta = \left(\frac{2\epsilon_0 c^2}{\omega \sigma_{dc}}\right)^{1/2} \tag{8.69}$$

In both cases, however, the skin depth scales as $\delta \propto n^{-1/2}$. The power absorbed thus depends on the volume into which the em wave can penetrate (area $A \times \delta$):

$$P = \frac{1}{2} j_\Theta^2 \frac{1}{\sigma} A \delta \tag{8.70}$$

Here, two cases can be distinguished depending on the vessel dimension d:

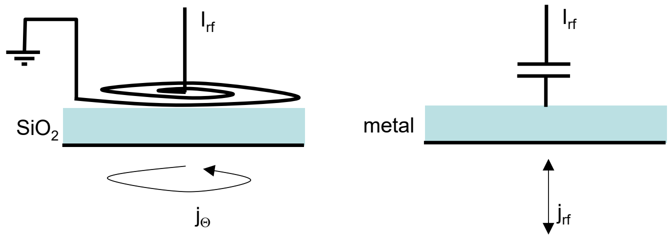

Figure 8.17: Difference between capacitive and inductive coupling

- $\delta > d$

  If the skin depth is very large at low electron density, the em wave can penetrate deeply, but the ability of the secondary winding "plasma" to carry the corresponding current I_{rf} is limited. The achievable current density j_Θ in the plasma is thus proportional to:

$$j_\Theta \propto I_{rf} n \tag{8.71}$$

  Thus, the absorbed power becomes ($\sigma \propto \frac{ne^2}{\nu_m m}$)

$$P_{abs} = \frac{1}{2} I_{rf}^2 n^2 \frac{1}{\sigma} A d \propto I_{rf}^2 n \tag{8.72}$$

- $\delta < d$

  If the skin depth is very small at high electron density, the entire current can be carried in the skin depth. However, the heated volume is now limited and the current density j_Θ in the plasma is proportional to (radius r of the plasma):

$$j_\Theta \propto \frac{I_{rf}}{\delta r} \tag{8.73}$$

  Thus, the absorbed power becomes

$$P_{abs} = \frac{1}{2} I_{rf}^2 \frac{1}{\delta^2} \frac{1}{\sigma} A \delta \propto I_{rf}^2 n^{-1/2} \tag{8.74}$$

From these dependencies of the power on the electron density and the current through the coil, the hysteresis of an inductive discharge and the different heating modes can be derived. This is illustrated in Fig. 8.18. The loss power in the plasma usually scales linearly with the electron density according to the electron collision-induced loss processes:

$$P_{loss} \propto n_g n \nu_{Ionization} \epsilon_{Ionization} \tag{8.75}$$

The electron density is set such that absorbed power and loss power are equal. Thus, three intersection points result in Fig. 8.18. (The increase of P_{abs} occurs more strongly than $\propto n$ with a more accurate estimate). The intersection point at low electron density corresponds to the capacitive mode (**E-mode or CCP: capacitively coupled plasma**); the intersection point at the highest electron density corresponds to the inductive mode (**H-mode or ICP: inductively coupled plasma**). The middle intersection point is unstable, since an increase in electron density increases the power absorption more strongly than the losses.

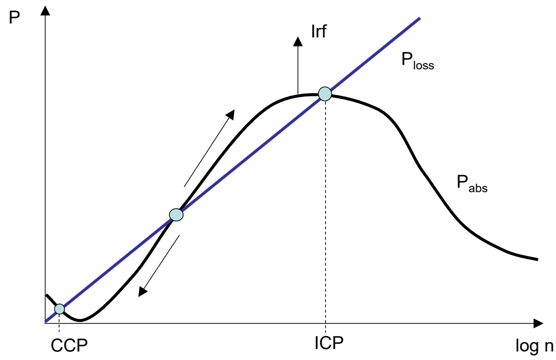

Figure 8.18: Operating points of the inductive discharge

When the current in the primary coil I_{rf} is increased, the curve of P_{abs} is shifted on the y-axis. Accordingly, the individual intersection points appear and disappear. This leads to a hysteresis between the E- and H-mode depending on the type of variation of I_{rf}, as illustrated in Fig. 8.19: In the pure CCP mode, only one intersection point is obtained at low electron densities; with an increase of I_{rf}, three intersection points are created. The discharge, however, remains in the CCP mode; only when the lowest intersection point disappears with further increase does the discharge jump to the ICP mode; if the current I_{rf} is now reduced again, the discharge *remains* in the ICP mode, characterized by the operating point at the uppermost intersection point of P_{abs} and P_{loss}; only when this intersection point disappears with further reduction of I_{rf} does one return to the CCP mode. i.e., a pronounced hysteresis is visible (see Fig. 8.19.

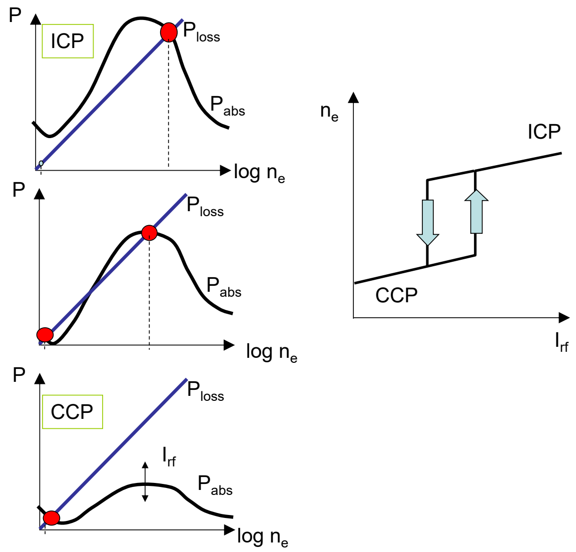

Figure 8.19: In the inductive discharge, only two stable operating points exist. When the power is varied, a pronounced hysteresis is observed.

8.4 Plasmas with Wave Heating

8.4.1 Microwave Plasmas

The plasma density can be further increased by directly irradiating waves. Microwaves ($\sim$ GHz) are often used for this purpose. Due to the frequency dependence of the energy transfer from the em wave to the electrons, the field strengths must be very high. Furthermore, it must be taken into account that the microwaves do not penetrate arbitrarily far into the plasma, since the cut-off is reached due to the high electron density. i.e., the plasma usually forms in front of the coupling window into the vacuum apparatus. This can only be prevented if a special design of the reactor is chosen, which is resonant to a standing wave in the plasma. Thus, a maximum field strength is first created at a certain distance from the coupling window.

8.4.2 ECR Plasmas

Plasmas with wave heating can also be realized resonantly, either by heating at the upper hybrid or by absorption at the cyclotron frequency. From the consideration of the refractive index for em waves in magnetized plasmas, it can be seen that the location of power absorption is fixed by the resonance condition. The em wave can penetrate to this location if the magnetic field strength on the path between the coupling window and the resonance zone is higher than the resonance field strength. One speaks of high-field coupling. This is illustrated in Fig. 8.20.

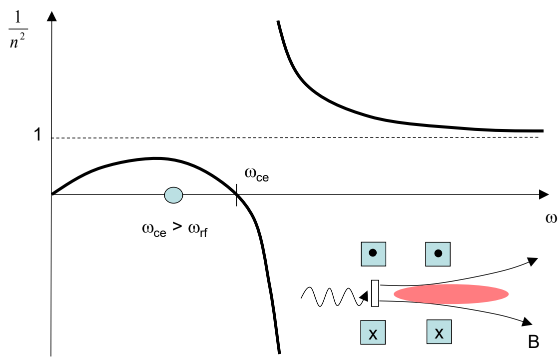

Figure 8.20: ECR discharge

In the resonant heating of the electrons, it must be noted that this takes place in very strongly *inhomogeneous* magnetic fields, i.e. the resonance condition is only satisfied in a very narrowly limited region, as shown in Fig. 8.21.
If electrons with a velocity v_0 pass through this resonance surface, they are accelerated. This is illustrated in Fig. 8.22.
The gradient in the magnetic field can be expressed by a local variation of the cyclotron frequency:

$$\omega_{ce} = \omega_{rf}(1 + \alpha z) \tag{8.76}$$

The path length z that an electron travels through, which passes through the resonance surface with the velocity v_0, is given as $v_0 t$. The velocity of the electrons in the radial direction is expressed in the sense of a phasor diagram by:

$$v = v_x + \imath v_y \tag{8.77}$$

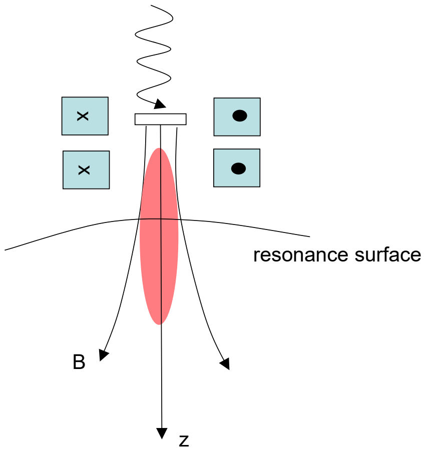

Figure 8.21: Heating of the electrons is only possible in the vicinity of a surface on which the resonance condition applies

Thus, the Lorentz force can be written as:

$$m\frac{dv}{dt} = -eE + e\imath vB \tag{8.78}$$

The gyration can be written as $v = v_r e^{\imath\omega t}$ and the field strength of the right-hand circularly polarized em wave as $E = E_r e^{\imath\omega t}$. Thus, we obtain:

$$\frac{dv_r}{dt} - i\omega_{ce}v_r = -\frac{eE_r}{m} \tag{8.79}$$

or

$$\frac{dv_r}{dt} - i\underbrace{\omega_{rf}(1+\alpha v_0 t)}_{\dot{\Theta}}v_r = -\frac{eE_r}{m} \tag{8.80}$$

Now, let $\alpha v_0 t$ be much larger than 1, and we can write for the temporal development of the angle $\Theta = v_x/v_r$:

$$\dot{\Theta} = \omega_{rf}\alpha v_0 t \qquad \text{or} \qquad \Theta = \omega_{rf}\alpha v_0 \frac{1}{2}t^2 \tag{8.81}$$

The extension to a time-dependent resonance condition is an essential feature of power absorption in ECR plasmas. Without this term, resonant heating would only be possible exactly on the resonance surface. This hard boundary condition is relaxed by the formulation of the time-dependent resonance

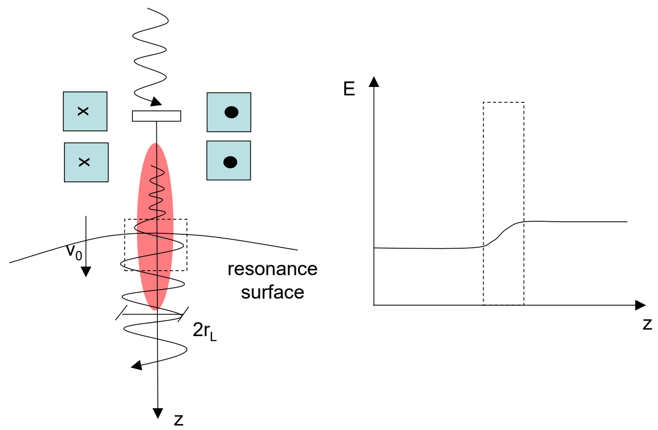

Figure 8.22: When passing through the resonance zone with the velocity v_0, the electrons are briefly accelerated

condition. Equation 8.80 is multiplied by $e^{-i\Theta t}$ and integrated over one revolution.

$$\underbrace{\int \frac{dv_r}{dt} e^{\imath\Theta t} dt}_{\Delta v_r \;\; per \;\; revolution} - \underbrace{\int \omega r f \alpha v_0 t e^{\imath\Theta t} dt}_{=0} = -\frac{eE_r}{m} \int e^{i\Theta t} dt \tag{8.82}$$

This gives:

$$\Delta v_r = \frac{eE_r}{m} \left(\frac{2\pi}{\omega_{rf} \alpha v_0} \right)^{1/2} \tag{8.83}$$

Thus, the energy gain per passage through the resonance surface is given by:

$$\boxed{\Delta\epsilon = \frac{1}{2} m \Delta v_r^2 = \frac{e^2 E_r^2}{m} \frac{\pi}{\omega_{rf} \alpha v_0}} \tag{8.84}$$

8.5 Atmospheric Pressure Plasmas

8.5.1 Arc Discharge

In an arc discharge, the current density in a DC discharge has reached a value at which the heating of the electrodes leads to thermionic emission of electrons. i.e. now a high voltage is no longer needed for electron multiplication in the gas phase, but the electrons are emitted directly from the cathode.

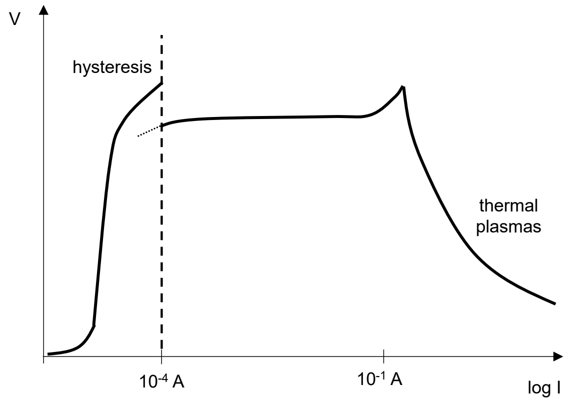

Figure 8.23: Characteristic up to the arc discharge

Thermal emission is described by the **Richardson equation**:

$$j = AT^2 \exp\left[-\frac{e\Phi}{k_B T}\right] \tag{8.85}$$

Arc plasmas are usually operated at atmospheric pressure, and the high pressure implies thermal equilibrium of the individual particle species, electrons, ions, and neutral gas.

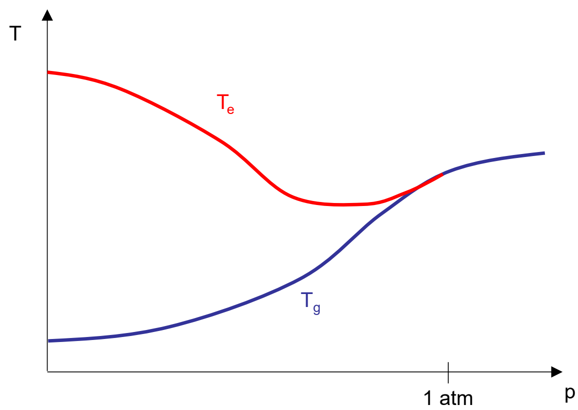

Figure 8.24: Equilibration of neutral gas and electron temperature in an arc plasma

The stability of the arc is characterized by the MHD equilibrium, as sketched in Fig. 8.24.

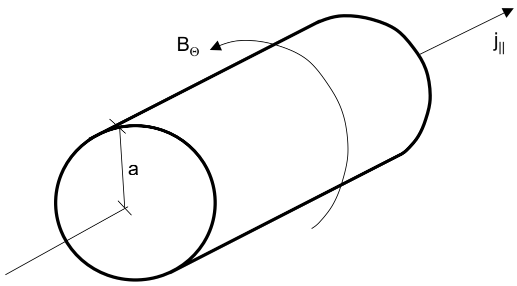

Figure 8.25: Equilibrium of a plasma arc

The current of the arc generates a magnetic field that limits the plasma via $j \times B$ forces. The magnetic field is given by:

$$B_\Theta = \frac{1}{2}\mu_0 j_\parallel r \qquad r < a \tag{8.86}$$

$$B_\Theta = \frac{1}{2}\mu_0 j_\parallel \frac{a^2}{r} \qquad r > a \tag{8.87}$$

and the MHD equilibrium as:

$$\vec{j} \times \vec{B} = \nabla p \tag{8.88}$$

Substituting Eq. 8.86 gives, by integration, for the pressure:

$$p(r) = \frac{1}{4}\mu_0 j_\parallel^2 (a^2 - r^2) \tag{8.89}$$

In the center of the arc, we have:

$$p(0) = p_0 = \frac{1}{4}\mu_0 j_\parallel^2 a^2 \tag{8.90}$$

The current flowing through the arc is $I = \pi a^2 j_\parallel$. Thus, we obtain:

$$p_0 = \frac{1}{4}\mu_0 \frac{I^2}{\pi^2 a^2} \tag{8.91}$$

This describes the pressure for a given extension of the arc and impressed current. Often, the current in thermal plasmas of plasma technology is smaller than that required for the arc to be stabilized by MHD forces alone. Therefore, such an arc is stabilized by a gas flow, by a twisting of the magnetic field lines, by an external magnetic field, or by wall contact.

The arc attachment itself is usually smaller than the extension of the arc. By localization on the electrode surface, the current increases, thus the temperature and thus the electron emission according to the Richardson equation. A **cathode spot** is created. Through this arc attachment, a pressure gradient is created between the electrode and the plasma volume, which drives the gas flow, the so-called **electrode jet**, as sketched in Fig. 8.26. The pressure difference is given by:

$$\Delta p = p_b - p_a = \frac{\mu_0 I^2}{4\pi^2}\left(\frac{1}{b2} - \frac{1}{a^2}\right) \simeq \frac{\mu_0 I^2}{4\pi^2 b^2} \tag{8.92}$$

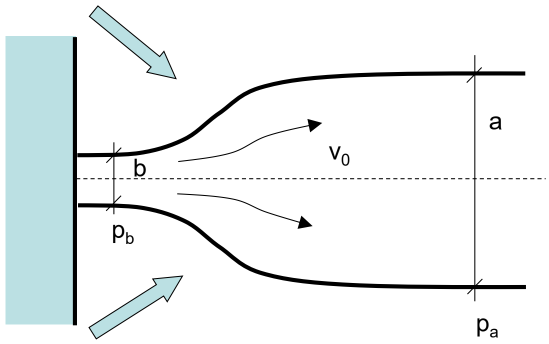

Figure 8.26: The pressure difference between the arc attachment point and the arc itself leads to a so-called electrode jet.

With the Bernoulli equation, the pressure difference can be converted into an outflow velocity according to:

$$\Delta p = \frac{1}{2}\rho v_0^2 \tag{8.93}$$

Thus, we obtain:

$$v_0 = \frac{I}{\pi b}\sqrt{\frac{\mu_0}{2\rho}} \tag{8.94}$$

This outflow velocity reaches up to 100 ms^{-1} and drives the gas mixing of the arc with the surrounding atmosphere (see Fig. 8.25).

8.5.2 Dielectric Barrier Discharge

Filamentary Discharge

If the formation of an arc is to be prevented, this can be achieved by inserting a dielectric barrier into the gas gap. After the ignition of an electron avalanche, these are deposited on the dielectric and thus reduce the field strength in the gas gap. The remaining ions can now flow to the cathode (streamer) and the discharge extinguishes again. These microdischarges occur in the form of individual filaments, which only burn for a short time in the range of nanoseconds and only have a spatial extent in the range of 10 to 100 nm.

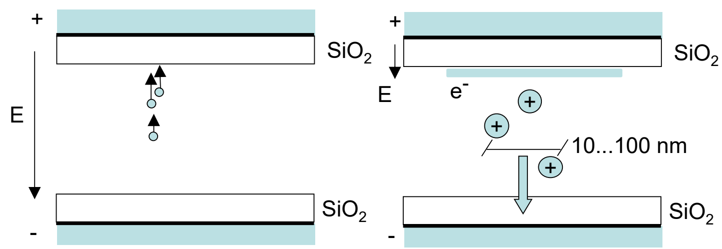

Figure 8.27: Filamentary barrier discharge

An important application of the dielectric barrier discharge is ozone generation for water treatment (see Fig. 8.28). Here, the fact is utilized that ozone decomposes very easily. In the short times of a local filament, the oxygen chemistry is only briefly initiated, and ozone has a significant probability of survival in these discharges. Another technical advantage is the fact that barrier discharges can be easily scaled.

Glow Discharge at Atmospheric Pressure

A disadvantage of barrier discharges is the fact that they are usually filamentary and thus the utilization of a gas flow can never be complete. Moreover, erosion of the surface can occur due to the high local current density in the filaments.
However, it has been shown that it is possible to generate a uniform glow discharge at atmospheric pressure at medium frequencies in the kHz range. To obtain a uniform discharge, it appears that the breakdown of the discharge in the form of a filament is suppressed in these plasmas. There are several explanations for the formation of such a discharge:

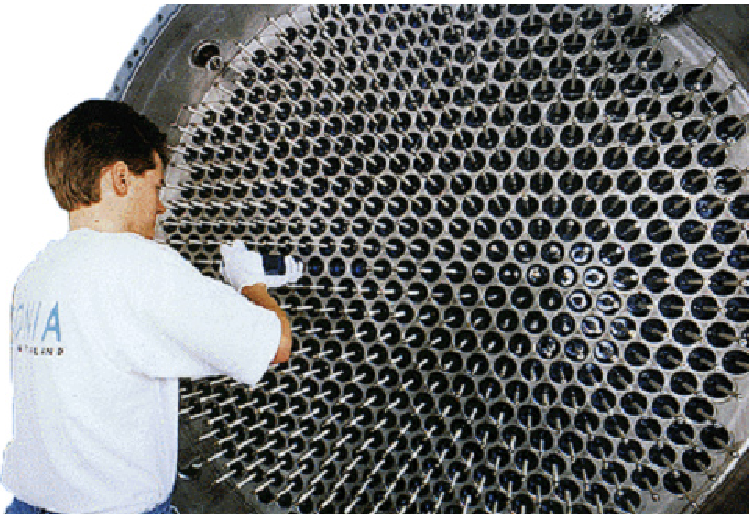

Figure 8.28: Ozone generation in barrier discharges for water disinfection

- **ion trapping**

  At a medium frequency, it can be achieved that the electrons can reach the surfaces while the slower ions are trapped in the oscillating E-field in the middle of the gas gap. In such a situation, one obtains a reduced electric field in the gas gap, and the discharge ignites only in the sheath, but does not break through anymore. This inertia separation of electrons and ions can be estimated from the equation of motion:

$$m\ddot{x} + m\nu_m\dot{x} = eE_0 \sin\omega t \tag{8.95}$$

  This has the solution:

$$x(t) = -\frac{eE_0}{m}\frac{1}{\omega^2+\nu_m^2}\sin\omega t - \frac{\nu_m}{\omega}\frac{eE_0}{m}\frac{1}{\omega^2+\nu_m^2}\cos\omega t \tag{8.96}$$

  If the deflection is averaged over an rf period, for $\nu_m \gg \omega$ one obtains:

$$x_{rms} = \left(\int_0^{2\pi} x^2 dt\right)^{1/2} = \frac{2}{\pi}\frac{eE_0}{m\omega\nu_m} \tag{8.97}$$

  The ions thus remain trapped in the gas gap if the deflection does not become larger than the width d of the gap ($x_{rms} = d$). With the field strength at a voltage V given as $E_0 = V/d$ one obtains:

$$\boxed{\omega = \frac{2e}{\pi m}\frac{1}{\nu_m}\frac{V}{d^2}} \tag{8.98}$$

i.e., at a certain combination of frequency, voltage, and electrode spacing, a uniform glow discharge can be generated at atmospheric pressure.

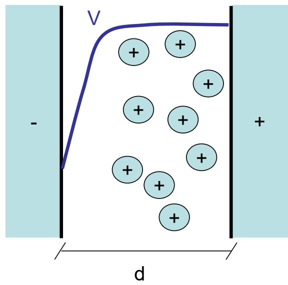

Figure 8.29: Selective inclusion of the ions by utilizing their inertia.

- **Memory Effect**

  The electron avalanche charges the surface. If this surface charge takes a finite time to flow off, it can also remain in the second half of the rf period and even enhance the external field. If the electron density in the gas phase, which was generated in the first half of the rf period, does not decay completely, the discharge can be more easily built up in the second half of the rf period.

- **Penning Ionization**

  If a reservoir of excited atoms is created in the discharge by generating metastables, new electrons can be continuously generated by Penning ionization. Penning ionization for argon is:

$$\mathrm{Ar}^* + \mathrm{Ar} \rightarrow \mathrm{Ar}^+ + \mathrm{Ar} + \mathrm{e}^- \tag{8.99}$$

  The longer lifetime ($\sim \mu s$) of the excited states compared to the lifetime of a single filament ($\sim$ ns) is decisive here.

8.6 Global Plasma Models

With the types of discharges and confinement mechanisms for low-temperature plasmas presented so far, simple dependencies for the temperatures in the plasma and the plasma density can be derived.

8.6.1 Particle Balances

Consider a plasma volume in which the charge carriers can reach the sheath without collision processes. In equilibrium, the loss of charge carriers must be balanced by ionization in the volume. i.e. the loss of ions in a plasma with surface A balances with the ionization in volume V with rate $k_{Ionization}$:

$$An_0 v_B = n_g n_0 k_{Ionization} V \tag{8.100}$$

Substituting the corresponding dependencies on the electron temperature gives:

$$An_0 \sqrt{\frac{k_B T_e}{M}} = n_g n_0 k_{Ionization,0} e^{-\frac{E_{Ionization}}{k_B T_e}} \tag{8.101}$$

From this dependence, one immediately recognizes that the temperature of the plasma must increase when the surface-to-volume ratio becomes larger, since only in this way can the losses be compensated. Also, if the ionization energy $E_{Ionization}$ increases, the plasma must become hotter to compensate for the surface losses. One can see that the *particle balance gives a determining equation for the temperature of the plasma.* This equation can be represented in a shortened form as:

$$\frac{k_{Ionization}}{v_B} = \frac{A}{V} n_g^{-1} \tag{8.102}$$

In the case of a diffusion-determined situation, the ion current Γ_i to the surfaces is limited by ambipolar diffusion. One obtains:

$$\Gamma_i = -D_a \frac{dn}{dx} \tag{8.103}$$

In a planar-parallel geometry, one obtains from the solution of the diffusion equation a dependence as:

$$\Gamma_i = -D_a \frac{n}{l} \pi \tag{8.104}$$

if l is the electrode spacing. In this ambipolar diffusion, the ion current can still be increased by ionization and one obtains:

$$\frac{\Gamma_i}{dx} = k_{Ionization} n_g n \tag{8.105}$$

This can also be linearized and one obtains by integrating a diffusion profile in n from 0 to $l/2$

$$\Gamma_i = k_{Ionization} n_g n \frac{l}{\pi} \tag{8.106}$$

Thus, one obtains:

$$\frac{\pi}{l} D_a = k_{Ionization} n_g \frac{l}{\pi} \tag{8.107}$$

With $D_a = \frac{k_B T_e}{M\nu_m} = \frac{k_B T_e}{M n_g k_m}$ one finally obtains:

$$\frac{(k_{Ionization} k_m)^{1/2}}{v_B} = \frac{\pi}{l} n_g - 1 \tag{8.108}$$

This is analogous to Eq. 8.102.

8.6.2 Energy Balance

In considering the energy balance, a certain power is coupled into a plasma and comes out of the plasma again essentially in the form of light, energetic ions, electrons, and excited neutral particles. The electrons carry a portion of T_e out of the plasma. The dominant contribution is the flux of energetic ions. These carry an energy E_{Ions} corresponding to their ionization energy $E_{Ionization}$ and the acceleration in the sheath with voltage V out of the plasma:

$$E_{Ions} = E_{Ionization} + V \tag{8.109}$$

The dominant contribution here is also the acceleration in the sheath. Thus, the loss power or the absorbed power P_{abs} on a plasma surface A is:

$$P_{abs} = e n v_B A E_{Ions} \tag{8.110}$$

Thus, the particle density n in the plasma is:

$$n = \frac{P_{abs}}{e v_B A E_{Ions}} \tag{8.111}$$

One can see that the plasma density can be derived from a balance equation for the absorbed power. The quantitative determination of the absorbed power for the case that only external quantities such as rf currents and voltages are known is, however, often not easy.

Chapter 9

Application: Nuclear Fusion

The development in plasma physics has been largely driven by the exploration of controlled nuclear fusion. To gain energy from the fusion of atomic nuclei, a plasma must remain confined at a sufficiently high temperature for a long enough time. Only then does the energy release in fusion reactions occur at a rate that maintains the plasma. This ignited thermonuclear plasma has not yet been realized experimentally. However, research has now reached a stage that allows, with an extrapolation to larger fusion experiments, the ignition of a thermonuclear plasma to be demonstrated. This is the declared goal of the international mega-project **ITER** *(Fig. 9.1).*

9.1 Fusion Reactions

The energy gain in nuclear fusion is based on the fusion of light atomic nuclei (see Fig. 9.2. A large amount of energy is released here because the binding energy per nucleon increases in the fusion product (deeper potential well). For fusion to occur, the distance between the atomic nuclei must be small enough for them to tunnel through the repulsive Coulomb barrier to reach the region of strong interaction (see Fig. 9.3). The fusion reactions of hydrogen isotopes with a high cross section are:

$$\mathrm{D} + \mathrm{D} \rightarrow^3 \mathrm{He}(0.8\mathrm{MeV}) + \mathrm{n}(2.45\mathrm{MeV}) \tag{9.1}$$

$$\mathrm{D} + \mathrm{T} \rightarrow^4 \mathrm{He}(3.52\mathrm{MeV}) + \mathrm{n}(14.07\mathrm{MeV}) \tag{9.2}$$

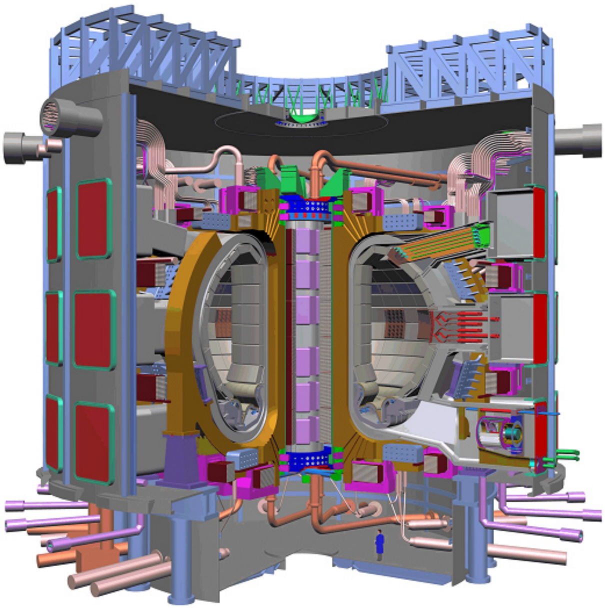

Figure 9.1: Future fusion experiment ITER

In the sun itself, the direct fusion of protons to helium occurs. In future terrestrial fusion reactors, deuterium and tritium will be used as fuel. Since tritium, however, has a short half-life of 11 years, it must be produced in the process. One possibility is to *breed* tritium in the fusion reactor. For this purpose, the fusion neutrons can be used, which, through capture in lithium in the reactor walls, breed tritium again (6Li(n,4He)T).
The fusion cross section in the merging of two atoms with atomic numbers Z_1 and Z_2 is determined by the tunneling process with a cross section:

$$\sigma_{Fusion} = S(E_s)\frac{1}{E_s}e^{-2\pi\alpha Z_1 Z_2 \frac{c_0}{v_s}} \tag{9.3}$$

E_s and v_s are energy and velocity in the center-of-mass system; α is the fine structure constant and c_0 is the speed of light. The exponential term is referred to as the **Gamow factor**.
The principal course of the cross sections is shown in Fig. 9.4. Current experiments are conducted in hydrogen or deuterium. In these, neutron production is low, and experiments can be conducted in a non-radioactive machine.
As an alternative concept to fusion, the μ-catalyzed fusion was investigated for a time. In this process, Mμons are generated in a target by an accelerator (3 GeV protons) with a lifetime of about 10^{-6} s. These Mμons can replace

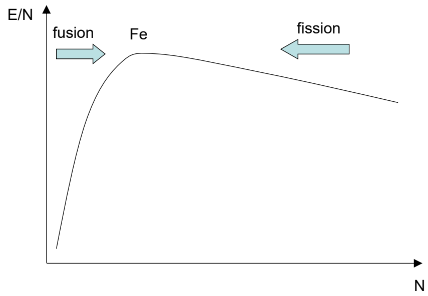

Figure 9.2: Binding energy per nucleon.

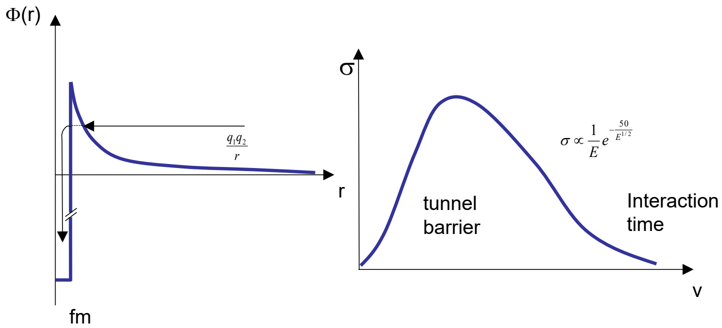

Figure 9.3: Fusion occurs through tunneling through the Coulomb barrier.

the electrons in deuterium or tritium in this target. μonic DT molecules are formed in which the Coulomb barrier is lowered by the smaller Bohr radius, and fusion can occur. With an efficiency of 99.4%, a helium nucleus is formed and the Mμon is released again. Thus, this Mμon can be used to catalyze further DT reactions. Unfortunately, in 0.6% of the DT reactions, muonic helium is also formed, and the muon is thus lost. In the experiment, it is therefore shown that only about 100 DT reactions occur per muon. This is too little to compensate for the energy input to generate the 3 GeV proton.

9.2 Ignition Criterion

To determine the limit from which thermonuclear ignition can occur, a power balance of the fusion plasma must be established. For this purpose, it is necessary to balance the energy gain through fusion processes with the losses due to a finite energy confinement time through bremsstrahlung and line

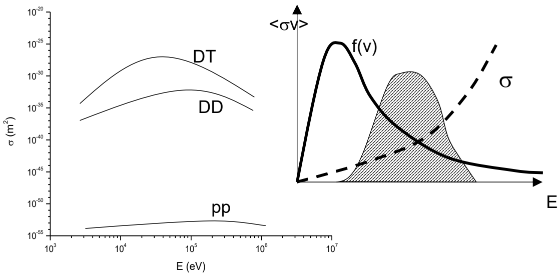

Figure 9.4: Cross sections of some fusion reactions.

radiation.

- **Fusion Energy**

  The rate of fusion reactions is given by:

$$R = n_1 n_2 \langle \sigma v_R \rangle = \frac{1}{4} n^2 \langle \sigma v_R \rangle \tag{9.4}$$

  Here, it is used that always 2 ions are needed for a fusion reaction ($n_1 = 1/2n$). The rate coefficient $\langle \sigma v_R \rangle$ results from a convolution of the distribution function with the cross section:

$$\langle \sigma v_R \rangle = A \int \sigma(v) \exp\left[\frac{mv^2}{2k_B T_i}\right] v3dv \tag{9.5}$$

  or as a function of energy ϵ:

$$\langle \sigma v_R \rangle = \frac{1}{(m\pi)^{1/2}} (k_B T_i)^{3/2} \int \sigma(\epsilon) \exp\left[\frac{\epsilon}{k_B T_i}\right] \epsilon d\epsilon \tag{9.6}$$

- **Bremsstrahlung**

  In fully ionized plasmas, the radiation losses are essentially bremsstrahlung of the electrons, which are deflected in the Coulomb field of the ions. The power radiated by a charge that is accelerated with acceleration a is given by:

$$P_e = \frac{e^2}{6\pi\epsilon_0 c^3} a^2 \tag{9.7}$$

The deflection in the Coulomb field is sketched in Fig. 9.5. Again, we consider small-angle collisions, in which the Coulomb force is expressed in a simplified manner with the impact parameter b:

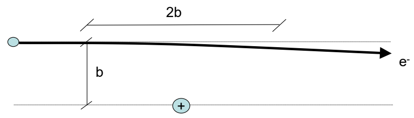

Figure 9.5: Deflection of electrons in the field of ions leads to bremsstrahlung losses of the plasma

$$F = \frac{Ze^2}{4\pi\epsilon_0 b^2} \qquad \text{or} \qquad a = \frac{Ze^2}{m_e 4\pi\epsilon_0 b^2} \tag{9.8}$$

According to Fig. 9.5, this force acts for a time τ, which is given by $\tau = \frac{2b}{v}$ with v the velocity of the electron. i.e. the energy lost in the collision is:

$$\epsilon = P_e\tau = P_e\frac{2b}{v} \tag{9.9}$$

The losses due to bremsstrahlung result from the rate at which these losses occur. Given a density of electrons and ions, for an impact parameter b, the contribution is:

$$P_{br}\mathrm{d}b = \epsilon n_e n_i v 2\pi b \mathrm{d}b = P_e 2b n_e n_i 2\pi b \mathrm{d}b \tag{9.10}$$

with v the relative velocity. Thus, we obtain:

$$P_{br}\mathrm{d}b = \frac{4e^6 n_e n_i Z^2}{3(4\pi\epsilon_0)^3 m_e^2 c^3 b^3} 2\pi b \mathrm{d}b \tag{9.11}$$

The total losses due to bremsstrahlung are obtained by integrating over all impact parameters. In this case, in particular, the minimum impact parameter must be considered. The distance of closest approach is given by the Heisenberg uncertainty relation:

$$\Delta x \Delta p = \hbar \tag{9.12}$$

The momentum uncertainty is $\Delta p = m_e v$ and the minimum impact parameter corresponds to the position uncertainty Δx. Thus, we obtain:

$$b_{min} = \frac{\hbar}{m_e v} \tag{9.13}$$

With this integration limit and the determination of the velocity from $\frac{1}{2}m_e v^2 = \frac{3}{2}k_B T_e$, the loss due to **bremsstrahlung** is:

$$\boxed{P_{br} = \frac{1}{4\pi\sqrt{3}\epsilon_0^3}\frac{e^6}{m_e^{3/2}c^3 h}(k_B T_e)^{1/2} n_e n_i Z^2 \propto (k_B T_e)^{1/2} n^2 Z^2} \tag{9.14}$$

- **Line Radiation**

  In fully ionized plasmas, line radiation plays a subordinate role. However, impurities that are introduced into the plasma by wall processes can strongly influence the power balance. The energy of **line radiation** scales with

$$\epsilon \propto \frac{Z^2}{n^2} \tag{9.15}$$

  n is the principal quantum number. For efficient energy radiation, an imbalance in the occupation is required. This scales in the simplest case according to Boltzmann occupation $\exp -\frac{\epsilon}{k_B T_i}$. This exponential factor can be expanded for large temperatures compared to the energy of the line radiation and one obtains as a dependence for the radiated power in this very simple estimate:

$$\boxed{P_{Linien} \propto \epsilon \exp\left[-\frac{\epsilon}{k_B T_i}\right] \simeq \epsilon^2 \propto Z^4} \tag{9.16}$$

  i.e. the radiation losses due to line radiation increase very strongly with the atomic number of the impurity. In pure hydrogen plasmas, they are negligible.

- **Confinement**

  Finally, the isolation of the plasma is essential for the power balance. This is expressed in the simplest approach by an energy confinement time τ_e for the energy in the plasma at equal temperatures of ions and electrons ($=\frac{3}{2}n_e k_B T_e + \frac{3}{2}n_i k_B T_i = 3nk_B T$):

$$P_{Einschluss} = \frac{3nk_BT}{\tau_e} \tag{9.17}$$

The individual terms of the power balance must be in equilibrium:

$$\frac{1}{4}n^2\langle\sigma v\rangle\epsilon_{Fusion} = P_{br} + P_{Linien} + \frac{3nk_BT}{\tau_e} \tag{9.18}$$

Line radiation is negligible, and one obtains:

$$\frac{1}{4}n^2\langle\sigma v\rangle\epsilon_{Fusion} = \xi n^2(k_BT)^{1/2} + \frac{3nk_BT}{\tau_e} \tag{9.19}$$

The prefactor of bremsstrahlung is abbreviated by ξ. Solving for the product $n\tau_e$ gives an equation for the power balance:

$$n\tau_e = \frac{3k_BT}{\frac{1}{4}\langle\sigma v\rangle\epsilon_{Fusion} - \xi(k_BT)^{1/2}} \tag{9.20}$$

However, it can also be assumed that the released power is reabsorbed by the fusion plasma and directly contributes to heating: (i) the helium nuclei, which are formed in fusion with 3.5 MeV, transfer their kinetic energy to the plasma; (ii) the bremsstrahlung is reabsorbed by the plasma; (iii) the power flows emitted outward are converted into electrical energy in power plant operation and fed back to the plasma via the various heating methods. Assuming that the loss power is partially reabsorbed with an efficiency η (typical values are $\eta \sim 0.4$), the power balance is:

$$\frac{3nk_BT}{\tau_e} + P_{br} = \eta\left[\frac{1}{4}n^2\langle\sigma v\rangle\epsilon_{Fusion} + P_{br} + \frac{3nk_BT}{\tau_e}\right] \tag{9.21}$$

Thus, the so-called **Lawson criterion** for the ignition condition of the thermonuclear plasma is obtained:

$$\boxed{n\tau_e = \frac{3k_BT(1-\eta)}{\eta\left[\frac{1}{4}n^2\langle\sigma v\rangle\epsilon_{Fusion} - \xi(k_BT)^{1/2}\right] - \xi(k_BT)^{1/2}}} \tag{9.22}$$

The course of the ignition criterion as a function $n\tau_e$ as a function of T is shown in Fig. 9.6.

If this criterion is reached, the fusion plasma burns *self-sustained* without external energy input! It should be noted that for the control of a fusion plasma, the energy input from the outside should not fall below a certain value. The experiment ITER is designed so that the generated fusion power is ten times higher than the externally supplied power. The ratio of generated

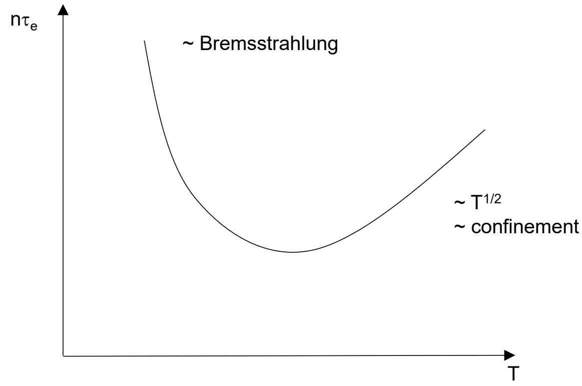

Figure 9.6: Ignition curve for thermonuclear burning.

fusion power P_{Fusion} to supplied heating power $P_{Heating}$ is referred to as the quality factor Q:

$$Q = \frac{P_{Fusion}}{P_{Heating}} \tag{9.23}$$

So far, the generation of helium by the fusion reaction has not been considered . Continuous helium production reduces the proportion of deuterium and tritium in the plasma, and the ignition criterion is also limited to large confinement times τ_e. i.e. the confinement must not be too perfect to be able to remove the ash (=He) of the fusion reaction.
This factor modifies the ignition criterion somewhat. The number of helium nuclei produced is proportional to the plasma density. Quasi-neutrality requires:

$$n_D + n_T + 2n_{He} = n_e \tag{9.24}$$

With $n_{He} = fn_e$ and initially ideal DT mixture (=1:1), we obtain:

$$n_D = n_T = \frac{1}{2} n_e (1 - 2f) \tag{9.25}$$

i.e., the factor $(1-2f)$ modifies the plasma density as it is used in the Lawson criterion.

9.3 Plasma Confinement

To achieve the thermonuclear ignition of the plasma, the main focus is on improving confinement. Accordingly, there are different concepts for generating a hot fusion plasma. Two classes can be distinguished: magnetic fusion, as discussed below, and inertial fusion, in which a fuel mixture of deuterium and tritium is brought to implosion by laser radiation. The latter will not be discussed here.

9.3.1 Tokamak

The first arrangements for magnetic confinement were made in mirror machines. However, at high densities, particles are scattered into the corresponding loss cones by collision processes, so that the confinement time remains limited.
The variant of short plasma duration but high densities, as in pinch discharges (z and Θ-pinches), is made difficult by the MHD instability of plasmas with high β.
The most advanced approach to magnetic fusion is the investigation of toroidal confinement to avoid the losses at the ends of a mirror machine or a z- or Θ-pinch.
This toroidal arrangement has fundamental consequences for the equilibrium condition of the plasma. Essential here is the fact that the magnetic toroidal field is larger on the inside of the torus than on the outside. A gradient in the magnetic field necessarily arises over the plasma cross-section (see Fig. 9.7).
Such a plasma configuration is initially still unstable. This can be justified both in the single-particle picture and in the fluid picture:

- **Stability of a toroidal plasma in the single-particle picture**

  With a gradient in the B-field, the ∇B-drift leads to a separation of the charge carriers. This creates an electric field that, according to the $E \times B$-drift, *pushes both* particle species outward (see Fig. 9.8. i.e. this configuration is not stable. This outward drift can be compensated by a shearing of the magnetic field lines, in which the guiding center of the particle motion is always guided back to the inside of the torus.

- **Stability of a toroidal plasma in the fluid picture**

  The MHD equilibrium is given by:

$$\nabla p = \vec{j} \times \vec{B} \tag{9.26}$$

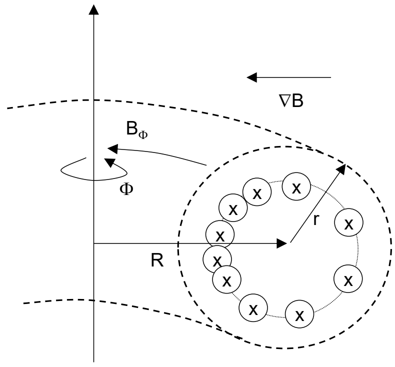

Figure 9.7: B-field configuration in a toroidal arrangement necessarily has a gradient.

The shearing of the magnetic field leads to a concentric arrangement of nested **flux surfaces** on which a uniform pressure is established by parallel transport. The cross-section of the torus thus consists of concentric circles, each corresponding to a certain pressure. Representing the MHD equilibrium on the inside and outside of a surface of constant pressure, the currents $j_\perp$, which would flow poloidally, must be different on the inside and outside, as sketched in Fig. 9.9.

$$\vec{j}_{\perp,1} \times \vec{B}_{\Phi,1} = \vec{j}_{\perp,2} \times \vec{B}_{\Phi,2} \tag{9.27}$$

This configuration is not possible, since we have no current sources in the plasma and thus always div$j = 0$ must hold. This implies that an additional current $\vec{j}|$ must flow, which induces a magnetic poloidal field B_p . The superposition of B_p and $B\Phi$ leads to a shearing of the magnetic field lines.

The relationship between current and magnetic field can be derived as follows. The diamagnetic current is initially:

$$\vec{j}_\perp = \frac{\vec{B} \times \nabla p}{B^2} \tag{9.28}$$

The current parallel to the magnetic field can be written as

$$\vec{j}_| = \frac{\vec{j}\vec{B}}{B^2}\vec{B} \tag{9.29}$$

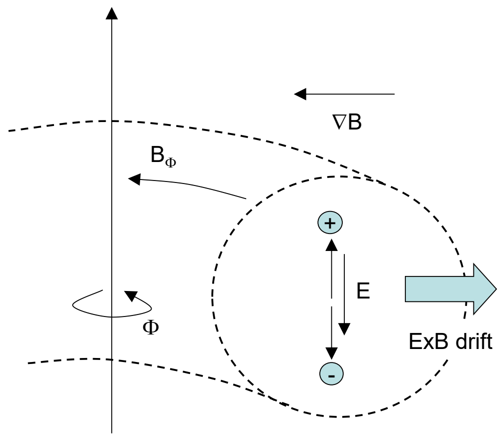

Figure 9.8: $E \times B$-drift in toroidal plasmas

From the condition div$j = 0$ it finally follows:

$$\nabla\left(\frac{\vec{B}\times\nabla p}{B^2}+\frac{\vec{j}\vec{B}}{B^2}\vec{B}\right)=0 \qquad \frac{\vec{B}\times\nabla p}{B^2}+\frac{\vec{j}\vec{B}}{B^2}\vec{B}=\text{const.} \tag{9.30}$$

i.e., the expression in parentheses must remain constant on a surface of constant pressure and thus determines the current profile and magnetic field configuration.

These arguments show that a toroidal MHD equilibrium in axially symmetric external magnetic fields can only be achieved if a toroidal current $\vec{j}_{|}$ also flows, which shears the magnetic field. This shearing of the magnetic field can be generated by a current in the plasma itself (= **Tokamak principle**). In this case, the plasma is operated as a secondary winding of a transformer. If the current in the primary winding is changed, a current is induced on the torus axis in the secondary winding, which generates the shearing of the magnetic field (Fig. 9.10). This shearing cannot be maintained in a steady state, since the current in the primary winding must be continuously changed.
This disadvantage is avoided by the alternative concept of the stellarator, in which a sheared magnetic field is directly generated by non-axially symmetric external coils (= **Stellarator principle**). However, the technical implementation is significantly more complex (Fig. 9.11).
The shearing of the magnetic field is described by the so-called **safety factor** q . q is the ratio of toroidal to poloidal turns of a magnetic field line, according

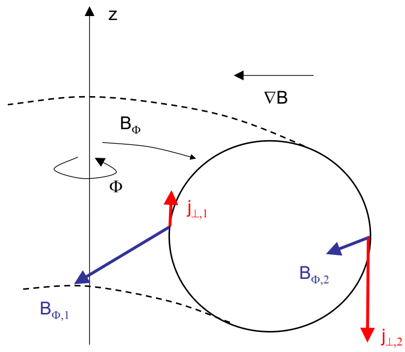

Figure 9.9: The non-uniform toroidal B-field B_Φ on surfaces of constant pressure leads to different currents $\perp$ to B_Φ on the inside and outside of the torus.

to Fig. 9.12. If N denotes the turns around the torus and n_t and n_p the toroidal and poloidal turns, respectively, q is defined as

$$q = \underbrace{\lim}_{N\to\infty} \frac{n_t}{n_p} \tag{9.31}$$

i.e. an unsheared magnetic field corresponds to $q \to \infty$ and a strong shearing corresponds to $q \to 0$. The parameter q is called the safety factor because it must only lie in certain ranges to ensure a stable plasma. This stability refers to large-scale deviations from equilibrium:

- **lower limit for q: q >2**

  If q is very small, the shearing of the magnetic field lines is very large. Accordingly, the poloidal magnetic field increases and the plasma becomes unstable against the **kink instability**. i.e., an outward deflection of the plasma increases the density of the poloidal component of the magnetic field, and the plasma is driven further outward (= **ballooning modes**), as shown in Fig. 9.13.

  A similar effect also occurs during plasma operation. As the plasma is built up, the conductivity increases just in the center of the discharge. i.e., the current $\vec{j}_|$ is now carried centrally in the torus, and a local increase in the poloidal field in the center results. Thus, a kink instability can again occur, which drives the hot central plasma outward. i.e., the plasma current suddenly breaks off again and must be rebuilt (= **sawtooth instability**).

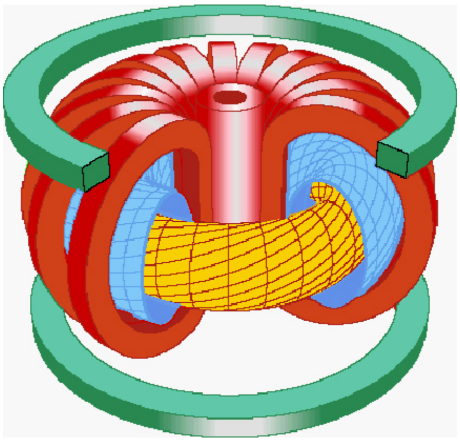

Figure 9.10: Tokamak principle.

- **upper limit for q**

  A large q is equivalent to a low shearing of the magnetic field. This situation is unstable against the **Rayleigh-Taylor-** instability!Rayleigh-Taylor or **interchange instability**. Now the plasma flows over a large distance on the outside of the torus with unfavorable curvature. The centrifugal force drives a large-scale interchange instability. Since this instability becomes particularly significant at large wavelengths of the deflection, it is dominant just at low shearing, as sketched in Fig. 9.14.

9.3.2 Limiter, Divertor

At locations where the magnetic field lines hit the walls of a fusion experiment, locally very high particle fluxes occur. To control the interaction of the plasma with the wall, the location or the manner in which the plasma comes into contact with the wall must be controlled. There are three concepts for this:

- **Limiter**

  A so-called limiter is placed at the edge of a plasma. At this location, the loss is maximized and thus the extension of the plasma is limited.

  The disadvantage of the limiter concept is, however, the spatial proximity between intense plasma and the limiter surface. The resulting transport of impurities into the plasma and the radiation losses limit the achievable temperatures and densities in the fusion plasma.

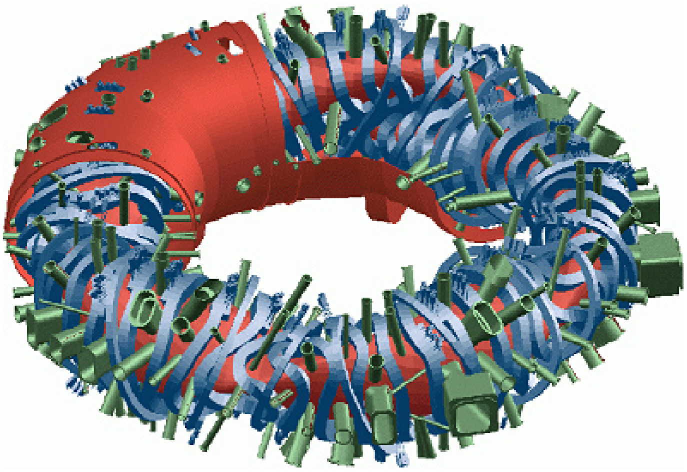

Figure 9.11: Stellarator W7X

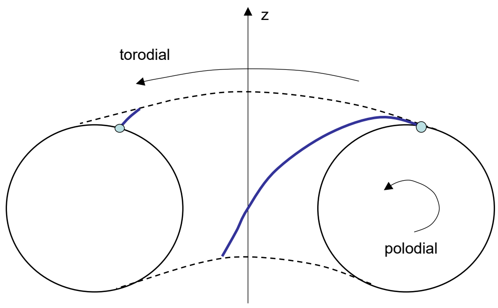

Figure 9.12: The safety factor q is defined as the ratio of poloidal to toroidal turns of a field line

- **Divertor (static)**

  A better concept for particle removal and edge control is that of a **divertor**. In this case, an **X-point** is created in the magnetic field configuration, generating a second separate plasma region at the top or bottom of the vacuum vessel. Particles that pass through the so-called **separatrix** reach the divertor plasma region on their magnetic field lines, where they hit special target surfaces.

  The spatial separation of plasma-wall interaction and main plasma allows fusion plasmas with very low impurity concentrations.

  In fusion experiments with a divertor, it was found that at higher heating powers the confinement improves abruptly. The regimes with poor

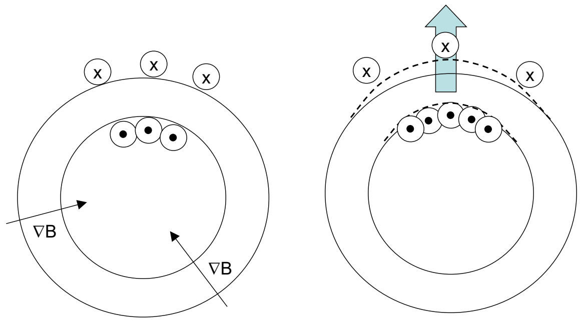

Figure 9.13: Kink instability of a toroidal plasma

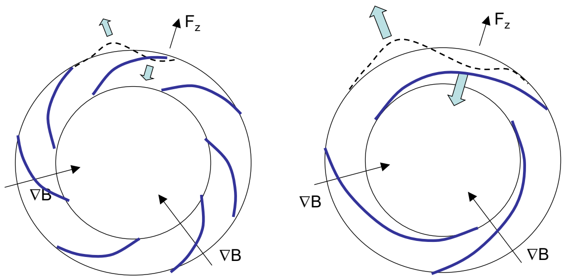

Figure 9.14: Interchange instability at large and small shearing of the magnetic field.

and good confinement are referred to as L-mode (low confinement) and H-mode (high confinement). In the H-mode, high temperature gradients are created by the good confinement, which lead to small-scale instabilities. These occur at locations of high temperature gradients at the edge and drive the hot plasma outward. These instabilities are referred to as ELMs (edge localized modes).

- **Divertor (dynamic)**

  A newer concept is based on turbulence of the magnetic field lines at the edge by generating time-varying magnetic fields. The location where the charge carriers hit the wall is distributed over a large area. The ideal case is achieved when this turbulence causes the trajectories of the particles in the edge region to become ergodized (i.e. every point in phase space is reached). Therefore, this concept is also referred to as the dynamic ergodic divertor (DED).

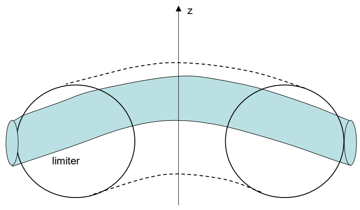

Figure 9.15: Limiter operation of a plasma

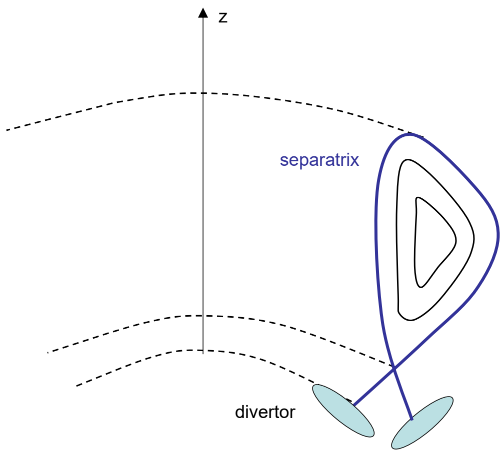

Figure 9.16: Divertor operation of a plasma

9.3.3 Transport in the Tokamak

The transport in a toroidal arrangement can be divided into several classes, depending on the length scale and collision frequency of the respective dominant transport processes:

Classical transport at high ν_m

As described in chapter 4, normal diffusion in unmagnetized plasmas is modified by the influence of the magnetic field. The diffusion coefficient perpendicular to the magnetic field scales as:

$$D_\perp = \frac{D_|}{1+\omega_c^2\tau^2} \propto r_L^2 \nu_m \tag{9.32}$$

If diffusion is considered as a random walk in real space, a step size according to the Larmor radius results.

Neo-classical transport at low ν_m

At low collision frequency, the particles experience fewer collisions and can thus follow the magnetic field topology undisturbed. In a sheared toroidal magnetic field geometry, however, the particles reach regions of alternately high (toroidal inner side) and low magnetic field (toroidal outer side). If the ratio of parallel to perpendicular velocity $\frac{v_{|}}{v_{\perp}}$ falls below a certain value, particles remain trapped in a mirror configuration, as shown in Fig. 9.17.

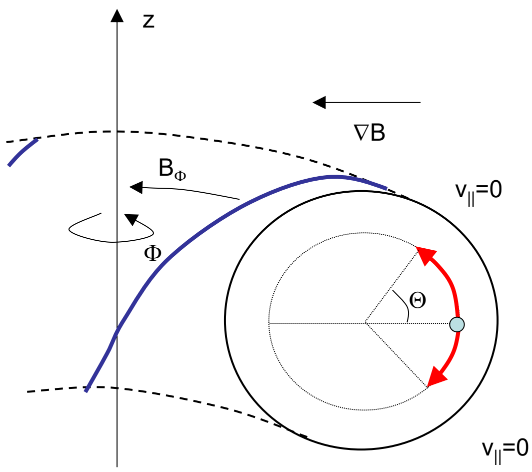

Figure 9.17: Pendulum motion of trapped particles in poloidal projection on a surface of sheared magnetic field lines or constant pressure. This corresponds to the banana orbit without considering drifts.

The pendulum motion between the two turning points is, however, superimposed by the ∇B and curvature drift. The ∇B drift was,

$$v_{\nabla B} = \pm \frac{1}{2} v_{\perp} r_L \frac{B \times \nabla B}{B^2} \tag{9.33}$$

and the curvature drift for a curvature radius R:

$$v_R = m v_{\|}^2 \frac{1}{|e| B^2} \frac{R \times B}{R^2} \tag{9.34}$$

Together, this gives for $v_{\|} \ll v_{\perp}$:

$$v_D = \frac{m}{|e| BR} \left(v_{\|}^2 + \frac{1}{2} v_{\perp}^2 \right) \simeq \frac{m}{2|e| BR} v_{\perp}^2 \tag{9.35}$$

This drift points perpendicular to the gradient of the magnetic field and the direction of the magnetic field of the toroidal field. This drift motion leads to a finite width of the banana orbit as shown in Fig. 9.18.

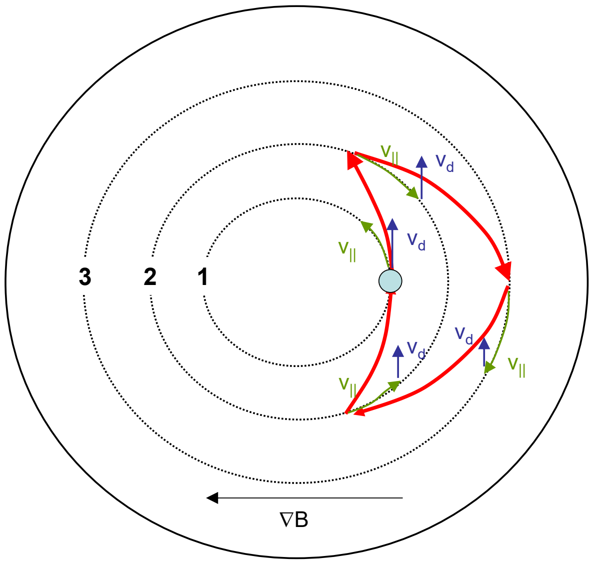

Figure 9.18: Banana orbit in poloidal projection taking into account the curvature and ∇B drift.

The distance a particle travels during the pendulum motion is denoted by L. It is given by the large radius R, the safety factor q and the opening angle $\Delta\Theta$ of the banana orbit in poloidal projection as:

$$L \sim qR\Delta\Theta \tag{9.36}$$

i.e., the time duration in which the banana orbit is traversed is $\Delta t = \frac{L}{v_|}$. Thus, the width of the banana orbit Δb becomes:

$$\Delta b = v_D \Delta t = v_D \frac{L}{v_\parallel} = r_L q \frac{v_\perp}{v_\parallel} \Delta\Theta \tag{9.37}$$

The maximum width is obtained at $\Delta\Theta \sim \pi$. Thus, an estimate for the diffusion coefficient for neo-classical transport is:

$$D_{neo} = (\Delta b)^2 \nu_m = r_L^2 q^2 \frac{v_\perp^2}{v_\parallel^2} \nu_m \tag{9.38}$$

The diffusion coefficient for neo-classical transport is typically 100 times larger than that for classical diffusion.

The course of the banana orbit in a plasma with density gradients can, however, also lead to a toroidal current flow. The argumentation is similar to that in the derivation of the diamagnetic drift. Considering two banana orbits according to Fig. 9.19, a net particle movement downward results from a volume element. Since only the poloidal projection was considered here, this net particle movement also corresponds to a net current in the toroidal direction of the magnetic field. This current is driven by the density gradient and is referred to as the **bootstrap current** .

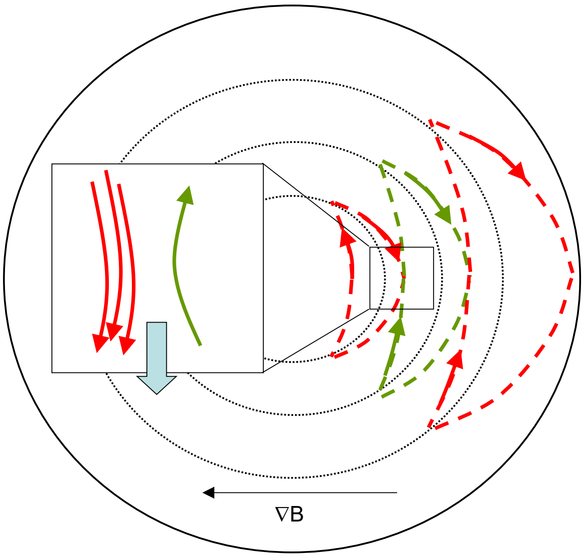

Figure 9.19: Generation of a bootstrap current by superposition of banana orbits in a plasma with density gradient.

The bootstrap current corresponds to a directed component of the parallel velocity of the trapped particles. The net current of the trapped particles, however, can be transferred to non-trapped particles through collisions (Fig. 9.20). A toroidal current is generated.
This opens up the possibility of driving the current by a density gradient to replace the current drive by induction. This would enable steady-state tokamak operation. This concept is referred to as **"advanced tokamak"**.

Anomalous transport

The previous consideration referred to normal transport processes that essentially take place on large scales. Small-scale transport perpendicular to the

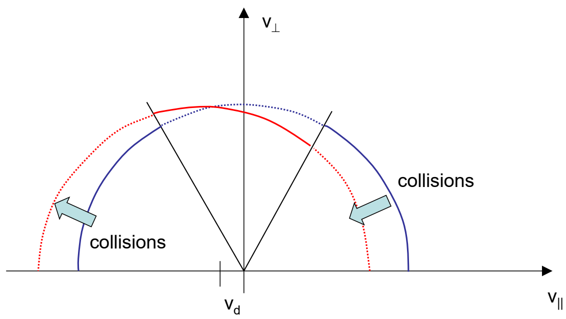

Figure 9.20: Transmission of the net current of the trapped particles to the free particles.

magnetic field can occur through instabilities or turbulence. A distinction is made between electrostatic and magnetic turbulence.

- **Electrostatic turbulence**

  As an example of electrostatic turbulence, the drift wave instability may be mentioned. At high pressure or temperature gradients, electric fields can arise. These lead to an $E \times B$ drift that drives the plasma outward (Fig. 9.21). This effect essentially limits the achievable temperature gradient in the plasma.

- **Magnetic turbulence**

  As an example of magnetic turbulence, the case of reconnection is shown, in which the magnetic field topology can change through dissipative processes. In ideal MHD, a change in the magnetic field topology is not possible because the condition of frozen-in flux must hold. With finite conductivity, however, adjacent flux surfaces can connect (= **reconnection**) and create so-called magnetic islands, as sketched in Fig. 9.22. These magnetic islands represent a radial short circuit of the plasma.

9.4 Plasma Heating

There are three main methods for heating a plasma:

- **Current Drive**

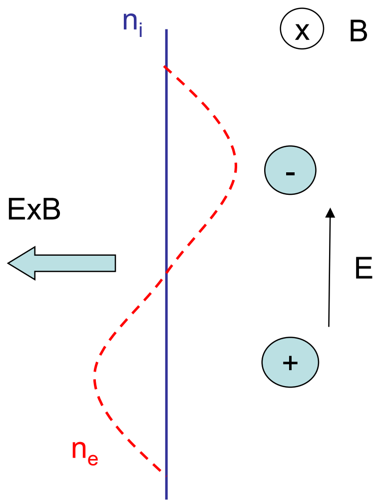

Figure 9.21: Drift waves as a possibility for the generation of small-scale electric fields that can drive anomalous transport.

By driving a toroidal current, the plasma is heated by Ohmic heating. However, the resistance decreases strongly at high temperatures, $\eta \sim T^{-3/2}$. Therefore, this type of heating plays a subordinate role in today's fusion experiments. Only for the buildup of the plasma at the beginning of the discharge is current drive important for heating.

- **Wave Heating**

  By resonant wave heating, the plasma can still be heated even at high temperatures. Ion heating is achieved by ion cyclotron resonance heating (ICRH) for em-waves parallel to $\vec{B}$ and the lower hybrid for em-waves perpendicular to $\vec{B}$. Electron heating is achieved at the electron cyclotron frequency (ECRH). At the high magnetic fields in future fusion experiments, the resonance frequencies of ECRH are in the range up to 200 GHz. The corresponding transmitters for these frequencies are technically very demanding. Finally, the penetration depth into the plasmas is limited by the heating itself.

- **Neutral Particle Injection**

  The most important heating for current and future fusion experiments is the injection of neutral particles of protons. In this process, ions are first accelerated, then neutralized, and can thus penetrate deeply into

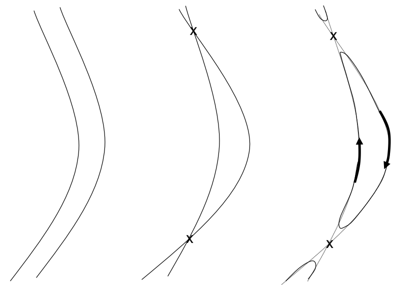

Figure 9.22: In plasmas with finite conductivity, the reconnection of magnetic field lines is possible. This creates magnetic islands that act as a radial short circuit for transport.

the plasma. In the plasma itself, they are ionized and then transfer their kinetic energy to the plasma. The injection can be perpendicular to the torus or tangential. In the case of tangential injection, a current can be driven in the plasma, which does not require an external transformer.

A schematic drawing of a neutral particle injector is shown in Fig. 9.23.

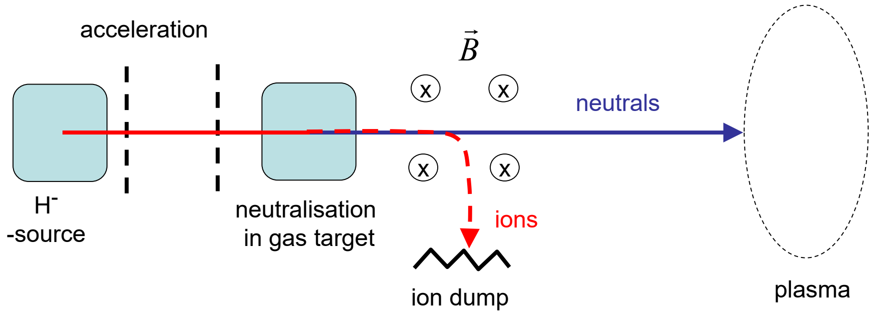

Figure 9.23: Neutral particle injection

To make neutral particle injection more efficient, high acceleration voltages are required. However, at higher voltages, the efficiency of neutralization for fast positive ions in a gas target decreases. This is not the case for the use of negative ions (the loss of an electron for a fast H^- is much more likely than the capture of an e- for a fast H^+)(see Fig. 9.24). The problem here, however, is the construction of efficient, high-power sources for negative ions.

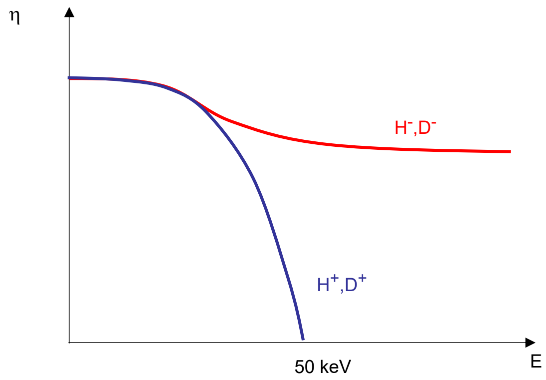

Figure 9.24: Efficiency for charge exchange

9.5 Materials for Fusion

The erosion of wall materials usually occurs through collision processes with energetic particles. For the evaluation of the threshold energy for this sputtering, is the kinematic factor and the surface binding energy of the material. The kinematic factor γ_{max} for a central collision describes the energy loss of the projectile:

$$\frac{\Delta E}{E} = \gamma_{max} = 4\frac{m_1 m_2}{(m_1 + m_2)^2} \tag{9.39}$$

According to Fig. 9.24, in the simplest case the relationship between threshold energy E_{th}, surface binding energy E_{SB} and kinematic factor γ_{max} is given as:

$$E_{th} = E_{SB}\frac{1}{\gamma(1-\gamma)} \tag{9.40}$$

One can see that the kinematic factor for protons as a projectile and lighter elements as wall material becomes particularly large, and thus the threshold energy for sputtering is very small. If sputtered wall material enters the hot fusion plasma, it contributes to the power loss through line radiation ($\sim Z^4$). For the selection of wall materials, there are two optimization possibilities: (i) on the one hand, the use of a **low-Z material**, which, although easily eroded, contributes only slightly to line radiation when introduced into the fusion plasma; or (ii) **high-Z materials**, which are only weakly eroded and thus can hardly enter the fusion plasma.

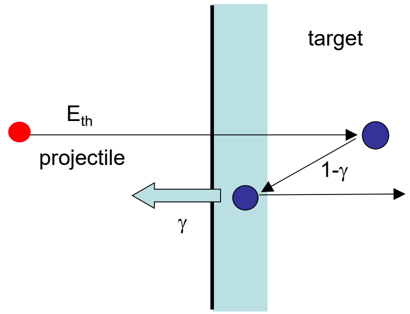

Figure 9.25: Sputtering by fast particles above a threshold energy E_{th} and kinematic factor γ.

In addition to these optimization variants, other factors also apply. These are thermal conductivity (should be high), shock resistance to high local, short-term particle fluxes (should not melt), low neutron activation and degradation of structural properties (should not become brittle).
From this long list of requirements, a material mix for the wall materials has now been established, which essentially consists of carbon for the divertor (high particle fluxes) and tungsten or beryllium for the first wall of the main plasma (low particle fluxes).

Appendix A

Question Catalog

A.1 Chapter 1: Introduction

- Define the plasma state?
- How are the plasma frequency and Debye length defined?
- When is the specification of a temperature for a plasma meaningful?
- What are degenerate, relativistic, and ideal plasmas and where do they occur?

A.2 Chapter 2: Description of Plasmas

- What types of plasma descriptions do you know and how do they differ?
- Describe the trajectories of charged particles in constant electric and magnetic fields. Which drifts occur and what is a guiding center?
- How are the Larmor radius and cyclotron frequency defined?
- Which drifts exist in non-uniform E and B fields?
- Which drifts do you know in time-dependent fields?
- Why is a shearing of the magnetic field lines necessary in a toroidal arrangement?
- What is the magnetic moment and why is it an adiabatic invariant in a mirror arrangement?

- Which adiabatic invariants do you know and when do they apply?
- What is a distribution function?
- How do the fluid equations arise from the Liouville theorem?
- What does the convective derivative describe?
- How does the diamagnetic drift arise, and what is referred to as plasma-β?
- Which drifts exist in the single-particle picture and not in the fluid picture and vice versa?

A.3 Chapter 3: Collisions

- Define mean free path, collision frequency, and collision time?
- How are collisions incorporated into the fluid equations?
- What do the cross section and the differential cross section denote?
- What is the cross section for momentum transfer?
- What is the scattering integral?
- How is the differential cross section for Coulomb scattering defined, or how does it scale with scattering angle and energy?
- What does the Coulomb logarithm describe, and what approximation is made to obtain a total cross section for Coulomb scattering?
- What is referred to as the Langevin capture cross section?
- What is the typical course of an ionization cross section with energy?

A.4 Chapter 4: Transport

- What is referred to as drift and diffusion, and how are they linked to the collision frequency?
- What is the fundamental mode of the diffusion profile in one dimension (parallel plate arrangement)?
- What is referred to as ambipolar diffusion, and how does it arise?

- How does diffusion scale with the magnetic field and the temperature of the particles in the case of charged-neutral collisions? How does the transport differ perpendicular and parallel to the magnetic field?
- Why do only collisions between particles of different charge lead to transport in fully ionized plasmas?
- What is the specific resistance of a plasma and how does it scale with particle density and temperature?
- How are the MHD equations for fully ionized plasmas derived?
- What is the generalized Ohm's law?
- How does diffusion in fully ionized plasmas scale with temperature and particle density?
- What is Bohm diffusion? What are possible causes for this?
- What is referred to as frozen-in flux?
- How does magnetic field diffuse into a plasma?
- What is a pinch and how does it work?
- Which mechanism is described by the Rayleigh-Taylor instability?
- How do drift waves arise and why are they unstable? What significance does this have for fusion?
- Explain the plasma-beam instability intuitively?

A.5 Chapter 5: Waves

- Distinguish between electrostatic and electromagnetic waves?
- When can electrostatic electron waves propagate?
- How do electrostatic electron and ion waves differ?
- Describe electrostatic electron and ion waves perpendicular to the magnetic field.
- What is the upper hybrid frequency?

- Sketch the dispersion of electromagnetic waves in unmagnetized plasmas.
- What is the refractive index of a plasma?
- How does plasma heating occur at the upper hybrid frequency?
- What is Faraday rotation?
- What is the idea of high-field coupling?

A.6 Chapter 6: Kinetics

- What does the distribution function describe?
- What does the collision term in the Boltzmann equation look like?
- What is the 2-term approximation?
- What assumptions underlie the Maxwell and Druyvesteyn distributions?
- What does the form of the distribution function look like depending on the interaction mechanisms?
- Explain the Landau damping intuitively?

A.7 Chapter 7: Plasma Sheath

- What is the Bohm criterion?
- What boundary conditions apply in the sheath and what in the presheath?
- What is the floating potential and what is the plasma potential?
- What are the assumptions in the Child-Langmuir sheath and how does the current scale with voltage and the thickness of the sheath?
- Describe the principle of a probe measurement.

A.8 Chapter 8: Low-Temperature Plasmas

- What is a Townsend discharge?
- How does the transition from an unself-sustained to a self-sustained discharge occur?
- Describe the Paschen curve.
- How do the individual zones of the DC glow discharge arise?
- Describe the current-voltage characteristic of a DC glow discharge.
- How does a magnetron discharge work?
- Sketch the voltage profile in a symmetric and asymmetric RF discharge.
- Describe the cause of the hysteresis in an inductive RF discharge.
- How does the absorbed power in an RF plasma scale with frequency and RF voltage?
- What is stochastic heating?
- How does a barrier discharge work?

A.9 Chapter 9: Fusion

- Describe the power balance of a fusion reactor?
- How do bremsstrahlung and line radiation scale with the atomic number?
- What is the Lawson criterion?
- How is the MHD stability of the toroidal arrangement achieved?
- What is a divertor?
- What is neo-classical transport?
- How does a tokamak work?
- Why will negative ions be important for plasma heating in the future?

Index

α/γ-mode, 184
μ-catalyzed fusion, 214
2-term approximation, 147

, 225

adiabatic invariant
  first, 39
  second, 41
  third, 44
advanced tokamak, 231
Alfven Waves, 141
Approximation
  local, 153
  non-local, 153
arc discharge, 204

B-field
  poloidal, 222
  toroidal, 221
ballooning modes, 224
banana orbit, 102
Bohm velocity, 164
Boltzmann equation, 144
Boltzmann relation, 11, 58
bootstrap current, 231
bremsstrahlung, 218

capacitive RF discharge, 187
cathode sheath, 182
cathode spot, 207
center-of-mass system, 69
Child-Langmuir sheath, 170
collision frequency, 66
collision time, 66
confinement
  Stellarator, 223
  Tokamak, 223
convection, 56
convective derivative, 50
corona discharge, 180
Coulomb logarithm, 73, 74
Coulomb scattering, 71
cross-section, 65
  differential, 67
cut-off, 201
Cyclotron frequency, 19

Debye length, 12, 58
Definition Plasma, 6
definition pressure, 54
dielectric barrier discharge (DBD), 208
diffusion
  ambipolar, 86
  Bohm, 101
  density profile, 86
  diffusion constant, 84
  Einstein relation, 84
  magnetic field, 104
  perpendicular to $\vec{B}$, 91
distribution function, 46, 47
Divertor
  dynamic, 227
  static, 226
Drift
  ∇B, 25
  $\vec{E} \times \vec{B}$, 21
  curvature, 26

diamagnetic, 59
gravitational, 22
drift
diamagnetic, 91

ECR plasmas, 202
electrode jet, 207
electrons
runaway, 94
ELM - edge localized mode, 227
equation
adiabatic, 46
Boltzmann, 50
continuity, 52
Maxwell, 46
state, 46
Vlasov, 49
Equilibrium
global thermal, 10
Eulerian description, 50

Faraday Rotation, 140
Fermi acceleration, 43
field reversal, 190
Fokker-Planck equation, 146
Fusion Reactions, 213

Gamow factor, 214
global model, 88, 89
guiding center, 21

H-mode, 227
heat conduction, 56
Heating
Current Drive, 232
Neutral Particle Injection, 233
Wave Heating, 233
heating
stochastic, 192
Helicon Plasmas, 139
Helium removal, 220
High-Field Coupling, 140
high-Z materials, 235

impact parameter, 67
inductive discharge, 197
E-mode, 200
H-mode, 200
hysteresis, 199
instabilities
dissipative, 116
resistive, 116
instability
drift waves, 113
interchange, 225
kink, 224
plasma-beam, 116
Rayleigh-Taylor, 109
sausage, 108
sawtooth, 224
interferometry, 132
Ionization, 76
ITER, 213

kinematic factor, 70, 235

Lagrangian description, 50
Landau damping, 159
Langevin cross-section, 75
Larmor radius, 19
Lawson Criterion, 215
Lawson criterion, 219
Limiter, 225
Liouville theorem, 49
Lorentz force, 18
loss cone, 32
low-Z materials, 235

magnetic mirror, 30
mirror ratio, 31
magnetic moment, 29
magnetic pumping, 41
Magnetohydrodynamics (MHD), 95
magnetron discharge, 185

Matrix sheath, 168
matrix sheath, 187
Maxwell distribution, 47, 145
mean free path, 66
MHD
  frozen-in flux, 106
  generalized Ohm's law, 97
  ideal, 105
  single-fluid equation, 96
MHD generator, 23
microfield, 12
microwave plasmas, 201
mobility, 84
moments of the Vlasov equation
  energy balance, 56
  momentum balance, 52
  particle balance, 51
multifrequency plasmas, 193

negative glow, 182
neoclassical transport, 102

Paschen curve, 182
pinch discharge, 107
pitch angle, 31
plasma β, 60
plasma frequency, 13, 121
Plasma Immersion Ion Implantation PIII, 169
Plasmas
  degenerate, 14
  ideal, 14
  relativistic, 15
polarizability, 74
polarization drift, 35
polarization scattering, 74
ponderomotive force, 35
positive column, 183
Potential
  floating, 166
  Plasma, 167

Ramsauer minimum, 76
random walk, 90
reconnection, 232
refractive index, 132
resistance
  specific, 93
Richardson equation, 205
Rogowski coil, 62
Rutherford scattering, 71

safety factor q, 223
scattering integral, 70
separatrix, 226
sheath
  Presheath, 164
  Space charge zone, 162
skin depth, 197
sputtering, 235

Townsend coefficient
  first, 179
  second, 181

unself-sustained discharge, 178

Vlasov equation, 144

wave equation, 131
Waves
  Electromagnetic, 130
  Electrons, 120, 122
  Ions, 124
  Lower Hybrid, 127
  Magnetosonic, 142
  Upper Hybrid, 126
waves
  cutoff, 136
  extraordinary, 133
  ordinary, 133
  resonances, 136
Whistler Modes, 139

X-point, 33, 226

